Engineering Surfaces to Control Neurogenesis

Rupert Wright

This thesis is submitted in acordance with the requirements of Keele University for the degree of Doctor of Philosophy Regenerative Medicine

March 2015

Keele University

Abstract

Producing therapeutic neural cell populations *in vitro* to treat neurodegenerative diseases is a key aim of regenerative medicine. Various protocols have been developed to produce a wide range of neural cell types in vitro, but the protocols are labour and resource intensive. Lower costs will take the cell therapy closer to clinical adoption. Cell-material interactions can be used to control cellular processes and behaviours in the place of expensive reagents. The thesis went about developing superior materials to culture neurons *in vitro* by using simple surface parameters. By using simple surfaces findings could be leveraged by incorporation in to other materials, and protocols to culture neurons.

We have investigated the responses of primary neural tissue derived from rat ventral mesencephalon (VM), interacting with a range of surface chemical functionalities and net molecular properties by using silanes. Specific substrate functionality leads to higher ratios of neurons, longer neurites and neurosphere spreading capacity. All of these characteristics indicate a high neuro-regenerative capacity.

Next it became important to optimize the amine functionalised surface with the addition of secondary amines in to the surface. The rational of adding secondary amines to the surface would produce functionalities which have a closer resemblance to biological molecules. The biomimicry in the surfaces provides extra scope for selective surface interactions to provide more control over neural cell culture which could steer protocols away from the use of expensive surfaces which are coated in extra cellular matrix molecules such as laminin.

Controlling differentiation with surfaces has long been an aim in regenerative medicine to deliver productive production protocols. It has been shown that surfaces can induce differentiation of stem cells; however there is little control where stem cells and adult cells are

simultaneously cultured. To achieve controlled differentiation of neural stem cells a surface gradient of amine polymer lengths, and polymer densities. That is in contrast to the surfaces used in previous chapters which had homogeneous presentations of surface chemistries.

Keywords

Neurons, stem cells, , microscopy, biomaterials, surface analysis, biomimicry and Gradients.

Acknowledgements

Thank you to everyone for help with the project. I would first like to thank my supervisors Dr Rosemary Fricker and Dr Paul Roach. For all the practical help I owe a large debt of gratitude to: Folashade Kuforiji, Síle Griffin, Munyaradzi Kamudzandu and Dr Rowan Orme. For use of equipment not at Keele I would like to thank: Tim Self at Nottingham University, Nexus at Newcastle University, David Smith and Dr Rob Thomas at Loughborough University. I would like to thank the Regenerative medicine DTC for recruiting me, and keeping me off the dole in very difficult economic times. For good times I would like to thank everyone in the Harvey and ISTM labs, and specifically: Hari Markides, Alan Weightman, Chris Adams, Deepak Kumar and Josh Price. My family deserves a lot of gratitude for all the help before, during and no doubt after the PhD project. The person who deserves the most thanks especially for the last year is Dr Antonella Lisella because she has provided everything.

List of Figures

Chapter I

1 Introduction

Biomaterials have a long history in medicine where clear improvements have been delivered with patients lives. The earliest example of success were total hip replacements pioneered by Sir John Charnley at Wrighington centre for hip surgery in the early 1960s. The intervention replaced the arthritic joint with metal/plastic implant cemented into the patients bone stock (Gomez and Morcuende, 2005). The implants were functional at the anotomical level where mobility was restored in patients, but the implants were inert at the biological interface. At the time it was probably a good thing because inflamation was poorly understood. Six decades later the bold new frontier for biomateials is with regenerative medicines and cell therapies, but success for biomaterials in this area will require materials to be active at the biological interface (Ratner and Bryant, 2004). Regenerative medicine will use transparented cells and cellular constructs derived from stem cells to treat diseases and injury.

Regenerative medicine has some challanges which need to tackled such as consistency of results, overuse of expensive rare chemicals, complex protocols which makes scalabilty challanging, useful and ease of analysis. All these issues can be solved by designing better biomaterials which can be engineered to be: cheap, do tasks such as enhance migration, and enhance the activity of other components. To address the problems important early goals include:

1. Find the simplest biomaterial parameters/characteristic which when manipulated will causes changes in cell response.

2. Find the best way to present chemical characteristics on a biomaterial.

3. Vary the chemical characteristic on a single surface to direct changes in cell response simultaneosly.

Biological Surface Interface

1.1.1 Protein Adsorption

The biomaterial/biomolecular interface controls the resultant cell response, because cells have specialist components for surface interactions such as extracellular matrix and adhesion molecules. Controlling the biological conditioning of biomaterials is the simplest way to achive cellular control with a surface. Proteins are 3D biological macromolecular polymers composed of 20 different amino acids in different abundances these present a range of chemical properties, and can be hydrophilic (postive or negatively charged at physiological pH) or hydrophobic. (**Figure** 1.1). Short polypeptide specific binding sequences are found in larger proteins, and adhesive sequences include Arginylglycylaspartic acid (RGD) (Ruoslahti, 1996). From the protein's chemical properties interactions with the surface can be engineered. The myriad of protein functions come from the fluid structures because proteins are amphiphilic macromolecules. In contrast most man-made polymers have a repetitive structure (excluding catalysts) the function is dependent on composition.

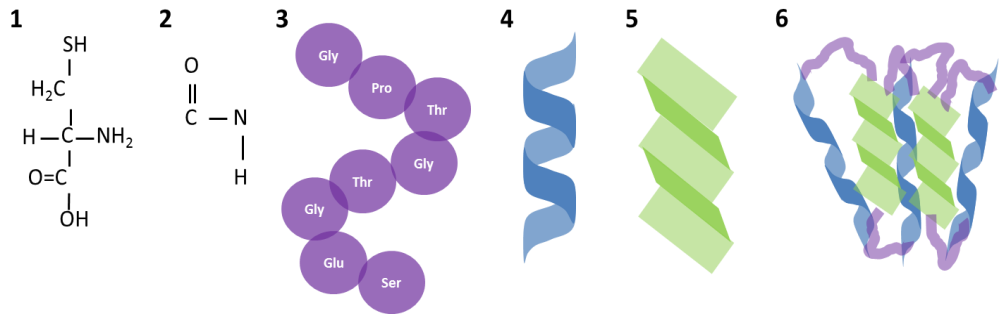

Figure 1.1 - The protein heirarchy in life. 1 is an amino acid (cysteine) which is the monomer unit of a protein. 2 is a peptide bond which links amino acids. 3 is a polypeptide which is the primary structure of a protein. 4 is the alpha helix which is a secondry structure. 5 is a beta sheet which is also a secondary structure. 6 is a teritary structure of a protein which combines primary and secondary structures.

1.1.2 Physical Science of the Biomaterial Interface

Engineering of the surface at the nano scale has highlighted how protein adsorption can be controlled, obeying physical laws to form mono- or multilayers, also impacting on the structure of the adsorpbed protein molecules (Roach *et al*., 2005). Most cell culture medias contain proteins, so controlling protein adsorption through designed surface engineering will rapidly lead to improved biomaterials with specific biological activity. Selectively absorbing proteins from biofluids can therefore improve biomaterial performance, through directing cell response. Interactions between proteins and biomaterials usaully centre around intermolecular bonds which depend on chemical characteristics. Therefore, key interactions between biomolecules and a surface should be considered in order to optimise the surface's biological performance. These will include, but are not limited to, the defined chemical and nano-topographical charcteristics, presenting charged and hydrophilic/phobic regions. Chemical interactions exist in form of discrete and formal bonds/ interactions, ranging from coulomb interactions to hydrogen-bonding. Synergistically these play a role in determining how protein molecules bind, and how their structure is presented in the adsorbed layer.

Coulomb interactions are defined as formal presentation of charged chemical groups, meaning that a negative molecule will be attracted to a positively charged surface; likewise a repulsive interaction will be observed between a positively charged biomolecule and positively charged surface (Dubiel *et al*., 2011) This concept was explored by Finke *et al*., 2007 where the authors compared positively charged amine surfaces to natural negatively charged hyaluronan coatings for osteoblast adhesion. The number of focal adhessions was enhanced by on positively charged surfaces.

Another consideration is that a biomolecule will interact with a surface based on a similar priniclple of wettability; which provides a simplistic measure of water interaction.

The most common measurement of hydrophobicity is water contact angle which looks at how a solvent behaves on a surface. General rules for wettabilities and protein adsorption were established by Whiteside's team in the late 1990s (Sigal *et al*., 1998). Small proteins tend to adsorb on to hydrophobic surfaces and the larger proteins tested (pyruvate kinase, fibrinogen and γ-globulin) also adsorbed best on the most hydrophobic surfaces. Hydrophillic surfaces tended to be more resistant to protein adsorption. On tissue culture plastic which is hydrophilic (WCA 56˚) (Chang *et al*., 2005), serum albumin readily adsorbs (Curtis and Forrester, 1984).

More generally, wettability can be used to describe how extracellular matrix (ECM) proteins interact with a surface, impacting directly to interface with cells. Surfaces of median wettability are known to better support protein adsorption, and therefore positively support cell adhesion (Sousa *et al*., 2005). Very wettable surfaces such as poly(ethylene oxide) (PEO) are, however, strongly resistant to protein adsorption due to the hyper-hydrated polymer brush-like structures preventing 'attachment' of the protein to the surface – this is particulrly evident under flow conditions (Jeon and Andrade, 1991) (Harder *et al*., 1998). Likewise, very hydrophobic surfaces show a similar effect (Koc *et al*., 2008). Wettability of a biomaterial is a very simple defining parameter of surface characterisitcs, but it has major impact on biomaterial performace.

1.1.3 Dynamics of the Interface

The biological interface is highly dynamic, with many considerations needing to be addressed to understand the mechanistic detail of the events occuring. There are numerous events working simultaneously, with many thousands of proteins/species competing for vacant surface sites. In a multi-protein system, such as a biological mileu, the surface changes over time as the material is goes through a so-called '*conditioning*'

process. Surface characteristics such as chemistry and nanotopography have been well documented to influence the adsorbing protein layer. The complexity of biological fluids drives adsorbing species competition for surface sites. This means that the composition of the adsorbed biolayer can be dictated by engineering the surface accordingly.

The stages of biological conditioning are described by (Roach *et al*., 2007):

1. Rapid hydration of the material (nanoseconds)
2. Protein conditioning (seconds to hours)
3. Cell/bio-interface interactions (hours)
4. Remodelling and integration with the host (days to years)

Koc *et al* demonstrated that nano-topography had a major influence on the ability of protein molecules to adsorb to a surface, with nano-hairs preventing adsorption, particulaly under flow conditions. (Koc *et al*., 2008) Further, the authors demonstrated that the surface chemisty acts synergistically with topography at this length-scale, with more hydrophobic chemistry giving rise to negligible protein adsorbed under flow. Others have shown in static systems that the binding affinity of proteins was lower as a result of nanotopography, but the absorption was very high on hydrophillic surfaces (Scopelliti *et al*., 2010). The packing and conformation of proteins has also been shown to be strongly influenced by surface nanotopography (Roach *et al*., 2006).

When coming in contact with a surface, proteins can denature, conformationally distorting to present native interior cytptic domains to the external environment. New hydrogen bonds can form in the new denatured protein conformation when previously there were weaker interactions (Roach *et al*., 2007). A functional study of the effects of protein adsorption and protein conformational changes was made by Roach *et al.* Bovine serum albumin (BSA) was found to adsorb in a one-step process, while fibrinogen

adsorbs in a multi-step process. Which means the adsorption process for target molecules should be considered for biomaterial design.

Vroman was the first to demonstrate the highly changeable nature of the biological interface. (Vroman *et al*., 1980) Using two proteins having differing affinities Vroman demonstrated how low affinity fibrinogen was displaced by the heavier high affinity kininogen (**Figure** 1.2).

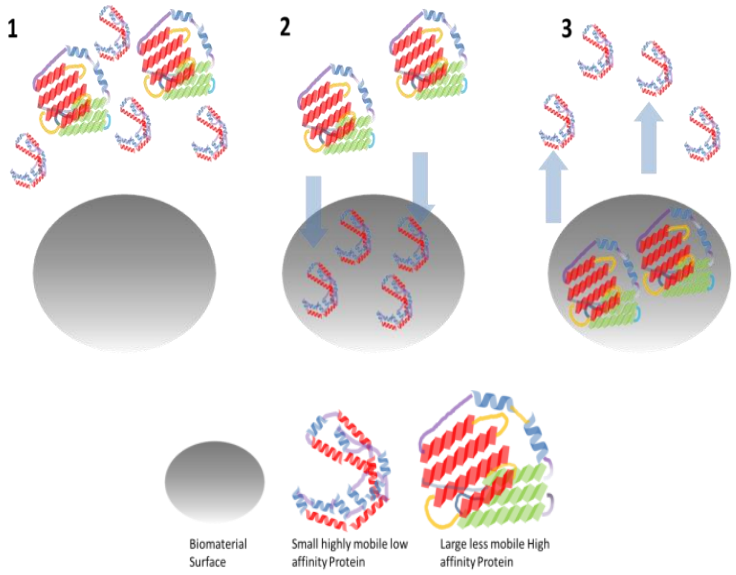

Figure 1.2 – A schematic showing the Vroman effect. a) hydration of the biomaterial surface with biofluid, b) biomaterial surface is first condition with low affinity highly mobile small proteins, and c) low affinity highly mobile small proteins are displaced by larger higher affinity proteins.

Competitive protein adsorption has been assayed with an osteoblast cell line (Wei *et al*., 2009). The influence of wettability was assessed for albumin and fibronectin, showing clearly that only the latter adsorbed well to both.

Fibronectin covered hydrophobic surfaces promoted osteoblast adhession, and to compare all albumin coated surfaces did not promote osteoblast adhession. Which is a manifestiation in cell response to chemical characteristics at the interface.

Cells respond in many ways to biomaterial conditioning. Osteogenic lineages are known to be responsive to topology from work by Dalby's team. Mesenchymal stem cells were well retained on surfaces with a random arrangement of nanoposts

(McMurray *et al*., 2011), and increased the expression of the stro1 marker. The randomness may have benefited the cells because of a lack of clear poles, and the immunocytochemistry shows that actin is in a random alignment which is a downstream result of focal adhesions. The nanotopography made the surface more hydrophobic (WCA 81-82˚). Nanotopology has the effect of super-hydrophobicity called the 'lotus-leaf effect' (Roach *et al*., 2008), which is the basis of biologically inspired materials. Surfaces roughness enhances the differentiation of mesenchymal stem cells down an osteogenic lineage (Dalby *et al*., 2007)**.** A possible mechanism was highlighted in (Giam *et al*., 2012) where dots of fibronectin were mapped to mesenchymal stem cell fate. Arrangement of the dots controlled the cell shape resulting in changes to cell fate. Microposts have also been shown to offer a slight raise in neural differentiation from pluripotent stem cells (Sun et al., 2014). One of the strengths was the integration of synthetic surfaces into the methodology, but the techniques are highly complex which makes the gains in differentaition marginal.

Control of the biological conditioning process is critical for the early cellular colonization process. Being able to control the condition would enhace the role for biomaterials, because colonization governs future cell attachment, cell proliferatation, and cell differentiation.

1.2 Cell Adhesion

After biological conditioning of a biomaterial cells will remodel the enviroment. Mammalian cells adhere to a surface with a variety of adhesion molecules in a receptor/ligand interaction, and cells will stick to each other through extra-cellular matrix

interactions. Adhesive molecules often have secondary functions in cell signalling and proliferation, so further highlight the importance of the cell surface interface.

Integrins and cadherins are the main adhesion molecules which attach cells to surfaces, and each other. Integrins are well studied cellular adhesion molecules present on most cells, and composed of an α and β unit. The role of integrins is not just for adhesion, communication messages with neighbouring cells can occur when integrins carry messages in-and-out of cells (Hynes, 2002). *Cadherins* are calcium dependent transmembrane cell adhesion molecules. Cadherin are transmembrane proteins which are calcium dependent and link cells together with the extracellular region. Cadherins play roles in cell communication and morphogenesis through the cytoplasmic region (Angst et al., 2001), and also cadherins are spescific to tissues. E-cadherin which was first discovered in the 1980s (Hyafil et al., 1981) is common in endothelial cells, in contrast neural cell adhesion molecule (NCAM) is common to neurons.

1.2.1 Extra Cellular Matrix

The ECM provides a chemo-mechanical surrounding connecting cells in most tissues, consisting of proteins including: laminin, collagen, fibronectin and vitronectin. The ECM has been exhaustively studied in terms of roles in neuroscience in cell migration, connections and structure of tissue.

The ECM is not a static entity because in processes along with cell migration, cell differentiation where tissues change shape through development, and specific to neurons synaptic strengthening/weakening (synaptic plasticity) (Dityatev and Schachner, 2003); the ECM is constantly remodelled *in vivo*, as well as during *in vitro* culture. For example, fibronectin is degraded in neural outgrowth because ECM is important as scaffolding in neural development (McGuire and Seeds, 1990). The findings have highlighted a new

target to prevent brain-injury which would be matrix metalloproteases, and their inhibits to prevent loss of neural connections in brain injury (Muir et al., 2002).

The ECM provides a chemical signaling enviroinment, wherein concentration gradients of proteinaceous species dictate positional information for cells, directing migratory effects such as axonal projection. Tissue architecture is therefore developed in this way, with cells migrating long distances to reach their target site (Emerling and Lander, 1996). Laminin has been shown to provide a cue for axons to extend and glycosaminoglycan (GAG) heparin sulphate as an migratory inhibiton, defining a cortical boundary in brain development. Emerling and Lander studied the portioning in slice culture where the partitioning of developing cortical lamellae was impacted by enzymic digestion of heparin sulphate, because there was innervation through the lamellae partitions. Heparin sulphate has also been demonstrated to control differentiation processes of neural stem cells (NSCs) (Nurcombe *et al*., 1993). Acting as a cofactor for mitogens including FgF1 & FgF2, the heparin sulphate surprisingly does not alter the conformation of FgF (Faham *et al*., 1996). One may expect that the highly charged heparin sulphate would interact strongly when binding to the FgF, and therefore cause a conformational change; this is not observed. Other studies have revealed that the heparin sulphate binding domain on FgF2 has a higher affinity for heparin sulphate (Naimy *et al*., 2011), highlighting that the charge of the FgF-heparin complex is important for cell receptor interaction.

A cells matrix takes part in various process, and some of which will not work without the ECM. Making the biomaterial conducive to cellular remodelling of extra cellular matrix will result in the physiological functions and architectures being established with less problems. To achive that specific features of the ECM have to be understood.

1.2.2 Laminin

The laminin component of ECM has been the **gold standard** for the culture and differentiation of neurons for two decades (Drago *et al*., 1991). The reason is because laminin contains various epitopes which direct cell response (Table 1). Laminin is at the basement membrane of developing tissues from which other ECM molecules bind to (Timpl *et al*., 1979). It is a large glycoprotein typically with a size around 900 kDa, presented in a 'cross' shape morphology (Beck *et al*., 1990). There are 15 laminin isoforms (Table 2), composed of variants of α, β & γ chains (Miner and Yurchenco, 2004) which are bound by disulphide interactions giving laminin its distinct shape (**Figure** 1.4) (Cooper *et al*., 1981). 15 genes encode for the laminin subunits and in mouse knockouts for γ1 subunits are lethal (Smyth *et al*., 1999), demonstrating the importance in development through lethality of knock-outs. Table 1 lists specific motifis which control nearly cell functions including: cell adhesion, stem differentiation and morphogenesis (Malinda and Kleinman, 1996). The expression of laminin and trafficking in the ECM is complicated, in contrast stationary cells such as keratinocytes laminin was expressed in a rosette pattern or in fribiular trials for migratory cells (Sehgal *et al*., 2006).

Xenogeneic and recombinant derived laminins have been used extensively for cell culture by enhancing cell attachment and spreading. In 1980 laminin was shown to enhance the attachment of the PAM 212 line of mouse epithelial cells compared to basement collagen (Terranova *et al*., 1980), also the authors highlighted specificity for certain cell types. Terranova *et al* demonstrated that laminin enhanced migration of polymorph nuclear neutrophils, whilst fibronectin inhibited migration (Terranova *et al*., 1986). This is an important insight showing that migration of cells is influenced by ECM proteins. In the late 1980's laminin was shown to cause axon extensions in Rugli human glioblastoma cells (Goodman *et al*., 1987). Goodman found latter that cell attachment

was driven by the Arginine-glycine-aspartic acid (RGD) peptide sequence which is the epitope for α1β1 integrin (Goodman *et al*., 1991). Cell culture of primary derived neurons was becoming far simpler and in the early 1990's laminin was shown to drive differentiation of primary murine mesencephalic neurons (Drago *et al*., 1991). The technique described became a gold standard in neural cell culture demonstrating that the surface (or biological interface) controlled neural differentiation. This has therefore been the gold standard for neural culture, when previously diffusible nerve growth factor (NGF) had been used to differentiate a neural cell line (Matsushima and Bogenmann, 1990). The effect of other ECM molecules including fibronectin and gelatine (hydrolysed collagen) were compared to laminin for embryonic stem cell derived neural precursors (Goetz *et al*., 2006b). The hypothesis was that areas of the brain are partitioned by different ECM molecules (Garcion *et al*., 2004). Neural stem cell fates were steered depending on which ECM protein was used to coat the surface. The findings were echoed in a similar publication which showed that laminin and fibronectin would stimulate the migration out neurospheres compared to other ECM molecules such as chondroitin sulphate proteoglycan (Kearns *et al*., 2003). The role for laminin in neural differentiation *in vitro* was shown in two publications where the colonization of laminin coated slides was characterised. The first the stages of neural differentiation were characterised in (Jacques *et al*., 1998). It was demonstrated that when a neurosphere comes into contact with a surface the first indicator of maturation is the first neurons migrate out in a process called chain migration (Jacques *et al*., 1998). This is stimulated by integrin α1β1 and α6β1, where the epitope can be found on laminin. Maintenance of neural stem in neurospheres is maintained by laminin 1, 2, 4 and 12 in a laminin rich environment (Campos, 2004). These laminins have peptide ligands corresponding for the β1 integrin. Laminin is considered essential in many of the neural differentiation protocols (Risner-Janiczek *et al*.,

2011)(Kriks *et al*., 2011a). The reputation has been earned, but expense and scaling problems have not been addressed. Arrays of ECM combination coated coverslips were tested in Nakajima *et al*. 2007 in an attempt to screen for optimum combination surface coating for neural differentiation. Fibronectin and laminin caused neural differentiation and were capable of other tasks when combined with soluble signals including NGF and EGF. Recently laminin-10 (α5β1γ1) has shown to be effective at retaining pluripotency in hESCs and iPSCs (Rodin *et al*., 2010). A clear advantage of the surface was the ability to retain karyotype stability in the pluripotent cell lines. The authors showed with antibody blocking that the α6β1 integrin was driving attachment to the surface. Numerous applications have been demonstrated by the use of laminin, but the disadvantages are the expense repeatability and lack of flexibility which are massive problems with scalability in medical translation. Another indirect problem is that the laminin tends to get used in complex protocols, so lots of exspensive reagents do not get used in an optimal way.

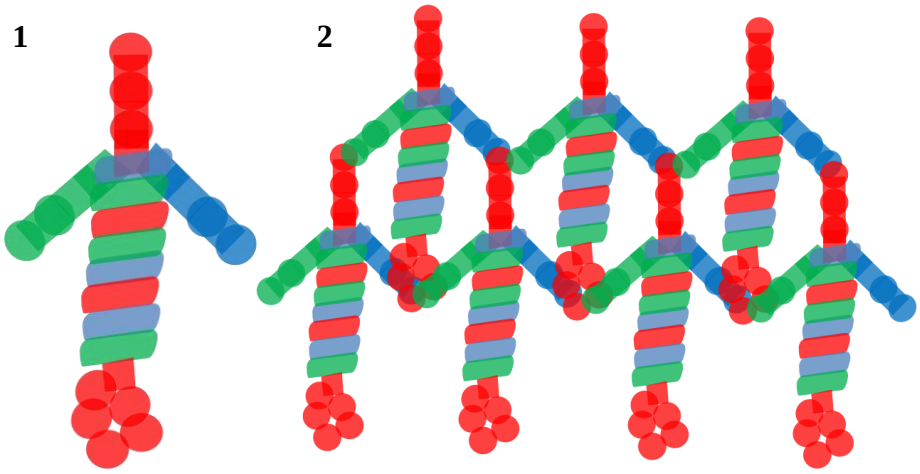

Figure 1.3– (1) Laminin's cross shaped structure (2) Laminin polymerization

Laminin plays an important role in the structure of tissues *in vivo*, because of the interactions with other ECM molecules. Which could be a possible reason for the laminin

coated surfaces as a gold standard for culturing cell types, because it is conducive to cellular remodelling. Electron microscopy in the 1980's was used to show that laminin specifically interacts with type IV collagen (Charonis *et al*., 1985). The laminin interacts with any of its globular domains with COOH-terminal non-collagenous (NC1) domain on collagen. Laminin can bind to other molecules in a process called laminin polymerization which was first observed by Yurchenco *et al* 1985. Blocking of the globular domains on the β chain can stop the polymerization process (Schuger *et al*., 1998). The amino terminal is also important in the polymerization process (Hussain *et al*., 2011). The polymerization of laminin is driven by calcium ions and the polymerization is halted with chelating agents including ethylenediaminetetraacetic acid (EDTA) (Cheng *et al*., 1997). Another interesting point about the chemistry of laminin is the interactions it forms with growth factors. Fractones which are formed from laminin interactions with collagen (Mercier *et al*., 2003), produce special catalytic sites allowing for the binding of bFGF to heparin sulphate (Kerever *et al*., 2007). In these areas the bFGF is more potent causing more proliferation of neural stem cells.

Laminin has an excellent track record, but has scalability problems. It is important to take the best features forward, and to engineer in to optimal presentations for various roles.

Table 1 – Neural specific sequences and related functions (Adapted from SANNA MURTOMÄKI-REPO 2000) which range from roles in neural adhesion, migration and differentiation.

Subunit Chain	**Peptide Sequence**	**Function**	**Reference**
α1 I	CSRARKQAAS IKVAVSADR	Cell adhesion, neurite outgrowth Stimulation of metastasis, collagenase production Bone cell differentiation Binding of 110 kDa cell surface protein Stimulation of plasminogen activation Signal transduction, cell growth Promotion of angiogenesis and tumor growth Tumour growth, colony formation Binding of APP T-lymphocyte adhesion Disruption of gastulation in sea urchin	Tashiro *et al*., 1989 Kanemoto *et al*., 1990 Vukicevic *et al*., 1990 Kleinman *et al*., 1991 Stack *et al*., 1991 Kubota *et al*., 1992 Kibbey *et al*., 1992 Yamamura *et al*., 1993 Kibbey *et al*., 1993 Weeks *et al*., 1994 Hawkins *et al*., 1995
α 1 G α 1 III	RGD	Endothelial differentiation Cell adhesion Cell adhesion, spreading,	Grant *et al*., 1989 Aumailley *et al*., 1990 Tashiro *et al*., 199
α 1 G	KQNCLSSRASF RGCVRNLRLSR	α3β1 integrin binding	Gehlsen *et al*., 1992
α 1 G	SINNNR	Cell adhesion	Chen *et al*., 1997b
α 1 G	KATPMLKMRT SFHGCIK,	Cell adhesion, heparin binding, neurite outgrowth	Skubitz *et al*., 1991
α 1 G	KEGYKVRDLNI TLEFRTTSK	Cell adhesion, heparin binding, neurite Outgrowth Binding of α3β1 integrin	Skubitz *et al*., 1991 Pattaramalai *et al*.,1996
α 1 G	KNLEISRSTFDL LRNSYGRK	Cell adhesion, neurite outgrowth	Skubitz *et al*., 1991
α 1 G	DGKWHTVKTE YIKRKAF	Cell adhesion, neurite outgrowth	Skubitz *et al*., 1991
α 1 G	RKRLQVQLSI	Neurite outgrowth	Richard *et al*., 1996
α 2 G	KNRLTIELEVRT	Neurite outgrowth	Richard *et al*., 1996
β1 III	YIGSR	Neural attachment	Graf *et al*., 1987
β1 III	YGYYGDALR	α2β1 integrin binding	Underwood *et al*., 1995
β1 I V	RYVVLPRPVCF EKGMNYTVR	Heparin binding, cell adhesion	Charonis *et al*., 1988
B1VI	RIQNLLKITNLR IKFVK	Heparin binding	Kouzi-Koliakos *et al*., 1989
β2 I	LRE	Motor neuron on stop signal, inhibition of neurite outgrowth Promotion of motor axon growth	Hunter *et al*, 1989b,1991 Brandenberger *et al*, 1996
γ1 I	RNIAEIIKDI	Neurite outgrowth, neurotrophic effect, neurotoxic effect Neural migration Axonal differentiation Axon guidance Modulation of electrical activity of neurons	Liesi *et al*., 1989 Liesi *et al*., 1995, 1996 Matsuzawa *et al*., 1996 Matsuzawa *et al*., 1998 Hager, *et al.*, 1998

Table 2 – Adapted from (Durbeej., 2010) shows all 15 isoforms of laminin, their constituent subunits and the locations in the body where each isoform is expressed.

Laminin Isoform	**Constituent Chains**	**Tissue Expression**	**Reference**
Laminin-1	α1β1γ1	embryonic epithelium, brain blood vessels	Timpl *et al*., 1979
Laminin-2	α2β1γ1	muscle, heart, peripheral nerves and testis	Ehrig *et al*, 1990
Laminin-3	α1β2γ1	placenta	Engvall *et al*, 1990
Laminin-4	α2β2γ1	muscle, heart, peripheral nerves and neuromuscular junction	Engvall *et al*., 1990
Laminin-5	α3β3γ2	epidermis, placenta and mammary gland	Rousselle *et al*., 1991
Laminin-6	α3β1γ1	epidermis and amnion	Marinkovich *et al*., 1992
Laminin-7	α3β2γ1	epidermis and amnion	Champliaud *et al*., 1996
Laminin-8	α4β1γ1	endothelium, smooth muscle, fat and peripheral nerve	Miner *et al*., 1997
Laminin-9	α4β2γ1	endothelium, smooth muscle and neuromuscular junction	Miner *et al*., 1997
Laminin-10	α5β1γ1	developing epithelium, mature epithelium, mature endothelium and smooth muscle	Miner *et al*., 1997
Laminin-11	α5β2γ1	mature epithelium, mature endothelium, smooth muscle, neuromuscular junction and glomerular basement membrane	Miner *et al*., 1997
Laminin-12	α2β1γ3	Placenta and testis	Koch *et al*., 1999
Laminin-13	γ4	Axon guidance for the neural floor plate	Serafini *et al*., 1994
Laminin-14	γ5	Axon guidance for the midline	Serafini *et al*., 1994
Laminin-15	γ6	Axon guidance for motor, sensory and sympathetic neurons	Wang *et al*., 1999

1.2.3 Integrins

Integrins are the main adhesion molecules which adhere cells to a biomaterial surface or biomolecular matrix. Integrins are well studied cellular adhesion molecules present on most cells, and composed of an α and β unit (**Figure** 1.4). The integrins are found in a transmembrane position the head of the protein (matrix end) is outside the cell while the tail end is inside the cell cytosol which is glued to actin filaments. The matrix end (receptor) binds to specific peptide sequences (ligand) frequently found on ECM proteins (Hynes, 1992), triggering cell adhesion and down-stream effects. The integrins can be used to communicate messages with neighbouring cells showing that integrins can carry messages in-and-out of cells (Hynes, 2002). By changing the integrin's conformation, cells can attach and detach, because the integrin is 'glued' to the internal cytoskeletal machinery of the cell facilitating migration in neural development (McKeown *et al*., 2013).

When the molecule is in the 'off' conformation it is not in an optimum conformation for binding, calcium and magnesium ions make integrins more adhesive but has to be in proportion to charge balance the structure because abundance of one integrin sub-unit over another makes integrins less adhesive (Chen *et al*., 2003).

Focal adhesions are integrin clusters where actin filaments are anchored in, and this affects cell: adhesion, migration, signalling and division. Focal adhesion stimulates the digestion and polymerization of actin which is a cytoskeleton protein important for movement and shape (Ballestrem *et al*., 1998). Densely packed RGD engineered peptide on engineered surfaces stimulate cell spreading (Cavalcanti-Adam *et al*., 2006a). The αvβ3 integrin is the receptor for the ubiquitous RGD ligand (Singer *et al*., 1988), which is effected by density of ligand. The reason is because when there are few adhesion complexes the cells are rounded and can detach easily. Lots of these complexes together as focal point mean more spreading because the cells are firmly bound to the surface (Cavalcanti-Adam *et al*., 2007).

Integrins have roles in neural stem cell maintenance and differentiation. Campos *et al* have shown that the β1 integrin is a marker for neural stem cells in neurospheres. This integrin causes increased expression of FGF2 in neural cell cultures which is a stem cell mitogen (Kinoshita *et al*., 1993). This shows the hierarchy of factors in cell niches. Using neurospheres and blocking the β1 integrin will cause a decreased expression of nestin (neural stem cell marker) presumably because the cells differentiate (Leone *et al*., 2005). *In vivo* β1 knockout experiments show that the neural crest development in chicks is effected causing trans-differentiation of attached epithelial stem cells (includes neural lineages) to migratory mesenchymal stem cells (Tucker, 2004). Antibody blocking of the α6Bβ1 integrin in neurospheres inhibits chain migration of neurons which is in an indicator of neural differentiation (Jacques *et al*., 1998). In the same paper antibody

blocking of α5β1 and α5β1 stopped proliferation. The α3β1 *in vivo* is important for the layering of the cortex in development, because silencing is thought to cause glial differentiation (Anton., 1999). Saha *et al*., 2007 modified surfaces with arginylglycylaspartic acid (RGD) and isoleucine lysine valine alanine valine (IKVAV) which demonstrated an ability to control neural cell fate. RGD was better at maintaining the neural stem cells because RGD is a ligand for β1 integrins (Humphries *et al*., 2006). In contrast IKVAV produced enhanced differentiation. IKVAV has been used to make fibres more adhesive in (Mandal *et al*., 2009) also the fibroblast cell lines aligned in the same directions of the fibres.

Neural alignment is thought be a result of aligned focal adhesion complexes (Ferrari *et al*., 2010). This was shown with confocal microscopy and substrates with imprinted gratings. The neural growth cone's position is stabilized by focal adhesions which has been shown with Rac1 (stimulated by focal adhesions (Rottner *et al*., 1999)) inhibition, this is the precursor step to neurite outgrowth.

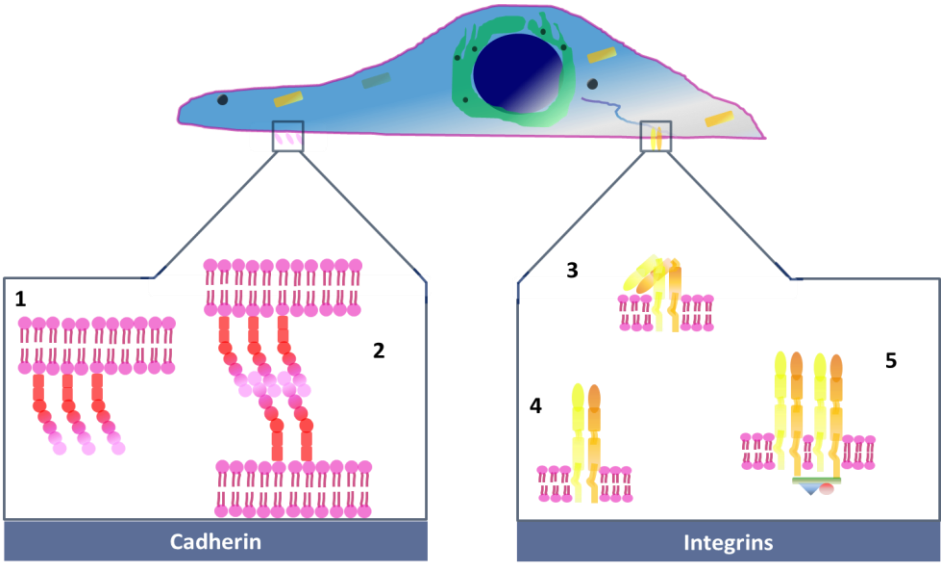

Figure 1 4 – cell adhesion with two cell adhesion complexes Cadherins and Integrins. 1 is an inactive cadherins. 2 is an active cadherin bond between neighbouring cells. 3 is an inactive integrin. 4. Is an active integrin. 5 is a focal adhesion complex where there are multiple integrins clustered together in close proximity.

1.2.4 Neural Cell Adhesion Molecule

Neurons adhere to glia with neural cell adhesion molecule (NCAM) which is a cadherin specific to neurons which is expressed on the surface of glia and neurons (Noble *et al*., 1985). NCAM is a glycoprotein expressed at the cell surface of neurons (Theodosis *et al*., 1999) and binds cells to cells through homophilic interactions (Kasper *et al*., 2000). NCAM binds to other NCAM molecules (**Figure**1.5). A cell to cell NCAM complex structurally has two-domains which resembles a cross-shaped antiparallel dimer. NCAM has a high preference for polysialic acid groups which means NCAM molecules can be selectively unbound for neural detachment (Cunningham *et al*., 1983).

The interaction is exclusive to NCAM and polysialic acid groups do not effect other adhesion molecules (Kleene and Schachner, 2004). In synaptic plasticity (neurons making new connections) this feature is important (Weinhold *et al*., 2005). Murine animal models deficient in polysialic acid had poorly developed brains in terms of connecting the nuclei. Polysialic acid is also important in injury and reinnovation where levels increase during injury (Franz *et al*., 2005).

In neural tissue, glia serve as the support cells for neurons and there are specific interactions between the two. *In vitro* neurons are frequently seen migrating on a bed of glia (Edmondson and Hatten, 1987). Therefore it is not common for the neurons to have a direct interface with the biomaterial or a bio-interface.

There are three isoforms of NCAM: NCAM180, NCAM140 and NCAM120. The name is dependent on the length of the cytoplasmic domain, for example NCAM180 has a cytoplasmic domain weighing 180 kDa. NCAM 140 is located in the growth cone and is typically associated with immature neurons (Persohn *et al*., 1989). In contrast NCAM180 is found at sites of cell to cell synaptic contacts in mature neurons. KYSFNY (KHIFSDDSSE)

is a peptide sequence made with FMOC chemistry which binds selectively to NCAM and prevents adhesion of cells (Rao *et al*., 1992).

KHIFSDDSSE is therefore the epitope for NCAM to NCAM binding. This peptide sequence has been used to functionalize materials in Kam *et al.* 2002 with silanized glass. The KHIFSDDSSE peptide enhanced the adhesion of astrocytes in both serum containing and serum free media. In Lu *et al*., 2006 very similar substrates were used which had the lowest surface coverage of neurons across the surface compared to other ligands such as IKVAV and a standard PLL surface. Boehler *et al*., 2012 produced a multi-array electrode to look at hippocampal neural networks *in vitro*. The authors were keen to look at the network in homeostatic conditions which were stimulated with drugs, so the hippocampal neurons were cell cultured with astrocytes. To get good attachment of the astrocytes in the non-electrode areas of the array and keep the reading neuron specific from the array, those areas where conjugated with KHIFSDDSSE. α2,8-linked sialic acid polymers have been used to culture rat Schwann cell and VM progenitors in Haile *et al*., 2007. A key advantage with the α2,8-linked sialic acid polymer surface was the ease of preparation, which was to just dissolve and leave overnight at room temperature. In serum containing media, the poly sialic surface compared well to the PLL control surface in measurements including cell numbers and viability. Collagen can be functionalised with poly(sialic acid) causing further extending axonal processes compared to normal collagen (Masand *et al*., 2012).

Cells have the relevent organelles to produce tissue patterning, so it is important that techniques utilize these. At this point it has been challanging to get neural cells to show the relevant patterning *in vitro*. If simple surface cues which stimulate the cells to pattern in physiologicaly relevant ways, then producing functional neural tissue *in vitro* will be an achievable goal.

1.3 Basic Science and Regenerative Medicine

The role of biomaterials in regenerative medicine of neurodegenerative diseases has been studied in fields such as tissue engineering, however clear applications have not been exploited. The section will include the principles, challenges in regenerative medicine and biological problems which have been solved using materials. Everything will be in reference to neuro regenerative medicine, so key principles such as tissue culture and differentiation will be highlighted along with successful material research and areas where better materials would have an impact.

Many tissues in the human body such as liver and skin have a strong ability to regenerate when damaged. Other tissues such as nerve cells and cardiac muscle cannot be restored to the same extent. With ageing populations where chronic disease is common, healthcare systems could breakdown; so a new paradigm of regenerative medicine is being developed, using cells to restore diseased or damaged tissue and cure chronic diseases which were previously only managed instead of cured.

Thus far cell therapies for neurodegenerative disease have been attempted in small scale pilot clinical trials. Material-based approaches have not been used with neurodegenerative diseases, but have been used in spinal-injury lesion animal models (Teng et al., 2002). Some functional recovery was seen when poly(lactic-co-glycolic acid) scaffolds seeded with neurons were implanted. The majority of translational projects have been purely cell based for instance, attempts have been made to treat Parkinson's disease with foetal neural grafts of cells directly dissected from foetal CNS tissue (Lindvall and Björklund, 2004). These foetal grafts have varied, from improving the disease progression reducing dependence on medications, to making the symptoms worse. A greater problem is that the cell source is scarce, and there is not enough foetal neural tissue to cover the demands of the patient population. In the long term cell therapies are

likely to have the most success in treating neurological disorders either as direct therapies to replace discrete cell populations, such as dopaminergic neurons which degrade in Parkinson's disease; or as an indirect means to deliver support factors, e.g. to treat auto-immune diseases such as multiple sclerosis.

1.4 Neurodegenerative Diseases

Key to a biomaterials success in treating neurodegenerative diseases will be the materials ability to cope with hallmarks of pathology in neurodegenerative diseases. In neurodegenerative diseases such as Alzheimer's the molecular basis is a spontaneous mutation causing the formation of Aβ amyloid (Selkoe, 2001). The Aβ amyloid aggregates and plaques causing death of sub-cortical neurons and lesion in the frontal cortex (Wenk, 2003). Similarly in Parkinson's disease dopaminergic neurons expressing the neurotransmitter dopamine are lost due to a mutation with α-synuclein which plaques to form lewy bodies in dopamine neurons (Leroy *et al*., 1998). Although the plaques are uqibquatinated for destruction the process fails due to inhibition of downstream enzymes (Shimura *et al*., 2001).

1.5 Stem Cells for Cell Therapies

To circumvent the need for large numbers of cells, stem cells will be used as a more scalable cell source for neural transplants. Using biomaterials in conjunction will lead to more control over stem cell transplants. Stem cells are found throughout the body and exist from development all the way through to adulthood. Stem cells are defined as cells possessing two main properties, self-renewal and the ability to become (differentiate into) other cell types depending on their potency.

Stem cells range from being:

I) Pluripotent – can differentiate into any cell type in the body

II) Multipotent – differentiate into multiple cell types but have a more restricted lineage, often forming cells of the tissue where they reside, *for example* neural stem cells

III) Unipotent/bipotent – make one or two cell types respectively

Stem cell therapies have been proposed to branch in two main forms:

Autologous: same donor and recipient. A personalized medicine that avoids immune rejection. This strategy will work best when there is a source of easily available adult stem cells that can either be re-programmed *in situ*: or removed from a patient, manipulated and returned in a transplant. If we are able to genetically re-programme cells, this will allow greater flexibility and produce a wide array of cell types that would be suitable for stem cell repair.

Allogeneic: Different donor and recipient. The advantage of using allogeneic stem cells is that these can be derived from more diverse sources than the patient, e.g. pluripotent embryonic stem cells. Close human leukocyte antigen (HLA) matching will be required for immune-compatibility, it is estimated that a cell bank of 150 embryonic stem cell lines would be required to cover 85% of the British population (Taylor *et al*. 2010).

1.5.1 Adult Stem Cells

Adult stem cells have been used extensively by clinical professionals. For example, stromal bone marrow and adipose tissue can provide a supply of mesenchymal stem cells (MSCs) which are multipotent. When a patient is given a bone marrow transplant for

leukaemia, the bone marrow stem cells replenish the recipient's supply of haematopoietic stem cells.

Adults possess a small pool of neural stem cells, with the potential to treat Parkinson's disease. However *in vitro* it is difficult to derive dopaminergic neurons from adult neural stem cells, also the cells are difficult to harvest. Through a process called trans-differentiation where a cell's lineage changes, dopaminergic neurons have been derived from bone marrow stem cells, which are more abundant and easier to access. The problem is that the cells express a lot of relevant markers but possess some non-characteristic phenotypes rendering these neurons medicinally unsuitable (Terada *et al*., 2002).

Due to the limitations progress has been slow for the last decade. Adult stems cells are clinically safest, but currently have a limited potential. The reason for safety in adult stem cells is because the cell fates are restricted, but expansion is limited because the cells will be limited on the potential number of replications. One problem is isolation of relevant cell types, secondly it is difficult to expand the cells into a large population for clinical use, and the biggest challenge is that the fates of the adult stem cells are often restricted.

1.5.2 Embryonic Stem Cells

Compared to adult stem cells, embryonic stem cells (ESCs) are pluripotent, i.e. they can form any cell type in the body. ESCs also show extensive self-renewal meaning large clonal populations can be produced. ESCs were first separated from mice in 1981 (Evans and Kaufman, 1981), human ESCs were isolated at the turn of the last millennium (Thomson *et al*., 1998). Human ESCs are derived from the inner cell mass of 6 day blastocysts from residual *in vitro* fertilisation (IVF) tissue. From a small population of ESCs

a limitless volume of cells could be produced; and be steered into many mature cell lineages with appropriate cues, meaning the potential to cure neurodegenerative disorders such as Parkinson's disease.

A major breakthrough was to differentiate pluripotent stem cells *in vitro* to neurons (Ying *et al*., 2003). The work shows a critical role for surfaces because gelatin at an early stage and laminin in the later stages were used different stages for lineage commitment. To achive therapeutic relevent populations the role of the surface was shown to be critical.

Some other challenges of working with ESCs have already been overcome to make the process more defined for clinical translation. Early problems such as karyotype abnormalities (incorrect numbers of chromosomes) have been avoided through stable culture protocols. Also, when human ESCs where first produced they had to be cultured on a feeder layer of irradiated cells (usually of non-human origin) or Matrigel® (containing extra cellular matrix proteins) to be maintained long-term. Now human ESCs can be cultured stably for long periods in a more defined environment using substrates such as recombinant laminin, and special plastics such as poly[2-(methacryloyloxy)ethyl dimethyl-(3-sulfopropyl)ammonium hydroxide] PDEMSAH (Villa-Diaz *et al*., 2010), reducing safety concerns when generating cells to be used in the clinic (Couture, n.d.). Similarly, ESCs tend to be cultured now with a defined knockout serum in the media, instead of undefined bovine serum, thus reducing safety concerns regarding animal/human pathogen transmission. It is critical to now get hESC systems to work in cost-effective ways, because billions of cells will be required in some of intended therapeutic interventions (Celiz et al., 2014). To produce 109 hESCs on peptides would cost over £10,000 while it be less than £1000 on synthetic surfaces. It is therefore critical to elimate the use of expensive reagents, and make cheap scalable surfaces.

1.5.3 Induced Pluripotent Stem Cells

Induced Pluripotent Stem Cells (iPSCs) have similar properties to ESCs but have none of the ethical problems because embryos are not essential. In 2006 pluripotent stem cells were derived from mature tissues through genetic reprogramming, these are labelled IPSCs (Takahashi and Yamanaka, 2006). iPSCs can potentially be derived from individual patients, therefore generating autologous cell types for transplantation.

Protocols to convert iPSCs to various types of differentiated cells emerged, showing that IPSCs can yield mature cell types *in vitro* just like ESCs. A number of research groups have now derived iPSCs successfully from Parkinson's patients and techniques have been developed to increase their safety (e.g. using excisable viruses for the genetic reprogramming and creating a more stable genetic profile, Soldner *et al*. 2009). In terms of efficiency it is possible to derive neural stem cells from mature tissues, thus omitting the naïve stages.

Safety concerns have been raised over about the four reprogramming factors, particularly the *c-Myc* gene because it is involved in cancer proliferation. However, more recent work suggests that iPSCs can be induced without using the *c-Myc* gene, and that reprogramming can be accomplished without DNA or viruses, instead using chemically modified proteins. These achievements have made the reprogramming process safer. Moving forward there are concerns that iPSC based terratomas are immunogenic compared to ESC based terratomas (Zhao *et al*., 2011). This is surprising because ESCs are not immunogenic until they differentiate, however this work shows that there is a new molecular basis for immunogenicity which will provide new targets for immune suppressants.

However there are key differences with ESCs, iPSCs have been found to be less efficient than ESCs in differentiating into neurons (Chin *et al*., 2009). A likely explanation

is because of genetic and epigenetic differences (Chin *et al*., 2009). Another concern raised is that iPSCs are not truly naïve like ESCs because they possess latent 'memories' of their original lineage; e.g. an iPSC derived from blood cells is more likely to turn into a haematopoietic cell. The expansion of iPSCs to achieve a large population is difficult and and time-consuming (months) which proves to be a big translational hurdle (Hanna *et al*., 2010). The relatively uncontrollable reprograming process leads to some of this difficulty (Hanna *et al*., 2009), with extra steps within the protocol necessary to remove remaining non-reprogrammed cells. This problem has recently be solved by depleting Mbd3 (an epigenic acetylase) which vastly increases the reprogramming and potency of iPSCs to produce stable populations quickly and efficiently (Rais *et al*., 2013).

The enhanced reprogramming efficiency of iPSCs would be benefical for drug response and disease modeling. iPSCs have been produced from sufferers of many diseases including: Duchenne muscular dystrophy, motor neuron disease, Parkinson's disease and Huntington's disease. A major finding from iPSCs generated from skin cells of a spinal muscular atrophy patient was that reprogrammed iPSCs differentiated into neurons that had the spinal muscular atrophy defects (Dimos *et al*., 2008). If neurodegenerative illnesses can be modelled more effectively these would provide accurate models which would be a valuable tool for the pharmaceutics industry and biotech companies, to test promising molecular candidates.

1.5.4 Neurons from pluripotent stem cells

Following the isolation and discovery of pluripotent stem cells various differentiation techniques have been devoloped. Dopamine neurons have been derived from embryonic stem cells using a variety of culture methods (Morizane *et al*., 2010)(Swistowski *et al*., 2010)(Yan *et al*., 2005). Effective methods include the use of co-

cultures to provide environmental cues, or the addition of known signalling molecules. To achieve the desired lineage using signal molecules the ESCs are cultured in the presence of various cytokines, mitogens, trophic factors or morphogens in a complex culture medium, to mimic the cells' natural environment.

The task of finding relevant signal molecules has become more efficient as a result of high-throughput gene and protein screening methods such as genetic micro-array technology and proteomic mass spectrometry. Our research group has utilised a mass spectrometry method to find new molecules to improve the differentiation of dopaminergic neurons from various stem cell sources (Orme *et al.*, 2010). Proteins were harvested from developing midbrain tissue and their expression patterns compared during neurogenesis. The key to finding the signal molecules was to characterise the midbrain developmental stages in rodent embryos, to identify precise regional development of the midbrain dopamine neurons and to target our search for specific protein signalling molecules by comparing their temporal expression. Thus we have identified novel and/or previously unidentified proteins that play key roles in dopaminergic differentiation.

Using genomic micro-arrays it is possible to look for gene products coding for intracellular signalling molecules. A team at the Karolinska Institutet using genomic micro-arrays found some key transcription factors for defining neural lineages (Panman *et al.*, 2011). Cells were isolated from differentiated cultures and compared with naïve ESCs for differences in gene expression.

However, identification is only the first step to achieving high yields of specific neuron subtypes from stem cells. A major challenge with developing optimal differentiation protocols is recreating the complex spatial and temporal signalling processes that are required to create specific cell types within organised three-

dimensional tissues and structures. Scaling the use of, and using these molecules effectively is an expensive task, will ultimately keep these as lab-based curiosities. The ecomonics and regulatory burden incurred through using these molecules mean that credible translational medical researchers should limit their use. However the pathways triggered by the molecules will remain a constant interest in regenerative medicine and drug research.

1.5.5 The Complexity of Stem Cell Differentiation

Cell therapies are made by differentiating the stem cells into disease specific populations. Currently one of the biggest challenges when using stem cells is to direct the differentiation of stem cells into mature cells (differentiation) with high efficiency and to create complex tissue structures which can replace diseased and damaged tissue. In terms of complexity some recent achievements might indicate that things are changing. Highly functional dopamine neurons have recently been derived from ESCs *in vitro,* following developmental principles (Kriks *et al*., 2011a). The key to the protocol was providing the cells with sequential media containing specific signal molecules that are up-regulated at different times in the development of dopamine neurons in the embryonic midbrain. With so many signal molecules, the key is to understand the dynamics of how stem cells experience signal molecules (i.e. the driving force of a system and its evolution during the process of development). The simplest dynamic is that different concentrations of signal molecules will push naïve stem cells down different lineages (**Figure** 1.5). Good examples are sonic hedgehog and WNT proteins that work in a concentration gradient during neural tube development (Ribes and Briscoe, 2009). BMP2 has been conjugated as gradient on to surfaces using streptavidin and BMP2 conjugated biotin (Lagunas et al., 2013)**.** The authors found that the gradient

caused changes in ALP activity, and cell density in the high BMP2 density areas. The creation of more complex spatial patterns such as stripes and spots can be described with Alan Turing's reaction/diffusion model, where activator and inhibitor signals spontaneously organize into binary patterns (Turing, 1952). Evidence has been shown in mouse folical spacing with WNT serving as the activator, and DKK being the inhibitor (Sick et al., 2006).

A big break-through in cell signalling biology was made by coupling mathematics and engineering methods in what is called 'systems biology'. Often biological signalling pathways in bulk analysis look 'noisy', however new systems biology methods show these pathways at a single cell level the activation of cells by the signals are heterogeneous (Cookson et al., 2005).

At the single cell level, some types signal molecules can elicit greater responses when delivered as a pulse rather than a steady dose (Ashall *et al*., 2009). Also heterogeneous cell responses can occur to the same stimuli through internal feedback loops within individual cells and interplay between neighbouring cells. Also the response of cells to these types of stimuli are digital, so part of a population will respond while other parts won't respond to the stimuli (Tay et al., 2010). These complex dynamics could be responsible for the lack of effectiveness in current differentiation protocols. There is a non-linearity to developmental systems and its modelling is likely to be important for future stem cell research. There are multiple opportunities to integrate computational methods in to stem cell science, for instance incorporating microfluidic designs to differentiation protocols. These advances will provide better understanding of cellular systems and improve the efficiency of stem cell differentiation, a crucial step for their translation towards clinical therapies.

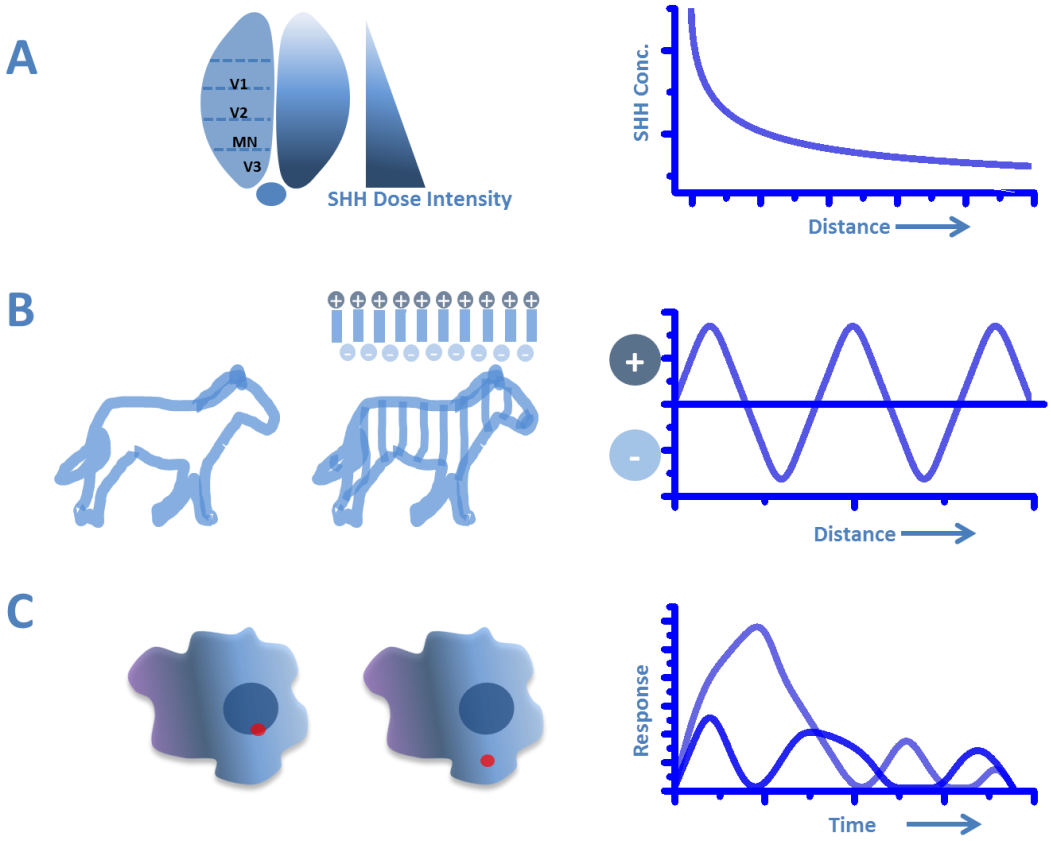

Figure 1.5 - Chemical morphogenesis. A) concencentration gradient of SHH which forms during brain devolopment. The gradient forms through diffusion, and the concentration of SHH gets weaker over distance causing cells to differentiate differently. B) reaction/diffusion explaining zebra stripes. Activator and inhibitor morphoghens spontateously organize forming elaborate natural patterns. Some cells become pigmentented because of the activator morphogen, and other cells are pigmentless because of the inhibitor morphogen. C) Pulsing. Cell's often have a heterogeneous response to stimuli, because frequency is an important signal parameter which is needs more consideration. The pulse is temporal, so complex infomation is encoded which is important for process where a varied and adaptable response is required.

1.5.6 Foetal Neural Stem Cells

The current strategies for clinical use of cell therapies to replace damaged tissue in neurodegenerative disease use foetal neural stem cells (FNSCs). A clear advantage to using FNSC is that differentiation is simpler to control. Dopamine (DA) neurons can be derived from FNSCs (Fricker-Gates and Gates, 2010). FNSCs are obtained from the developing central nervous system of mammalian embryos. Dissections of neural tissue contain a mixture of nervous cell types with sections of the tissue being isolated where particular subtypes predominate (Gage 2000). Transferring the dissected cells to media containing neurotrophic proliferation factors such as basic fibroblast growth factor (bFGF)

and epidermal growth factor (EGF) disallows cells from adhering to the tissue culture plastic (and therefore differentiating). This causes the formation of proliferating cell clusters termed *neurospheres* (Vescovi *et al*., 1993a). Reducing bFGF concentration causes the neurospheres to attach and differentiate. Additional additives can influence neurospheres to differentiate into DA neurons. Yu *et al.* cultured DA neurons from FNSCs (Yu *et al*., 2007). Heparin can be added to enhance differentiation to tyrosine hydroxylase (TH) expressing neurons; TH is the enzyme responsible for converting L-tyrosine to L-dopa, the first step in the biosynthesis of DA, and therefore is a marker of mature DA neurons. Heparin is known to cause neurite outgrowth (Lauri*et al*. 1998), and during development of the substantia nigra (SN) DA neurons lengthen their axons sending projections to their target structures: the caudate nucleus and putamen (collectively called the striatum) (Tepper, Damlama & Trent 1994). This inspired Tepper *et al;* they seeded neurospheres onto polylysine and laminin coatings with addition of βFGF, heparin and B27 media supplements; resulting in about 40% conversion to DA neurons when using heparin in combination with laminin (Tepper, Damlama & Trent 1994). Despite this enriched differentiation *in vitro*, when the expanded cells were implanted into a mouse model of PD they failed to engraft in the host tissue.

Recently Rosler and others have examined the use of sonic hedgehog (Shh) which is a morphogen, FGF8 and Wnt1 (external proliferation and differentiation factors) as soluble factors to induce DA neuron differentiation (Rössler *et al*., 2010) (Rossler, Boddeke & Copray 2010). Some of the neurospheres were engineered to over express *msx1* (a morphogenesis control gene). This mutation however was found to have little effect on conversion into DA neurons. However the addition of ventralization factors without the histone deacetylation inhibitor trichostatin A (TSA) did increase conversion. The authors claim about 40% conversion to dopaminergic precursors. The precursors

were characterised by the Pitx3 marker (a gene controlling morphogenesis), but these cells had a low expression of TH.

The effects of hypoxic (low oxygen surface tension, 3±2% O_2) culture conditions have also been explored for its effect on DA neuron differentiation (Studer *et al*., 2000). βFgF, vascular growth factor (VEGF) and erythropoietin (EPO) were added to the culture media. A higher cell count and increase in DA neuron yield was observed in hypoxic conditions compared to normal incubation (20% O_2). Liu *et al.* also examined the effects of hypoxia using a striatal cell conditioned media (SCM) (Liu *et al*., 2009). Under hypoxic conditions higher cell counts of neural and glial cell types was observed. Significantly more dopamine production was found when combining hypoxia and SCM compared to 20% O_2 and SCM. The authors argue that SCM was the main contributing factor in DA neuron production because more dopaminergic markers such as TH were found in populations differentiated under these conditions.

A big advantage to using FNSCs is transplantation into animal models (Kim, 2011). This is because FNSCs can only be differentiated into neural cells and often do not divide significantly following transplantation. Therefore patients are not exposed to the risk of teratoma which are tumours containing cell types from all three germ layers, these are caused by uncontrolled differentiation of rapidly dividing stem cells. Teratomas are usually used as an indicator for pluripotency as they are tumours that contain many types of differentiated cells. Unlike FNSCs, ESCs often retain their division potential when transplanted *in vivo*, which creates more risks because the cells may continue to divide post transplantation and give rise to tumours containing many different cell types. None of the approaches have exploited biomaterials meaning that the approaches can be improved with engineered surfaces which can make everything controllable. Conversely, the disadvantages of using FNSCs are their limited cell numbers and expansion capacity.

1.6 Key Lessons to Improve Biomaterial Design

1.6.1 Neurospheres

There are scalability problems with FNSCs, so neurospheres provide a way to improve scalability. The simplest way to culture neural stem cells is as neurospheres which are structured 3D multicellar floating structures. *In vitro* neural stem cells and progenitors are grown as neurospheres (Vescovi *et al*., 1993a). Attempts have been made to characterise murine neurospheres (Singec *et al*., 2006a). It is estimated that a neurosphere consists of 80% astrocytes, 17% neurons, and 1-3% oligodendrocytes. It is believed that neural stem cells make up about 0.16% of total cells within any neurosphere (Singec *et al*., 2006a). Some think that neurospheres contain different populations of neural stem cells (Tropepe *et al*., 1999). When E8.5 murine telencephalon cells were cultured with FGF2 or EGF different effects would occur. Only FGF responsive precursors exist in primitive stages, at low density FGF caused more proliferation and responses were differential. This information is irrelevant until cell divisions and passages are taken into account. Neurospheres do not necessarily contain neural stem cells, the important point about these spheroids is that they can only be reformed and passaged a few times (Kim and Morshead, 2003). Clonal neurospheres which derived from fluorescently sorted neural stem cells can be passaged for longer and also get uniformly smaller with each passage (Louis *et al*., 2008).

Glioblastoma tumourspheres (a 3D heterogeneous proliferating cluster, grown from gliablastoma biopsies) are structurally organised (Vik-Mo *et al*., 2011). In the tumourspheres, cancer stem cell markers were confined to the core, while cells expressing mature glia markers were located at the periphery. When neurospheres were produced from primary neural tissue the spheroid were structured (Lia S Campos *et al*., 2004). The neural stem cells markers (nestin and sox2) are found at the periphery

as are a majority of dividing cells. More mature markers such as Tuj1 and GFAP are found in the centre. Cells have also been shown to migrate within the spheres which has been shown with confocal microscopy that single fluorescently labelled neural precursor cells migrate within the neurosphere. This shows that although the spheroid is structured there are dynamics too (Wang *et al*., 2006). Adding further evidence is work done at Keele University. In the publication, neurospheres were transfected with green fluorescence protein (GFP) using magnetic nano particle vectors (Pickard *et al*., 2011). The distribution of GFP was not static to any area, therefore transfected cells were migrating throughout the spheroid.

Due to the merging of neurospheres (Singec *et al*., 2006a), clonality of the sphere population cannot be taken for granted as an experimental factor. Therefore efforts have been made to culture neurospheres from single cells (Cordey *et al*., 2008a). Single cells were taken and placed in PEG hydrogel microwell plates (r= 50 µm) and clonal neurospheres were generated. A problem with the technique is that attrition was high with a lot of cells unable to produce neurospheres. Neurospheres in culture are believed to be heterogeneous, one reason for this is because cells are in different stages of the cell cycle (Bez *et al*., 2003). Also it is thought that any cell in a neurosphere can create the other cell types within the neurosphere (Alvarez-Buylla *et al*., 2001). This point actually goes further because germ layers can be created from neural stem cells (Clarke *et al*., 2000a), demonstrating the engraftment of NSCs in to primitive embryos and later showing relevant germ layer markers.

Heterogeneity in neurosphere size has been addressed by using poly(methacrylate)(PMMA) microwells with a PEG surface, it has been shown that single rat neurosphere size can be controlled (Eiraku *et al*., 2008)(Sakai *et al*., 2010). A linear relationship was demonstrated between where neurosphere diameter and microwell

diameter. For example after 10 days of culture, a 200 µm microwell would restrict neurospheres to a diameter of 50 µm. An 800 µm microwell equated to a neurospheres with a greater diameter (225 µm).

1.6.2 Advanced Spheroid Culture Methodologies

The best demonstrations of organs made *in vitro* comes from work on spheroids cells self-organize and differentiate to produce tissue-like structures were natural physiological behaviour can be established through the relevent mosaic of cells. The first structure to be made from murine pluripotent stem cells was cortical neuron lamella spheroids from (Eiraku *et al*., 2008). The authors used a combination of FGF8b FGFR3-f BMP4 and Wnt3a and hydrophobic tissue culture plates to achieve neural aggregation. Spheroids were found to self-organized in to a recognizable lamella structure of a cortex with relevant markers in relevant positions and folds. The tissue displayed functional activity which was characterised with Ca imaging characteristic of neonatal cortical tissue showing large-scale very fast oscillatory Ca^{2+} waves over large distances. The same team produced a 3D optic cup following a similar approach (Eiraku *et al*., 2011). Stem cells were induced into a neural ectoderm spheroid which would organise and a rx+ zone would evaginate. The zone would then invaginate forming the optical structures of the eye. An a similar approach (Eiraku *et al*., 2008) has been used to create human derived cortical organoids from hESCs and IPSCs with an extra step with ECM embedding and bioreactor culture which makes the process more scalable (Lancaster *et al*., 2013). Some of the IPSC lines used were from sufferers of microcephaly (small brain disorder), the authors' observed premature differentiation in these organoids which is a characteristic of microcephaly. These recent accomplishments are achieved by paracrine

signalling and thermodynamic cell sorting within the spheroid, which shows minimal interventions, can produce excellent results when cells are left to recreate their niches.

Thermodynamic cell sorting was first described in the 1960's where a 3D spheroid will form when free energy of the liquid (cell culture media) overcomes free energy of a surface (hydrophobic surface) so aggregates form (Steinberg, 1963). If there are multiple cell types in the aggregates the populations sort out on the basis of different adhesion molecule having thermodynamic stability (like with like). This was demonstrated with an excellent experiment where two cell types were dyed and after aggregation sorting was observed (Foty and Steinberg, 2005). As this is a natural cell sorting mechanism mutations to cell adhesive molecules affects tissue organization shown in **Figure**1.6 (Kane *et al*., 2005).

Spheroid culture systems have a lot of biological advantages and these culture systems can be engineered. One concern of spheroids was heterogeneity of size (Reynolds and Rietze, 2005) this concern has legitimacy due to spatial dynamics changing in different sized spheroids with the same signalling molecules (Peerani *et al*., 2007). Indeed size maters with the cell fate of spheroids (Bauwens *et al*., 2011). Larger spheroids will take on a cardiac identity and smaller spheres have a more neural identity, because the proportion of endoderm/ectoderm changes. If shear induced phenotypic changes (Mammoto *et al*., 2011) are a concern, sphere size can be homogenized in static culture conditions (Ungrin *et al*., 2008). This was done in hydrophobic PDMS microwells and now morphogen eluting microparticles have been incorporated into these (Bratt-Leal *et al*., 2011) which has been shown to improve efficiency. pNIPAAm hydrogels have been used to produce substrates for controlling spheroid geometry which is thermally adjustable (Tekin *et al*., 2012). The authors produced a thermo-sensitive microwell which is interesting because interventions could

be made in off-target cell cultures. To make things more flexible it would be great to control spheroids with surfaces which can be incorporated into more experiments. Currently free-floating methods are used to culture spheroids, so if spheroids were adhered to the surface different culture techniques could be used. That would provide a way of getting the controllability of surface engineering to present specific motifs and functionality with the intricate self-organization of cells and populations within the spheroid cultures.

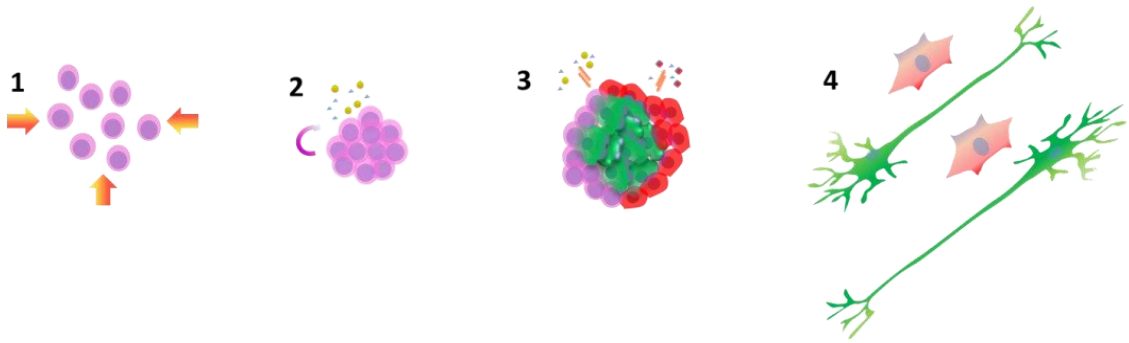

Figure1.6 –Steinberg's DAH in reference to neural stem cell culture: (1)Thermodynamics drive aggregation of NSCs (2) NSCs are sustained in neurospheres in bFgF media (3) Proliferation forms new cell types and thermodynamics causes sorting (4) Adhesion and differentiation neural stem cells and progenitors by removing bFgF and adding a 'sticky' laminin coated surface.

1.6.3 Niches

Stem cells have the innate ability to self-organize into proliferative and differentiating niches which combines different cell types, soluble and insoluble factors. A surface which provided cues to control these behaviours would eliminate the interventionism common in most current stem cell techniques. Lutolf & Hubbell, 2005 and Discher *et al*., 2009 make excellent points about complexity in these niches with factors never in isolation (because of signal cross-talk and impedance in pathways), and difficulty controlling all these factors simultaneously. Key publications have recently shown that ESCs can be used to produce dopamine neurons and chondrocytes (Kriks *et al*., 2011a) (Oldershaw *et al*., 2010). The work demonstrates that good 'functional' tissue can be derived from embryonic stem cells by niche mimicking, but these are extremely

tricky protocols utilizing numerous growth factors, morphoghens and ECM protein coated surfaces. The problem is that complexity means a lack of scalability, difficult to control, and not productive because of redundancy (Whitesides, 2013).

The niche provides stem cells with specific cues for survival, maintenance, proliferation and activation (Solozobova *et al*., 2012). These are rich in ECM, specific cell signals and paracrine signalling regimes (Scadden, 2006). These signals are very powerful which was shown by trans-differentiation of neural stem cells into less differentiated germ layer stem cells (Clarke *et al*., 2000a). The niche is multi-cellular entity with the cells sorted out into specific positions. The signalling in the niche is extremely complex with differences throughout. For example in the *Drosophila* ovary *glass bottom boat* which is similar to human BMP is found in cells in the outer sheath and is absent in cells found at the inner sheath (Song *et al*., 2004). SMAD which is a transcription factor associated with mesodermic differentiation in pluripotent stem cells (Lagna and Hemmati-Brivanlou, 1999) is inhibited by bone morphogenic protein (BMP) signalling (Xu *et al*., 2008). This is important for retaining pluripotency in embryonic stem cells. Niche signalling has dynamics with size dependent signalling gradients (Peerani *et al*., 2007). By inhibiting growth differentiation factor-3, BMP2 and Smad1 signalling the differentiation of the stem cells stopped. Controlling the embryoid bodies with Matrigel islands was effective at retaining the undifferentiated state. Size must therefore be considered an important factor with *in vitro* niches. Another dynamic is that transforming growth factor beta (TGFβ) signalling in embryonic stem cells inhibits cardiac differentiation, but when the TGFβ receptor degrades when the mesoderm forms the cells are unresponsive to TGFβ which is biphasic response (Willems *et al*., 2012). The most talked about dynamic in neural development is the shh ventral to dorsal signal gradient. The gradient is seen *in vivo* to cause proliferation of progenitors,

and can be partially recreated *in vitro* because a dose dependence can be seen in simple cell culture systems (Lai *et al*., 2003). More faithful recreations of the shh gradient have been made in microfluidic chips (Park *et al*., 2009). Another advantage of this set-up was that the gradient affects cell differentiation of the neural progenitors.

Signalling is also thought to be important in the organization and structure of the niche, because ephrin is important in tubule organization in kidneys (Ogawa *et al*., 2006). The ephrin receptor is richly expressed in structures such as medulla cortex nephron. Similar functions are fulfilled in cardiac tissue (Genet *et al*., 2012) in tissue organization. Ephrin signalling has been shown to have importance with gastric differentiation for the organisation of stem cells into more mature structures (Batlle *et al*., 2002). Crypt and villus cells interact without the intervention of ephrin. Ephrin-B1 knock-out mice displayed bad tissue organization and too much stiffness in cardiac tissue where elasticity is important. The signalling effects are very powerful where bone marrow stem cells can take on a neural lineage even though they have a separate germ layer lineage (Mezey *et al*., 2000). The process can work the other way with neural stem cells taking on a blood lineage when transplanted into bone marrow (Bjornson *et al*., 1999).

Adult neural stem cells have a distinct niche (Shen *et al*., 2004). Neural stem cells in the adult brain reside near endothethial vascular cells where the neural stem cells are maintained by the release of soluble factors from endothethial vascular cells triggering the Notch and Hes1 pathways in neural stem cells. In cortical and sub-ventricular N-cadherin (a calcium dependent neural cell/cell adhesion) triggers β-catenin which is retains neural progenitors (Zhang *et al*., 2010). This is a mechanism to allow cells to the progenitors to divide and organize, which was shown with knock-outs. In a histology paper the architecture of the neural stem cell niche in the ventricular zone was revealed

(Mirzadeh *et al*., 2008). It has 'pin-wheel' architecture with neural stem cells next to an ependymal cells with a blood vessel running on the basal process which the neural stem cells are adhered to. The extracellular niche and the adhesion molecules play a crucial role in the neural stem cell niche. In α6 integrin knock-out experiments would lead to abnormal development of the retina and cerebral cortex of mice (Georges-Labouesse *et al*., 1998). This was because lamination in those structures was poor. Knock-outs with small interfering RNA on the β1 integrin will prevent the adhesion of neural stem cells to fibronectin and reducing the cells sensitivity to EGF and βFGF (Suzuki *et al*., 2010). The β1 integrin can be blocked with galectin-1 which is glycoprotein (Sakaguchi *et al*., 2010), and highlights a mechanism to control neural stem cell adhesion. Another mechanism put forward for the balance of neural stem cells to neural progenitors is EGFR and Notch pathways (Aguirre *et al*., 2010). Where the EGF signalling would cause a doubling of neural stem cells. Interactions and changing the balance of between the two (Notch for neural stem cells division and EGFR for neural progenitor identity) caused changes in cell identity.

The niche is an obvious target to try and engineer with biomaterials by immobilizing ECM proteins and soluble signalling factors in precise configurations. The advantages of immobilizing the factors strong signal sources can be presented (Keung *et al*., 2010) and prevention of endocytosis which enhances and sustains the signalling factors activity (Tayalia and Mooney, 2009). FGF-2 has been covalently attached to nanofibrillar surfaces (Nur-E-Kamal *et al*., 2008). Showing higher potency than the soluble FGF-2, also having a longer half-life when attached to surface. Due to surface interactions the structure and function of the FGF was more stable. Experiments with a fibroblast cell line, showed increased biocompatibility. The covalently bonded FGF-2 was 100 times more effective at retaining cell viability. Leukaemia inhibitory factor (LIF),

maintains the pluripotency of mESCs (Williams *et al*., 1988), and is widely used in mESC culture protocols. One form of LIF is a non-diffusible form (Robertson *et al*., 1993) which associates with the extra cellular matrix. This type of LIF has been immobilized onto poly(octadecene-alt-maleic anhydride) (POMA) in (Alberti *et al*., 2008). The POMA immobilized LIF was effective for retaining pluripotency of ESCs. N-hydroxysuccinimide (NHS ester) is versatile for attaching proteins to surfaces NHS esters are commonly used molecules for bioconjugation in Yao *et al.* 2007 horseradish peroxidase and chicken immunoglobulin were attached to polymer brushes by utilizing NHS esters (Yao *et al*., 2008) which shows the NHS ester is used to attach proteins selectively. Alternatively, poly (carbonate urethane) (PCU) scaffolds can be used instead. The PCU scaffolds were grafted with acrylic acid using a copper catalyst (PCU-AA) (Dubey and Mequanint, 2011). The PCU-AA was next immersed in NHS to form PCU-AA-NHS Fibronectin. Fibronectin conjugation was assessed with bicinchoninic acid assay, this assay tells us about total protein levels. The conjugation method meant that a lot of the fibronectin stayed attached which leads to more cell attachment. So the method that Dubey and Mequanint document can be used to attach other proteins (Dubey and Mequanint, 2011).

As proteins are expressed at varying levels, it would be useful to have proteins immobilized in a concentration gradient. The concentration gradient for patern formation during morphogenasis based on diffussion was first put forward in the 1970s (Gierer and Meinhardt, 1972). Through conjugation materials can present a concentration gradient. bFGF has been successfully immobilized in gradients on poly(ethylene glycol) PEG hydrogels using NHS ester bonds (DeLong *et al*., 2005). The authors showed that cells would migrate in the direction of the gradient.

Using surface science it was shown that 440 nm distance between RGD ligands would cause cell spreading through the αvβ3 integrin, and a spacing of 140 nm would cause the cells to form stronger focal contacts (Massia and Hubbell., 1991). Fifteen years later Calalcanti-Adam *et al.* 2006 developed another method to specifically space RGD molecules on gold nanoparticle surfaces (Cavalcanti-Adam *et al*., 2006a). RGD is an integrin binding sequence. The authors found that spacing is a controllable factor with accurate spacing between the particles. It was demonstrated that a spacing of 58nm caused the most integrin clustering.

With heparin binding shh, neurotrophin-3 and pdgf have been attached to fibrin scaffolds (Willerth *et al*., 2008). The strategy was good at causing the proliferation of neural cell types, but controlling the fractions was hard. A new fabrication technique for biochemical gradient has been presented in (Jeon *et al*., 2013). The authors produced RGD gradients and dual TGFβ and BMP2 gradients which were made in a microparticle dual injection system. The authors achieved osteogenic following the BMP gradient but did not achieve the chrondrogenic differentiation in the opposite direction.

As ECM is a combination of proteins the most sensible way to probe interactions *in vitro* is as an array of combinations. A famous example of ECM arrays was shown in Flaim *et al*., 2005 where 32 different ECM combinations were assessed the impact on embryonic stem cells. Promising combinations were found, another advantage was because it was a spot array it driven hepatic differentiation through architecture. The role of ECM proteins on neural cell cultures are well established, however high throughput array methodologies might yield further incites because of the scale. On a PEG substrate with islands of NHS conjugated protein combinations for cell to attach. Combinations of laminin and jagged-1 were an effective combination for stimulating the notch reporter cell line which is for neural stem cell maintenance (Roccio *et al*., 2012). A

similar high throughput approach has shown that immobilized Jagged-1 was good at retaining neural stem cells, and bmp4 drive a glia differentiation of the stem cells (Soen *et al*., 2006). A recent approach is to combine the ECM arrays with different shapes (Solanki *et al*., 2010). By having laminin in different patterns the neuron numbers were affected. The fraction of neurons was increased in a grid morphology and the cells take-up the morphology which could lead to more applications. The ECM arrays are useful tool for finding key endogenous and exogenous signals are un-scalable (Kirouac and Zandstra, 2008). Therefore a key aim is to be able to g*et al*l the advantage ECM interactions without specifically using these expensive proteins.

The next step would be to produce a synthetic biomaterial causing cells to self organize into proliferative and differentiating niches. The optimum state would be to achieve niche engineering without using any exspensive reagents, so that would mean no highly purified or recombinant proteins. If the engineering was precise enough differentiating and proliferating niches could isolated to different parts of the same material. If that could be achived next generation high efficiency biotechnology production methods such as consolidated bioprocessing (Lynd et al., 2008) would be possible in cell therapy production. To achieve such methodologies in cell therapy production the philosophy of interventionism has to change, so more of the stem cell's natural abilities are utilized.

I – Aim

The aim of the work is to enhance the role of the surfaces in neuroscience and regenerative medicine. To accomplish that aim there were three critical steps:

1. Find the simplest biomaterial parameters/characteristic which when manipulated will causes changes in cell response.

2. Find the best way to present chemical characteristics on a biomaterial.

3. Vary the chemical characteristic on a single surface to direct changes in cell response simultaneously.

II Objectives

In the first experimental chapter the purpose of the work was to characterise and study the cell response of neurons to a range of interfaces. Currently the protocols to produce dopaminergic tissue for cell therapies are labour and resource intensive. Lower costs will take the cell therapy closer to clinical adoption. Cell-material interactions can be used to control cellular processes and behaviors in the place of expensive reagents. We investigated the responses of primary neural tissue derived from rat ventral mesencephalon (VM), interacting with a range of surface chemical functionalities and net molecular properties, because the most rational place to start in biomaterial design is at the material/biological interface. The different chemical functionalities were chosen because of their effects on the biological conditioning process. Six silane surfaces were tested against the PDL laminin coated gold-standard surfaces. The self-assembled silane monolayers presenting different head groups and net properties were fabricated on glass coverslips. Samples were fixed and stained to highlight Tuj1 (neuron), glial fibrillary acidic protein (GFAP is a glia marker) positive cells and 4', 6-diamidino-2-phenylindole (DAPI) as a nuclear stain. The neural cell responses were controlable using the different surface functionalities, because specific substrate

functionality leads to higher ratios of neurons, longer neurites and neurosphere spreading capacity. The primary amine functionalised surfaces caused a similar response to the PDL laminin surfaces in terms of adhession, spreading and maturation. All of these characteristics indicate a high neuro-regenerative capacity.

The second experimental chapter built on the success of the primary amine functionalised surfaces from the first experimental chapter. There was further scope to optimising the primary amine surface, because by adding further secondary amines the surfaces would have a closer resemblance to biological molecules. secondary amines feature in peptide bonds which are a major part of proteins. Therefore the interactions between the surface and proteins are can be more selective because specific motifs on the protein are targeted. In the material bio-design paradigm the role biological chemical functionalities have not been properly established. The advantages gained by following these principles would confront a key concern with the translation of protocols to produce of dopamine neurons to treat Parkinson's disease which is the use of ECM coated surfaces. Using a synthetic surface instead would be a major benefit for keeping costs down and simplifying the translational process because it remove xeno and/or recombinant proteins from the process. In this chapter the neurosphere response is compared between the primary and secondary amine surfaces. In the early stages of the experiment.

The third experimental chapter's purpose was to study a simultaneous neural cell on an amine gradient. Patterning plays an important organizational role in biology in terms of cell type localization in tissues and development. A key challenge of regenerative medicine is for cell differentiation protocols to incorporate patterning to improve on current protocols. Currently the best differentiation protocols use a myriad of soluble proteins which feature prominently in development, but the proteins are

expensive and have overlapping roles reducing process control. An orthogonal gradient was produced following a first principles approach to biomaterial design which controlled neural differentiation. The orthogonal gradient concentrated differentiated neurons and neural stem cells/progenitors (present in neurospheres) to different areas of the surface in the same media. Neurospheres size was controlled with the gradient providing new insights into the neural niche. The gradients surfaces allowed simultaneous culture of naive cells and mature cells without expensive reagents leading towards more productive and controllable tissue culture strategies.

Chapter II

2 Methods

2.1 Preparation of Functional Surfaces

The coverslips used were 13 mm coverslips (Thermo). The coverslips were left in 70% industrial methylated spirit for 24 hours minimum to remove dust and unwanted debris, and the slides were rinsed in isopropyl alcohol (IPA) and air dried immediately prior to use 5 functionalities (amine, hydroxyl, methyl, phenyl and thiol, as shown in **Figure** 2.1) were prepared by adding 5 mLs of toluene (Fisher, Epsom) to a glass vial, then adding 50 µL of silane to the vial which binds to the glass coverslips. 30 coverslips added to the vials individually. These were left for 24 hours; the coverslips acquire the functionality through a condensation reaction. The glass coverslips have hydroxyl groups at the surface, which is the bond site for the silane. The coverslips were finally rinsed in toluene and stored in a desicator until used. A range of surfaces functionalities were afforded included SH, CH, Ph, NH and OH in a single step process. The carboxylic acid functionality was prepared in a two-step process. First the coverslips were prepared with the amine functionality as described earlier, using aminosilane. After the rinse with toluene the coverslips were placed in a second vial which contained toluene plus 0.005 moles of dissolved succinic anhydride to form the carboxylic acid functionality through a condensation reaction, where the succinic anhydride reacts with the terminal amine to form a new carboxyl terminal group to the amine group. These were left for 24 hours then rinsed in toluene, the resultant coverslips were stored.

2.1.1 Self-assembled Monolayers Reaction Engineering

There are two seminal reviews on the kinetics and chemistry of self-assembled monolayers (Ulman, 1996) (Schwartz, 2001). The first stage of the reaction is that the silane molecules in the liquid phase are transported to the surface solid phase through diffusion and convection. The silanes next adsorb on to the surface following Langmuir type kinetics, the speed to which silane from the liquid phase absorbs on to the surface is limited by reaction sites on the surface and diffusion/convection of the silane. The silane molecules in terms of 'reactivity' are asymmetrical with very reactive ethoxy/halogen groups and a less reactive head-group. The ethoxy groups will react with glass because it is energetically more favourable, minimising Gibbs free energy of the system, Equation 1. bonds between the siloxane terminus and the glass surface are covalent, and drive the overall adsorption, with Van der Waals lateral interactions between neighbouring adhered silanes adding to energy efficient ordered state. Ethoxy on the silane reacts with hydroxyl on the glass surface in a condensation reaction to anchor the silane on to the glass. The packing occurs when more silane molecules absorb on to the surface and reaction sites on the glass get filled and a highly ordered covalent siloxane bond network.

$$\Delta \boldsymbol{G} = -\boldsymbol{T}\,\Delta \boldsymbol{S} \qquad \text{Eq(1)}$$

$\boldsymbol{\Delta G}$ is the change in Gibbs free energy
$\boldsymbol{T}$ is temperature
$\boldsymbol{\Delta S}$ is the entropy change

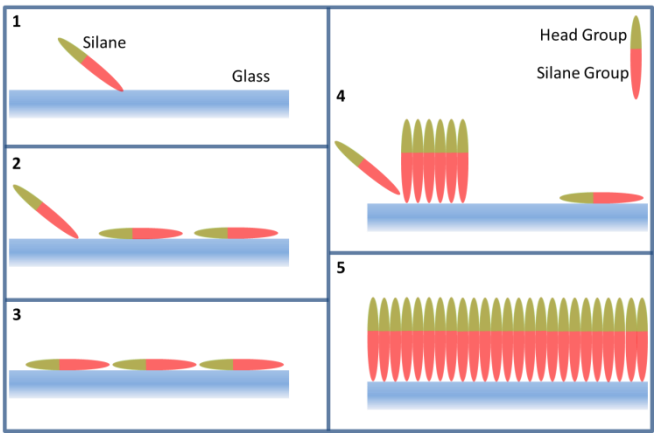

Figure 2.1 – Functional silane monolayers form on glass. 1+2 silane is adsorbed from the liquid phase to the glass surface in the solid phase. 3 silanes have a disordered conformation on the surface. 4 packing starts where an ordered covalent bond network begins to form. 5 closely packed functional monolayer.

2.2 Preparation of the NIPAAm Gradients

The polymerisation reaction to make the N-isopropylacrylamide (NIPAAm) polymer gradients is called atom-transfer radical-polymerization (ATRP) which was first described simultaneously in the 1990's by Toshinobu Higashimura's and Krzysztof Matyjaszewski's groups (Kato *et al.*, 1995) (Wang and Matyjaszewski, 1995). The kinetics of ATRP is well understood for different polymers (Matyjaszewski *et al.*, 1997) (Zhang *et al.*, 2001). The key aspects show that polymerization is a first order process with respect to initiator concentration, so the ATRP polymerization reaction is easy to control and terminate. There are more advantages to ATRP such as: polymer branching being easy to control, concise methodology only requiring widely available reagents and cheap apparatus (Patten and Matyjaszewski, 1998). Numerous polymer systems can be synthesized with properties that can be tailored for the task. Synthesis, polymers and functionalization is extensively reviewed in (Barbey *et al.*, 2009). A range of polar and non-polar solvents can be used providing environmentally friendly processes.

2.2.1 Reaction Engineering NIPAAm Gradients

The ATRP polymerization reactions works has four smaller reactions occurring: initiation, propagation, transfer and termination (Braunecker and Matyjaszewski, 2007).

Initiation

Initiation dissociation (radical formation from initiator)

$$I \xrightarrow{K_d} 2\mathrm{R}^{\bullet}$$

Eq(2a)

Initiation of polymerization

$$\mathrm{R}^{\bullet} + M \xrightarrow{K_i} M\mathrm{I}^{\bullet}$$

Eq(2b)

Propagation

$$M_i^{\bullet} + M \xrightarrow{K_p} M_{i+I}{}^{\bullet}$$

Eq(3)

Termination

$$M\mathrm{n}^{\bullet} + M\mathrm{m} \xrightarrow{K_{tc}} M_{n+m}$$

Eq(4)

The ATRP stages were adapted from a PhD thesis (Bergenudd., 2011). Eq(2a) is the radicalization of the surface bound initiator through the loss of bromine in our specific case. Eq(2b) is the initiation of the ATRP polymerization from monomers. Eq(3) represents the propagation of the polymer through the radicalized polymer or monomer combining with a non-radicalized polymer. Eq(3) is transfer the of radicals when it is independent of radicalized monomers or polymers. Eq(4) is the termination of the reaction. The use of a catalyst reduces the energy of activation through chemical co-ordination.

Radical polymerization (Rp) and degree of polymerization (DP_n) was adapted from (Braunecker and Matyjaszewski, 2007). Rp is a function of efficiency of polymerization initiation (*f*) and the rate constants (rate of a specific chemical reaction) of radical initiator decomposition (kd) which is the initial radical, propagation (kp) and termination (kt). Eq5 shows a the first order stage of the reaction where the initiation rate (kd) is a lot larger than the termination rate. When the reaction is in the zero order phase the initiation rate and termination rate are equal. Eq6 shows the degree of polymerization (Dp_n) when independent radical transfer does not have to be considered. The degree of ATRP polymerization is a reciprocal of the square root of radical initiator concentration, as shown in Eq6.

Radical Polymerization Rate

$$Rp = k_p[M\,](fk_d[I]_o/k_t)^{1/2}$$

Eq(5)

Degree of ATRP Polymerization

$$Dp_n = k_p[M\,](fk_d[I]_o k_t)^{-1/2}$$

Eq(6)

2.2.2 Orthoganal NIPAAm Gradients on Microscope Cover Slides

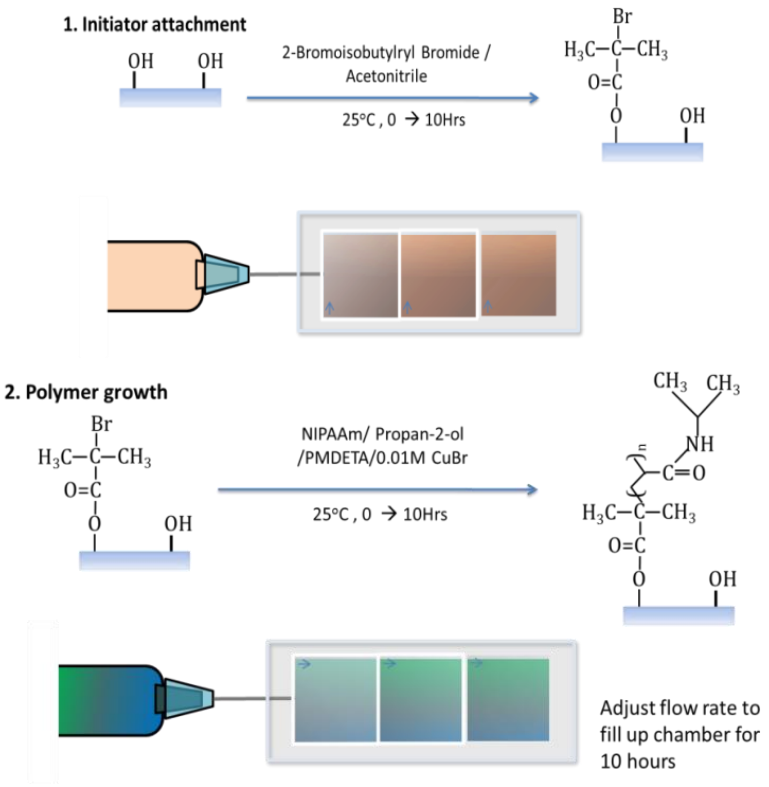

Figure 2.2 – NIPAAm gradients were prepared in two main stages. An initator gradient was made first. The slides were flipped round, and the chamber was gradually filled with polymer solution to produce the dual orthogonal gradient. The NIPAAm polymer brushes were formed a 'grafted from' reaction.

Figure 2.2 shows the preparation of the NIPAAm gradients. 18 mm * 18 mm square microscope coverslips (Fisher/Menzel Glaser) where immersed in Piranha etch solution 3:1 sulphuric acid: hydrogen peroxide (Sigma). The purpose was to clean the surfaces through oxidation with removal of organic matter and addition hydroxyl groups to the cover slide surface for ATRP. The oxidized cover slides were washed with distilled water to remove the piranha solution and washed with methanol to remove residual distilled water. The coverslips were scored with an arrow so the backside to indicate directionality of the intended gradients. The treated cover slides were stored in plastic Petri-dishes (Grenier) and sealed with parafilm, and placed in a desiccator to prevent long term condensation.

The mould for the ATRP was made out of PDMS. 45 mL of potting compound was mixed with 5 mL of bonding agent (Farnell) in a 50 mL disposable centrifuge vial (Dow-Corning). The PDMS was set for 5 days in a square Petri dish (Sarstedt). Once the PDMS was firmly set, it was removed and cut with a scalpel to the dimensions to hold six microscope slides (26X76mm) (Fisher). The reactor was cut with the dimensions of 17 mm * 53 mm which made space for three 18 mm * 18 mm square coverslips could fit where they sat on a slight lip to hold the coverslips. The reactor volume was roughly 3.6 mL. It was important to have the arrow on the outside of the reactor, and the arrow pointing upward. A 26 mm * 76 mm microscope slide was placed on the outside round the 18 mm * 18 mm square cover slides to create a seal and held together with bulldog clips, under constant pressure to ensure the seal was kept throughout the experiment

The chemistry and the fabrication method used to make the orthogonal gradients is adapted from (Wu *et al*., 2003) by combing ATRP and filling. A syringe needle was placed in the top of the reactor to allow the displacement. A polymer density gradient was made by having a seeding the surface with an initiator. Infilling the chamber with NIPAAm reactant soutuion, with a pre-ATRP initiator coated coverslip held in the chamber onto which the polymer could be grown from. A syringe was filled with 2% α-bromoisobutylryl bromide in acetonitrile. A needle was running out in to the reactor and the syringe was placed in a syringe pump, and the reactor was filled over a 9 hour period at 22˚C. The reaction was stopped by washing the samples in acetonitrile. The reaction works by one of the bromines on the from the α-bromoisobutylryl bromide dissociating and the remnant molecule bonding with silinols on the piranha etched microscope coverslip.

A NIPAAm polymer gradient was grafted on to the 2-bromoisobutylryl bromide initiator density gradient. The glass slides where flipped over to have an orthogonal gradient. NIPAAm, copper bromide and N,N,N',N'',N''-pentamethyldiethylenetriamine (Sigma) were dissolved in propan-2-ol (Fisher). The solution was sparged with nitrogen gas and stirred for 20 minutes to remove oxygen radicals. Once sparged the polymerization solution was taken into a 20 mL plastic syringe (BD sciences). A syringe needle was placed in the top of the reactor to allow the displacement, so inflow was a smooth process. A needle was running out in to the reactor from the syringe and the syringe was placed in a syringe pump (Hamiliton), and the reactor was filled over a 9 hour period at 22˚C. The filling process was done in a nitrogen atmosphere to prevent the loss of radicals which would halt the reaction. The ATRP polymerization of NIPAAm was stopped by washing the slides with propan-2-ol. The slides were stored until they were used. The reaction works by having the CuBr (catalyst) dissociate in the presence of N,N,N',N'',N''-pentamethyldiethylenetriamine (ligand) creating Cu ions that will catalyse the NIPAAm polymerisation. The NIPAAm polymerization reaction is initiated by the NIPAAm monomer bonding to the α-bromoisobutylryl bromide (initiator) anchored to the surface. The bonded NIPAAm monomers are radicalized so polymer brushes can be propagated.

2.3 Surface Characterisation

2.3.1 Water Contact Angle (WCA) Measurements

WCA is a measure of chemical polarity at the biomaterial surface interface. WCA will affect the protein conditioning process meaning some proteins controlling cell adhesion or signalling will bind differently. The measure was made by adding water (polar solvent) droplets to a surface; and depending on the interfacial polarity the droplet will either maximise it's exposure (hydrophilic), or minimise it's exposure (hydrophobic). Hydrophobic materials attract proteins such as c3 fibronectin and vitronectin. Hydrophilic surfaces attract proteins like albumin.

In the method a droplet of water is added to a surface and the spread of the droplet is assessed. If the water droplet has a low angle (0-30˚) the surface is hydrophobic, if the droplet has a low contact angle the surface is hydrophilic (>90˚).

50 mLs of Ultra-pure water (Millipore, Watford) was collected. The NI-IMAQ camera was put into focus; 5 µL of the water was added to the coverslip with a Hamilton syringe. 20 droplets were placed and imaged on the gradient surface with the varying wettabilies recorded. Using Measurements & Automation software (National Instruments corp), pictures of the droplet are taken. This was repeated five times. The contact angles were measured with Imagej (http://rsbweb.nih.gov/ij/) using the LB-ADSA plugin (http://WWW.epfl.ch/demo/dropanalysis/). Water droplets images were taken from immediately after addition to the surface. Individual drops were imaged across each of the surfaces produced, taking a mean average of at least 3 drops.

2.3.2 Fourier Transform Infrared Attenuated Total Reflectance (FTIR-ATR)

FTIR-ATR (Nicolet instruments, ThermoSpectroscopy Cambridge) was performed. Infrared spectroscopy is a technique where a sample is subjected to various wavelengths of infrared energy. Chemical bonds are characterised as a vibrational energy, so if the sample receives the corresponding wavelength of infrared energy, the IR will resonate with bond energy resulting in adsorption. The absorbed wavelengths are attenuated (loss of intensity) by the absorption process, which is detected. The following step is for a Fourier transform algorithm to transforms the time based function into a frequency based function which is relevant to chemical bonds (because a bond vibration is a frequency). The spectra which is analysed has to be coherent which is a signal processing principle about the relationships and differences between signals. In FTIR-ATR it would be about the difference in the input/output signals.

Background measurements of air were run for every sample to eliminate spectral noise arising from vibrational atmospheric water bands. Samples were handled with needle tip forceps (Squires Tools) and placed on the measurement stage. Samples were analysed on a thermo scientific is 50 fitted with a germanium single bounce ATR. An air background was taken immediately prior to each sample, with 124 scans being averaged at a resolution of 4 cm^{-1}. Data was collected using Omnic v9, being exported as CSV for data analysis within Originlab v9.

2.3.3 X-Ray Photoelectron Spectroscopy (XPS)

XPS provides a technique to look at the elemental composition, film depth and the electronic state of a surface. XPS does not require any sample preparation, and is done under vacuum because of the sensitivity of the method. The main principle of XPS is that a sample is irradiated with monochromatic beam of x-rays which causes excitation of the chemicals on the surface which causes a release of photoelectrons (K_e). From the number of electrons and kinetics the chemical composition can be elucidated. K_e is unique for atoms and their various states (Ratner *et al*., 1993). The surfaces are excited with xrays.

XPS has a penetration depth of roughly 100 Å (Ratner *et al*., 1993), and in polymers the depth is lower at 30Å. Dependant on the energy used and x ray angle of incidence. The inelastic mean free paths of photoelectrons in the material are limited, thus emitted photoelectrons cannot escape the material beyond that depth, making XPS a surface specific technique. For samples with heterogeneous coverage angle resolved XPS works best because it shows the different intensities of the photoelectrons at different emission angles.

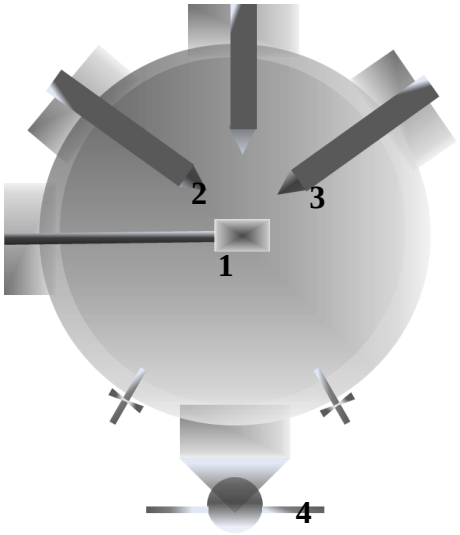

Figure 2.3 – Schematic of an XPS rig. The sample is placed on a stage where it is exited at an angle to get depth penetration of the sample. The measurements are made under vacuum to get accuracy from the detector. 1 sample deck. 2 excitation probe. 3 measuring probe. 4 vacuum pump.

The XPS surface analysis was performed using the Theta Probe instrument equipped with a monochromated AlKα source (Thermo Scientific) which was the excitation source in the national EPSRC XPS user's service (NEXUS) facility at Newcastle University. A pass energy of 200 eV (which works like a high-pass filter where electrons under a certain energy are filtered out) and a step size of 1.0 eV was employed for all survey spectra while a pass energy of 40 eV and a step size of 0.1 eV was used for high resolution spectra of the elements of interest. A flood gun was used for charge compensation which was used to cope with electron loss from the sample.

The gradient was measured at 25 different regions across the gradient surface in a five by five grid, allowing data on element composition and to verify that the chemicals were properly covalently bonded to the surface. Amine content was analysed via the N1S band along with C1S for carbon units (Table 3).

A pass energy of 200 eV and a step size of 1.0 eV was employed for all survey spectra while a pass energy of 40 eV and a step size of 0.1 eV was used for high resolution spectra of the elements of interest. A flood gun was used for charge

compensation. Data acquired was analyzed using CasaXPS software. pKa of surface presented molecules was calculated from structural information using ACDlabs software v12.

Table 3 – Relevent XPS element energies

Energy / eV	Element	Level
69	Br	3d
168	S	2p
284	C	1s
399	N	1s
532	O	1s

2.4 Cell Culture On Silane Surfaces

2.4.1 Cell Culture Functional Surface Studies

To better model the neurons affected in Parkinson's disease primary midbrain neurons were dissected from E12 rats. Primary VM tissue was used because it contains a diverse and natural cell population of purely neural cell types. A benefit of using rat tissue is the similarity to human neurospheres (Reynolds and Weiss, 1996), without the trouble of producing high quality neurons from stem cells. Rats gestate for 22 days (E0-E21), so E12 midbrain dissections were selected because classic radiolabelling experiments show that the first dopamine neurons emerge around E12 (Altman and Bayer, 1981).

Tissue used in the experiments was from E12 Sprague Dawley rat embryos in accordance to UK Home Office animal's act 1986. Pregnant rats on the first day form a vaginal plug, these are designated 'E0'. At E12 (12 days after a plug was spotted) the pregnant rat was sacrificed following schedule 1 guidelines. An incision was made in the abdomen using scissors, the uterine horn was removed, and embryos were removed and placed in cold (4˚C) dissection media, listed in appendix 11. The embryos were removed from sacs, under a dissection microscope (Leica UK); ventral mesencephalon (VM) tissue was removed. The method was to first make a 'V' shaped cut at the top of the embryo's brain to remove the midbrain as shown in **Figure** 2.4. The next step was to cut along the top to unfold the tube-like structure. The resultant pieces usually resembled a butterfly, from that the VM was removed (the central part), the process is shown in **Figure** 2.5.

VM dissection tissue was placed in 0.1% trypsin in Hanks balanced salt solution (Worthington Biomedical Corp) for 30 minutes at 37˚C to dissociate the structure. A pellet formed through natural sedimentation, after supernatant aspiration the pellet was washed three times with 200 µL of 0.05% DNase in dissection medium (Worthington Biomedical Corp.) to digest extracellular nucleic acid released by lysed cells, the structures were dissociated mechanically with a pipette. On the third wash, the pellet was centrifuged at 700 RPM for 5 minutes.

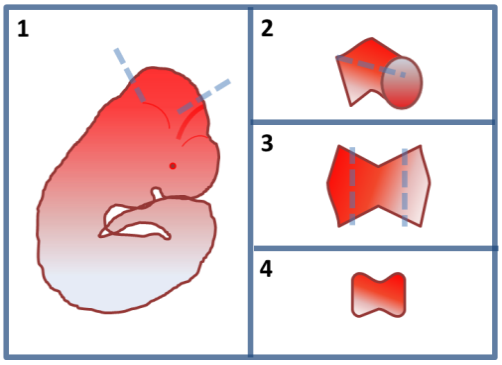

Figure 2.4 – Dissection of the developing midbrain from E12 rat embryos. 1 Neural tube removal. 2 Opening of the neural tube. 3 isolation of developing midbrain. 4 Tissue which produces neurospheres.

2.4.2 Neurosphere Culture

To derive neural stem cells and progenitors for experiments neurospheres were cultured. To quench proteolytic activity of any residual and trypsin, following centrifugation, the DNase was aspirated and the pellet was re-suspended in 1 mL of NPC media (Appendix 11). Cell counts were performed with a haemocytometer and T25 flasks (Greenier Bio-One) were seeded with one million cells/ mL. Once seeded 7 mLs of NPC media was added, NPC contains bFGF which causes formation neurospheres which grow because of proliferation; these were incubated at 5% CO_2 and 37˚C. After 24 hours a further 3 mLs of NPC was added. Every 48 hours fresh NPC media was added to replace old media which was aspirated. The T25 flask was placed

upright and left for five minutes; this caused sedimentation of the neurospheres, preventing accidental removal. To avoid excess media 2 mLs of NPC was removed, and then 2 mLs of fresh NPC media was added to the T25.

2.4.3 Neurosphere Passage

Smaller neurospheres were used for various reasons including: increased supply of food, more uniformed spheres, and making the microculture technique and analysis easier. In normal cell culture passaging is the process where cells are detached and transferred to fresh media. In the context of neurospheres; passaging is the process of splitting up the spheres into single cells and transferring them to fresh media.

Neurospheres were passaged after 7 days in culture. The neurospheres plus NPC media were taken from the T25 and centrifuged at 700 RPM for five minutes to create a pellet. The NPC was aspirated off and the neurospheres pellet was re-suspended in 0.5 mLs of fresh NPC. This was transferred to a 1 mL Eppendorf tube (Eppendorf UK, Cambridge). The neurospheres were dissociated mechanically into single cells using a pipette. The single cell solution was transferred to a fresh T25 with 7 mL of NPC to provide a high yield of neurospheres. The T25 was incubated (37˚C, 5% CO_2) for three days to facilitate division and the formation of smaller neurospheres.

2.4.4 Neurospheres Microculture

Microculture is a method to miniaturize cell culture experiments. The primary advantage is being able to test a lot of experimental conditions with limited biological

material, usually cells and proteins. The microculture ensures that the neurospheres adhere to the various glass coverslips and not the well plate, before the well is filled with media. Micro-culturing was performed on all surfaces which is depicted in **Figure** 2.5.

The P2 neurospheres were taken from the T25 and centrifuged down at 700 RPM for 5 minutes. The supernatant NPC was aspirated off, and the neurospheres pellet was re-suspended in 1 mL culture media (Appendix 11). Neurosphere counts were performed using a haemocytometer. A stock solution of neurospheres and culture media was made to provide 30 µL micro-cultures containing 200 neurospheres; in the method the microculture solution was continuously rocked manually during seeding to prevent settling of the neurospheres. 30 µL was pipetted into the centre of a surface within each well in a 24 well-plate (six of each surfaces was seeded). The coverslips were incubated at 5% CO_2 and 37˚C overnight, next morning 0.5 mL of culture media was added to every well. Every 48 hours afterward 0.5 mLs of culture media was added to each well.

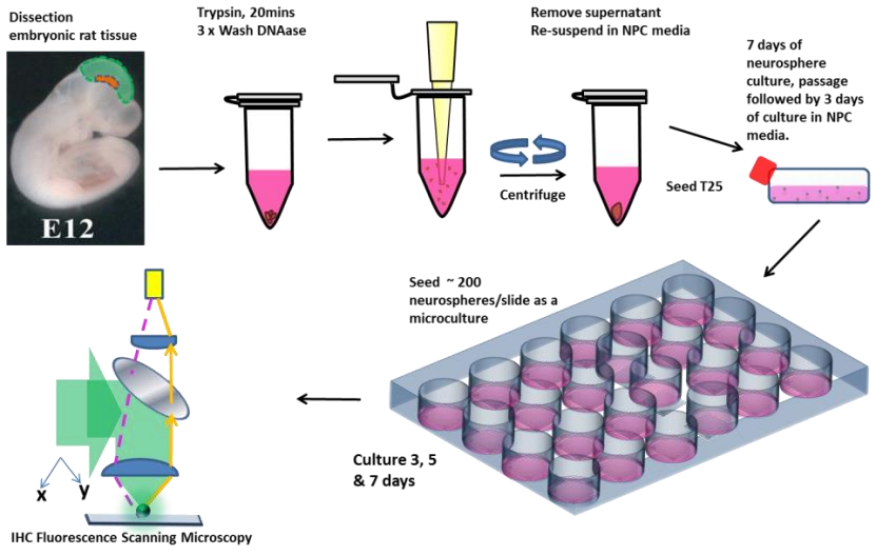

Figure 2.5 – Workflow for cell culture in all the functional monolayer surface work. First there was dissection, then neurosphere culture, experimental cell culture and analysis.

2.5 Cell Culture Gradients

Cortical neurons were chosen for these studies because cortical neural progenitors and neural stem cells can be sourced from this area over a long period. At E8 50% of the cells in the developing CNS are neural stem cells (Kalyani *et al*., 1997). The population of neural stem cells fall to 1% on P1 (Kalyani *et al*., 1997). Neurospheres have been derived E14 rat neurons in EGF media stem cell media (Reynolds *et al*., 1992). The neurogenesis of cortex of rats continues for 15 days post natal, which was shown with thymidine-H^3 radio labelling (Altman and Das, 1965).

2.5.1 Primary Rat Cortical Neurons

Primary rat frontal cortical tissue was removed from timed pregnant Sprague Dawley on the 16th day of gestation (E16). The pregnant rat was sacrificed in accordance to Home Office standards (schedule 1). An incision was made in the abdomen using sterile standard scissors, the uterine horns were removed. Using needle tip forceps the embryos were removed from the ovules placed in cold (~4˚C) dissection media. The following dissection steps are carried out using a dissection microscope (Leica UK). Heads were removed from the bodies, so the developing brain could be removed with needle tip forceps. Next the meninges are peeled with needle tip forceps which exposes the frontal cortex that was cut out with fine surgical scissors (Fine Scientific Tools). The dissected cortical pieces where digested to form single cells with 0.1% trypsin in DMEM for 30 minutes at 37˚C. A pellet formed through natural sedimentation and the trypsin solution is aspirated away from the pellet which was washed three times with 200 µL of 0.05% DNase in dissection medium (Worthington Biomedical Corp.) to digest extracellular nucleic acid released by lysed cells making the

solution less viscous. Once the DNase is aspirated the cells and washed with media, centrifuged for 3 minutes at 700 RPM and aspirated to remove any residual enzyme. The cell pellet is suspended in media and mechanically dissociated to get single cells.

2.5.2 Seeding the NiPAAm Gradients with Primary Cortical Rat Neurons

From the dissected pieces cell counts are performed to calculate the cell number. The cell solution is diluted with culture media to get 100,000 cells/ mL. **Figure** 2.6 shows the cell culture workflow on the NIPAAm gradients. The NIPAAm gradients are placed in a 6 well plate (Greiner) and stuck down with silica grease (RS components). The gradients are drawn round with a PAP pen (Dako) to confine the micro-culture. 0.7 mL of cell culture media solution is pipetted on to the gradient and the droplet is spread around the gradient surface to provide homogenous coverage. The coverslips were incubated at 5% CO_2 at 37˚C overnight, and the wells were flooded with culture media and incubated to the 4 day time point.

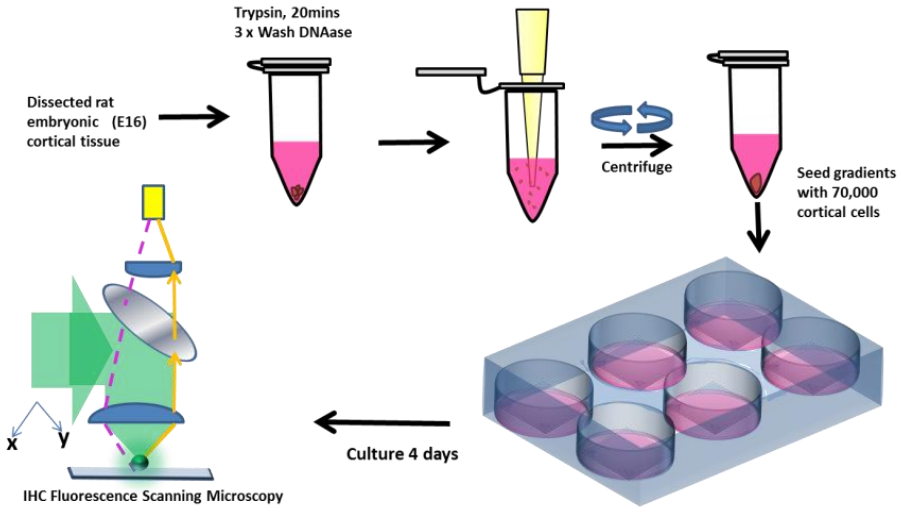

Figure 2.6 – Workflow for gradient cell culture. What the work flow shows is a simplification of the earlier workflow in **Figure**2.5.

2.5.3 Neurospheres

To provide a comparison to show the extent of tissue sorting in the gradient surfaces neural spheroids (neurospheres) that retain the neural stem cells free floating neurospheres were compared to gradient neurospheres. Single rat cortical neurons were prepared as described previously cell counts were performed with a haemocytometer and T25 flasks (Greenier Bio-One) were seeded with one million cells/ mL. Once seeded 7 mLs of NPC media was added, NPC contains bFGF (stem cell mitogen) which causes formation and proliferation of neurospheres that serve as the *in vitro* niche for neural stem cells (Vescovi *et al*., 1993b); these were incubated at 5% CO_2 and 37˚C. After 24 hours a further 3 mLs of NPC was added. Every 48 hours fresh NPC media was added. The T25 flask was placed upright and left for five minutes causing sedimentation of neurospheres which prevented accidental removal. To avoid excess media 2 mLs of NPC was removed, and then 2 mLs of fresh NPC media was added to the T25.

2.6 Fixing and Immunohistochemistry (IHC)

IHC provides a technique of exposing cellular antigens meaning cell types can be identified. The principle is simple: a primary antibody (*e.g.* murine β-III-tubulin) attaches to an epitope on a cell structure. Next a secondary (e.g. goat anti-mouse) is added which contains a fluorophore. The fluorophore is important because it is excited by fluorescent light which can be viewed with fluorescent microscopy, therefore cells positive for the specific antigen will fluoresce.

At the 4 day time-point cells were fixed for IHC. First media was removed from the wells and cells immobilized/fixed in 3 mL of 4% paraformaldehyde (PFA) solution

for 15 minutes in a water bath at 37˚c to stop the cells detaching. After a wash with tris buffer solution (TBS) the wells were inspected for the presence of cells under a standard upright lab microscope. Three out of six wells were selected for staining; non-specific binding sites on the cells were blocked by serum with 2 mLs of 5% goat serum block solution for 1 hour at 4˚C. After a wash with TBS 2 mLs of primary antibody solution containing β-III-tubulin (neural marker 1 in 500 dilution) and GFAP (glial marker 1 in 1000 dilution) antibodies to show cells with mature neural phenotypes. SOX2 (1 in 1000 dilution) and nestin (1 in 300 dilution) primary antibodies were added to stain for neural stem cells and progenitors. The samples were incubated with primary antibody solutions overnight at 4˚C. Following a TBS wash step a secondary antibody solution containing the FITC and TRITC fluorophore tagged antibodies (Cheshire Sciences) were added. Which were left in a dark place for two hours. The cells were washed one final time in TBS. The samples were mounted on microscope slides with hard-set DAPI mounting media (Vector Labs). The DAPI is a fluorescent dye that binds to nuclear material within the nucleus.

2.7 Microscopy

2.7.1 Bright-field Microscopy

Phase contrast bright-field is a simple form of microscopy where the refractive differences between materials where some light is retarded which creates an effect that the objects are out of phase making contrast greater. This is done with specialist objective lenses or phase plates which focuses on the specimen and retards the scattered light.

Bright-field colour images of the cells on the gradients were taken so neurosphere size and location can be recorded. Samples were viewed with an automated scanning XY stage Nikon Ti microscope (Nikon Instruments Europe). Images were taken using a 10X phase contrast objective lens with a split colour/monochrome ICCD DS-Qi1 CCD camera (Nikon Instruments Europe). Images were saved as meta files in the ND2 format and opened in ImageJ using ND2 reader plugin (http://rsbweb.nih.gov/ij/plugins/nd2-reader.htML) and resaved as TIFF metadata encode image files. The images were split into 25 images using a custom Python script written by at Keele University by Dr Paul Roach.

2.7.2 Epi-Fluorescence Microscopy

Fluorescence microscopy works on a simple principle that is when a flurophore conjugated antibody or fluorescent dye is exited at one wavelength it emits at another. High intensity light is split into fluorescent light wavelengths with a florescence filter. The excitation fluorescent light makes its first pass through the dichromic filter which lets light of one wavelength through and light of another wavelength out. On the Nikon Ti microscope the dichromic filter and fluorescence filter are consolidated into a unit called a filter block.

The florescent light goes through the object and is focussed on to the sample which excites stains on the sample causing a fluorescent emission. The emitted light goes through the objective lens which also magnifies the sample, and then through the dichromic mirror. In a phase contrast system the goes through a phase plate to heighted the contrast between the contrast between materials. The emission is detected by an ICCD camera (intensified charged coupled device) to provide an image.

Fluorescence images of the neurons on the gradients were made to assess attachment, migration and differentiation. The cells were viewed with an automated scanning XY stage epi-fluorescence Nikon Ti microscope (Nikon Instruments Europe). Images were taken using a 20X phase contrast objective lens with a split colour/monochrome ICCD DS-Qi1 CCD camera (Nikon Instruments Europe). Pictures were taken under three filters listed in Table 4 second of exposure was used for DAPI images 15 seconds of exposure was used for the FITC and TRITC images. All images were acquired with 1X gain.

Table 4 – Excitation and emission wavelengths of the filters from fluorescence microscopy in the experiments.

Filter	Excitation Wavelength	Emission Wavelength and Colour	Colour
DAPI	358 nm	461 nm	Blue
FITC	488 nm	518 nm	Green
TRITC	541 nm	572 nm	Red

Images were stitched together with 5% overlap using NIS Elements advanced research version 3.2.1 (Nikon Instruments Europe).

Image measurements and analysis were performed with a combination of ImageJ (http://rsbweb.nih.gov/ij/) and NIS elements advanced research version 3.2.1 (Nikon Instruments Europe). After cropping and rotating a 5X5 grid is placed over the image. The biological responses assessed were: glia and neuron migration, glia and neuron lengths, neurosphere areas. Data was imported into excel for validation and manipulation, using Origin v9 for statistical analysis and further presentation of data

2.7.3 Single Photon Confocal Microscopy

Imaging 3D samples is very challenging and expensive specialist imaging equipment has to be used to image the sample. Confocal laser scanning microscopy (CLSM) is used for 3D imaging and is popular because of the sectioning in the images

which provides high quality depth profiling. The concept is that high intensity laser light is aimed into precise areas of the sample with scanning mirrors, and motorized sample stages. Only focused emitted light gets to the detector because of a pinhole aperture, because normal fluorescent microscopy will let unfocussed light through which means lesser quality of the sectioning and the illumination of the sample is not as powerful which makes imaging the insides of the sample very hard. The focused emission is measured and collected with a photon multiplier tube which can detect low light intensities. Confocal microscopes comes in various forms shown in **Figure** 2.7 with different advantages and disadvantages which are listed in Table 5.

Table 5 – Advantages and disadvantages of different methods of confocal microscopy

Type	**How it works**	**Advantage**	**Disadvantage**
Single photon confocal laser scanning microscopy	With a combination of excitory lasers and a motorized stage, the ROI is scanned. The sectioning quality of the z stack is a result of the confocal aperture.	Sectioning quality Flexibility with lasers, filters and samples Ubiquity and innovation	Slow image acquisition (not optimal for live cell experiments)
Multiphoton photon confocal laser scanning microscopy	Two low intensity infrared photons (penetrates further than visible light) cause emission of one photon from the stain which is detected. The section quality is a result of the highly localized excitation.	Highest penetration depth Excellent *point of spread* function	Limited to red and green detection Slow scan speed Un-flexible
Spinning disk confocal microscopy	Instead of scanning mirrors there is a spinning disk with apertures which excites multiple parts of the sample. There is a second spinning disk with the confocal apertures which lets focussed emissions on to a high quantum efficiency ICCD camera. The system requires sophisticated controllers and computers to make images.	Fast image acquisition, so it is brilliant for live cell experiments	Lower robustness due to moving parts Lesser sectioning quality

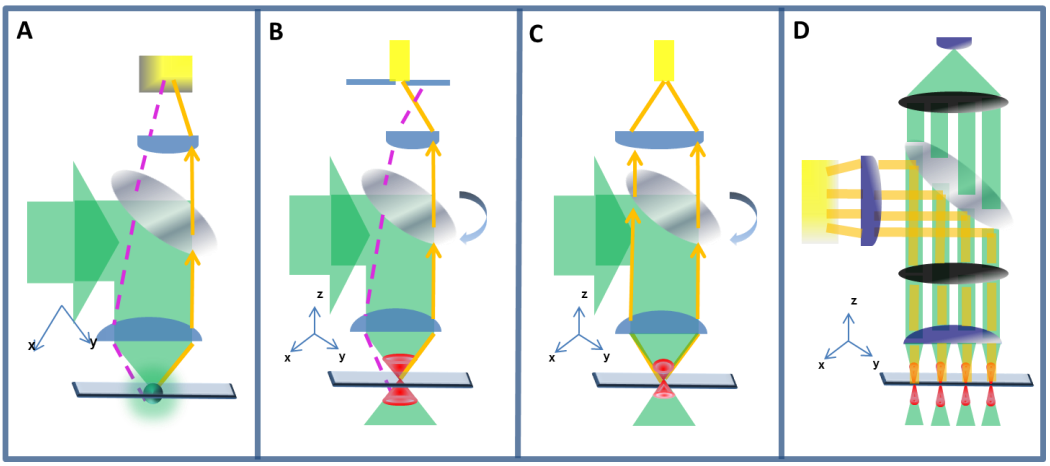

Figure2.7 – Different schematics of fluorescent microscopy. Orange arrows are focused emissions, and purple dotted lines are unfocused emissions. A standard epi-fluorescence microscopy. B single photon confocal microscopy. C multi-photon confocal microscopy. D spinning-disk confocal microscopy.

To demonstrate cell sorting within neurospheres according Malcolm Steinberg's differential adhesion hypothesis single photon confocal microscopy was performed on parts of the gradient samples and whole neurospheres fixed neurospheres using a Olympus FluoView FV1200 confocal laser scanning microscope. Samples were imaged with multiline argon lasers at (453/488/515 nm). Signals from the samples are picked-up with photon multiplier tube GaAsP detector unit. Images were taken with a UPLSAPO40XS 40x oil immersion objective to verify the localization of markers to a cell. The images were taken in the XYZ axis to inform on sample depth and encompass whole neurospheres in one image because whole neurospheres can not be imaged in one field of view, because a neurosphere spreads across multiple Z steps.

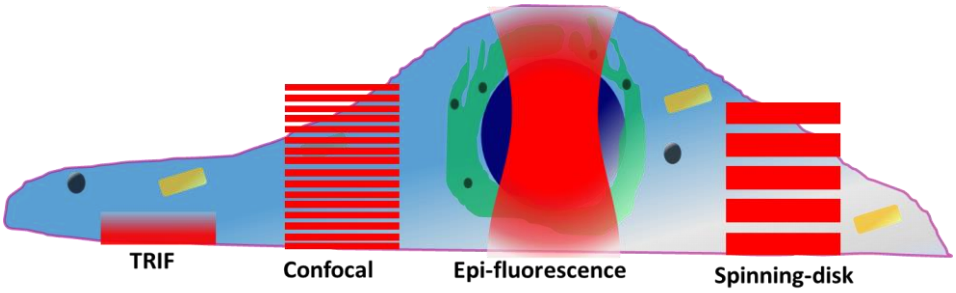

Figure 2.8 – Different resolutions and sectioning qaulity of microscopy techniques. Block-red means focused, and faded red is un-focused.

Images were taken were imported into ImageJ using the import plugin. Kalman filtering was used for to increase the signal to noise ratio and 3D image composites were also made in ImageJ using plugins.

2.7.4 Silane Confocal

Single photon confocal microscopy at University of Nottingham to characterise the 3D neurosphere biomaterial colonization process on silane functional surfaces. The microscope used was a Zeiss LSM 710 confocal laser scanning microscope with 20x objective. A key aim was to build-up a better picture of where the different cell populations were found by using 3 wavelengths to excite the immune stains (488 nm argon laser, 543 nm HeNe laser and propidium iodide laser).

2.8 Quality Controls and Statistics

The outputs of cell response to surfaces were validated using statistical quality control. High quality will inform on parameter robustness and repeatability. Once established the main effects of the parameters can be established, which can be further optimized in a clear way making the surfaces or the design principles more productive.

QQ plots were also produced as a judge of normality. A guide to interptreting QQ plots is shown with **Figure** 2.9, so skews in the data sets are made more obvious in QQ plots compared to histograms. QQ plots are quantile-quantile which shows two probability distributions plotted against each other. This makes qq plots superior for quality control compared to histograms, because real judgements can be made. The dots are quantile values which are a cumulative distribution function of a random variable, and the blue line is a normal distribution reference line. QQ plots can be interpreted by looking at where the values fall with regards to the normality reference line. In a normal distribution all the values are directly on the line. In a normal distribution with fat tails, most the values fall on the reference line except the values at the lowest and highest end which move away from the line. In a distribution with a positive skew (where values are mostly at the low end, small dominates) the values curve upward on top and away from the normality reference line (upward parabolic curve). If the distribution has a negative skew (most values fall in the top end, big dominates), the values curve downward below and away from the normality reference line (downward parabolic curve, like a kinetics graph) to perform standard comparative statistical tests such analysis of variance (ANOVA) normality of the data set has to be proven.

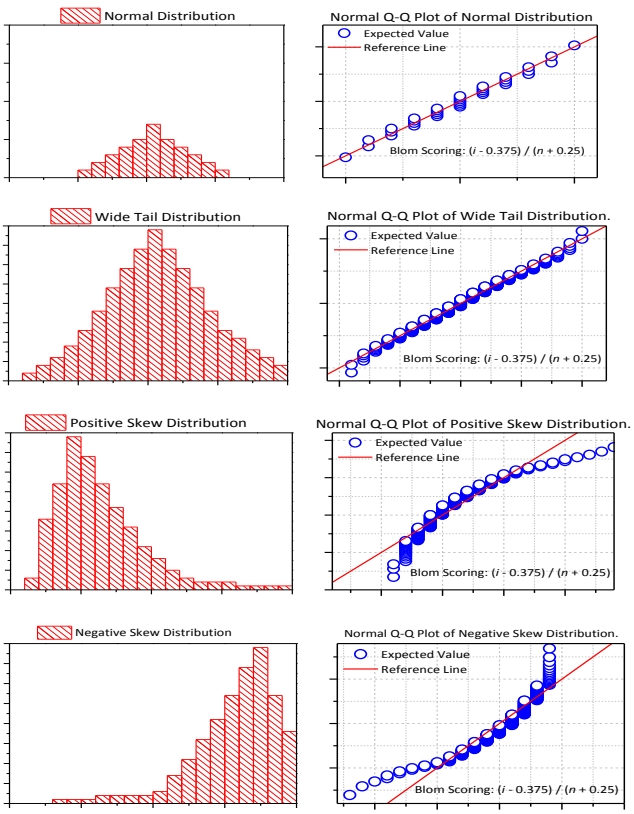

Figure 2.9 - QQ plots showing the different skews of data compared to normal distributions which provides a powerful tool to inform on any data transformations.

QQ plots were produced for each set of combined measurement data outputs, and were judged using QQ plots To cope with skews which were shown in the combined data sets transformations were performed using an online calculator found at (http://vassarstats.net/trans1.htML) to make the data follow a normal distribution which is an important prerequisite for statistical testing (Howell, 2012). To verify that the distribution of all the data sets used have an equal distribution to test the distributions of data were equal which is another prerequisite for statistical comparisons a Levene's test was performed in Originlab V9. Levene's test showed that the distribution between the groups.

The purpose of statistical testing is to test whether a null hypothesis (a treatment has no effect) can be rejected. In all the experiments there where more than two experimental groups which ruled out parametric A/B tests such as t-test. If

multiple t-tests are used instead of multiple groups the chances of getting false positives is raised. Therefore analysis of variance (ANOVA) was performed to compare multiple means. The ANOVA tests if the overlap of variance (spread of data) between multiple groups. The data is re-plotted as an f axis to compare the means of the groups. Strictly speaking a *P value* has to be calculated from an F value which is:

$$F = \frac{found\ variation\ of\ the\ group\ averages}{expected\ variation\ of\ the\ group\ averages}$$

A large F value means it is more likely that the null hypothesis can be rejected. The expected variation is the overall average made from all the data. The individual group averages are compared against the overall average.

A *P value* of less than 0.05 was judged as significantly different, and that the null hypothesis can be rejected. The *P value* serves as a summary of experimental the data assuming a specific null hypothesis. Significance is 1-confidence interval. The confidence interval provides an estimated range of values (the interval) which is likely to include an unknown population parameter (the probability value in % units), the estimated range which is calculated from sample data. The confidence interval of 95% comes from statistical tables written by Karl Pearson about hundred years ago (Pearson, 1914), which were a staple of statistical testing before automate computerized techniques were used. It is important to understand limitations of any statistical technique. In a recent article it was highlighted that the *P value* for example of 0.01 being the probability of the result being a 1% chance of the data being a false positive, and the actual probability is 11% (Nuzzo, 2014). To work out the probability of a false positive a second piece of information is required (the underlying probability of a true effect) to infer that.

Chapter III

3 Control of Primary Neural Stem Cell Fate, Adhesion and Morphology with Defined Surface Chemistry

3.1 Introduction

Great progress has been made over the past decades towards the regeneration of single tissues (e.g. skin, bone) and more complex organs; however regeneration of nervous tissue remains a challenge. Solutions to the produce better stem cell therapies to treat neurodegenerative diseases such as Parkinson's disease could be solved using approaches from physical sciences. Current drugs and treatments for Parkinson's disease such as levodopa and deep brain stimulation surgery only treat symptoms not disease progression. Neural stem cell transplants in a rat lesion model of Parkinson's disease have demonstrated site specific migration, engraftment and transcription (Fricker *et al*., 1999).

A key aim for biomaterial design is to get a better resemblance of the cell niches *in vitro*. The complexity of the niche environment and necessity to achieve neural alignment and specific re-connectivity is challenging. Interaction between cells and their microenvironment provide the conditions for tissue growth, which is important for regeneration of complex neural architecture. Poor clinical outcomes are largely associated with the limited capacity of the central nervous system for self-repair, with glial scarring following damage to neural tissue that compromises the ability to regenerate neural circuitry. Strategies to minimize such inhibitory effects whilst enhancing neural cell re-growth are key in terms of nerve engineering. Cell replacement strategies for the treatment of neurodegenerative diseases such as Parkinson's currently focus on the use of primary neural stem cell-derived populations, harvested from embryonic, developing ventral mesencephalon (VM) mid-brain tissue due to the abundance of dopaminergic neurons. The preclinical research has been met with limited

success due to the low differentiation efficiency of stem cells to specific neural populations, the inability to remove dividing cells from transplants leading to overgrowth *in vivo* and inhibition of axonal outgrowth by the adult brain microenvironment. By controlling cell-material interactions we aim to control cellular processes which enhance regeneration capacity by addressing all three shortcomings.

Stem cells which will be the basis of cell therapies reside in specific niches, here the stem cell divide and their key properties are retained. Another property of the niche is to keep the stem cell populations confined, preventing uncontrolled growth (Scadden, 2006). It is notoriously difficult to recreate the niches *in vitro*. In the adult brain a small population of neural stem cells are retained in a sub ventricular niche (Tavazoie *et al*., 2008) to provide a capacity for intrinsic repair. The adult niche provides feedback and cell signaling which influences the activation, maintenance and differentiation of the neural stem cells. The best way to recreate the neural differentiation niche *in vitro* is to use laminin coated surfaces.

Success of bio-materials can mainly be attributed to the biological/surface interface, and a few key molecular properties are in action at the interface. In the past biomaterial studies have looked at the impact where the authors showed that cell attachment was effected by surface wettability, (Mei *et al*., 2009) with stem cell embryoid body formation observed upon interaction with surfaces of mid-ranging wettability. Others have shown a relationship between the calculated partition coefficients of amino acid functionalised surfaces (logP of un-tethered group) and cell spreading (Rawsterne *et al*., 2007). In addition surface chemical and nano-structure characteristics influence protein layer composition and activity of adsorbed proteins. Functional groups presented at the surface therefore play a key indirect role in the control of cell responses, mediated through proteins deposited on the substrate surface.

Neural culture protocols commonly make use of laminin-coated surfaces to mimic the laminin-rich niche (Drago *et al*., 1991, Perrier *et al*., 2004, Kriks *et al*., 2011b). The extracellular matrix protein promotes adhesion and axonal extension, enhancing cell attachment initially through its positive charge followed by selective integrin binding (Letourneau *et al*., 1994). Typically laminin is used in complex differentiation protocols of stem/progenitor cells requiring cocktails of factors to direct cells towards a particular lineage. These mixtures of biological signaling factors are designed to mimic the biological niche environment, with researchers looking at the relationship between different cell types in co-culture to further understand cell-cell signaling control of specific biological processes (Sørensen *et al*., 2007). We have recently shown that co-culture of neurons with supporting radial glia has been advantageous for the attachment and alignment of neurons (Roach *et al*., 2012).

The reason for the success of laminin and other ECM coated surfaces in stem cell protocols such as matrigel was because of adhesion molecules including integrins on the cell surface. Laminin contains various specific ligands which allow adhesion of specific integrins on various cell types. A biomaterial's relationship with adsorbed proteins is the key lever on the cell response. The protein conditioning process of biomaterials was described in detail in Roach (Roach *et al*., 2007) and Volger (Vogler, 2012). Once proteins adsorb structural changes can occur exposing previously unavailable domains on the protein (Roach *et al*., 2005), presenting binding sequences for anchoring molecules including integrins which are triggered by extra cellular matrix proteins (Hynes, 1992), the peptide sequences which cause astrocyte/glia adhesion are in (Kam *et al*., 2002). NCAM (Rutishauser *et al*., 1988) is a specific adhesion molecule for neural cell types where the binding is homophillic between molecules, the sequences which cause binding were elucidated in (Rao *et al*., 1992).

By using surface engineering techniques production of cell therapies to treat neurodegenerative disease can become defined. The aim of making the inputs more defined has been to make the process of manufacturing stem cell therapies more stable (Couture, 2011). Early on the importance of the surface to the culture of pluripotent stem cells, where Matrigel has been a popular surface coating, because of the mixture physiochemical cues provided (Ludwig *et al*., 2006). Complexity represents a huge problem because perturbations which can disturb the system can set in form any number of places, so it would be more favorable to make culture systems which require fewer interventions harnessing the ingrained ability of stem cells to proliferate, organize and differentiate. So there have been reports where the authors to simplify the culture by using only laminin (Rodin *et al*., 2010), or using synthetic substrates (Melkoumian *et al*., 2010). However in these two publications the surfaces have been simplified, but the culture media and culture technique remain highly complex. The problem is that the surfaces have not been designed to control cell behavior (and therefore control the ingrained abilities of the cells), but to compare favorably to pre-existing materials. These are valuable findings because a better surface will be far cheaper than optimized culture conditions which are requiring ever equipment spiraling in cost, and lack flexibility to incorporate into pre-existing workflows. Materials can be engineered to be incorporated into pre-existing processes, or inspire creative new processes which were previously not possible. An important part of the design process was to select behaviors of cell which would be good to control with materials. To add to that the behaviors have to be things which can be controlled by a surface, because it is probably ineffective to try and trigger biological pathways where there are many steps. This is because the cue from the surface can be impeded by various other things.

In the experiments neurospheres were used because they provide the proliferative niche for neural stem cells and progenitors *in vitro*. Neurospheres are 3D spheroids which expand with the addition of βFGF or EGF to culture media, and the deprivation of serum proteins (Reynolds and Weiss, 1992). The structure of neurospheres has been characterised in (Lia S. Campos *et al*., 2004), thus demonstrating the neurosphere has the properties of a micro-environment as opposed to clusters and aggregates. Neural stem cells grow at the edge of the structure where there was a high frequency of MAP-kinase signaling which is typically related to the β1 integrin, glia progenitors are found at the outer core of the structure, neural progenitors and found at the core of the structure. Another important point was that the niche environment is rich in laminin which activates the β1 integrin. Surface induction of stem cell differentiation is nearly perfect to look at with neurons, because in the differentiation process the 3D neurosphere flattens in to a 2D monolayer. The colonization of neurospheres on laminin coated surfaces has previously been characterised in (Jacques *et al*., 1998) When a neurosphere comes into contact with a surface the first indicator of maturation was that the first neurons migrate out in a process called chain migration. Which was stimulated by integrin α1β1 and α6β1, where the epitope can be found on laminin. Indeed long term culture of neurons has been achieved using laminin coated surfaces in (Ray *et al*., 1993), where hippocampal neurons have been cultured for 24 passages.

In the present study neural stem cells and progenitors, in the form of neurospheres, were seeded on surfaces having defined terminal chemical functionality. Self-assembled monolayers (SAMs) provide a versatile platform to present defined chemical functionalities at surfaces (Bain and Whitesides, 1988) and are used widely in the study of biological interactions at solid interfaces. The purpose of the study was to provide first principles in to the design of a new generation of biomaterials or pre-existing ones where

the simple characteristics can easily be stacked to produce better biomaterials purposely design for the job. In cruder high throughput (Mei *et al*., 2009) the mechanisms which can be used to rationally design better materials are lost, however in the newer Pareto efficiency lead computionational design models which are beginning to come online for drug design (Besnard *et al*., 2012). What these approaches provide which others neglect is the fact that trade-offs have to be made for more fit-for-purpose biomaterials, and Pareto efficiency computionational design models take into account these trade-offs. A key area of biomaterial research which needs to be developed is to find where the trade-offs occur. Currently these new approaches cannot be effectively be incorporated into stem cell research because we have been failing to do fair comparisons where individual effects can be ascertained. A classic example is in (Caldwell *et al*., 2001) where different morphogens and growth factors were compared for maintained and differentiation of neurospheres. The problem was that although the inputs and outputs were clear which was a strength of the experiment, however there is a poor assumption. There is an assumption that the different proteins which are used in the experiment all behave the same way in cell culture, and that is not the case because diversity of properties inherent to proteins.

Previous studies have demonstrated that silanes can be used to tailor chemical functionalities on a surface and control interactions with biomolecules (Roach *et al*., 2005 & Arima, Iwata, 2007). Adhesion and guided spreading of neurons has been demonstrated, using hydrophobic fluorinated surfaces to hinder axonal interaction along with amine-rich poly(lysine) providing adhesive tracks(Kwiat *et al*., 2012). Similarly simple amine containing silanes have been used to direct neural cells, using poly(ethylene glycol) (PEG) as a hydrophilic attachment inhibitor.(Sweetman *et al*., 2011).

The studies where the authors have been using silanes have a big advantage over other biomaterial work, because focus is placed on the key mechanisms controlling cell response rather over emphasising cell culture technique (Dubiel *et al*., 2011). Scaffolds are frequently made out of *generic* polymers such as poly(lactic-co-glycolic acid) (PLGA) (Kanczler *et al*., 2009), but PLGA as molecule has clear characteristics in terms of wettability (Paragkumar N *et al*., 2006) and charge (Astete and Sabliov, 2006). Molecular properties such as charge and wettability will have a real effect on protein adsorption (Sigal *et al*., 1998) which is the key process in biomaterial conditioning (Roach *et al*., 2007), and hence the principle area where a biomaterial can control cell response. Over-looking the mechanisms means that the cell response tends to be characterised at the end, rather than engineering the control in the biomaterial as a starting point for biomaterial design. A work-around has been to pre-adsorbed proteins on the surface or conjugating proteins on to the surface. The rational is good, because if a specific protein is congugated to the biomaterial will elicit a specific response (Ratner and Bryant, 2004). Ranging from morphogens to cause stem cell differentiation (Wylie *et al*., 2011) to extra cellular matrix for enhanced cell adhesion (Koh *et al*., 2008). However evidence from nanoparticles shows problems with this type of strategy. In a physiologically relevant cell culture conditions (which contains serum which contains over 3000 proteins (Anderson and Anderson, 2002) rapidly forms a protein layer termed the ‘corona‘. The corona multi-layer forms rapidly (in about half a minute) containing over 300 proteins (Tenzer *et al*., 2013). It has been shown that functionaling a nanoparticle surface with conjugated with proteins can be rendered irrelevant by the protein corrona (Salvati *et al*., 2013). A principle strength of the experiments in Curran and Hunt was the experiments were designed as striped back mechanistic biomaterial studies. The behaviour of mesemchymal stem cells was characterised on surfaces presenting different headgroups and the

biomaterial interface. So there was just one factor being studied, and the authors showed that the simple surfaces could control the stem cells behaviour. As the study was put together in a methodical way the under-pinning mechanism could be unpicked. In (Roach *et al*., 2005) the authors shown that the kinetics of protein adsorption could be controlled with a biomaterial property as simple as the headgroup. This type of study is going to be important in the translation of future biomaterials, because of the high regulatory hurdles (Prestwich *et al*., 2012). Ultimately that could be an insumountable hurdle for protein conjugated biomaterials, because there are numerous overlapping roles for proteins were relevant assay could be impossible to develop.

A key direction of our work is to improve the control of neural cell responses by presenting a well-defined micro-environment. The aim of the study was to assess the response of ventral mesencephalon (VM) stem/progenitor cells cultured as neurospheres (spheroids of proliferating cells) on a wide range of defined surface functionalities. We report that surface chemical functionality can be used to direct fractional populations of neurons vs. glia derived from VM neural stem/progenitor cells. Defined SAMs were prepared to present amine (NH_2), hydroxyl (OH), carboxyl (COOH), alkane (CH_3), phenyl (Ph) and thiol (SH) functional groups. Neurospheres varied in their response to specific chemical functionalities, in their ability to attach to and populate the surface; differentiation and migration of neurons and astrocytes, and neurite elongation, was either promoted or retarded in comparison to control laminin-treated surfaces. We show that the presentation of surface chemical cues provides a route to improve the robustness of neural culture methods, controlling multiple cellular responses commonly attributed to cell-surface interactions.

3.2 Results

Well defined surfaces presenting a range of terminal functional groups were produced via self-assembly of silanes on glass coverslips. Primary rat neural tissue was dissected from E12 VM tissue and manipulated to form a single cell suspension, and further cultured to produce neurospheres after 7 days. Neurospheres were then directly seeded onto chemically defined substrates and cultured for a further 3, 5 and 7 days, with paraformaldehyde fixation and staining carried out at each time point. Poly(D-lysine) (PDL)-laminin was used in the study as a reference to the current '*gold-standard*' surface used to support neural cultures *in vitro*. All surfaces were fully characterised by attenuated total reflection Fourier transform infrared spectroscopy (ATR FT-IR), x-ray photoelectron spectroscopy (XPS) and drop shape analysis (DSA) to confirm the presence of the SAM modification (**Figure** 3.1).

The XPS data in **Figure** 3.1 show that the relevent peaks for silanes were present. The XPS peaks show the states of the surface functional groups. Carbon, nitrogen and oxygen were chosen because all six of the chemical surface treatments contained carbon, and amine plus hydroxyl groups were chosen to be more specific to the amine, hydroxyl and carboxcylic acid surfaces. On hydroxyl functionalised surface strong carbon and oxygen peaks were present with a weak amine peak. Amine peaks were clearest on the amine and carboxylic acid surfaces. A strong carbon signal was found on the methyl, phenyl, carboxylic acid, and amine surfaces. carboxylic acid, and amine silane functionalities had akyl chains, and in contrast the carbon peaks would have come from the functionalities on the methyl and phenyl functionalised surfaces. The clearest oxygen peaks were on the carboxcylic acid and hydroxl functionalised surfaces. The laminin coated surface had strong peaks for carbon, hydrogen and nitrogen which are all common in protein.

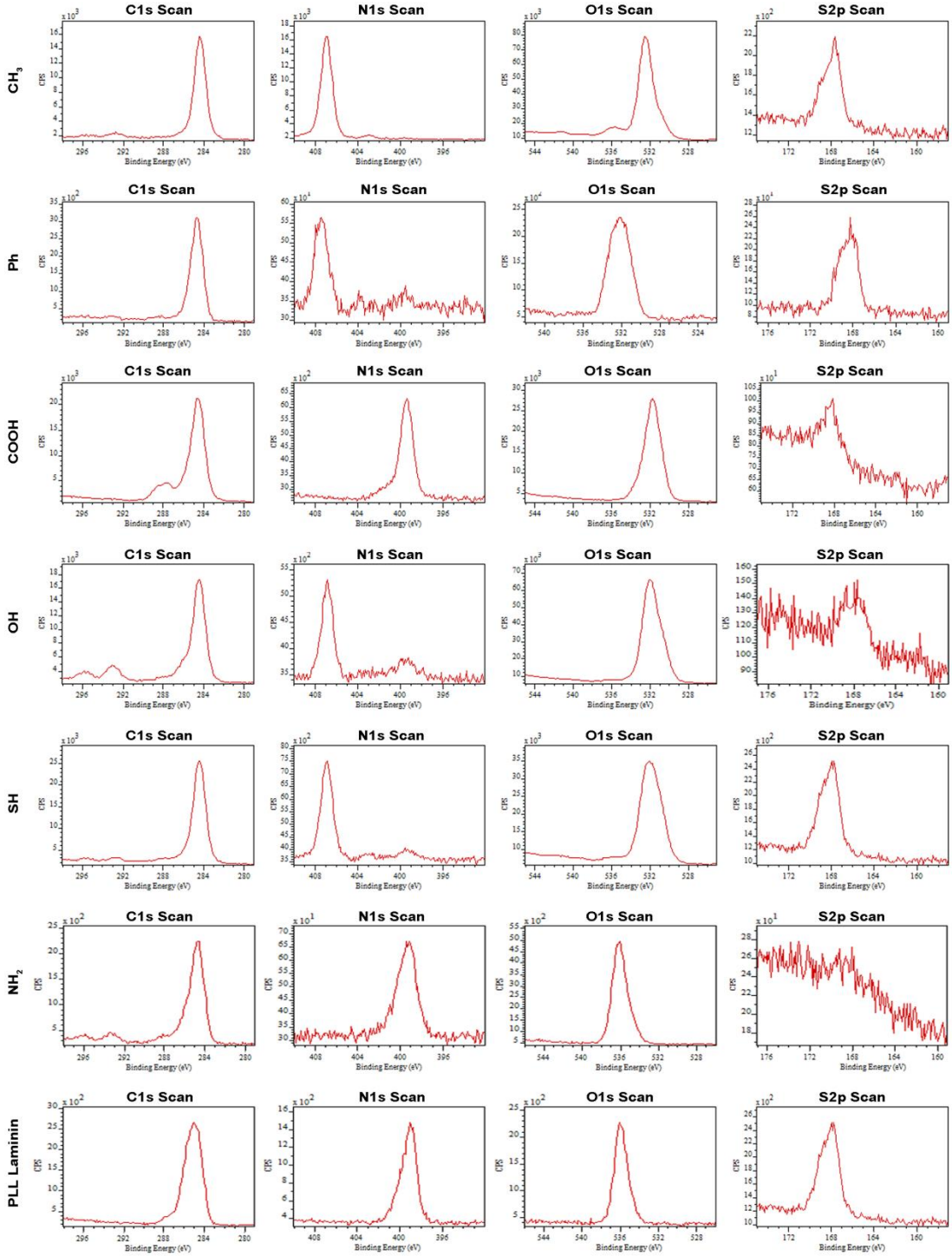

Figure 3.1 –XPS data from the silane functionized surfaces and the PdL laminin gold standard surface.

3.2.1 Qualitative Observations

PDL Laminin coated glass microscope cover slides provided a gold standard to which the functional silane head groups were compared to, because it is well established for neural cell culture (Drago et al., 1991). The behavior of neurospheres on the laminin

coated surfaces was clear with a flattening of neurospheres, spread out population of neurons, and clear axonal processes. All these qualitative descriptions show differentiation of neural stem cells and progenitors with representative images in **Figure** 3.2.

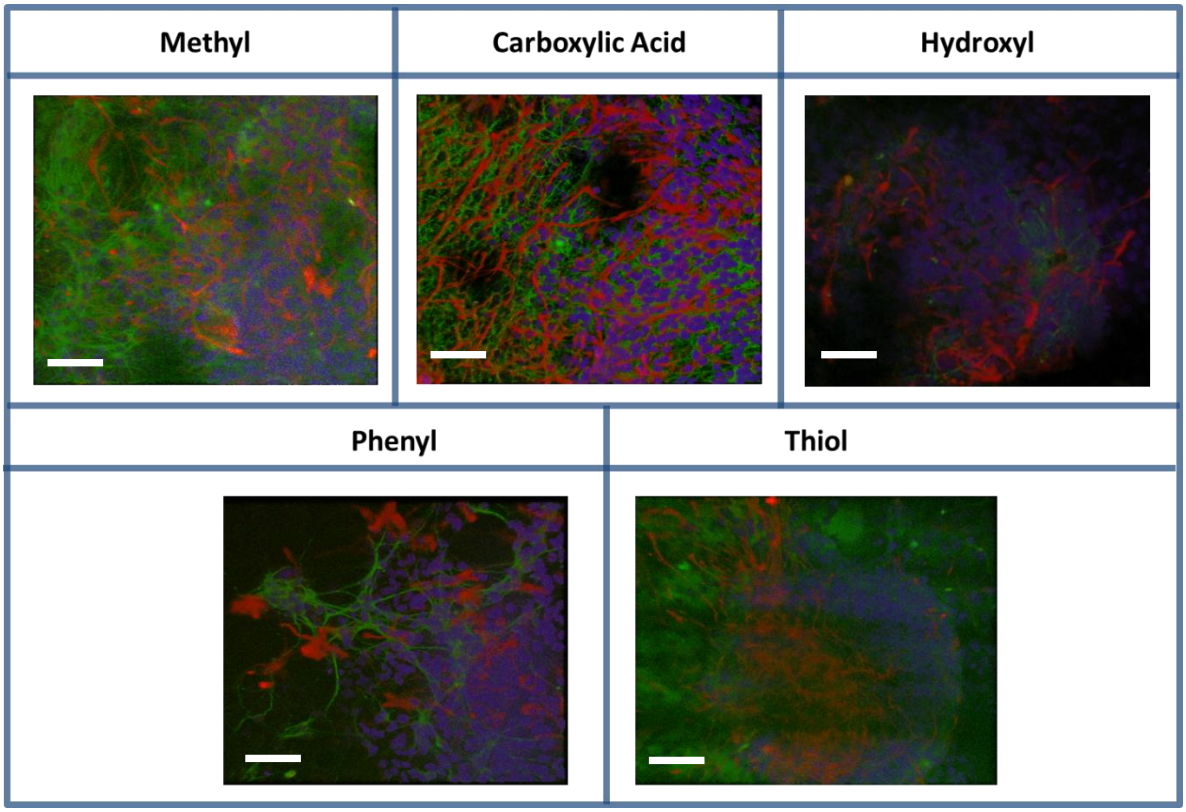

Figure 3.2 – Confocal images taken on silane functionalised surface of rat e12 VM neurospheres after 3 days of cell culture. The blue is DAPI which stains the cell nucleus. Green is tuj1 which is a neural specific marker, and red is GFAP which is a glia cell marker. White scale bar represents 50 µm.

The surfaces which were functionalised with amine head groups caused a similar cell response from the neurospheres as with the laminin coated surfaces. The similarities were with the long axons and rapid flattening and mixing of neurons and glia on the monolayer. On both the laminin and amine surfaces there was plenty of cell migration of both neurons and glia over a range of distances. Similarly the axonal processes were longest on the amine and laminin surfaces with wide trunks, and fine processes which were indicative of the neurons searching out new processes. On the CH, SH and Ph surfaces the cells were minimizing their exposure to the hydrophobic surface interfaces by remaining in the neurosphere. The hydrophobic interface with the reduction in

polarity will have affected the composition of the serum proteins which adsorbed on to the surface. There was some spreading with some short colonizing processes coming out from the neurosphere. Along with the similarity the PDL laminin coated surfaces with the amine functionalised surface was an interesting range of behaviors on the hydroxyl terminated surface. As the pictures show (**Figure** 3.2) the neurons remained in the neurosphere with the glia migrating out. To provide stronger evidence of the observation was provided by single photon confocal microscopy to provide accurate depth profiling of the three dimensional structure. What the confocal microscopy showed was that depending on the depth the composition of cells changed. At the lowest depth near the surface glia dominated, and within the spheroid the neurons dominated. Showing the potential of a new way to separate the two populations producing more effective cell therapies. On the amine and laminin surfaces the confocal microscopy did not show anything particularly interesting, because different neural populations were mixed with deconstruction of the neurospheres. On the Ph, CH and SH surfaces the smaller three dimensional spheroids were fairly intact. There was some evidence of structuring within the spheroids with neurons found in the core of the sphere, and glia found at the periphery to the core (Lia S. Campos *et al*., 2004).

3.2.2 Neurosphere Spreading

Neurosphere response to surface chemistry was investigated by fluorescence microscopy using markers to identify glial and neural cell populations. The neurospheres were observed to initially attach to all surfaces after 1-2 hours, with those cultured above more hydrophobic surfaces generally taking longer to attach (data not presented). A two way ANOVA in **Figure** 3.3 showed a significant difference between the population means of all surfaces tested at all time-points (surface variable – P value 0; time variable – P value 0), highlighting the impact of surface chemistry on neurosphere-surface interaction. Temporal effects were also observed. A Tukey's post-hoc test was performed to identify significant differences between test populations. Some differences were observed between repeat samples, with these increasing in significance with increasing culture time.

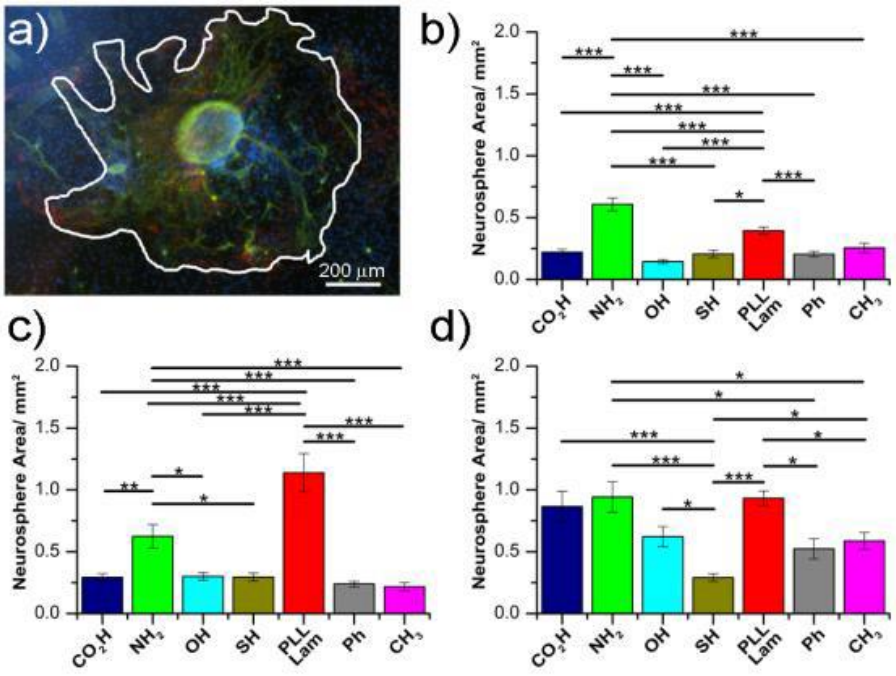

Figure 3.3 - Neurosphere spreading capacity on different surface chemistries**;** a) fluorescence microscope image of neurosphere on an hydroxyl functionalised surface at day 3 depicting area boundary as white line (green – β3-tubulin, red – GFAP, blue- DAPI nuclear stain); plots show area measurements after b) 3 days, c) 5 days and d) 7 days culture. ∗ $p \leq 0.05$, ∗∗∗

When neural stem cells and progenitors are cultured as three dimensional neurospheres a clear indicator of differentiation is the independent adhesion and migration of cells out of the spheres which causes flattening. The first stage of the differentiation of the neurosphere is the attachment of neurospheres to a surface with high affinity. PdL laminin surfaces are popular, because laminin proteins have plenty of adhesion ligands specific for neurons. The neurosphere tends to deconstruct and differentiate with first a migration of the glia away from the sphere, which simultaneously provides a the foundation layer for neurons to migrate away on (Edmondson and Hatten, 1987), and release of trophic factor for maintance of neurons. Alternately the neurons can make short range migrations out of the spheres independently of the glia in a process called chain migration (Jacques *et al*., 1998). The key mechanism to control the maintenance of neurospheres and the switch to differentiated monolayers are changes in the integrin adhesion molecules (Lia S. Campos *et al*., 2004). The spreading of neurospheres is a relevant measurement to the differentiation of neural stem cells. Another advantage of these experiments was to factor in the response of the cells measured over multiple time points. The ideal *in vitro* measurement would inform on how the implant might perform *in vivo*. In ideal circumstances where the implantation site can be kept free of large inflammatory responses, biological condition would be followed by stem cell recruitment and remodelling of the implantation site.

The neurosphere spreading was assessed by imaging the surfaces at three time points which were 3, 5 and 7 days. 3 days was selected because it was the shortest time point where the samples were robust enough for cell fixation and antibody staining. The three day time point informs on the biological/material interface. Whilst the seven day timepoint was selected to inform on biological remodelling of the environment. Also seven days was selected as the longest time point, because exceeding the time point

would mean that passaging the cells would be necessary which is extremely challenging with differentiated neurons. Once the sample were fixed and stained the xy scanning images were taken on a Nikon epi-fluorescent microscope with a 20X objective lens which is a 200X magnification. The resultant images were taken into Imagej, and the spread areas were measured with the freehand area tool.

In general, populations migrating away from the neurosphere edges were found to stain positive for both glial and neural cells rather than stay in a naïve undifferentiated state. Glial cells were observed to migrate further from the neurosphere boundary providing a bed on which neurons attached (**Figure** 3.2). The glia bed is most pronounced on the hydroxyl surface, highlighted in confocal microscopy with pure glia populations found at the surface interface. Migration of cells was quantified in terms of neurosphere spreading. The presentation of the neurospheres depended greatly upon interaction with differing surface chemical groups, with the proportion of each cell being found to differ in their distribution across the range of surfaces tested (**Figure** 3.3).

After 3 days in culture there was low variation in neurosphere spreading (**Figure** 3.4) and degree of cell migration from the parent neurospheres on individual surfaces (i.e. deviation amongst sample repeats was low (**Figure** 3.3). The results show that the interaction between cells and surfaces was comparable on each of the chemical surfaces tested. However distinct spreading patterns of neurons and glia from the spheres were observed, being dependent upon the surface functionality, **Figure** 3.3. Amine terminated surfaces gave rise to the largest spreading neurospheres (0.61 ± 0.05 mm^2) being larger than those on PDL-laminin surfaces (0.39 ± 0.03 mm^2). All other surfaces were relatively similar to each other, with lowest spreading capacity presented by hydroxyl SAMs (0.14 ± 0.02 mm^2). Differences observed in neurosphere spreading

across the range of surfaces tested did not appear to follow a direct trend with respect to surface wettability.

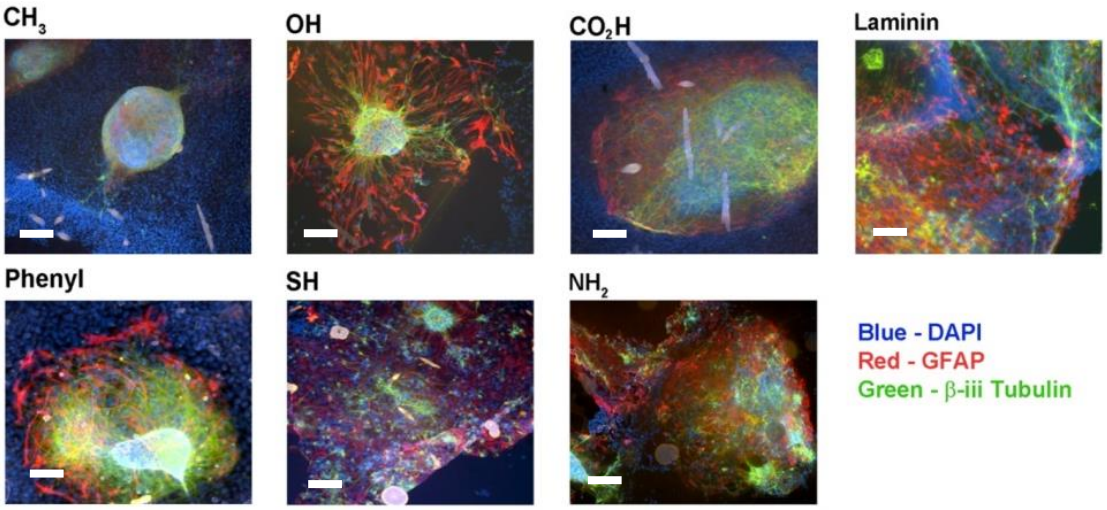

Figure 3.4 - Images of neurospheres attached to a range of defined surface chemistries using fluorescence microscopy (scale bar is 100 μm). Cells shown after 3 days in culture.

A marked increase in neurosphere spreading was observed on PDL-laminin after 5 days in culture (1.14 ± 0.16 mm^2) and hydroxyl (0.30 ± 0.03 mm^2) coated surfaces on day 5 compared with day 3, and other surfaces were showing either slight or no increase in neurosphere spreading area (**Figure** 3.5). The largest neurosphere spread areas after five days in serum rich media were on the PdL Laminin surfaces which increased from about 0.4 to over 1mm^2. The amine surface had also caused a significant increase in the spreading of neurospheres. The lowest spread area was on the methyl functionalised surface which had changed little from the previous timepoint.

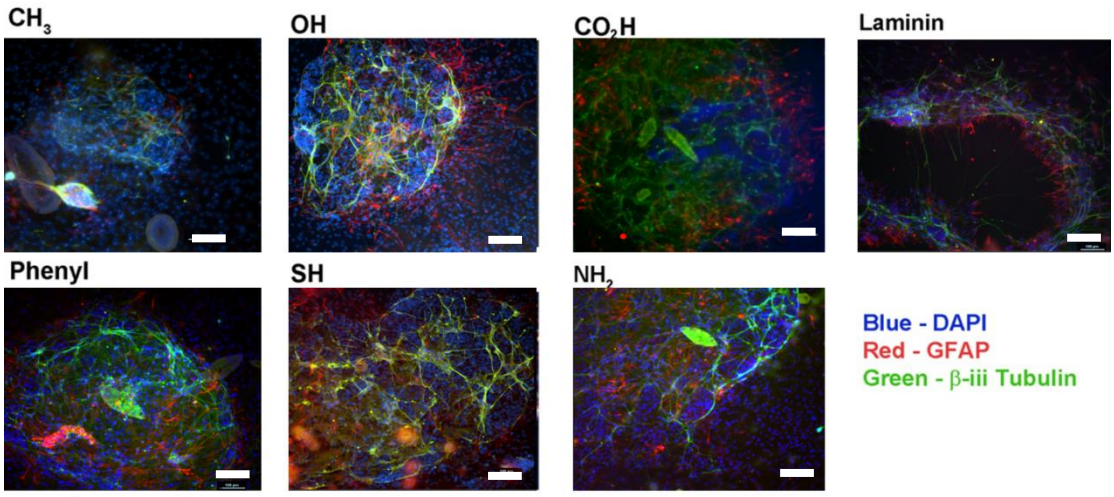

Figure 3.5 - Images of neurospheres attached to a range of defined surface chemistries using fluorescence microscopy (scale bar is 100 μm). Cells shown after 5 days in culture.

The final time point used to meause the attachment and spreading of neurospheres was at seven days (**Figure** 3.6). The most spreading was seen on the PdL laminin and amine surfaces, and suprisingly the COOH functionalised surface was only a little short of the PdL laminin and amine surfaces. the neurosphere spread area tripled on the COOH surfaces which was the largest increase of spread area across the experiment. Increases of neurosphere spreading was achived on all the other test surfaces, except for the thiolated surfaces where spreading did not increase from five to seven days. There were increases of neurosphere spreading on the OH, Ph and CH surfaces. The area doubled on the Ph, OH and CH functionalised surfaces.

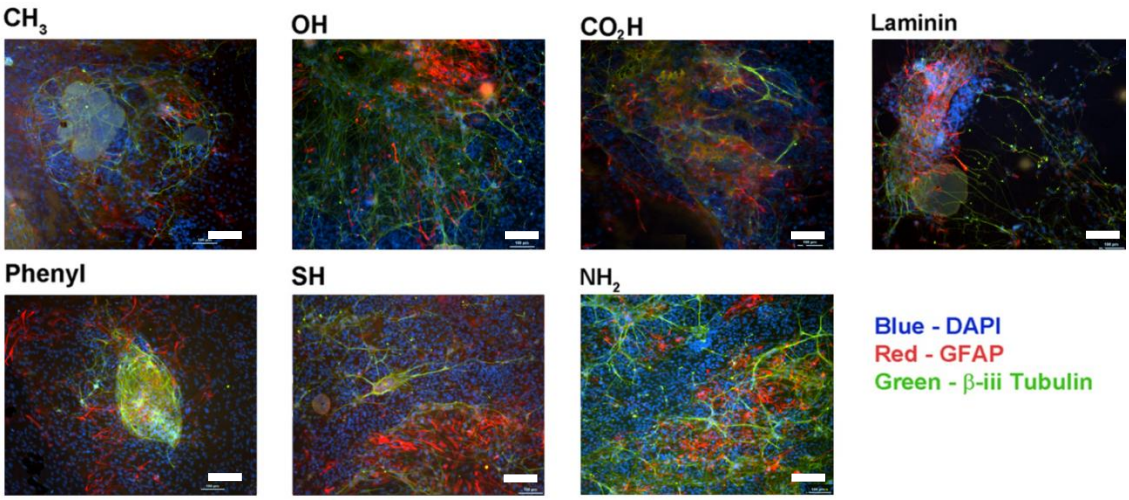

Figure 3.6 - Images of neurospheres attached to a range of defined surface chemistries using fluorescence microscopy (scale bar is 100 µm). Cells shown after 7 days in culture.

A significant increase in neurosphere spreading, demonstrated by two way ANOVA, was observed on almost all surfaces, compared with spread at day 3 (**Figure 3.3**). Neurospheres cultured on thiolated surfaces were the exception, showing no increase in spreading from 5 to 7 days and no significant spreading over the whole culture period. No apparent direct trend was observed relating neurosphere area to surface wettability according to the Pearson's R values (3 day = 0.256, 5 day = -0.365, 7 day = 0.187).

3.2.3 Neuron Density

The amount of neurons supported in culture is of primary importance for the delivery of successful cellular therapies to regenerate nervous tissue. Cells across the neurosphere area were counted as a means of quantifying the capacity of neural progenitors to be steered towards neural lineage as presented in **Figure** 3.7.

A key element to translating the cell culture techniques into large scale process is to keep costs down, so increasing the density of transplant relevant populations is important. New ways have to be found where defined surfaces increase cell numbers, because a defined culture surface would be cheaper and more controllable than the alternatives such as specialist cell culture media, and environmental culture conditions such as hypoxia. At the early 3 day time point the neural density measurement informs on

neural differentiation because a high density means that neurons are retained within the neurosphere. A low neural density at the three day time point is a strong indicator of differentiation. At the five and seven day time point the measurement is more relevant to proliferation, because Gage's team observed that it takes 4 days for hippocampal neurons to divide (Ray *et al*., 1993). So if neural density remains similar and the spread area is increasing, neurons are dividing to compensate for the expansion. A low cell density means a preference of cells towards autocrine signalling, whereas high cell densities will favour paracrine cell signalling (Lindholm *et al*., 1996). Neural density therefore provides a simple measurement of profound consequences.

Results were taken after days 3-7 time points with neurospheres becoming flattened enough, for reliable measurements, i.e., no cells were obscured by the depth of the neurosphere mass (**Figure** 3.7a). Quantification of neuron numbers were normalized to surface area on which they resided due to differences in initial neurosphere size and cell numbers.

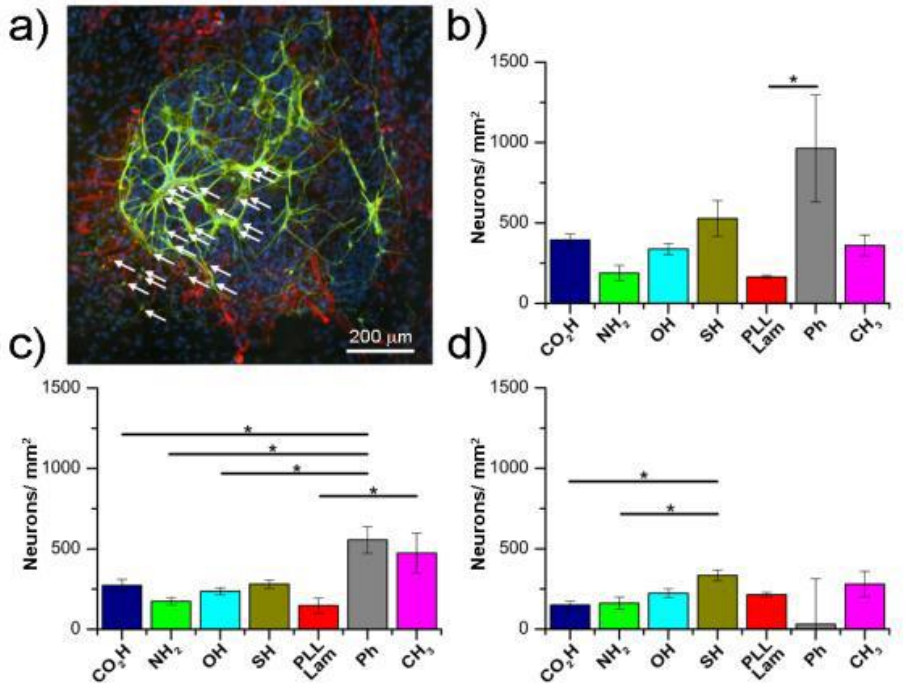

Figure 3.7 - Neural cells derived from neurospheres; a) fluorescence microscope image of neurosphere on an amine functionalised surface at day 5 indicating a selected number of neurons by white arrows (green – β3-tubulin, red – GFAP, blue- DAPI nuclear stain); plots show measurements of neuron densities as a function of surface area, after b) 3 days, c) 5 days and d) 7 days culture. ∗ p ≤ 0.05, ∗∗ p 0.05, ∗∗∗ p ≤ 0.005 . Surface functionalities are ordered in decreasing wettability, left to right.

Normalised neural cell densities were measured by counting the Tuj1 positive cells present in the neurosphere spread area. The neuron number was then divided by the area, so normalised comparisons could be made the surfaces. The measurement informs on the surface's impact on the numbers of transplant relevent cells, because it is optimal to have more neurons. Large images were taken from the samples, neurons were counted in the neursphere spread area (staining positive for Tuj1). It was important to normalize because bigger neurospheres have more cells which would ruin the measure. The measurements were made in Imagej using the free hand area tool and the cell counter plugin, a ratio was made from these values in Originlab 9.

Two way ANOVA analysis conducted over the 3 repeat samples for the 3 repeat tissue collections (i.e. 9 samples overall) indicated significant differences between population means of all surfaces (P value 4.24317 X 10^{-6}), and at all time-points tested (P value 0.00673). The interaction between the two factors was not significant. A Tukey's post-hoc test was also performed to assess individual differences between test populations showing significantly higher density only on phenyl surfaces.

Neuron densities were found to be generally similar on individual surfaces tested at day 3 (**Figure** 3.8) with some variance being observed across cell densities counted on hydroxyl and thiol terminated surfaces. This demonstrated overall reproducibility with the experiments. Most surfaces after 3 days in culture presented a similar neuron density, with a significantly higher neuron density only being apparent on phenyl surfaces, (**Figure** 3.7b). Cell densities were found to be ~500 neurons/ mm^2, with a highly significant difference observed between PDL laminin (~160 ± 10 mm^{-2}) and phenyl (~960 ± 330 mm^2).

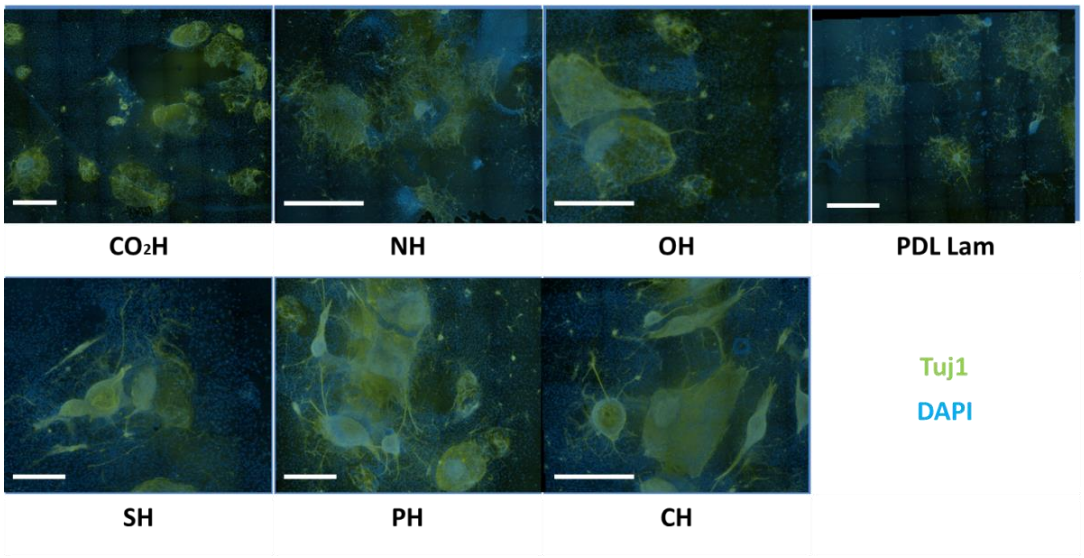

Figure 3.8 - Three day neural density on the seven surfaces taken as tiled images to provide a greater field of view to judge the response of many neurons. The two channels are FITC and DAPI taken at 20X zoom, and the white scale bars show 600µm.

By day 5 little difference was found between replicates on each surface (**Figure** 3.9). Significant differences were found (at a level $P \leq 0.05$) comparing surfaces to phenyl, with the exception between phenyl and alkane surfaces, which were not significantly different. Which suggests a good correlation between surface wettability and density of neurons. The highest values for neural density were on the phenyl and methyl surfaces, suggesting maintenance of stem cell and progenitor niche (neurosphere). Decreases can be seen on the other surfaces which points towards maturation of the cells, and being in more advanced stages of the neural colonization of biomaterial surfaces.

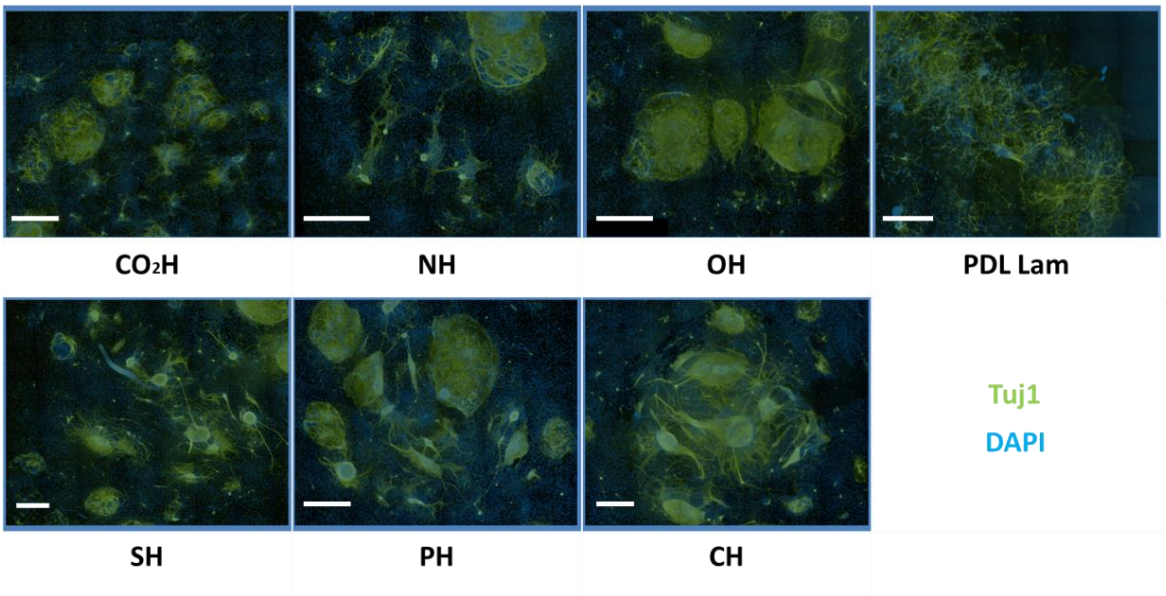

Figure 3.9 - Five day neural density on the seven surfaces taken as tiled images to provide a greater field of view to judge the response of many neurons. The two channels are FITC and DAPI taken at 20X zoom, and the white scale bars show 600µm.

Less change between the surfaces was observed for neuron densities measured at 7 days (**Figure** 3.10), with significant differences only being observed when comparing measurements made on carboxyl and amine surfaces to surfaces presenting thiol termination, (**Figure** 3.7d). Importantly, neuron densities were found not to decrease significantly over time, even though neurosphere areas increased. The only surface on which a decrease in cell density was observed was that with phenyl terminal chemistry.

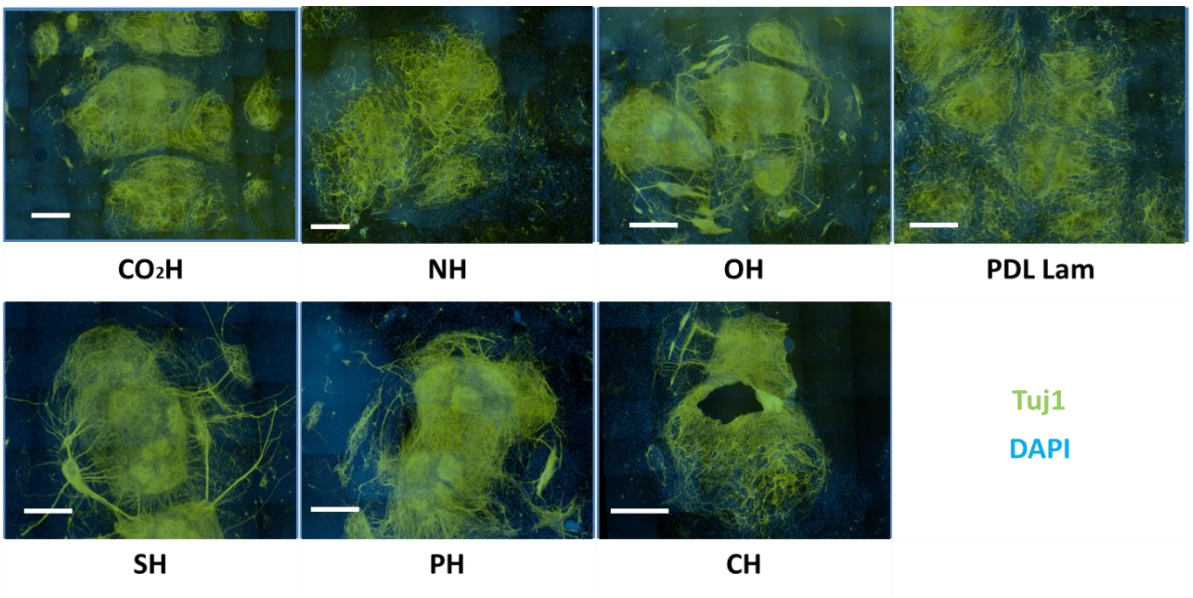

Figure 3.10 – Seven day neural density on the seven surfaces taken as tiled images to provide a greater feild of veiw to judge the response of many neurons. The two channels are FITC and DAPI taken at 20X zoom, and the white scale bars show 600µm.

3.2.4 Neuronal vs Glial Cell Populations

Although the regeneration of electrically functional neural tissue requires high numbers of neurons, supporting glial cells are often found to dominate cultures due to their proliferation. Normalization of neural densities to account for total cell numbers afforded from neurospheres (neurons and glia) serve as a better indicator for differences in cell-surface responses.

Controlling cell fate is a key aim in regenerative medicine, which is notoriously difficult. Indeed a critical quality attribute for a cell therapy is the purity of transplant populations (Rayment and Williams, 2010), so increasing the proportion of neurons is the key challenge in translating basic stem cell science into cell therapies. Normally the glia cells will dominate the cell culture, which is not ideal because neurons tend to be affected in the pathology of neurodegenerative diseases. Cell therapies for Parkinson's disease have been used in trials in (Politis *et al*., 2011) one adverse side effect was an increase in uncontrolled movements (dyskinesia) in recipients due to serotinergic contamination of the transplant populations. The long term source of dopaminergic neurons to treat Parkinson's disease will be derived from pluripotent stem cells which bring new and unique risks such as terratoma (Fricker-Gates and Gates, 2010). So increasing the proportion of neurons is important because it is the transplant relevant population. This is particularly true in neural cell cultures where supporting glia and astrocytic fractions tend to dominate cultures with the neurons which are of interest for Parkinson's, Alzheimer's and stroke therapies in the minority. Asymmetric cell fates after division of neuron and glia progeny is a probable explanation, and the fate is controlled by the transcription factor called neurogenin2 (Miyata *et al*., 2004). The effect of surfaces on this part of cell culture is unclear, so any advantage gain with surfaces would be beneficial.

Understanding the relation of neural cell division and time is important, so surfaces can be designed and optimised to control cell fates in stem cells.

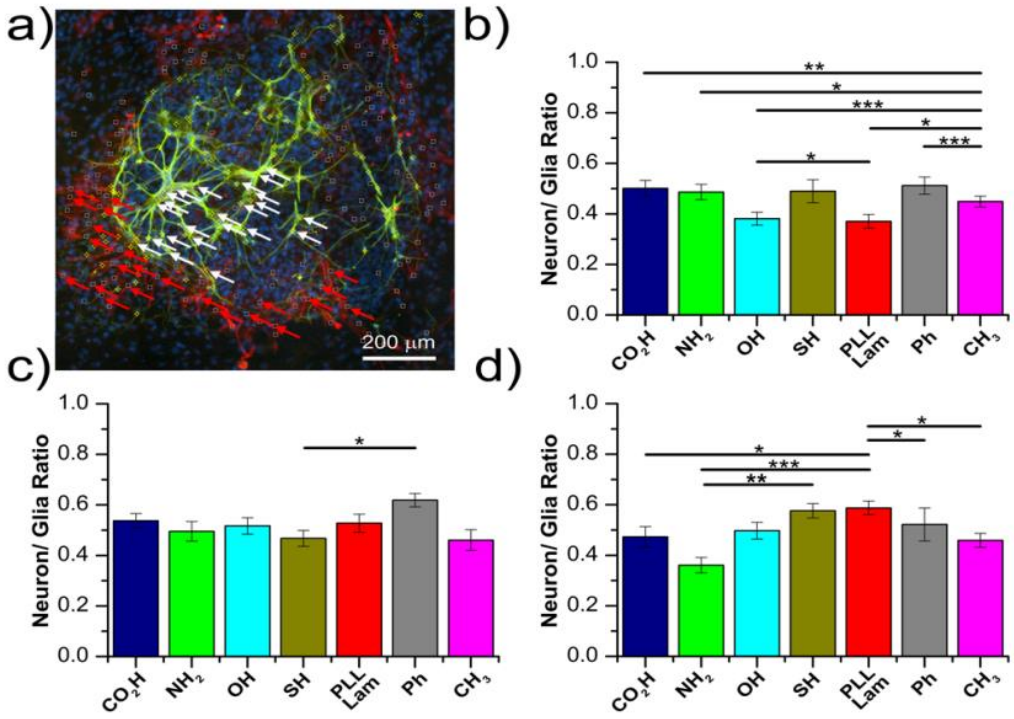

Figure 3.11 - Ratio of neurons/ glial cells derived from neurospheres; a) fluorescence microscope image of neurosphere on an amine functionalised surface at day 5 indicating a selected number of neurons by white arrows and glia with red arrows (green – β-III tubulin, red – GFAP, blue- DAPI nuclear stain); plots show measurements of neuron densities as a function of surface area, after b) 3 days, c) 5 days and d) 7 days culture. ∗ $p \leq 0.05$, ∗∗ $p \leq 0.0$, ∗∗∗ $p \leq 0.001$. Surface functionalities are ordered in decreasing wettability, left to right.

Normalised neural cell densities were divided by normalized glia cell densities which provided the basis of neuron to glia ratio. The measurement informs on the surface's impact on cell fate, so if the proportion of one lineage fate can be promoted over another. Neuron to glia ratio provides a better indicator for differences in cell-surface responses. From all the large images taken from the samples, mixture of neuron and glial cells were observed on the surfaces tested (staining positive for β-iii tubulin and GFAP respectively). The measurements were made in imagej using the free hand area tool and the cell counter plugin, a ratio was made from these values in Originlab 9.

On all surfaces tested a mixture of neuron and glial cells were observed (staining positive for β_3-tubulin and glial fibrillary acidic protein (GFAP) respectively), shown in

Figure 3.11a. Two-way ANOVA analysis showed significant differences between population means of all surfaces tested at all-time points ($p < 0.05$).

Ratios at day 3 indicated higher amounts of glia present on all surfaces, with neuron/glia ratios ranging from ~0.36-0.52. Lower proportions of neurons were observed on hydroxyl and PDL-laminin coated substrates compared to all others tested (**Figure** 3.12). A significant difference was observed between all samples compared to the alkane CH_3 terminated surface, (**Figure 3.11b**) and cell populations presented on phenyl and hydroxyl surfaces showing the highest level of difference.

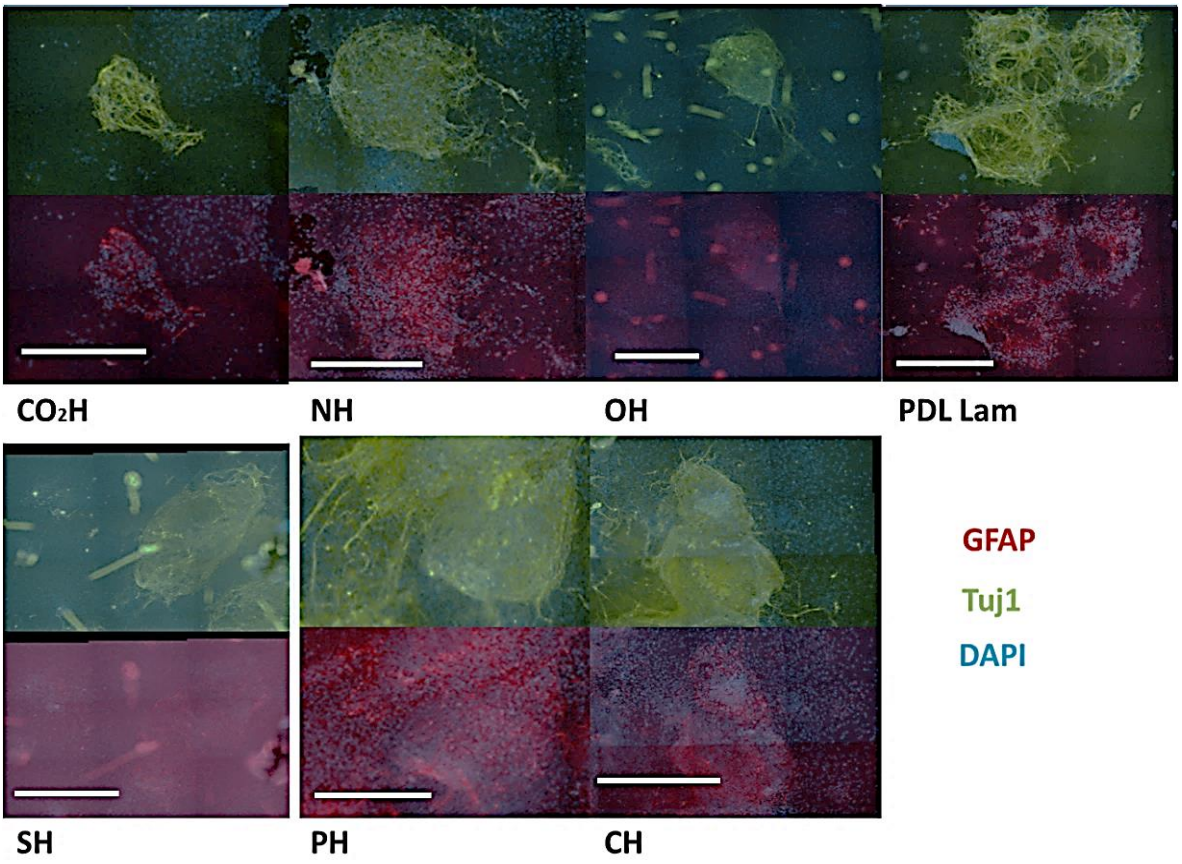

Figure 3 12 - Neural and glia densities at three days on all seven surfaces. Top row has the Tuj1 (green) and DAPI (blue) channels. For comparison the row underneath has glia (red) and DAPI (blue) from the same area. Scale bar is a 600 µm.

However, over longer culture periods this variation was found to reduce with population ratios becoming relatively uniform on repeat samples of individual surfaces.

At day 5 similar ratios were observed, with fewer differences found from surface to surface (**Figure** 3.12). Both hydroxyl and PDL-laminin presented population ratios much

closer to other surfaces at ~0.52. Only neuron/ glia ratios presented on thiol and phenyl surfaces was significantly different at a level of $p < 0.05$, with highest neuron populations being observed on phenyl surfaces. At this time point the highest neural to glia ratio is on the phenyl at roughly 0.6 neurons to every glia, and that is an increase in the ratio of neurons from the first measurements. The ratio of neurons to glia were lowest on the thiol functionalised surfaces with below 0.45 neurons to each glia. As cell culture had continued the ratio of neurons to glia declined, because at the three day time point thiolated surfaces had one of the highest ratios of neurons to glia.

Further culture to 7 days showed an increased difference between cell ratios (**Figure** 3.13). A reduction in neuron fraction on amine surfaces was observed down to a ratio of ~0.38, being significantly different to thiol ($p < 0.01$) and PDL-laminin ($p < 0.001$). The two later samples showed the highest ratio of neurons to glia at ~0.6. On the thiol functionalised surfaces which had the lowest ratio of neurons to glia at the five day time point increased by the final time points to have one of the highest ratios at the final time point. The PDL laminin surface and the thiol functionalised surface had the highest ratio of neurons to glia. Both around the 0.6 neurons to each glia, so there was an increase on the gold standard surface too. On the phenyl surface which had the highest ratio at the previous time point had a slight decline to 0.5 neurons to each glia. At the previous time point that would have been regression to the mean, but at the final time point there was no mean between the surfaces because the values diverged so much. The lowest ratio of neurons to glia was on the amine functionalised surfaces were the amine functionalised surfaces with the ratio around 0.38 neurons per glia. All the measurements apart from the neuron ratio the amine functionalised surface stacked up favorably to the PDL laminin gold standard surface.

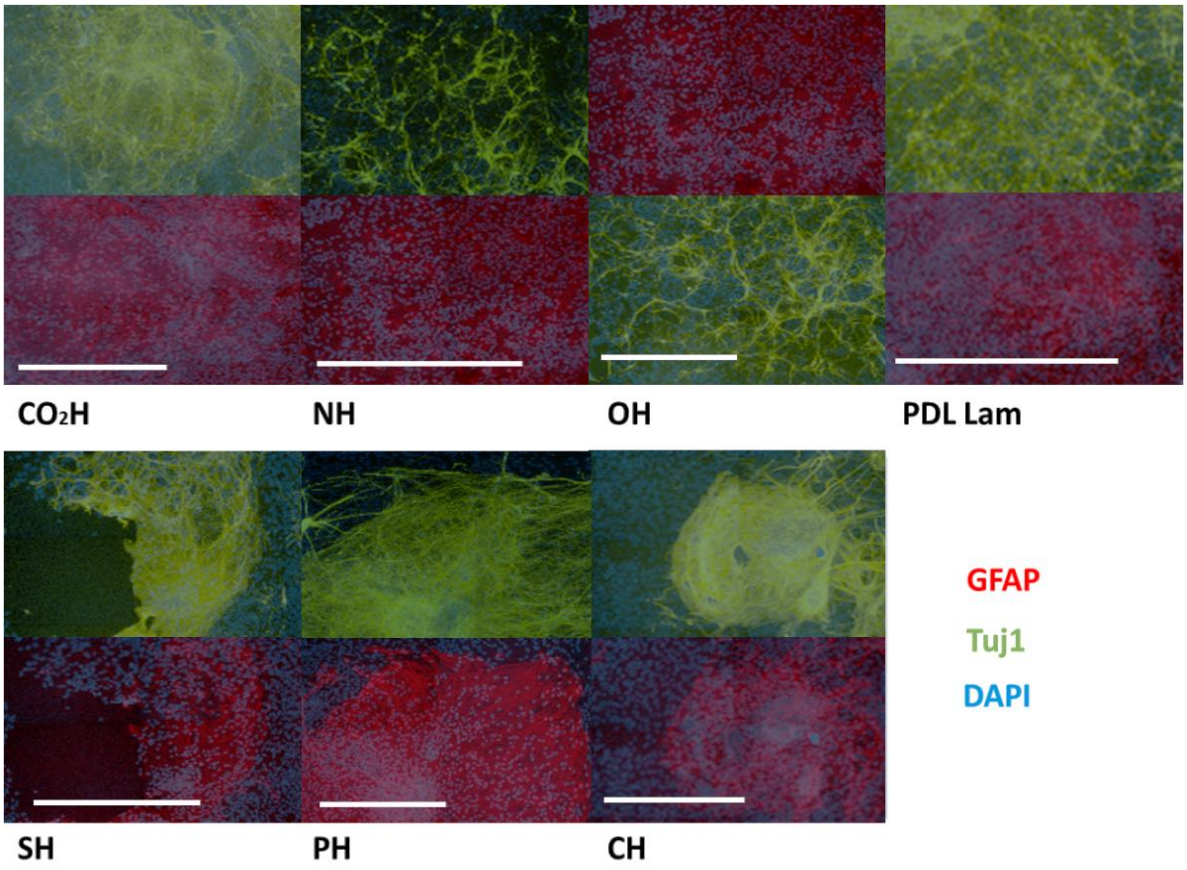

Figure 3.13 - Neural and glia densities at seven days on all seven surfaces. Top row has the Tuj1 (green) and DAPI (blue) channels. For comparison the row underneath has glia (red) and DAPI (blue) from the same area. Scale bar is a 600 µm.

3.2.5 Axon Length

Regeneration of nerve tissue relies heavily on the ability of neural projections to effectively communicate to neighbouring cells, so that electrical conduction across large sections of tissue can be established. Axon lengthening caused by the material is a key indicator of this *in vitro.* One of the biggest promises of neuro-regenerative biomaterial is to grow and guide neurons to specific injured areas, re-wiring compromised neural circuits. Biomaterials are ideal for this is because of a phenomena called 'contact guidance' coined by (Weiss, 1934) neurons follow features on a biomaterial surface. This feature has been exploited successfully with nanofiber surfaces with neurons being aligned by the surface (F. Yang *et al*., 2005). The key challenge is to find simple ways or principles to control the lengthening of neurons which will provide the basis of rewiring neural circuitry in effective stem cell therapies.

The measurement was made by counting the length of individual axonal processes because extension is the next phase of neural colonization of a biomaterial surface. Axonal processes which β-iii-tubulin positive were measured with the free hand line tool in NIS elements (Nikon UK). The values for axon process length were collated, analyzed and graphed in Originlab 9.

Axons were measured for ~300 neurons per surface, taking only those cells where tuj1 clearly defined the entire neurite length. From each surface a distribution of lengths was obtained as would be expected due to differing time of individual cell-surface interaction. These are presented as histograms allowing direct comparison between surfaces at varying time points (**Figure** 3.14).

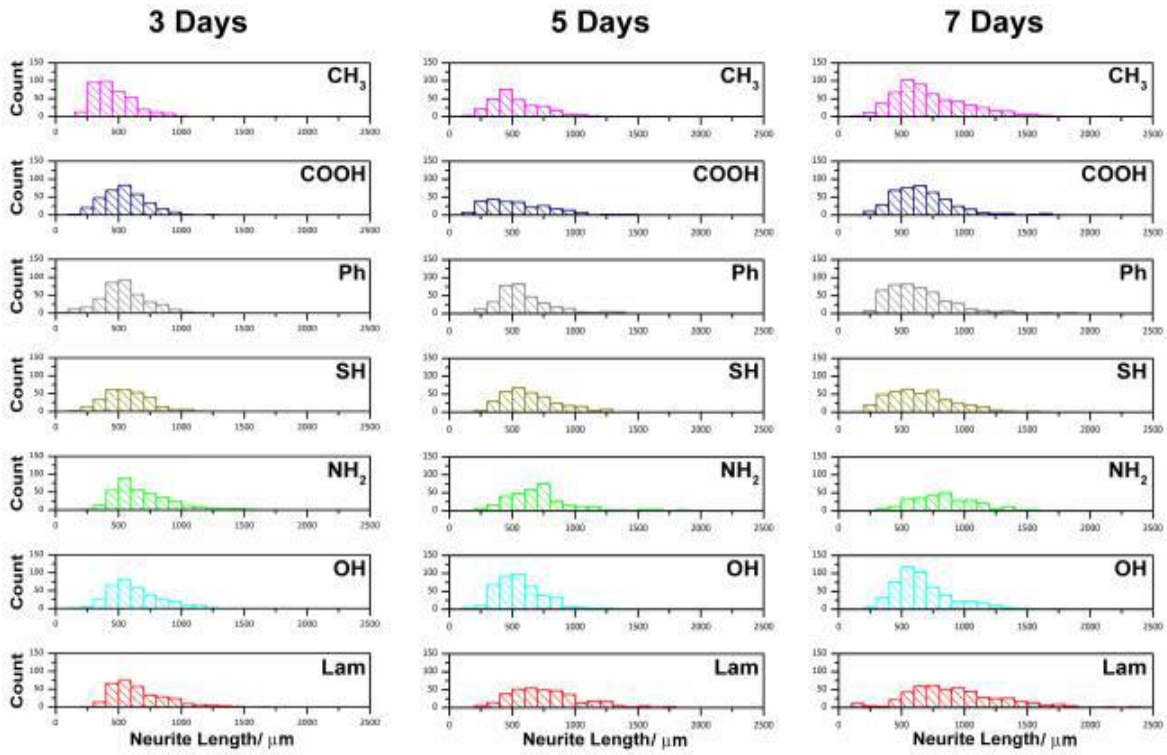

Figure 3.14 - Axon length distributions measured on surfaces presenting differing surface chemistries; fluorescence microscope image showing a representative neuron on an amine functionalised surface at day 7 (green – β3-tubulin, red – GFAP, blue- DAPI nuclear stain); plots show.

After 3 days in culture axonal length distributions were found to be highest on PDL-laminin surfaces, with the smallest population distribution obtained on alkane terminated surfaces. Alkane surfaces also produced the shortest axons by mean average,

with approximately 110 of the axons measuring over 500 µm. The longest axons at day 3 were found to be ~750 µm, with both PDL-laminin and amine functionalised SAMs being comparable.

The distribution in axonal length was not found to significantly increase by day 5, with similar trends observed to those at day 3. The largest axons remained on the amine and PDL-laminin surfaces with average lengths now increased to ~750 µm.

By day 5 the hydroxyl surface has 425 countable lengths, which is highest at this time-point. The phenyl and methyl surfaces both see declines in the number of countable lengths. The thiol surface sees a rise from 291 to 330. With the carboxylic acid, phenyl, hydroxyl and methyl the mean value for neuron lengths is in the 400-600 µm range. With the thiol surface mean value is in the 600-800 µm range, also the 8.8% of the neurons fall in the 1000-2200 µm range, which is nearly as high as the amine surface.

At the seven day time-point 18.3% of the neurite lengths fall within the 1000-2200 µm which is the highest proportion outside the PLL laminin and amine surfaces (**Figure** 3.15). The methyl surface had 568 which is the highest number of countable lengths; the second highest number was on the hydroxyl surface, which produced 518 countable lengths. The mean value for neuron length lies in the 600-800 µm range which is an increase from the two prior time-points, demonstrating that time has a very important role in the lengthening process. The largest distributions of axon length were observed after 7 days in culture. PDL-laminin presented the broadest spectrum of axon lengths, with amine surfaces supporting lesser-defined axons in general. Again amine and PDL-laminin surfaces gave rise to the longest axons, being ~1000 µm compared to those on other surfaces reaching average lengths of ~650 µm.

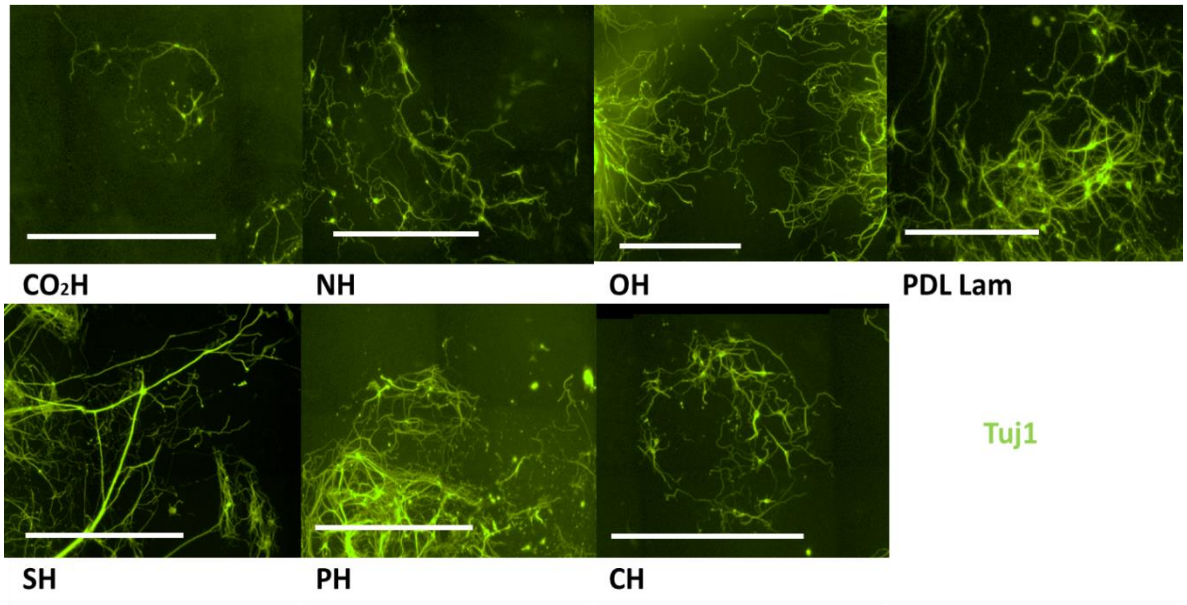

Figure 3.15 – Representative images of axon lengths in the Tuj1channel taken at seven days on all seven surfaces. The scale bar is a 600 µm.

3.3 Discussion

Neural stem / progenitor cell responses have been investigated in repose to culture over a range of selected substrates having defined surface chemical characteristics. The ability of cells to respond to their local environment is of key importance when considering the design of biomaterials for optimum cell culture *in vitro* and *in vivo.* By understanding specific cell-substrate interactions, and how they might lead to specific responses, biological surface engineers hope to be able to strongly influence cells, from differentiation to directed morphological control. Through controlled differentiation processes researchers are attempting to increase selected populations of cells necessary to enhance regeneration of clinical therapies. Numerous protocols to produce dopamine neurons have been developed aiming to treat Parkinson's disease using varying biological cocktail protocols to alter cell state *in vitro* to enrich the fraction of dopamine neurons. These cells die during the progression of this disease and cannot regrow naturally. We investigate the use of defined cell culture substrates to alter cell processes, with an overall aim being to increase neural populations and therefore in the future possibly increase interesting sub-populations. We report the responses of cells derived from E12 Sprague-Dawley rat VM, chosen to maximize the potential of forming dopaminergic neurons (Altman and Bayer, 1981).

3.3.1 Consideration of Surface Characteristics

Although surface chemistry has been widely investigated in terms of directing cell responses, there are no overarching correlations between the chemical property of the surface and its impact on biological response. Functional head groups presented at the surface are often used as a measure of change at the surface, e.g. amine vs carboxylic acid surfaces. Although these labels allow comparison of substrates, it is acknowledged

that they are far from appropriate for the full characterised. An amine surface, for instance, is an umbrella term for a huge variety of amine containing units that could be tethered to a surface with any number of linking groups, being linear or branched and containing any number of other chemical functionalities. In general both amine and carboxyl terminated surfaces have been used to provide a mimic of biological surfaces, and therefore are generally known to support cell adhesion and spreading (Curran et al., 2005).

In the present study a selection of defined self-assembled monolayers were fabricated such that a comprehensive investigation of surface chemical parameters could be assessed with respect to their ability to impact on neural stem cells in the form of neurospheres. Methyl (CH_3), phenyl (Ph), amino (NH_2), hydroxyl (OH), carboxyl (COOH) and thiol (SH) functionalised silanes were fabricated with a direct comparison between PDL-laminin modified glass substrates, which is the current 'gold standard' onto which neural cells adhere and spread well. Glia, however, proliferate rapidly on these substrates therefore the enrichment of neural populations are not favored. Complex protocols involving costly, animal derived biological cocktails are used in conjunction in attempts to direct desired cell responses. Therefore a need has developed to understand material-cell interactions to aid the next generation of advanced biomaterials.

3.3.2 Neural Cell-Surface Interaction

Neurospheres cultured on the range of surfaces tested showed very different characteristics, which evolved differently over the 7 days of culture. Where PDL-laminin surfaces are currently the accepted gold standard surface for neural cell culture, here we demonstrate the potential to increase the capacity of neuron differentiation, along with enhanced axonal elongation. Due to the significant differences in the cell responses

observed, migratory and morphological characteristic control could be accomplished using defined self-assembled monolayers. Upon interaction with surfaces, cells within neurospheres were found to differentiate forming neurons and glia; these migrated away from the neurosphere at different rates depending on the cell-substrate interaction (**Figure** 3.2). Neurons were found to remain within the body of the sphere on methyl and hydroxyl surfaces, whilst spreading well on all other surfaces tested. Glia cells were found to spread well on all surfaces with initial slow migration out of the neurosphere body before 7 days in culture. Silane surfaces have previously been studied by Yong-Juan Ren, *et al*., 2009 where the authors observed cortical-derived neurosphere response to surface functionalization.(Ren *et al*., 2009) The neural specific marker β-III tubulin was expressed at higher levels on carboxyl compared to amine surfaces indicating a degree of control over neural stem cell differentiation.

3.3.3 Neurosphere Spreading

In vivo and *in vitro* the neural stem and progenitor cells reside in distinct niches (Ren *et al*., 2009) (Doetsch *et al.*, 2002) which maintain self-renewal, division and differentiation because the niche provides a good environment for cell-to-cell signaling and region specific signaling (Campos *et al* 2004). As the neural stem and precursor cells develop into mature post-mitotic neurons their density decreases substantially to develop adult tissues and structures (Fuentealba et al., 2012). Low neural density is therefore considered an indicator of tissue maturation. The process is driven by the interaction of cells with 'adhesive' environments, allowing differentiation and in the case of neurosphere attachment to surfaces *in vitro*, driving a homeotypic short range migration *en masse* out of the neurosphere body (Lois, 1996).

In the present study the spreading capacity of neurospheres was measured as a function of the surface area covered by cells as they migrated. Laminin coated surfaces acted as a positive control, showing good adhesion and spreading. Generally it was observed that phenyl surfaces hindered initial migration, **Figure** 3.3. Amine surfaces, commonly suggested to be chemically similar to laminin due to the presence of many multiple primary amine containing residues along its backbone, also showed high levels of spreading. After 3 days in culture amine surfaces in fact showed a significantly higher ($p < 0.001$) average surface area of neurosphere contact at ~0.6 mm^2 compared to those on laminin surfaces, ~0.4 mm^2. After 7 days of culture neurospheres on both surfaces had increased in size to ~1 mm^2 with no major differences between these two surfaces. This The indication was that the initial cell adhesion was enhanced on amine surfaces, with prolonged culture giving rise to comparable cell spreading for amine and laminin surfaces, **Figure** 3.7. For these surfaces a rapid migration of glia was observed away from the neurosphere body, observed at day 3, with subsequent neuron migration observed at day 5. Mats of mixed cell population were formed giving higher area of cell spreading than all other surfaces, because neurons tend to migrate on a glia bed (Edmondson and Hatten 1987).

Thiol, phenyl and carboxyl terminated surfaces showed a similar response to each other, although cell migration occurred somewhat slower compared to amine and laminin surfaces. Carboxyl and thiol surfaces produced cell mats to a lesser extent compared to amine surfaces with an average surface area of ~0.25 mm^2 housing mixed populations of neurons and glia. Negatively charged carboxyl surfaces showed similar trends in terms of neuron/glia ratios, whilst the measured densities of neurons were found to decrease significantly over time. Migration of neurons from the neurosphere body gives rise to much larger spreading areas and therefore lower neural densities in these regions. This

finding demonstrates the enhanced migration of neurons on the carboxyl surface compared to amine and PDL-laminin, suggesting a weaker attachment to this surface. All surfaces gave rise to an increase in neurosphere spreading towards 7 days except thiol terminated surfaces. This was somewhat unexpected due to the nature of thiol to form disulphide bridges with proteins containing cysteine residues on their periphery, and thus form a bound protein, cell-mediating layer. It is possible that the thiolated surfaces promoted disulphide attachment to high abundant, non-adhesive proteins, e.g. serum albumin, thus restricting the ability of cells to attach (Kawamura *et al*., 2013). It is interesting to note that although neurosphere adhesion initially occurred before 3 days in culture, spreading of neurospheres only took hold between 5 to 7 days on all surfaces except those terminated with amine or coated by laminin.

The data collected for neurosphere spreading shows no correlation with regard to wettability at any of the time points analyzed. Surfaces classified either as hydrophilic or hydrophobic present with low spreading (COOH vs CH_3), as well as surfaces of mid-ranging wettability (SH), (**Table 6**). Which demonstrated that chemical functionality plays an important role, further to that denoting the surface wettability. Possibly the largest of the umbrella terms used to define surface characteristics is wettability. This is a generalized term that does not fully characterise the surface presented, with only a proportion of surface-tethered molecules contributing to observed contact angles (Bain and Whitesides, 1988). Surface charge is also often discussed with respect to cell adhesion in terms of associated surface charge accommodating that of the cell membrane (Liu *et al*., 2006). pK_a values can be used as an indicative measure of chemical charge as they represent equilibrium constants for molecular ionization. PDL-laminin coated surfaces could not be assigned a pK_a value due to the complexity of such a large

molecule, possessing many ionisable groups within its structure, although it has an apparent pI ~5 suggesting a net negative charge at pH 7.4.

No correlation was observed between surface chemical pK_a and neurosphere surface area for 3 and 5 days. After 7 days in culture a trend towards higher neurosphere spreading was observed, with both high and low pK_a. A clear demonstration of the influence of pKa was that both positive and negative surface charge plays an important role in determining cell-surface interaction. Less wettable surfaces (Ph and CH_3) also supported neurosphere spreading, with a minimum being observed for mid-ranging SH presenting surfaces.

Table 6: Surface chemical characteristics

Functionality	**WCA /^{o} ± SD**	**ALogP**	**pKa**
-COOH	24.9 ± 2.2	-0.16	2.00
-NH_2	29.2 ± 6.6	0.42	10.71
-SH	45.6 ± 8.2	1.73	11.94
-OH	32.1 ± 7.4	0.65	15.70
-Ph	64.2 ± 2.6	2.84	43.00
-CH_3	65.3 ± 3.5	0.78	48.00
PDL Lam	60.4 ± 7.2	N/A	pI ~ 5

All cell culture was carried out under buffered conditions at pH 7.4, meaning that all surfaces excluding those presenting carboxyl termini were protonated. Both charged and non-wettable surfaces are known to drive protein adsorption through different processes: charge stabilization and hydrophobic interaction (Morgenthaler et al., 2007). Our results highlight surface polarity and charge to be dominant factors affecting neural cell interaction strongly suggesting that the protein layer adsorbed at the surface plays a key role in mediating cell attachment and subsequent responses.

The spreading capability of neurospheres was directly related to the ability of neurons and/ or glia to migrate away from the body of the neurosphere. It is therefore very useful to look at the migration capacity of each of these populations to further

understand biological processes occurring. Cell population densities were normalized to surface area in order to negate any changes related to increasing amount of cells possible to count as they migrated out of the neurosphere body. As spreading on laminin surfaces was observed to increase with increasing culture time but neural density remained relatively constant, it must be assumed that the number of neurons migrating out of the neurosphere also increased over time. This suggests either:

1) longevity of the differentiation process with naïve cells coming into contact with the surface over the 7 days migrating out of the neurosphere body before differentiating into neurons, or

2) Initial cell-surface interaction from within the body of the neurosphere initiates differentiation and these more mature cells reorient within the neurosphere before migrating later (Campos et al, 2004 and Jacques et al, 1998).

3.3.4 Cell Morphology

When dealing with neural cultures, the morphology of neurites is often considered as a good measure of population characteristics; longer neurites are considered to be better for neural connectivity due to increased ability for communication /engraftment of these cells in culture or during transplantation. Specific peptide epitopes derived from laminin are known to steer elongation of neurites, most notably IKVAV (Tashiro *et al*., 1989), with others including KEGYKVRDLNI (Skubitz *et al*., 1991), YIKRKAF (Skubitz *et al*., 1991), RKRLQVQLSIRT (Richard *et al*., 1996) and KNRLTIELEVRT(Richard *et al*., 1996). Our findings support this, with the longest neurites measured on PDL-laminin surfaces, **Figure** 3.14. Amine surfaces did however also demonstrate potential to support neuron elongation, possibly through electrostatic interaction between the surface and the membrane wall, else through the directed adsorption of laminin from culture media.

Initially CH_3 terminated surfaces gave rise to the highest proportion of short neurites (<500 μm), suggesting low level of first interaction of neurons on this surface, which increased with increasing culture time. This is supported by the increasing ability of neurons to migrate over carboxyl terminated surfaces, evidenced by decreasing neural density (**Figure** 3.11). Neurospheres cultured on phenyl surfaces showed a similar trend, although no significant differences were observed between phenyl and hydroxyl presenting surfaces. An indication was that the initial cell interaction might be steer early neurite outgrowth, with adsorbed proteins from media/ secreted from cells during adhesion, act to mediate later stage neurite outgrowth. On all surfaces neurites were found to increase in length over the 7 days in culture. Others have reported similar measures, with no definitive surface characteristic being primarily critical to late stage neurite elongation; Liu (Liu *et al*., 2006) and Nakajima (Nakajima *et al*., 2007) showed neural guidance and tethering of neural signaling factors using amine-rich poly(ethylenimine) tethered surfaces. Lengthening of axons and migrational (extensional) guidance is directed through ECM protein interaction, of being influenced by amine functionalities.

3.3.5 Neural Population

The ability to increase the neural fraction *in vitro* is critical to producing better cell transplant populations for neurodegenerative disorders. Neuron density on amine functionalised surfaces was found to be very similar to PDL-laminin coated surfaces at ~150 neurons mm^{-2}, remaining relatively consistent within standard deviation across the 7 days in culture (**Figure** 3.7). This finding is particularly relevant when considering laminin is the 'gold standard' for neural cultures *in vitro*, with a general drive towards the 3R's tending towards non-animal derived materials.

Initial observation at 3 days suggested that neuron migration was hindered on phenyl surfaces, showing significantly higher neural density compared to laminin substrates ($p< 0.01$, ~1000 neurons mm^{-2}). After 5 days the neural density for all surfaces had either remained constant or reduced, indicating that for some surfaces neuron migration was slower than the increasing neurosphere spreading rate. Neuron densities on phenyl surfaces had reduced to ~550 neurons mm^{-2}, now presenting significantly higher values compared to all other surfaces tested except methyl ($p< 0.01$). The similarity of the non-wettable phenyl and methyl surfaces highlights the importance of surface hydrophobicity in determining cell interactions. However, a simple trend relating neuron density was not found with respect to either wettability nor pK_a as has been shown with other cell types (Mei *et al*., 2010). Suggesting a complex process, likely impacted due to mixture of cell types in this co-culture system. Cell-surface and cell-cell communication results in an elaborate conditioning process wherein differentiating glia and neurons mediate their environment through the deposition of signaling proteins. Attempting to fit such a complicated system to one variable, such as surface wettability, has been discussed in the literature by Dubiel *et al.* as being impossible (Dubiel *et al*., 2011). The balance of contributing factors may be difficult to fully interrogate within this study, although it is clear that surface functionality is an effective leaver on neural density.

Our findings suggest surface chemistry has significant impact on neuron to glia ratio (ANOVA, $F_{(6, 20)} = 3.59$, $p < 0.01$). Culture time was also found to be a significant factor (ANOVA $F_{(2, 20)} = 4.12$, $p < 0.05$). On the PDL laminin control surface the fraction of neurons was found to increase over the three time points, **Figure** 3.11. Amine functionalised surfaces showed very competitive characteristics in terms of initial responses being similar to laminin coated surfaces. Neuron to glia ratios were, however, found to decline over the 7 days in culture, with neural density staying constant

(**Figure** 3.11). This suggests that initial interaction for neural differentiation was very positive on both surfaces, with glia starting to dominate by 7 days on amine surfaces. A Bonferoni *post-hoc* statistical test reveals that the difference between the PDL-laminin and amine functionalised surfaces are not statistically significant, highlighting the potential of these simple, non-animal derived materials to support neural cultures, being of major benefit in terms of the 3Rs.

3.3.6 Differentiation Potential

Materials play an important role in stem cell fate decisions.(Marklein and Burdick, 2010). A key aspect of cell fate decisions are intrinsic and extrinsic signals. Neurospheres are tri-potent mixed cell spheroids of neural stem cells, glia and neural progenitors (Pastrana *et al*., 2011), therefore a useful property of functionalised surfaces would be to influence neural stem cell fate decisions. Neural and glia progenitors arise from neural stem cells through a process of symmetric and asymmetric division (Noctor et al., 2004). Through temporal modulation notch signaling means commitment can be influenced towards glia or neuron phenotype (Grandbarbe et al., 2003). Transcription factors such as STAT3 pathway activation has been shown to control neural stem cell differentiation either towards neuron or glia lineage.(Yanagisawa *et al*., 1999). Complex association of factors affecting gene switching, and therefore protein production, are often difficult to control within a mixture of cells in co-culture, leading to expensive and time consuming methods for production of transplantable cell populations (Kirouac and Zandstra, 2008). An alternative is to influence stem cell commitment with passive forces such as presentation of specific micro-environmental factors through material characteristics. Surface hydrophobicity has been shown to impact on differentiation potential of embryonic stem cells, through control of embryoid body size during culture (Valamehr *et al*., 2008). Stupp *et al.* demonstrated the degree of biological control using laminin

derived peptide IKVAV to steer neural stem cell differentiation towards neural lineage (Silva et al., 2004). Presentation of this bioactive epitope is well known to control neurite outgrowth during cell-surface interactions. Similarly Iwata *et al.* showed two-fold increase in adherence, along with selective and rapid expansion of human neural progenitor cells using surface tethered epidermal and basic fibroblast growth factors (Konagaya et al., 2013). In a similar approach we have shown control over neural stem cells, with a number of factors including *wettability* playing dominant roles in cell responses.

3.4 Chapter Three Conclusions

- Through the presentation of different surface functional groups neural progenitor response was controlled in terms of cell spreading, and proliferation.
- The different chemical properties at the interface affected many stages of the neural biomaterial colonization most effected was: neurosphere spreading, neural density and the proportion of neurons.
- In qualitative and quantitative measures, the gold-standard (PDL Laminin) was matched and exceeded by the amine functionalised surface.

Chapter IV

4 Rationally Bio-Designing Surface Chemistry to Control of Neural Stem Cell Fate

4.1 Introduction

A new theme with biomaterial design is to be 'biologically inspired'. Currently the best known achievements have been incorporation of natural structures into materials such as super-hydrophobic surfaces (Roach *et al*., 2007) and super-adhesive surfaces (Geim *et al*., 2003) in the macro-sense. The respective biological-inspiration comes from lotus-leaves and gecko feet. Systematic approaches to assess surface functional groups that mimic charged regions on proteins should be developed to further exploit natural features with materials. Biological systems have a strict hierarchy: chemicals (DNA, RNA, simple sugars and amino acids), macromolecules (proteins, lipids and long-chain carbohydrates), organelles (mitochondria, cytoskeleton), cells, tissues, organisms and populations (Castner and Ratner, 2002). Therefore it would be ideal to study the effect of commonly occurring chemistry which occurs in nature to build a hierarchical biologically inspired material. Natural chemistry such as those in peptides are the next obvious place to look. because the tissue and macromolecular scale features have an effect at the single cell level, and the lowest rung of the hierarchy means insights could easily be translated into materials at higher rungs in the hierarchy.

4.1.1 Application of Synthetic Surfaces to Solve Problems in Stem Cell Culture

Without using bio-design principles materials have already been applied to solve some pre-existing problems for the culture of stem cells. Originally pluripotent stem cells were cultured on a layer of irradiated non-dividing mouse fibroblasts, termed a *feeder*

layer. The feeder layer secretes cytokines including TGFβ (James *et al*., 2005) and growth factors such as bFGF (Levenstein *et al*., 2006) maintaining pluripotency. In terms of producing a cell therapy or a reliable bank for drug testing the feeder layer method is non-scalable because of variability, costs and preparation. The next surface innovation in embryonic stem cell culture was matrigel, which is xenogeneic extra cellular matrix. Pluripotent stem cell culture utilizing matrigel surfaces are robust (Xu *et al*., 2001), maintaining stem cell properties for long periods. There were fears of xenogenic contamination although clinical grade Matrigel^{tm} is available, the principle problem is that there is batch to batch variability, undefined formulation and it is difficult to scale production (Meng *et al*., 2010). New synthetic culture surfaces have been produced to address these problems. Villa-Diaz *et al.* demonstrated the use of poly[2-(methacryloyloxy)ethyl dimethyl-(3-sulfopropyl)ammonium hydroxide] for support of pluripotent stem culture maintaining relevant markers (oct4 and sox2) for 25 passages in serum supplemented media and 10 passages in defined serum-free media. Peptide-acrylate surfaces were developed by (Melkoumian *et al*., 2010) to expand pluripotent stem cells in defined conditions adding robustness to a process with repeatability problems. Cells were expanded presenting an undifferentiated phenotype and a stable karyotype. Synthetic surfaces are becoming a valuable tool for culturing pluripotent stems cells and made a notoriously difficult cell type more manageable.

4.1.2 Surface Features (Topology) (Tissue Scale)

In the bio-inspired materials paradigm the most success has been with tissue scale features such as topography and stiffness. MSCs/multipotent stem cells have been difficult to culture and engineered surfaces have been designed to improve the culture of MSCs. MSCs reduce inflammation and are freely available so therapies utilizing MSCs for

orthopaedics (Evans *et al*., 2013) and inflammatory diseases (Nasef *et al*., 2008) are close to clinical adoption. Robustness is a positive characteristic of MSCs, however *in vitro* expansion is difficult due to spontaneous differentiation and loss of potency. McMurry *et al.* highlight tissue culture plastic as a problem leading to heterogeneous populations. Their solution was to have a poly(caprolactone) (PCL) surface with nanopits (McMurray *et al*., 2011). It was shown that a disorganized pattern of nanopits was more effective at retaining stem cell potency compared to an ordered array. The majority of cells were found to express *Stro1* for prolonged periods on randomized surfaces. MSCs *in vivo* have slow metabolism, analysis illustrates that the random nanopit surface lowers the cells metabolism.

To design rationally, parameters which influence cell behaviour have to proven and incorporated in to biomaterial design. A clear inspiration is nature by characterisation of physiological and developmental processes. Incorporating physiological and physiochemical cues that influence cell decision making into a biomaterial is labelled as bio-inspired design (Fisher *et al*., 2010). It is thought that substrate stiffness can influence cell fate (Wang *et al*., 1993). Evidence was presented in Engler *et al.* where hard Poly(methyl methacrylate) (PMMA) hydrogels produced hard tissue phenotypes. In a process called mechantransduction (Wang *et al*., 1993) where cells sense environmental mechanics through receptors causing changes in the cytoskeleton. Cardiac muscle tissue has been cultured on material similar to a beating heart which expands and contracts (Song *et al*., 2011). Addition of electrical stimulation the cells would cause the construct to expand and contract.

Hydrogel material is mainly composed of water, so it is ideal to encapsulate soluble extra cellular signalling factors. Changes in stiffness can be coupled with release of biological factors. Adjusting linking between the polymer strands in the hydrogel, changes

pore tortuosity meaning the release of factors can be increased or slowed down (Zhang *et al*., 2009). Different factors are released at different times *in vitro* during the development process, hydrogels can be modified to release separate proteins at different times (Elisseeff *et al*., 2001).

4.1.3 Macromolecular Chemistry Bio-Design (Molecular Scale)

In the bio-design hierarchy the next rung is the macromolecular level, so that would include polypeptides and proteins. Good examples include materials incorporating peptides into the surface. The problem with using extracellular matrix (ECM) proteins to control differentiation are cost and scalability; synthetic surfaces are required to address these challenges. One strategy is to use smaller and synthetic cell adhesive ligands such as peptides or carbohydrates. Maheshwari *et al*., 2000 demonstrated enhanced migration of NR6 cells on poly(ethylene glycol) (PEG) hydrogels with YGRGD 1000-200,000 ligands per micrometre tethered using star shaped poly(ethylene oxide) (PEO). Similarly the cells migrated faster with higher ligand densities. Similarly the α5β1 integrin binding ligand on fibronectin PHSRN was immobilized in Feng *et al* 2004 on gold alkanethiol self-assembled monolayers. Cell adhesion and cell spreading were enhanced on 3T3 fibroblast cells. Surfaces have been modified with KHIFSDDSSE (NCAM ligand) for neural cell adhesion (Kam *et al*., 2002). The KHIFSDDSSE ligand selectively enhanced adhesion of astrocytes in a astrocyte/fibroblast mixed culture. RADA-IKVAV is a neural binding sequence found on laminin controling neural differentiation (Silva *et al*., 2004). This sequence has been used to differentiate PC12 cell lines on planar surfaces (Li and Chau, 2010) and murine progenitors on three dimentional nanofibres (Silva *et al*., 2004). The problem with using the IKVAV peptide sequence is the sequence has to synthesized, and that brings seperate problems such as tricky production, purification, and surface presentation.

4.1.4 Chemistry (Atomic Scale)

The foundation of the biologically-inspired design hierarchy is biologically relevant chemistry. In terms of directing cell response the biological functionalization would effect interactions with biomolecules which cells respond to. Surfaces with biological functional groups can deliver the advantages of ECM coated and peptide surfaces without the preparation difficulty. Curran *et al*., 2005 have demonstrated that a simple molecular layer on the surface of glass can drastically change cell response.

Amine is a common chemical group present in nature in all proteins. Amine groups on biomaterials have positive effects on cell attachment and cell proliferation (Griesser *et al*., 1994), which has been known for 20 years. Amine functionalised surfaces have been used to culture a variety of cell types including cell lines, mesenchymal stem cells, adipose cells, endothelium and osteoblasts (Griesser *et al*., 1994, Curran *et al*., 2006, Chieh *et al*., 2013). Amine-rich polymers provide the basis for *smart* thermo-responsive polymers allowing cell sheet removal to create complex tissues *in vitro* (Cole *et al*., 2009). A further advantage is that amino alky silanes are compatible with lithographic processes for applications such as neural guidance through photolithography (Stenger *et al*., 1992).

The benefits of amino silanes are clear but there are stability issues (Ayala *et al*., 2011). When amino silanes are exposed to water at physiological temperatures the silane is hydrolyzed (Asenath Smith and Chen, 2008). Amine layers where produced by and vapour phase self-assembly at room temperature. The authors found that the surfaces became more hydrophobic after being immersed in water at 40˚C for 48 hours. The layers made in the vapour phase showed the largest change because of patchy multilayer coverage highlighted by atomic force microscopy (AFM). Wang *et al*., 2005 found that the amine functionalised monolayer on a silicon wafer was altered in 10 days when incubated in salt water at 37˚C to model physiological conditions. Water contact angle and surface

topography we observed to alter in the 10 days along with changes in the XPS spectra. By increasing the alkane chain length the stability of the monolayer increased. The reason for the instability was attributed to the lack of order on the aminopropyl, when the chain length is increased the layers become more ordered and stable. Surface energy is an important design parameter, taking into account two material proprieties (Lamour *et al*., 2009):

(1) Cohesion – the degree to which similar molecules *stick* to one another through attraction

(2) Adhesion – the extent to which two dissimilar particles stick to one another

Free energy has been shown to effect lengthening of neurons.

The surface energy was modified by increasing the proportion of amine functionalities. Water contact angle which is attributed to surface free energy is affected by the placement of functionalities (Bain and Whitesides, 1988). By changing the depth on an alkyl chain to which a the functional group was placed it was shown that the water contact angle would stop being affected once the akyl chain length went beyond propyl. This matters because the first stage of biological conditioning the material is rapidly hydrated (Roach *et al*., 2008). The protein absorption which dictates the success of a biomaterial occurs at a solid liquid interface (Mrksich, 2000) meaning conditioning does not occur deep in a polymer network, it is limited to a functional interface.

Keselowsky 2003 *et al.* showed the structure of fibronectin is altered by head group surface chemistry (Keselowsky *et al*., 2003). The head groups controlled cell adhesion and spreading, hydrophilic domains exposed the α5β1 integrin binding domain. However Prime and Whitesides showed quantitatively that polymer chain length affects protein adsorption. When long chain polyesters are hydrolysed more fibrin and collagen was adsorbed (Atthoff and Hilborn, 2007). Surface analysis techniques including quartz

crystal microbalance (QCM) and XPS demonstrated that when more COOH groups throughout the chain were exposed through enzymatic hydrolysis more proteins would adsorb. SEM show that the collagen and fibrin organize into fibrous networks due to charge. So in the design of new biomaterials it is important to take into account more than just wettability because these measures only inform on surface head groups when more properties of the molecule need to considered. Wettability can account for the adsorption of small proteins on hydrophobic surfaces (Sigal *et al*., 1998).

Better tissue culture plastic (TCPS) incorporating biologically relevant chemistry would be good because it has an instantly recognisable yet versatile format which has been used to culture mammalian cells for decades. TCPS is polystyrene which has been plasma treated, introducing surface charge and in some cases roughening too (Barker and LaRocca, 1994). The brilliance of TCPS is the versatility, because polystyrene can be moulded into any shape making it compatible for all. TCPS is transparent, so cells in TCPS can be imaged using un-sophisticated microscopes. However TCPS was not developed with any particular job in mind, so it never achieves optimal results and works best with robust cell lines (Roach *et al*., 2010). Different cell types to the contrary have different needs in terms of cell culture surfaces. Another problem is that from supplier to supplier the TCPS varies (Zeiger *et al*., 2013) which is surprising because the manufacturing process is so similar (Barker and LaRocca, 1994).

One solution which would not disrupt existing workflows is hydrogels coatings of cell culture surfaces to improve the surface interface, and there are already kits available to introduce new surface properties to TCPS (Dow-Corning). Hydrogels which have high water content, the properties such as chemical composition and stiffness are adjustable. Natural hydrogels like collagen and matrigel have been used, this is probably the reason for hydrogel's success is because of hydrogels similarity to ECM (Dalton *et al*., 2002).

Synthetic hydrogels offer the most scalable solution because the properties can be precisely tuned and can be bulk produced through self-assembly. If the hydrogel has good bulk properties but performs badly at the interface modifications can be made. In (Cai *et al*., 2012) poly(ethylene glycol diacrylate) (PEGDA) hydrogel was modified with poly(lysine) which enhanced the culture of neurons. It should be noted that this type of scaffold requires the use of laminin and other expensive reagents.

Chemical functionalization can be patterned for specialist applications. In an attempt to make bone cells grow in a defined tissue architecture photolithography was used to make patterns of N-(2-aminoethyl)-3-aminopropy-trimethoxysilane and dimethyldichlorosilane. In a serum free system where 'sticky' adhesive and non-adhesive zones, sticky vitronectin adsorbed on the N-(2-aminoethyl)-3-aminopropyl-trimethoxysilane patterns. Cell adhesion also occurred in these areas. The amine functionality is extremely important for the adhesion and spreading of cells compared to other chemical surfaces (Faucheux *et al*., 2004). Interesting the authors look at protein adsorption too, and bovine serum albumin (BSA) would adsorb on to all the surface and vitronectin only adsorbed onto the NH_2 surface. Fibronectin however never-adsorbed at detectable levels, possibly indicating fibronectin has to be adsorbed for specific cell responses. Much work has gone into designing fibres for neural cell culture because of the promises of directed migration called *'contact guidance'* (Weiss, 1934). Neurons are typically require specific culture surfaces (Roach *et al*., 2010), and fibres which can guide neurons tend to be polymer such as poly(lactic acid) which have wettability around 70˚ (Navarro *et al*., 2008), and readily dissociates (meaning for the molecule to ionize). This means it is not an ideal surface for neurons because these are not surface characteristics tailored with neurons in mind. So functionalization provides an attractive alternative because it is a method to improve the biological interface.

A simpler approach to biologically functionilize is the amination of fibres as shown in Nisbet *et al.*, 2008. Untreated fibres caused the formation of neurospheres, because the cells wanted to minimise the exposure to the surface. While the amine coated surface caused the cell to adhere more directly and elongated which shows differentiation.

4.1.5 Ideal Surfaces for Stem Cells

The ideal surface for culturing neurons will have to heavily refrence the bio-design paradigm providing the benefits of ECM without the direct use of animal or recombinant ECM molecules to recreate the biological niches. The reason for limiting their usage is because of financial reasons. Another difficulty is translation into animal models and accredited manufacture for cell therapies (Daadi and Steinberg, 2009). Those types of trials require all materials are GMP grade, and have secure supplies.

To meet the potential cell requirement of a neural cell therapy, materials that drive neural stem cell expansion will be required. Neural stem cells (NSCs) will provide the basis for neurodegenerative cell replacement therapies. NSCs are grown in 3D mixed formations called neurospheres (Vescovi *et al*., 1993a) in the presence of bFGF or EGF. Conti *et al.* developed a monolayer method through serum deprivation and using gelatin coated plasticware (Conti *et al*., 2005), the methodology resulted with more nestin positive (neural stem cell marker) cells (Konagaya *et al*., 2011). EGF tethered to poly(styrene) is effective for proliferation of neural stem cells (Konagaya *et al*., 2011). The advantage of the surface was tethered making EGF more stable. On a similar array chip to test growth factors for neural stem cells with solution of recombinant proteins with His residues to bond with the surface. The combination of recombinant bFGF and EGF caused lots of neural stem cell proliferation, the two factors were potent on their own (Konagaya

et al., 2011). What is interesting is EGF and bFGF are diffusible factors and this immobilized form does not affect their activities.

Extra cellular matrix proteins provide instructive cues for cell fate decisions by providing the cell with tissue specific spatial information. Drago *et al*., 1991 demonstrated that laminin surfaces evokes the proliferation and differentiation of neural stem cells, which is basis of gold standard tissue culture protocols of neural cells. Compared to other ECM components including fibronectin and matrigel (mainly collagen) enhances neurite extension, cell division, neuron number and migration (Flanagan *et al*., 2006). The first advantage found was that laminin enhances the activity of EGF and FGF signalling for proliferation which means that laminin modulates cell signalling. Corroborating evidence can be found in Campos *et al*. 2004 because proliferating neurospheres are rich in laminin. Also Flannagan found that α6 integrin is important for neural differentiation, in reverse the β1 integrin is important for maintaining the neural stem cell niche (Lia S. Campos *et al*., 2004). The *REST* gene and its transcription factor product are important for laminin expression *(lama1, lama2, lamb1 and lamc1*) by neurons, this gene is important to prevent the neural phenotype and premature expression (Sun *et al*., 2008). Once the *REST* is down regulated more laminin genes are expressed. The LN-511 isoform produces the longest dendrites (Fusaoka-Nishioka *et al*., 2011). The roles for laminin occur early on in development because it is the first ECM component to be expressed and is found at the inner cell mass stage of development (Darr *et al*., 2006). Surface charge is important for the activity of laminin because denatured laminin by acid washing enhances neurite outgrowth compared to non- denatured laminin (Freire *et al*., 2002). The reasoning is as shown in Roach *et al.* proteins will change conformation upon adsorption surface interface. Different extra cellular matrix proteins can steer neural lineage (Goetz *et al*.,

2006a). Poly(ornethene) laminin surface enrich neural populations while gelatin coated surfaces increase the number of glia.

Morphogens controlling differentiation *in vitro* interact with the extra cellular matrix providing more roles with ECM in embryonic development. The activity of sonic hedgehog (SHH) is closely linked to glycoprotein in extracellular matrix called vitronectin (Pons and Marti, 2000). Also SHH interacts with glycoproteins at the cell surface other than the patched receptor. When SHH interacts with glypican-3 at the cell surface activity is inhibited, and causes endocytosis SHH for degradation (Capurro *et al*., 2008). BMP2 is a morphogen in bone development with specific heparin binding domains (Ruppert *et al*., 1996). The ECM is rich in heparin once bound diffusion of BMP2 is restricted the through the matrix, whilst versions of BMP2 without heparin binding domains are unrestricted. Heparin sulphate is essential for FGF (which is a growth factor) signal transduction (Ornitz, 2000). Adhesive motifs, poly (orniethene) PDL/PLL Laminin, interactions with morphogens, modulation of cell signalling.

Many of the differentiation protocols to manufacture dopaminergic neurons require numerous expensive recombinant proteins; cheap controllable inputs such as tissue culture plastics will improve the differentiation protocols. The materials can be engineered to work in predicatable ways, whereas that is extremely challenging to do with biomolecules.

4.1.6 Material Discovery and Design Rational Using High-Throughput Techniques

The Interactions of biological molecules with materials is complicated, therefore high-throughput techniques will have to be used to get the best results from the *biologically inspired* approach. An assortment of high-throughput biomaterial arrays have been developed to find better biomaterials for stem cell proliferation and differentiation.

The advantage of the array format is that a large assortment materials can be put on a single surface in different combinations. The automation of analysis means hundreds of measurements can be taken from a single image (Zanella *et al*., 2010). In one example Mei *et al*. 2010 form 22 monomomers through photo-polymerization an array of 496 new biomaterials were produced to discover a synthetic surface inducing pluripotent stem cell proliferation, a number of 'hit' materials were found (Mei *et al*., 2010). The method was adapted from Anderson 2004 where a library is synthesized by using a robotic liquid handler adding dots of monomer mixture to the substrate using a mixture of ink-jet and dip-pen deposition methods to cope with different viscosities following a computer designed experimental matrix. The key factor governing biomaterial success is biological interface (Vogler, 2012). Arrays of ECM surfaces have been produced using a similar automated format (Flaim *et al*., 2005). 32 different combinations were produced from 5 ECM proteins. Different proteins have different affinities for surfaces to confirm adsorption, an array was produced which had fluorescently labelled components and imaged. With embryonic stem cells high collagen content steered hepatic differentiation. Recently this ECM array was used to model malignancy (cancerogenic colonization of secondary organs and tissues) *in vitro* (Reticker-Flynn *et al*., 2012). The authors found a new role for α3β1 integrin in the malignancy process. A similar format has been applied for testing neural stem cell proliferation (Konagaya *et al*., 2011). The array confirmed that a combination of EGF and bFGF are effective at driving neural stem cell proliferation. This has been known for a long time but it has never been shown with high-throughput arrays. Arrayed surfaces could be used to also study neural surface markers (Ko *et al*., 2005) which would be useful for drug testing or analysing rare neural subpopulations.

A problem with high-throughput biomaterial screening is that some factors that are more important than others to control cell response. Having some factors can also come

at the cost of others. A new design methodology is emerging where key factors can be used as the basis for Pareto simulations that trade-off factors to produce the best possible result (Besnard *et al*., 2012). The Pareto front are a concept from economics to find the best possible designs when that are trade-offs of requirements that can oppose each other. The main use will be to find an optima, the ability to perform different tasks is compromised which is termed Pareto efficiency. Protein adsorption is the principle factor for controlling cell response (Dubiel *et al*., 2011) through volumes adsorbed and the conformations of adsorbed proteins. Proteins contain many domains with different affinities for a range of properties (Lynch and Dawson, 2008), and Pareto fronts will lead us to materials which perform better when a range of properties need to be considered and difficult trade-offs are required.

4.2 Results

4.2.1 Qualitative Observations

Cells which were fixed and stained after three, five and seven days, and with the early stages of surface colonization being at three days across all three surface functionalities (**Figure** 4.2). On the primary amine surface; the neurospheres showed the most spreading where contact with the surface was maximised. Neural processes extended out of the large cell masses, and albeit the processes were quite short around 400μm**.** The attached neurospheres were quite close together at this time point, but few processes extended from mass to mass demonstrating initial colony networks formation. The extension of processes out of the attached neurospheres was dominated by chain migration as described in (Lois, 1996), where the axons where migrating independently of glia. The glia cells had adhered to the surface but remained present in the core of the attached neurospheres. In these experiments migration and colonization was very much lead by the neurons with the glia in support ***(all shown in Figure 4.1)***. Similarly on the diamine surface the glia were present in their largest numbers in the attached neurosphere interior as shown in **Figure** 4.1. Neurospheres were observed close together on diamine surfaces. Generally the attached neurospheres on the diamine were less mature (with less migration out of the neurospheres) than the primary amine surfaces, but there were some surprising differences such as the outward neural processes. In contrast these were quite long, and some extended into other large cell masses meaning the colony network had started to diversify cell communication away from diffusible signals. The immature look (where neurospheres were mainly intact) was a characteristic of the neural tissue on the triamine surface also. **Figure** 4.1 shows that the processes tended were short with little connection between the spheres at the three day time

point. In contrast to the other two surfaces, the neurospheres were far apart on the triamine surface.

After 5 days of cell culture, colonization had advanced from the previous observations. Neurospheres residing on the primary amine surface had flattened which is indicative of maturation. The axonal processes became longer and more distinguished. Chain migration of neurons was observed, however glia very much lead the migration out if neurospheres at five days because they had projected out furthest. A small number of individually migrated neurons were observed, along with a lot of individually migrated glia cells. Long processes (600 um) reached into many neighbouring spread neurosphere localities. Axonal processes were extending between spread neurospheres on the diamine surface. The extra time in cell culture had caused more flattening of the neurospheres, and there was a range differently sized axonal processes. In the flatter areas, neurons were intermingled with glia, and tended to reside on top of the glia. The migration of neurons and axonal processes was driven by the glia. The furthest outreaches of the cells were glia, which were actively colonizing the diamine surface. In contrast the neurons were leading the colonization of the triamine functionalised surface. Chain migration was the main driver of neural migration on this surface, whereas glia were the driver on the other surfaces. The extra time in cell culture differentiation media had caused maturation of the cells. The triamine surface supported the proliferation of neurons, also the neurons had a clear definition. The connections between the spread neurospheres were thick and numerous.

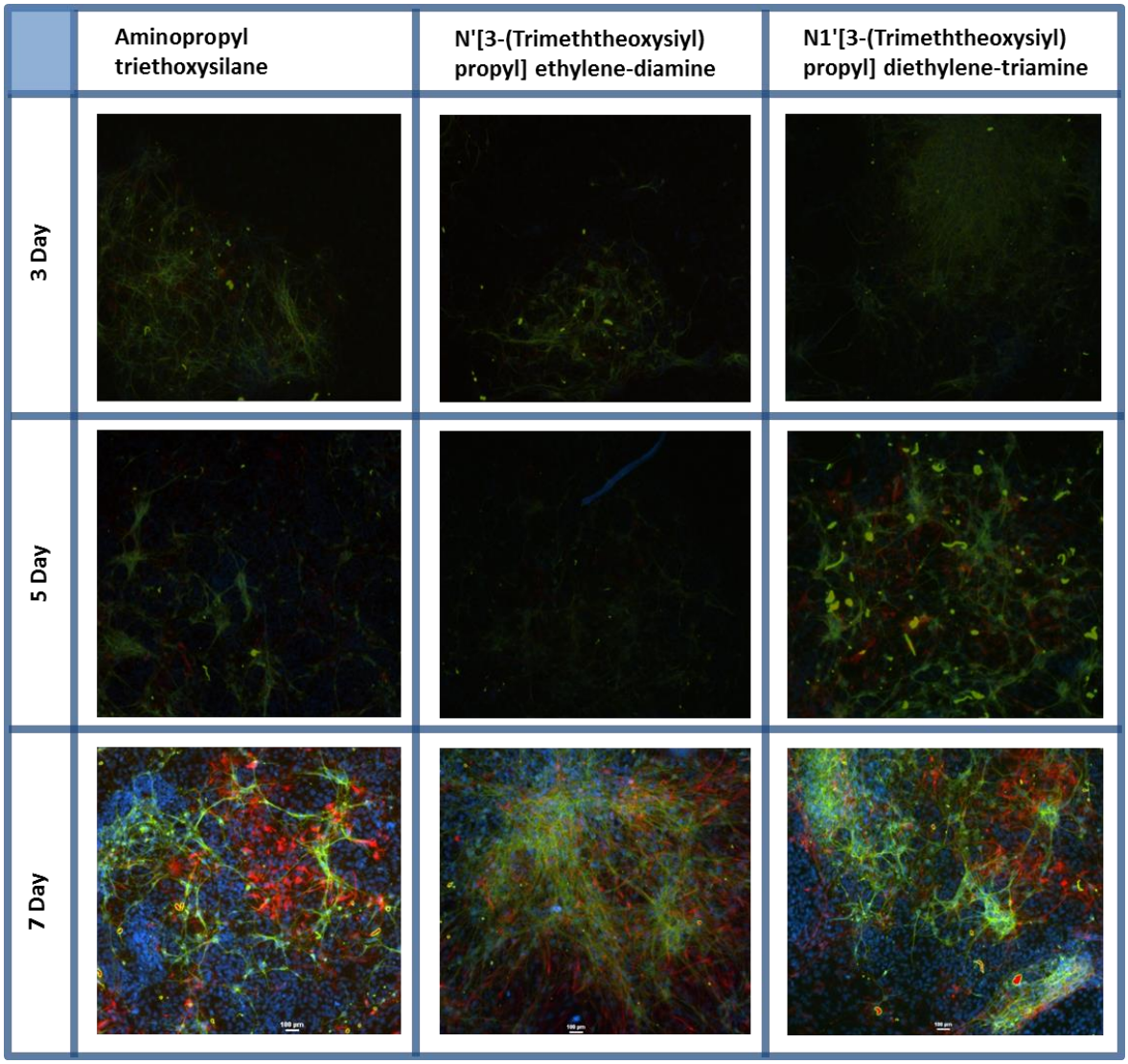

Figure 4.1 –Reprentative fluorescent images on the 3 test surface over the three time points. Aminopropyl triethoxysilane which was the primary amine surface. N'[3-(Trimeththeoxysiyl)propyl] ethylene–diamine (diamine) and N1'[3-(Trimeththeoxysiyl)propyl] diethylene-triamine (triamine). The blue DAPI stains the cell nucleus. Green is Tuj1 which is a neural specific marker, and red is GFAP which is a glia cell marker.

The neural cells continued to mature up to seven days in terms of morphology on the primary amine surface, where there was a low density look was maintained on the primary amine surface. The spreading had continued with a very large area of the surface being covered by the neurons. The neural processes were long and thick indicating there were well developed lines of communications between the cells. The response of the neural cells on the two secondary amine surfaces was contrasting because the cells looked less mature with a retraction of the spread area. The 3D neurospheres (which the surfaces were originally seeded with) were being re-established on the diamine and

triamine surfaces. In terms of the neurosphere maturation, the spheres had quite a small central 3D mass surrounded by a bed of cells largely in monolayer. Within this surrounding area many axonal projections were evident. We refer to this as the 'fried egg' look. On the diamine surface the outward neural processes were dominated by the glia cell populations. The reforming spheres were also quite close to one another on the diamine surface. There were very few axonal processes running between the spheres. The cell response of the neurons to the triamine surface was similar to that presented by the diamine surface. The secondary amines surfaces have altered between the five and the seven day time points because the cell response has altered so drastically.

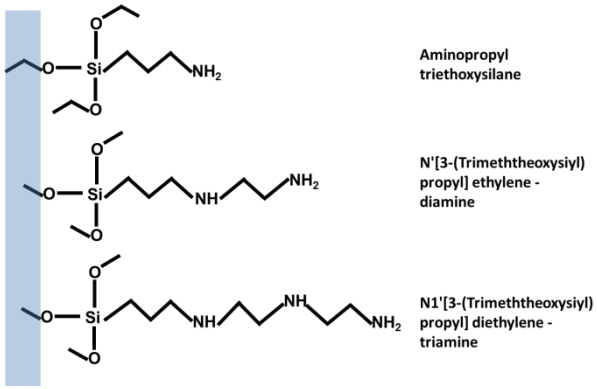

Figure 4.2 – Chemical structure of the aminosilanes used to functionalize the glass microscope coverslides used in the experiments.

4.2.2 Water Contact Angle

Water contact angle (WCA) is a simple and reliable measure of surface wettability, or surface polarity at the interface. Three water contact angle measurements were taken for each surface for reliability purposes, being performed at room temperature. Results are shown in Table 7, showing reproducibility between the repeats.

Table 7 – Water contact angle with standard deviations

Surface	WCA	StDev
Aminopropyl silane	62.3	1.1
Diamine	52.3	0.4
Triamine	40	1.7

Adding more amine made the surfaces more wettable, and more amination caused a linear decrease in wettability (R^2 = 0.9929). The polarity of the biomaterial interface will have a big effect on the biological condition process which was shown with cells.

The XPS data in **Figure 4.3** shows spectra for the primary and secondary amino silane functionalities. Carbon and nitrogen were chosen because all three chemical surface treatments contained alkyl chains, and amine groups. All three surfaces had strong amine spectra. The XPS peaks show the states of the surface functional groups. The amine peak increased in height as amine content per functionalty inceased, so primary amine had the shortest peak and triamine had the highest amine peak. A similar trend was evident with carbon. Small changes to carbon peak height were evident as the length of the akyl chains increased. The primary amine surface had the shortest peak height, while the di- and triamine surfaces had similar carbon peaks heights. The oxygen peaks on the spectra could have been a result of the bonding, glass or contamination. were on the carboxcylic acid and hydroxl functionalised surfaces. The trend for oxygen peak height was the oposite of the nitrogen peak height because decreasing amine content meant that oxygen peak got higher. The primary amine had the highest oxygen peak, and the triamine had the shortest oxygen peak.

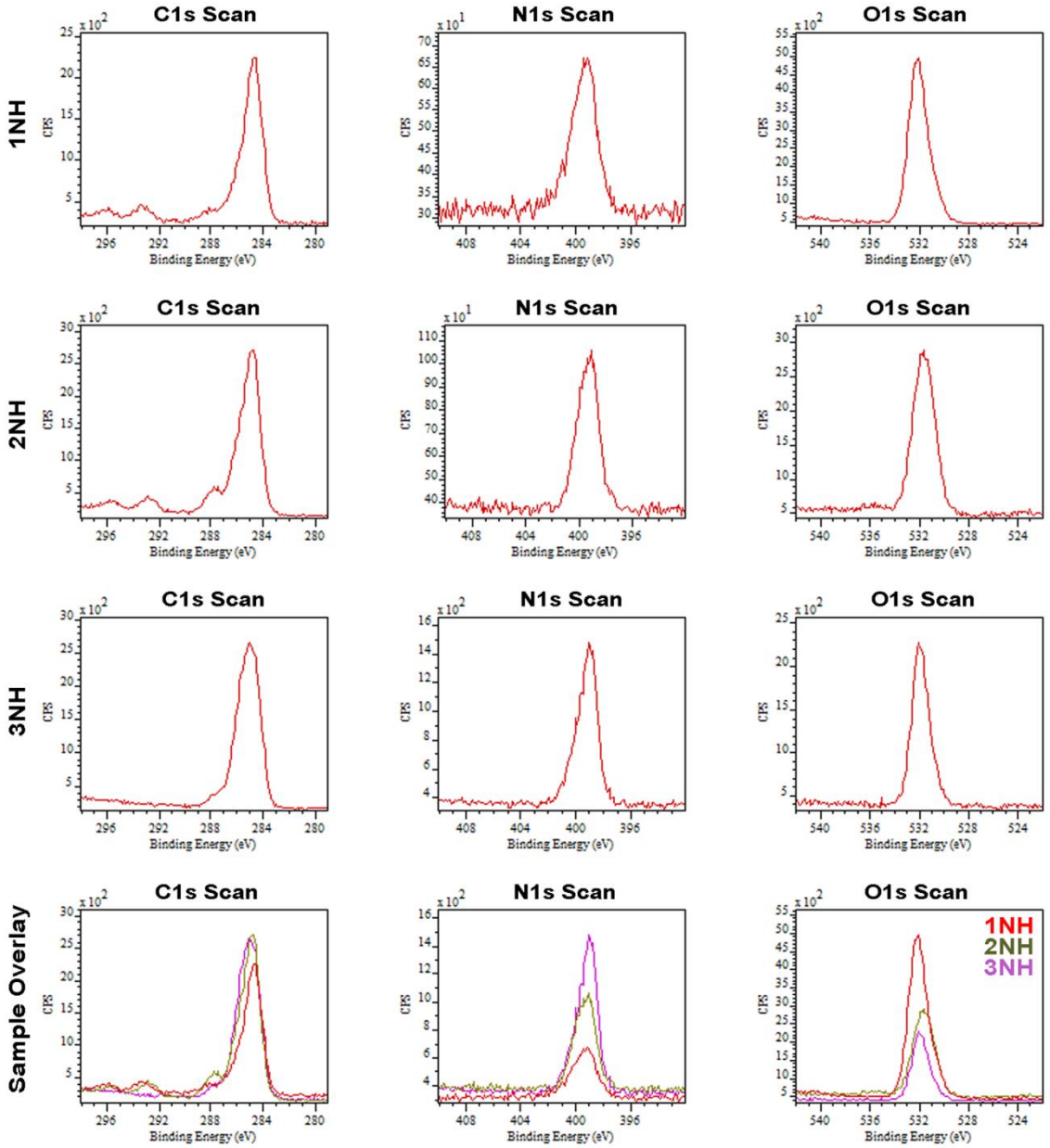

Figure 4.3 - XPS data from the primary and secondary amine silane functionized surfaces. Spectra of three elements are displayed: carbon, nitrogen and oxygen.

4.2.3 Neurosphere Spread Area

The spreading of neurospheres is a relevant measurement to the differentiation of neural stem cells. When neural stem cells and progenitors are cultured as 3 dimentional neurospheres a clear indicator of differentiation is the independent adhesion and migration of cells out of the spheres which causes flattening (Duval *et al*., 2002). The first stage of the differentiation of the neurosphere is the attachment to a surface with high affinity. PDL laminin coated surfaces is the most used surface because of the support of

neural differentiation in cell culture. Here we found the neurosphere tends to be deconstructed and differentiate with first a migration of the glia away from the sphere, which will provide the bed for later neurons migration (Altman and Bayer, 1981). Alternately the neurons can make short range migrations out of the spheres independently of the glia in a process called chain migration (Jacques *et al*., 1998). The key mechanism to control the maintenance of neurospheres and the switch to differentiated monolayers are changes in the integrin adhesion molecules (Lia S. Campos *et al*., 2004).

Neurosphere spreading was assessed to provide a measure of neural colonization by imaging the surfaces at three time points which were 3, 5 and 7 days (**Figure** 4.4). 3 days was selected because it was the shortest time point where the samples were robust enough for cell fixation and antibody staining. Seven days was selected as the longest time point because exceeding the time point would mean that passaging the cells would be necessary which is extremely challenging with differentiated neurons. Over the three time points and the three surfaces the spreading on the surfaces was fairly unique. From three days to five days linear increases occur on all the surfaces. At the seven day time point there was a retraction of neurosphere spreading on the secondary amine surfaces.

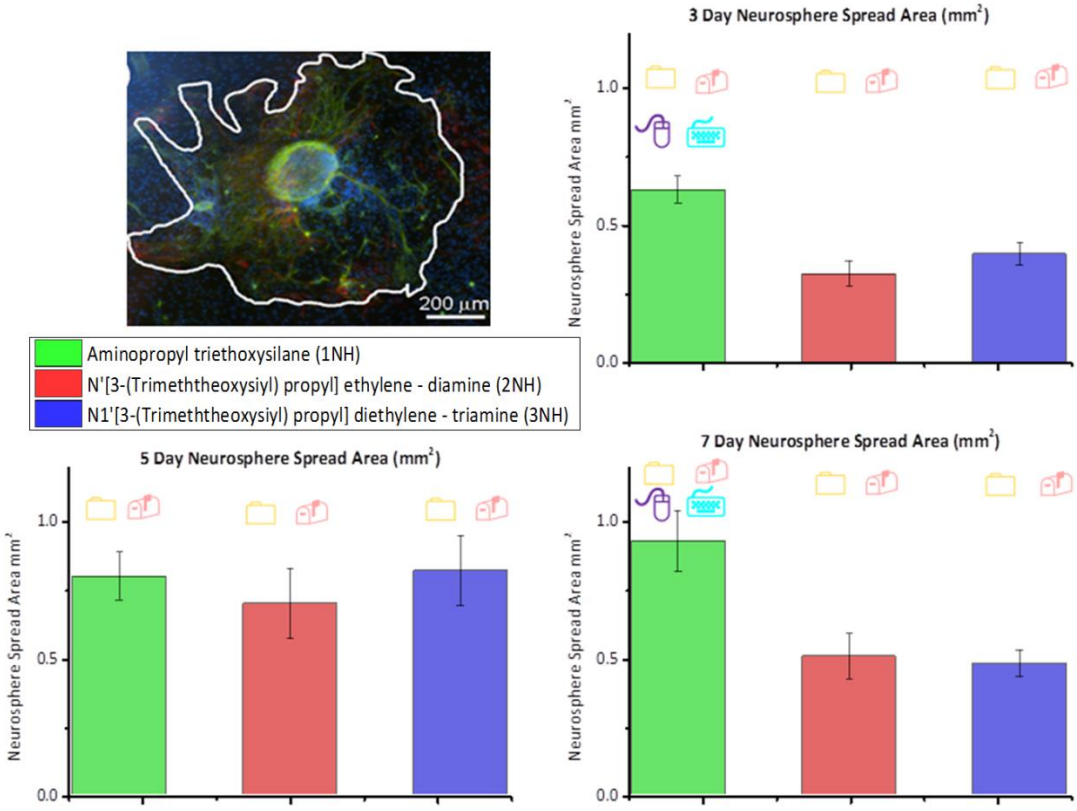

Figure 4.4 – Neurosphere spread over three time points on primary and secondary amine surfaces. The statistics are shown too. One way ANOVA = Significantly Higher Than primary amine = Significantly Higher Than diamine = Significantly Higher Than triamine . Two way ANOVA. = The Means of Time Points are Significantly Different = The Means of Amine Groups are Significantly Different

The most spreading after three days was on the primary amine functionalised glass surface with an average spread area of 0.6 mm^2. The spreading of the flattened rosette far exceeds the size of the original spheroid which means a rapid differentiation of neural stem cells and progenitors. The median spread area was on the diamine functionalised surface which is similar to primary amine but contains an additional secondary amine group. The average spread area on the diamine surface of 0.4 mm^2. The surface which caused the least spreading of the neurospheres was the triamine functionalised surface which had an amine functionality and two secondary amines in the molecule with an average spread area of 0.25. Therefore a trend is highlighted at the three day time point, which is the addition of amines specifically the addition of more secondary amines inhibit the spreading of the neurosphere. Neurosphere spreading was evident on all three surfaces to some extent at the initial three day time point.

Five days of cell culture increased the spreading on all the surfaces with the average spreading converged to a similar point on all the surfaces meaning that a steady trend for spreading was evident at the five day timepoint. This means that the neural cell types on the two surfaces with the secondary amine were able to finally remodel the surface to make the surface interface more conducive to spreading and hence differentiation. The largest value for the spreading was 0.8 mm^2 on the triamine surface. The primary amino and diamino surfaces caused very similar on these two surfaces with both around 0.75 mm^2. The error bars slightly overlap between the data between the two surfaces which means the differences are slight between the surfaces. The largest increase of spreading was seen on the triamine surface increasing by 0.5 mm^2, and the spreading increased by 0.35 mm^2 on the diamine surface. The spreading increased slightly on the primary amino surface, however an upward trend is evident on all the surfaces.

After seven days of cell culture a dramatic change in cell response with the surfaces with the secondary amines (primary amine and diamine) surfaces occurred. The spreading of neurons on the primary amine surface continued its upward trend, and the area increased to 0.9 mm^2 from 0.75 mm^2. On the secondary amine surfaces the observations are very different, because the neural rosettes have decreased in area. On the diamine surface which had one secondary amine the area of the rosette decreased from 0.75 to 0.3 mm^2. The observation on the triamine surface is similar where the rosette spreading decreased from 0.8 to 0.4 mm^2.

Quality control and statistical testing was performed on the neurosphere spreading measurements which were collected from the primary aminosilane surfaces over the three time points. QQ plots (Appedix 4) were made to compare the data collected from the experiment to a normal distribution. Data collected from the experiments (the blue circles) were re-plotted by a cumulative distribution function of the

random variable, and the red line is a reference line. The QQ plots for neurosphere spreading measurements data collected from the aminosilane functionalised surfaces tended to have a negatively skewed distribution. Data from the 3 day QQ plots shows that the data tended to have a negatively skewed distribution most clearly on the diamine surface. The primary amine and triamine surfaces had more normal distributions. The five day QQ plots show that the primary amine and diamine aminosilane surfaces produced negatively skewed neurosphere spreading distributions, and the triamine aminosilane surfaces the distribution was more normal. This was similar at 7 days. To cope with the negative skew the data was transformed following $\log_n$ transformation.

With the aim of maximizing the power of the ANOVA statistical tests the numbers of groups were cut from 25 sampling squares down to 4. The four squares represented the more extreme ends with the purpose of not including transition data which leads to instability in the model. QQ plots were produced for each set of combined neurosphere data groups, and the graphs revealed very negative skews (Appendix 4). To cope with very negative skews in the combined data sets natural logarithmic transformations were performed using an online calculator found at (http://vassarstats.net/trans1.htML) to make the data follow a normal distribution which is an important prerequisite for statistical testing (Howell, 2012). To verify that the distribution of all the data sets used have an equal distribution to test the distributions of data were equal which is another prerequisite for statistical comparisons a Levene's test was performed in originlab. Levene's test showed that the distribution between the 25 sampling squares was not significantly different after the data transformation.

One way and two way ANOVA was performed on the *log*n transformed neurosphere spreading measurements data which followed a normal distribution and there was equal variance between the groups. What the graph shows in **Figure** 4.4 was

that there was a significant difference at the 3 day time point between the groups in the one way ANOVA. Tukey's post-hoc test shows that the primary amine surface caused significantly more spreading than the diamine and triamine . At the five day time point the one way ANOVA could not detect any differences. In the one way ANOVA at the seven day time point the results were similar to the three day time point. The two way ANOVA showed that the population means of the time points were significantly different, and the population means of surface chemistries were significantly different. The interactions between time points and surface chemistries were significantly different. The statistics show that a small change in surface amine content has a significant effect on the spreading of neurospheres on biomaterials determining the early stages of neural differentiation.

4.2.4 Neural Cell Density

A key element to translating the cell culture techniques into large scale process is to keep costs down, so increasing the density of transplant relevant populations is important. New ways have to be found where defined surfaces increase cell numbers, because a defined culture surface would be cheaper and more controllable than the alternatives such as specialist cell culture media, and environmental culture conditions such as hypoxia. The changes in neural cell densities are displayed in **Figure** 4.5. At the early three day time point the neural density measurement informs on neural differentiation because a high density means that neurons are retained within the neurosphere. A low neural density at the three day time point is a strong indicator of differentiation. At the five and seven day time point the measurement is more relevant to proliferation, because Gage's team observed that it takes four days for hippocampal

neurons to divide (Ray *et al*., 1993). Therefore in the VM neurospheres we would not expect to notice cell division until the second five day time, because it takes around six to seven days for cells to double (Ostenfeld et al., 2002). So if neural density remains similar and the spread area is increasing, neurons are dividing to compensate for the expansion. A low cell density means a preference of cells towards autocrine signalling, whereas high cell densities will favour paracrine cell signalling (Lindholm *et al*., 1996). Neural density therefore provides a simple measurement of profound consequences.

Neurons across the neurosphere spread area were counted as a means of quantifying the capacity of neural progenitors to be steered towards neural lineage by the silane surfaces. The counts were made on samples being positive for Tuj1 neuron marker. Neurospheres became flattened enough by day three to allow repeatable, reliable measurements, so none of the cells were obscured by the depth of the larger central neurosphere mass. Due to some variability in neurosphere size, all quantification of neuron numbers were normalized to the neurosphere spreading area on the overwhelming majority of neurons were found. The measurements were made in ImageJ using the free hand area tool and the cell counter plugin, a ratio was made from these values in Originlab 9.

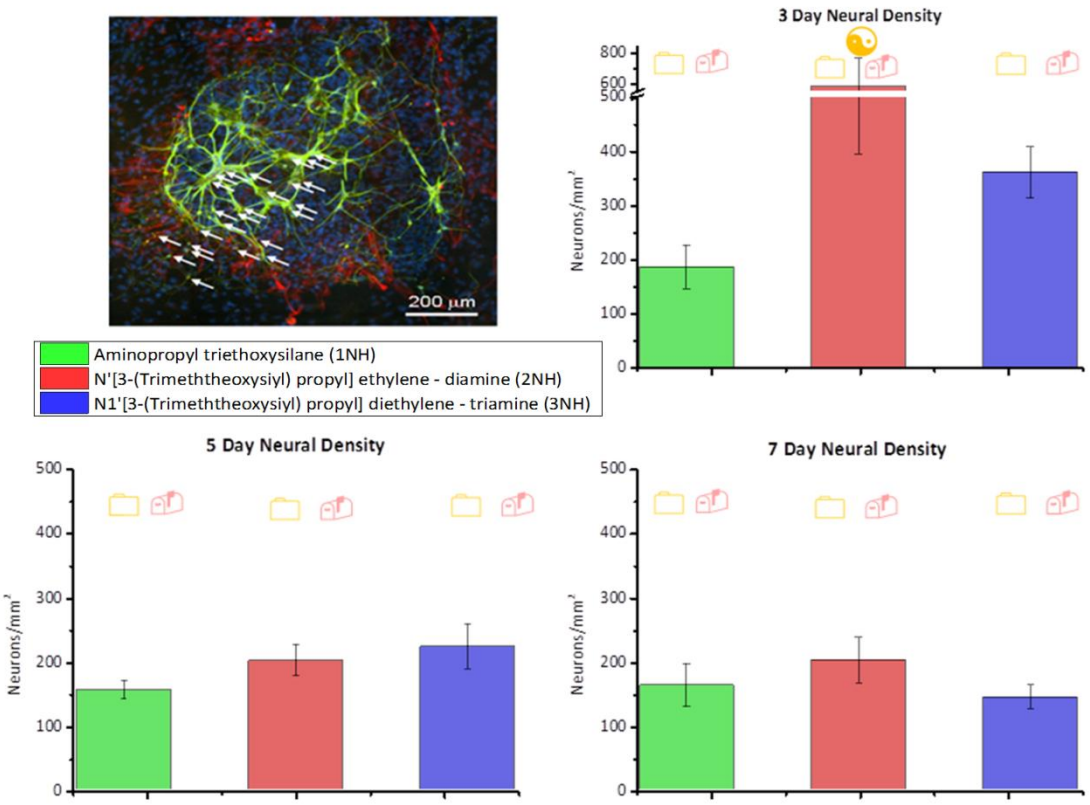

Figure 4.5 – Neural cell density over three time points. The statistics are shown too. One way ANOVA = Significantly Higher Than primary amine = Significantly Higher Than diamine = Significantly Higher Than triamine . Two way ANOVA. = The Means of Time Points are Significantly Different = The Means of Amine Groups are Significantly Different.

The three day time point showed that the neural density measurement was influenced strongly by amine content on the surface (**Figure** 4.6). The most striking observation was that higher amine content means higher neural density, so the differentiation of neurons can be controlled with something as simple as surface amine content. On the primary amine surface the neural density was lowest with 200 neurons per mm^2, which implies a rapid differentiation on the primary amine surface when a link is made with the area measurement. The second lowest neuron density was on the diamine surface above the 200 neurons per mm^2. The big difference with the primary amine surface is that the spread area was much lower, so the diamine surface contains fewer neurons generally. The highest overall neuron density was on the triamine surface with 400 neurons per mm^2. The spreading area on the triamine surface was lowest, so the high density should be viewed as an indicator for inhibition of neural differentiation.

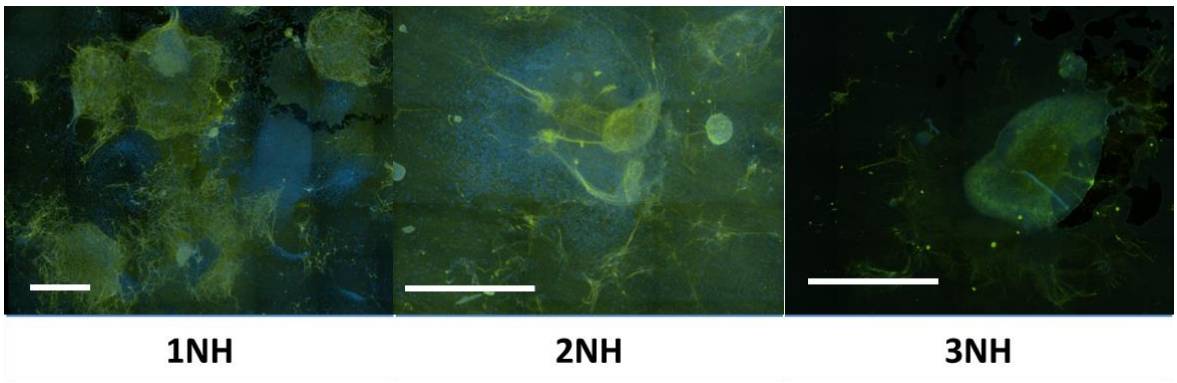

Figure 4.6 – Three day neural density on the primary amine, diamine and triamine functionalised surfaces. The images are tiled 20X images. The green channel is Tuj1 and the blue channel is DAPI. Scale bar is 600µm.

Biological conditioning plays the most important factor in governing the cell responses to the surface at the early time points, so the slight differences in the surfaces through the addition of secondary amine groups were shown to have a big effect on the neural density. Generally, the values for neural cell density converged towards 200 neurons per mm^2 at the five day timepoint (**Figure** 4.7). Which equates to the neural density remaining very similar on some surfaces over time, and the neural density declining a lot on the other surfaces. The neural density showed little alteration from three to five days on 1 amine surface with a neural density of 175 neurons per mm^2, but the spread area increased by about 30%. To compensate for the increase in spread area of the neural rosette the neurons will have proliferated to retain a similar density. The diamine surface caused a slight decrease of neuron density (175 neurons per mm^2) when the measurement was made after five days, however the average spread area has doubled from the three day time point. On the triamine surface the neural cell density decreases by half with the five day samples. There were 400 neurons per mm^2 at three days which declined to just above 200 neurons per mm^2 by the five day time point. At five days the triamine surface also had the highest neural cell density compared to the other surfaces used in these experiments. The decline in neural density was accompanied by a

large increase in the spread area on triamine surface. Which shows the neural colonization is in the early stages on the triamine surfaces.

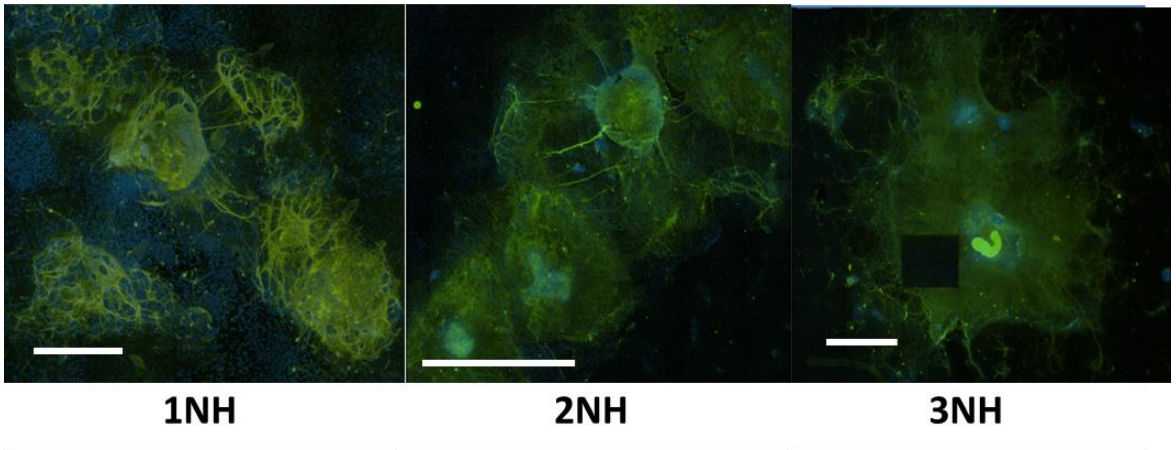

Figure 4.7 - Five day neural density on the primary amine, diamine and triamine functionalised surfaces. The images are tiled 20X images. The green channel is Tuj1 and the blue channel is DAPI. White scale bar is 600µm.

Neural density observations made from the final time point which was seven days showed interesting familiarities and divergences from the previous neural density measurements (**Figure** 4.8). The neural density was normalized to the spread area, and as the seven day time point. On the primary amine surfaces neural densities remained around 200 neurons per mm^2, signifying more steady proliferation across all time points on the primary amine surface. The area increased to 0.9 mm^2 at seven days, so there was a lot of proliferation to compensate for the increase in area. The diamine and triamine functionalised surfaces caused an increase in neural density from just under 150 neurons per mm^2 at five days to just over 200 neurons per mm^2 by day seven. Between the five day and seven day time point spread area halved. Between the five and seven day time point there has been a loss of neurons to account for the increase in density, suggesting some sort of alteration to the surfaces containing secondary amines. The neurons which remain were reforming the neurosphere micro-environment to deal with the changes with adhesion areas at the cell surface interface. The alternative explanation was that the neurosphere reformed, and we were observing re-colonization

of the changed surface. Triamine functionalised surface produced decreases in neural density by about 50%, which was down to 100 neurons per mm^2 from 200 neurons per mm^2. This observation should be coupled with a large decline in neural rosette area which signifies a large loss of neurons between the five and seven day sets of samples. The neural density measurement is similar to the spread area measurement, because there was a big difference between the five and seven day time point. The key to these drastic changes lies in the additions of secondary amines which cause a new response, or are changed during the cell culture.

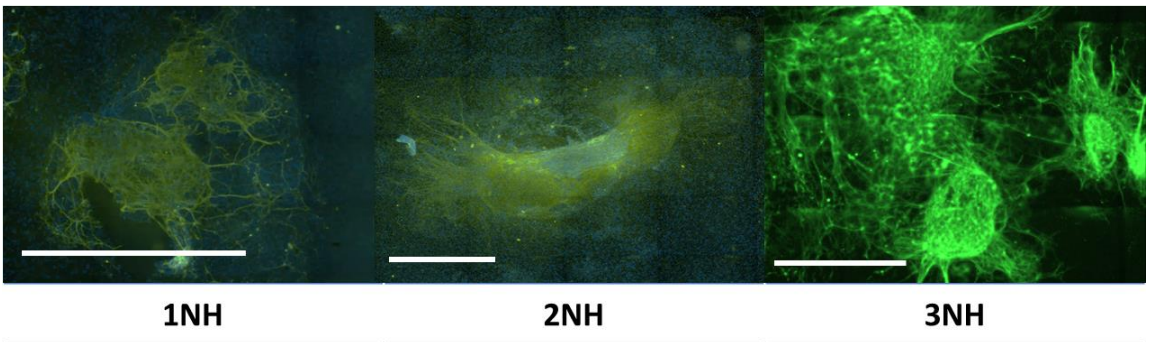

Figure 4.8 - Seven day neural density on the primary amine, diamine and triamine functionalised surfaces. The images are tiled 20X images. The green channel is Tuj1 and the blue channel is DAPI. White scale bar is 600µm.

QQ plots were made to compare the data collected from the experiment to a normal distribution (Appendix 5). The QQ plots for neuron cell density measurements data collected from the surfaces tended to have a slightly negatively skewed distribution. Data from the three day QQ plots shows that the data tended to have a negatively skewed distribution on the primary amine and diamine surfaces. The triamine surfaces had a more normal distribution. The five day QQ plots show that the primary amine, diamine and triamine aminosilane surfaces produced a slightly negatively skewed distributions for neuron cell density. The seven days QQ plots had slightly negative skew. To cope with the slight negative skew the data was transformed to deal with the problems using a square root transformation.

One-way and two-way ANOVA was performed on the square root transformed neuron cell density data which followed a normal distribution indicating equal variance between the groups. What the graph shows in **Figure** 4.5 was that there was a significant difference at the three day time point between the groups in one way ANOVA statistical testing. Tukey's post-hoc test shows that the primary amine surface had a significantly higher cell density than the diamine and triamine aminosilane functionalised surfaces. Which could be due to the increased wettability and surface charge on the di- and triamine sirfaces. At the five and seven day time points the one way ANOVA could not detect any differences. The two way ANOVA showed that the population means of the time points were significantly different, and the population means of surface chemistries were significantly different. The interactions between time points and surface chemistries were significantly different. The statistics show that a small change in surface amine content has a significant effect on the density of neurons. The findings demonstrate cell spacing is a controllable factor.

4.2.5 Neuron to Glia Ratio

A critical quality attribute for a cell therapy is the purity of transplant populations (Rayment and Williams, 2010); increasing the proportion of neurons is a key challenge in translating basic stem cell science into cell therapies. Cell therapies for Parkinson's disease have been tested (Politis *et al*., 2011) one adverse side effect was an increase in uncontrolled movements (dyskinesia) in recipients due to serotinergic contamination of the transplant populations. The long term source of dopaminergic neurons to treat Parkinson's disease will be derived from pluripotent stem cells which bring new and unique risks such as terratoma (Fricker-Gates and Gates, 2010). So increasing the proportion of neurons is important because it is the transplant relevant population. This is particularly true in neural cell cultures where supporting glia and astrocytic fractions trend to dominate cultures with the neurons which are of interest for Parkinson's, Alzheimer's and stroke therapies in the minority. Asymmetric cell division of neuron and glia progeny is a probable explanation, and the fate is controlled by the transcription factor called neurogenin 2 (Miyata *et al*., 2004). Understanding the relation of neural cell division and time is important, so surfaces can be designed and optimised to control cell fates in stem cells.

Neurosphere spread area normalised neural cell densities were divided by normalized glia cell densities which provided the basis of neuron to glia ratio. The measurement informs on the surface's impact on cell fate, *i.e.* if the proportion of one lineage fate can be promoted over another. Neuron to glia ratio (**Figure** 4.9) provides another indicator for differences in cell-surface responses. From all the large images taken from the samples, mixture of neuron and glial cells were observed on the surfaces tested (staining positive for Tuj1 and GFAP respectively). The measurements were made

in Imagej using the free hand area tool and the cell counter plugin, a ratio was made from these values in Originlab 9.

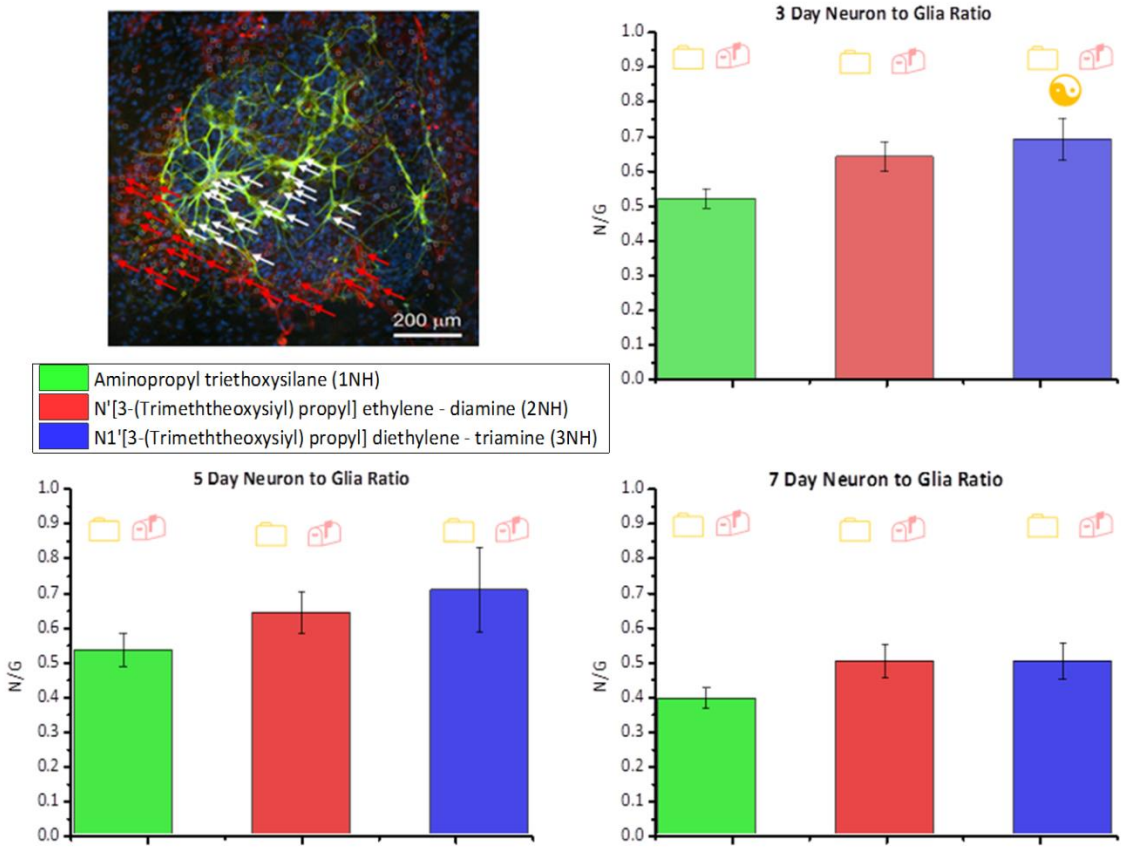

Figure 4.9 – neuron to glia ratio over three time points on the primary and secondary amine surfaces. The statistics are shown too. One way ANOVA = Significantly Higher Than primary amine = Significantly Higher Than diamine = Significantly Higher Than triamine . Two way ANOVA. = The Means of Time Points are Significantly Different = The Means of Amine Groups are Significantly Different.

All the test surfaces had a high proportion of neurons which was a positive indicator for the surfaces tested (**Figure** 4.10). The general trend was evident: higher amine content meant higher proportions of neurons found on the surface. When the proportion is compared to the spread area more neurons are present when there was less spreading on the surfaces with more amines. Which was probably due to the influence of neurospheres retaining neurons. The primary amine surfaces had the lowest proportion of neurons with a ratio of just below 0.5 neurons per glia cell. Spread area was highest on the primary amine surface. Median average was on the diamine surface,

because there were 0.6 neurons per glia. This was the first noticeable rise in neurons to glia because of the addition of a secondary amine. The highest proportion of neurons to glia found at three days was on the triamine surface where we measured 0.7 neurons per glia cell. The values show a perfect incremental increase with neural ratio with the addition of amines at the three day time point. This shows that the stem cell fate decisions can be influenced with the surface at the three day time point; because different ratios were observed on the three surfaces and clear trends were evident.

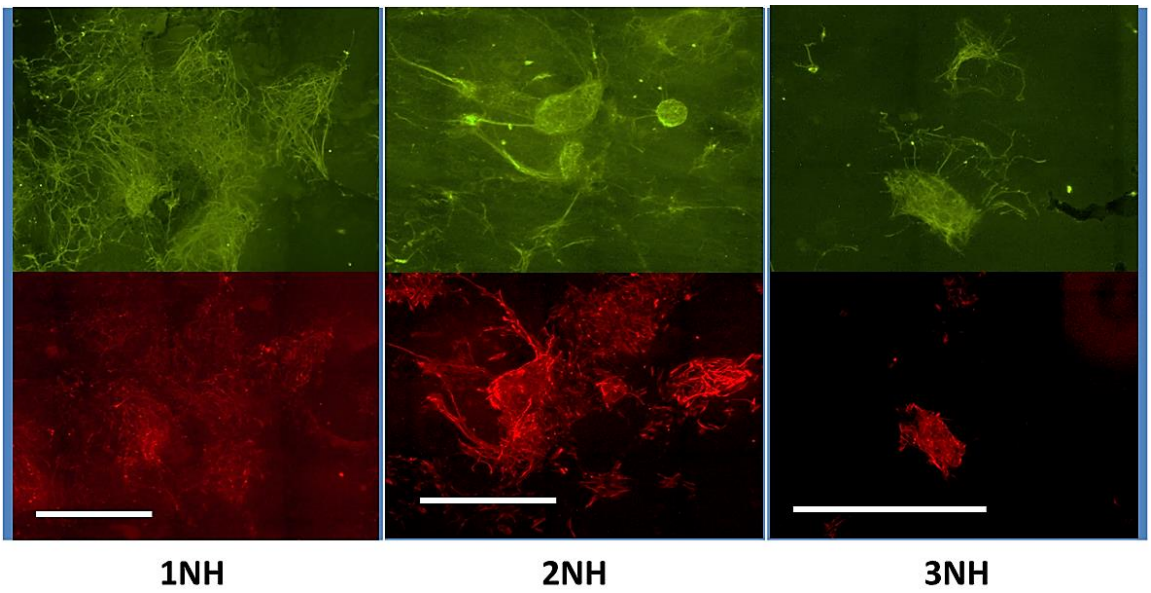

Figure 4.10 –Neural and glia densities at three days on all amine functionalised surfaces. The images are in order of amine content; so 1NH (primary amine) has lowest amine content, and 3NH (triamine) has the highest. Top row has the Tuj1 (green) channel. For comparison the row underneath has glia (red) from the same area. Scale bar is a 600 µm.

When the neuron to glia measurement was made at the subsequent five day time point the upward trend was evident (**Figure** 4.11). An increase in the neuron to glia ratio was still evident when the five day measurement was made. Simultaneous to the increase in the spreading was short range migration of neurons from the original spheroid. Which provides a clear indication that some surfaces are better for culturing neurons on, because increases in cell numbers. On the primary amine surface the ratio of neurons to glia stays around the 0.5 neurons to glia at the five day mark. With the extra proliferation the proportions of neurons remains similar, and about 75% of the population is glia. The

diamine surface had the median neuron to glia ratio of 0.6 neurons to every glia. The diamine surface saw a big increase in spreading and some proliferation, and retained a high proportion of neurons. In a repeat of the three day measurement the triamine surface still had the highest average proportion of neurons to glia (0.7). At this stage there had been a big increase of neuron numbers on the triamine surface, and the neuron concentration was high. These two points mean that the optimum conditions for the most numerous neural populations for potential transplants were at five days on the triamine surface, because numbers and purity of neurons were highest.

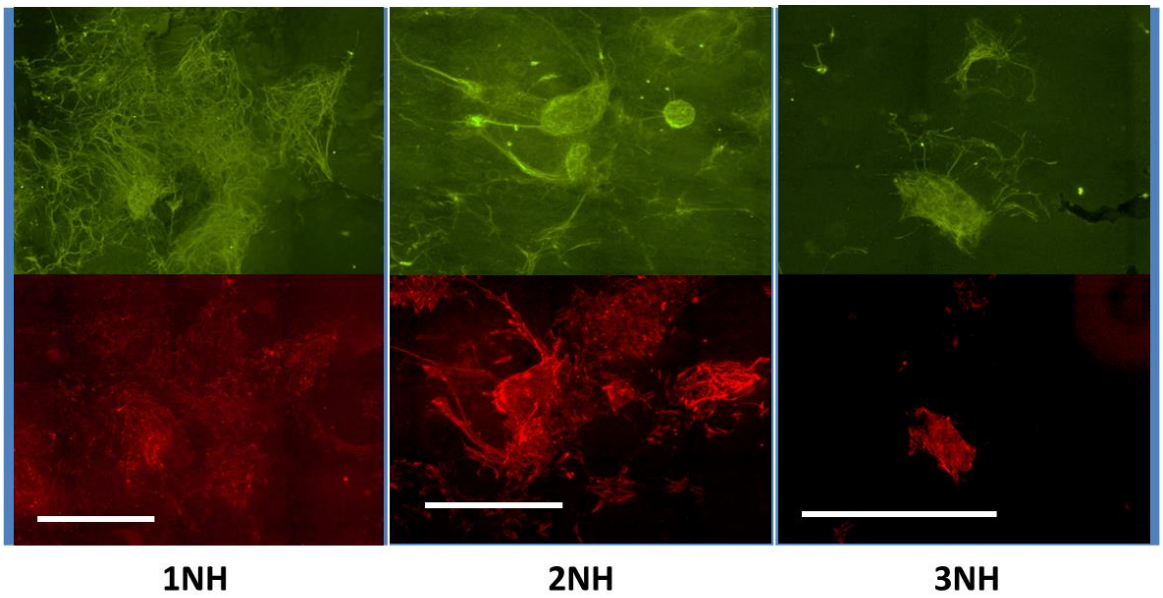

Figure 4.11 – Neural and glia densities at five days on all amine functionalised surfaces. The images are in order of amine content; so 1NH (primary amine) has lowest amine content, and 3NH (triamine) has the highest. Top row has the Tuj1 (green) channel. For comparison the row underneath has glia (red) from the same area. Scale bar is a 600 µm.

The change in trends that has been seen at seven days in regards to the other measurements made such as spread area and neural density were also present in the neuron to glia ratio (**Figure** 4.12). In general there were neurons to glia at the seven day time point compared to the five day time point. The culture of neurons on all the amine surfaces is a time dependent process, because decline happened without exception. On the primary amine amine surface the proportion declined to 0.3 neurons per glia from

0.5. The primary amine surface had the lowest fraction of neurons to glia after seven days of cell culture. In contrast to the primary amine surface the diamine surface had the highest fraction with 0.5 neurons to each glia cell. This value also represents the small decline of the fraction of neurons to glia from five days to seven days. Coinciding with the slight decline in the neurons to glia was retraction of the spread area and reformation of the spheres. Which means the composition of the new spheroid will be different because there are less Tuj1 positive cells in the reformed spheroid. The steepest decline in the fraction of neurons to glia was on the triamine surface, because at seven days there were only 0.4 neurons to each glia. Which was a decline by 0.3 from the five day value. The surface possibly altered at five days. The secondary amine surface tested decreased in terms of neural density and spread area at seven days of culture, but the neuron to glia ratio was uneffected by secondary amine surfaces.

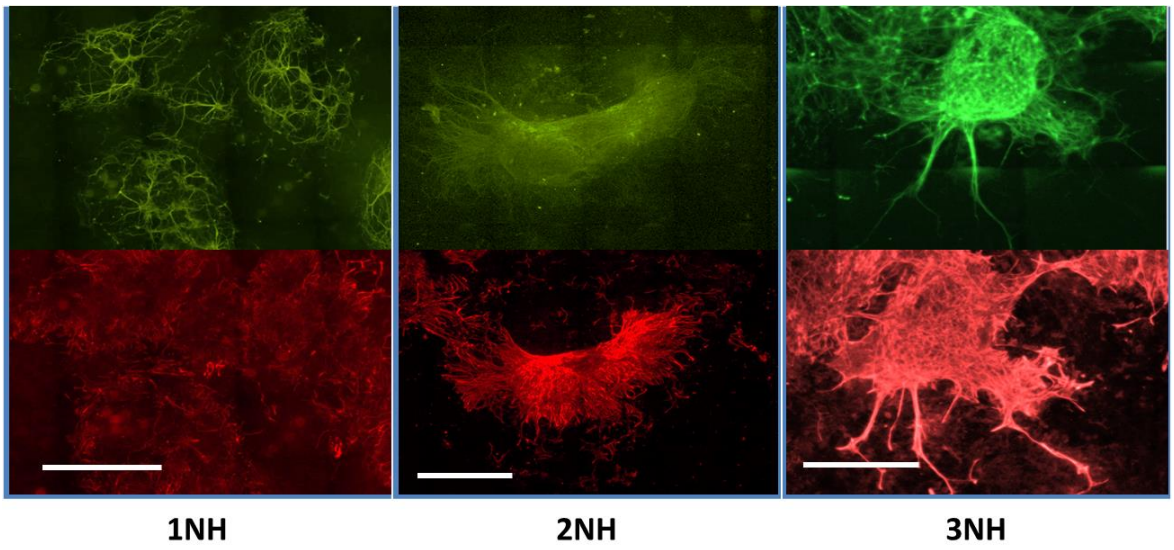

Figure 4.12 - Neural and glia densities at seven days on all amine functionalised surfaces. The images are in order of amine content; so 1NH (primary amine) has lowest amine content, and 3NH (triamine) has the highest. Top row has the Tuj1 (green) channel. For comparison the row underneath has glia (red) from the same area. Scale bar is a 600 µm.

QQ plots and Levene's variance test showed that the data collected for neural to glia ratios required no transformation for statistical testing (Appendix 6). One-way and two-way ANOVA was performed on the neuron to glia ratio measurements which

followed a normal distribution and there was equal variance between the groups. One-way ANOVA statistical testing at the three day time point between the groups showed a significant difference. Tukey's post-hoc test shows that the primary amine surface and diamine aminosilane functionalised surfaces were significantly different. At the five and seven day time points the one way ANOVA could not detect any differences. The two way ANOVA showed that the population means of the time points were significantly different, and the population means of surface chemistries were significantly different. The interactions between time points and surface chemistries were not significantly different. The statistics show that a small change in surface amine content has a significant effect on the fraction of neurons to glia on the surfaces which shows that a surface influences cell fate.

4.2.6 Axon Process Lengths

One of the biggest promises of neuro-regenerative biomaterial is to grow and guide neurons to specific injured areas. In a phenomena called 'contact guidance' coined by Weiss, 1934 when neurons follow features on a biomaterial surface. This feature has been exploited successfully with nanofibre surfaces with neurons being aligned by the surface (F. Yang *et al*., 2005). The key challenge is to find simple ways or principles to control the lengthening of neurons which will provide the basis of rewiring neural circuitry in effective stem cell therapies.

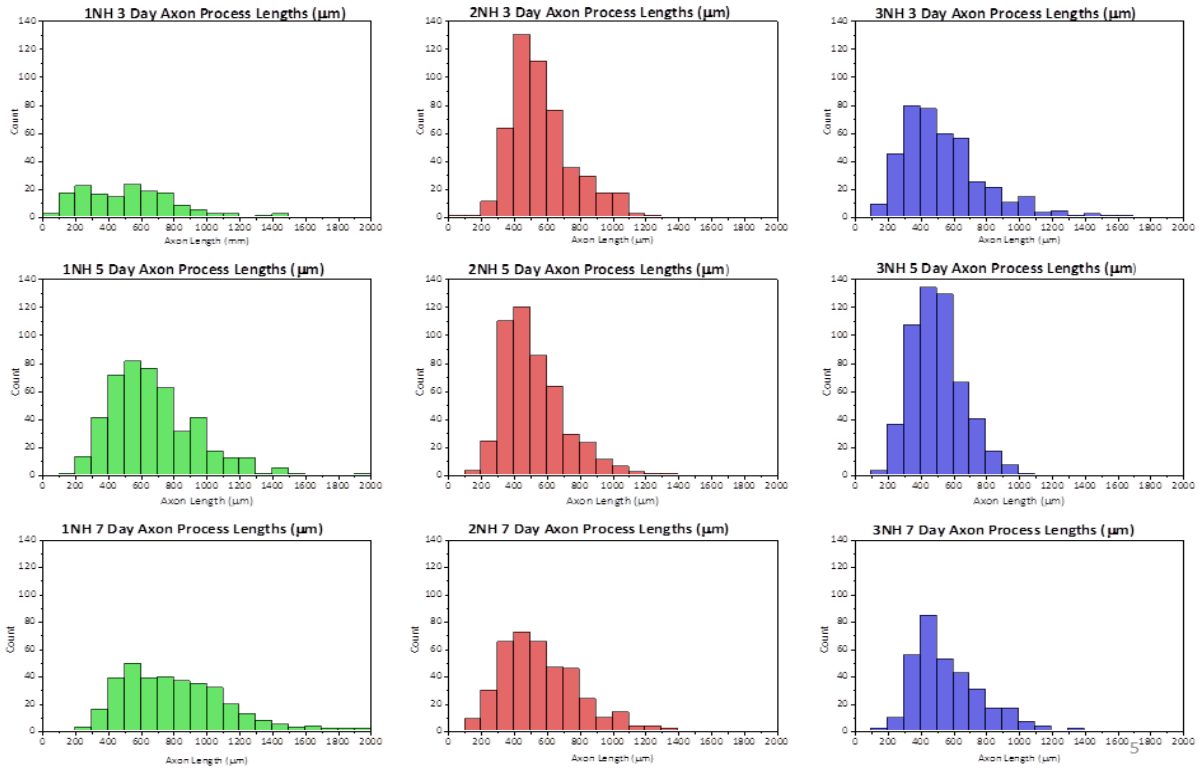

Figure 4.13 - Moving histograms of single axonal process lengths over three separate time points (3, 5 & 7 days)

The measurement was made by counting the length of individual axonal processes because the aim was to control the lengthening of axons using surface chemistry. Axonal processes which Tuj1 positive were measured with the free hand line tool in NIS elements (Nikon UK). **Figure** 4.13 presents histograms informing on outputs such as distribution, frequency, and QQ plots (Appendix 7) to compare theoretical distribution against measured distribution which makes trend spotting simpler.

In accordance to the other measures, axonal process were first measured 3 days into culture (**Figure** 4.14). The primary amine functionalised surfaces which was used in the previous chapter had a wide distribution of axon lengths. The distribution centres around the 500-600 µm mark for the mean. The mode value was around the 400 µm mark. A few extremely long processes were observed which measured 1400 µm. The QQ comparative plots show that the observed data had a positive skew when compared to the normal distribution reference line. The distribution of axonal process lengths on the

centered around 500 - 600 µm on the first secondary amine surface tested (diamine). The mode of axonal lengths appeared around 400 µm on the diamine surface. The QQ plots show that the distribution had wide tails with extreme values appearing at both ends. All the axonal process lengths were very similar at the three day time point the mean and the mode values were the same on the other secondary amine surface tested (triamine). The distribution itself had a positive skew like the primary amine surface, however the conclusion at the three day time point is that axonal process length is not effected by the tested surfaces.

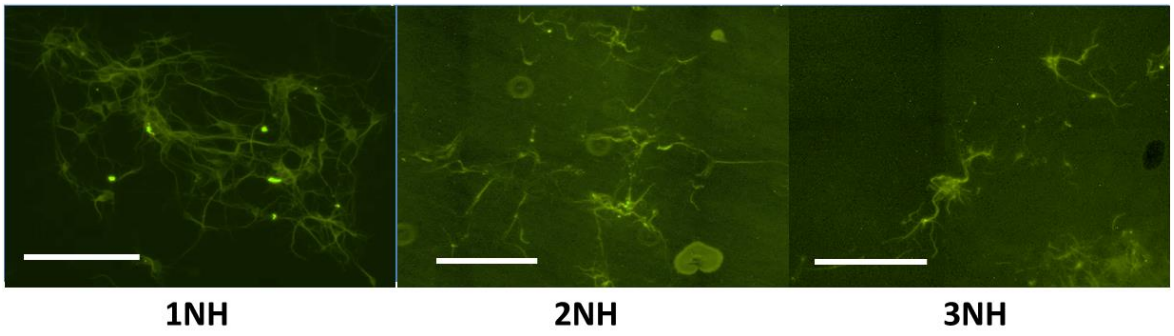

Figure 4.14 - Reprentative images of axon lengths in the Tuj1channel taken at three days on all amine functionalised surfaces. The images are in order of amine content; so 1NH (primary amine) has lowest amine content, and 3NH (triamine) has the highest. The scale bar is a 100 µm.

The observations made at five days show the axonal process lengths were more affected by the surfaces, and particularly the edition of secondary amines (**Figure** 4.15). On the primary amine surface which had a primary amine on the head group position of the molecule caused the values of axon process lengths shifted to the right. The mean for process length on the one amine surface was around 700 µm, and the median value was around 600 µm. The QQ plot show the collated data for axonal process lengths on the primary amine surface retained a positive skew. Compared to the measurements at three days the axonal process lengths did not alter noticeably from 3 to 5 days of culture on the diamine surfaces. The mean and mode values did not change, indeed the exact same stationary response was observed on the triamine surface too. The only differences were

revealed with the QQ plots which showed the distribution of axonal process lengths on the diamine had a positive skew. In contrast QQ plots showed that the data distribution for axonal process lengths had characteristics of a wide tailed distribution. Five days of cell cultured showed that lengthening of axonal processes was inhibited by the addition of secondary amines to the biomaterial surface.

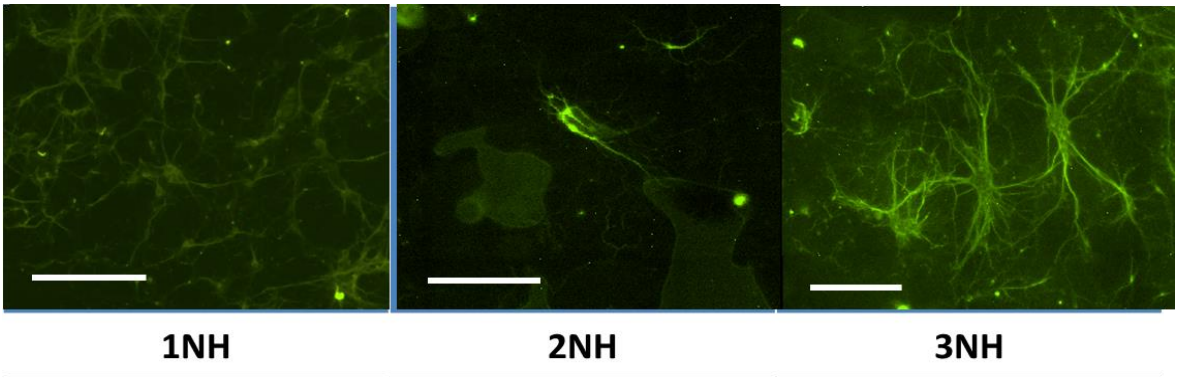

Figure 4.15 - Reprentative images of axon lengths in the Tuj1channel taken at five days on all amine functionalised surfaces. The images are in order of amine content; so 1NH (primary amine) has lowest amine content, and 3NH (triamine) has the highest. The scale bar is a 100 µm.

The trends witnessed at the second time point carried over into the third and final time point at 7 days of cell culture (**Figure** 4.16). The histogram shifted further to the right on the primary amine surface, so repeats a clear trend that the primary amine surface was permissive to the lengthening of axonal processes. The mean axon process length had increased to 800 µm, but the mode still remained at 600 µm. The QQ plot shows that the distribution of axonal process lengths retained the positive skew which was seen with the other two time points. Another interesting observation is that the primary amine surface provided the right environmental conditions for a small population of neurons with very long axons (> 1200 µm) at the three time points which were not witnessed on the secondary amine surfaces. The histograms remained stationary on the di- and triamine secondary amine surfaces, and the QQ plots remained similar.

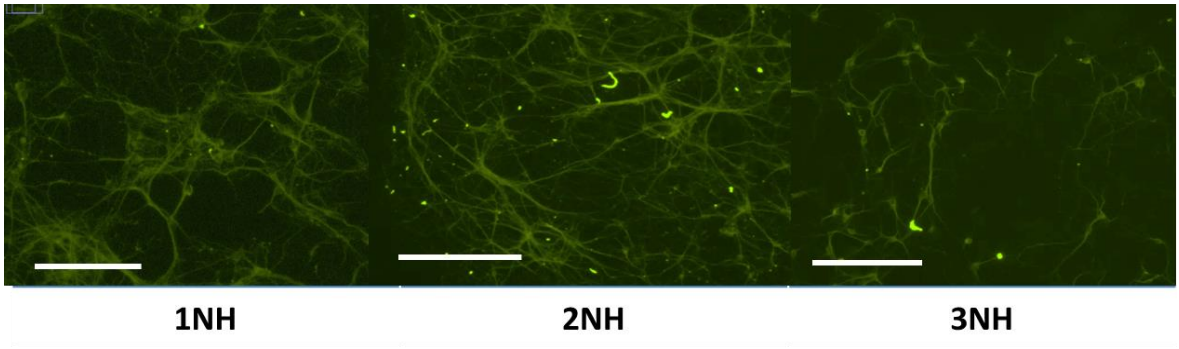

Figure 4.16 - Reprentative images of axon lengths in the Tuj1channel taken at five days on all amine functionalised surfaces. The images are in order of amine content; so 1NH (primary amine) has lowest amine content, and 3NH (triamine) has the highest. The scale bar is a 100 µm.

4.3 Discussion

Translation of stem cell therapies to treat incurable diseases is an important aim for healthcare providers because of the expansion in costs. To expedite the translation of cell therapies surfaces have been highlighted as an ideal tool (Couture, 2011,. Pashuck and Stevens, 2012), because surfaces are simple to define when properties can be introduced in a controllable way. Controlling cell responses in terms of process such as division, differentiation, and migration are difficult to control. A common area of biomedical research is to optimise factors or conditions to achieve better control of cell response. The aim of the work was to follow on from previous work in chapter three, and optimise the surface to control cell response with clear comparisons where only slight changes were made. Frequently in stem cell differentiation research proteins from the development process are added to cell culture media, and proteins which cause the desired response are viewed as being more effective (Caldwell *et al*., 2001). The problem is that the developmental proteins behave differently in cell culture media compared to their natural surroundings in niches, and even when not taking into account dynamics. So when for example two growth factors are compared for cell expansion it is treated as a factor when it should be treated as a condition which requires a different type of analysis and interpretation.

The rational of the experimental design was to compare three different aminosilanes to elicit different neural cell responses. In the biologically inspired designed paradigm the chemistry of the materials is a lower rung in the hierarchy (Castner and Ratner, 2002), but the incorporation of biologically relevant chemistry into future materials will mean some of nature's amazing chemistry can be engineered into materials in a simple way. Secondary amines are the perfect starting point for this approach for biologically inspired design, because of abudance of secondary amines in nature. By

stripping the experimental design into a simple comparison between primary and secondary amine surfaces, speed and versatility was added to the experiment. The analysis of biological responses was simple to analyse with widely available microscopes, and the experiments followed a simple rational which would simplify future optimization. High throughput surface discovery methodologies have emerged (Anderson *et al*., 2004) the cornerstones of the methodology are arrayed surfaces, high content surface and biological characterisation, and multivariate statistical analysis (Mei *et al*., 2009). The problem of these methods is specialist equipment is required for preparation, and correlations between surface properties and cell responses are non-existent (Mei *et al*., 2010), because of the way experiments were put together (R^2 = 0.39 for a linear correlation between colony formation and roughness, and the best correlation was between colony formation and elastic modulus R^2 = 0.88). Unless a 'hit' is found, the principle rational cannot be unpicked to rationally designed better materials. In contrast we used a simpler rational of changing the amine content on the surface.

4.3.1 Colonization of the Surfaces

Currently most biomaterials used in medicine are designed not to interact with the host, and that is problematic in long term implantations. Neurospheres instead of single cells were used in the experiments to assess the biological conditioning of the surface, because the flattening and dismantling of neurospheres provide good indication of differentiation. Over the three time points the primary amine surface had more neurosphere spreading compared to the secondary amine surfaces. When the spreading was next measured at the five day time point spreading had increased on all the surfaces, and the difference between the primary and secondary amine surfaces were negligible. Which means the spreading really caught-up on the secondary amine surface. The final

time point where the spread area was measured was after seven days. On the primary amine surface the spreading of the neurospheres increased, however on the secondary amine surfaces the spreading contracted was observed to reduce. Selection of the time points was about incorporating different parts of the cell material biological conditioning. The three day time point informs on the biological conditioning, and five days was to inform on cell mediated conditioning of the environment where ECM turnover was the key process (Lawrence and Madihally, 2008). The seven day retraction in neurosphere spread might be explained with something on the surface changed which manifested in a spreading retraction. It has been established that serum is important for the attachment of neurospheres to biomaterials as shown in poly(vinyl alcohol) (PVA) poly(ethylene-co-vinyl alcohol) (EVAL) biomaterial comparisons (Hung and Young, 2006). The EVAL and PVA are similar polymers with lots of hydroxyl groups, with the PVA being more hydrophilic. In similar experiments it has been shown laminin adsorbs better on EVAL substrates compared to PVA which was seen with superiors neurosphere spreading (Li *et al*., 2012). Similar observations have been made with fibronectin, however fibronectin enhanced the proportion of neurons (Kearns *et al*., 2003). The early biological conditioning will have made a big impaact on the neural colonzation of the amine functionalised surfaces by being the foundation.

4.3.2 Neuron Lengthening

In neurodegenerative diseases such as Parkinson’s and Alzheimer's the pathology of the disease in the advanced stages have characteristic lesions to the affected areas. In cell therapies to treat Parkinson’s disease, the cell therapy will have to be accompanied by factors which dampen the inhibitory cues present in the hosts to allow for axonal regrowth and functional regeneration (Lindvall *et al*., 2004). For example in spinal injury,

the area concerned will form a glial scar in the early stages where immune cells come in to stabilize the site (Silver and Miller, 2004). The consequence is that axonal growth cones which would reinnervate the site and regenerate function face inhibition. Animal models of Parkinson's disease point towards a number of different chondroitin sulfate-bearing proteoglycans being the main inhibitory cue (Moon *et al*., 2001). To aid regeneration in the animal models the authors used chondroitinase. Material-based solutions are needed to enhance the therapeutic action of cell therapies which will have to overcome the inhibitory cues present in the pathology of neurodegenerative disease. Currently the transplant interventions are highly attrition with limited engraftment, and limited interactions with a majority of the transplanted cells (Ben-Hur *et al*., 2004a).

The findings show a factor to control the lengthening of neurons was controllable due to a simple characteristic of the surface. Indeed the relationship between axon processes and materials have been studied extensively. 'Contact guidance' was first described by Wiess in the 1930's where neurons would align and fellow features of the environment. Early attempts showed neurons could be grown in tracks which allowed for patterning (Kleinfeld *et al*., 1988). Another more precise axon guidance of individual neurons controlled with surface topography was achieved by (Dowell-Mesfin *et al*., 2004) with single cell guidance. Others have shown that the combination of topology and synthesised peptide ligands can mimic the effects of ECM molecules, but in a more precise and controlled manner (Saneinejad and Shoichet, 1998). In terms of getting the surface scale features into more three dimentional constructs fibres provide an attractive option. Alignment of neurons on three dimentional fibre constructs has been shown in (F. Yang *et al*., 2005) where the authors compared the alignment of axons of random and ordered fibres. The axons did not align on the random fibres, but aligned when the fibres where aligned. Fibres can also be functionalised to add further control as shown in (Silva

et al., 2004), where differentiation could be effected by synthesised peptide epitopes. Neural guidance can be controlled with physical feutures on materials, but where the primary and secondary amine surfaces are interesting is that the lengthening of axons is controllable using simple surface chemistry.

In these experiments the first time point measured was at three days of cell culture. At this time point the distribution of axonal process outgrowths centred around 500 µm on the primary and secondary amine surfaces. However as the cell culture progressed on the primary and secondary amine surfaces, it was clear outgrowth of axons was only happening on the primary amine surface. On the secondary amine surfaces, the outgrowth of individual axonal process did not move out further. The histograms of axonal processes outgrowths remain tight on the secondary amine surface over the three time points compared to the primary amine surfaces. One mechanism could cause the outgrowth of individual axonal processes at three days, but secondary processes/mechanisms which caused further lengthening were inhibited on the secondary amine surfaces at the three and five day time points. The distribution of axonal processes lengths might have been wider on the primary amine surfaces, because it could facilitate a wider range of surface/biological mechanisms which cause outgrowth.

Numerous mechanisms have been researched as the cause of axon elongation and guidance and can be broadly classed as: molecular, physiological, and physical. The classical view of axon guidance is that a soluble protein factor will serve as a chemo-attractant. The best established chemo-attractant is nerve growth factor (NGF), where NGF causes the outgrowth of axons. NGF was first isolated after observation of *in vivo* experiments (Levi-Montalcini, 1987). In a comparison between Glial cell line-derived neurotrophic factor, Brain-derived neurotrophic factor, and NT3 in a rat dorsal column lesion model. When NT3 solutions were applied to the lesions, the strongest regeneration

was demonstrated (Bradbury *et al*., 1999). In an interesting knock-out experiment it has been show SHH displays chemoattractant properties with axons (Charron *et al*., 2003). The authors knocked-out Nestrin1 which would take away guidance, when shh was introduced chemo-attractive behaviours would return to the axons. Efforts have been made to get these signals into materials where shallow NGF immobilized gradients the axons from neurospheres extended furthest (Joddar *et al*., 2013). Biomaterials can therefore be used in complicated ways to achieve goals.

The area which will have been most affected by the primary and secondary amine surfaces will have been physical factors. It is well known that epitopes on ECM cause the outgrowth of axons (Skubitz *et al*., 1991, Liesi *et al*., 1989, Kanemoto *et al*. 1990). On the laminin ECM basement protein the epitopes which promote axon outgrowth include: KEGYKVRDLN (Skubitz *et al*., 1991), RNIAEIIKDI (Liesi *et al*., 1989), and IKVAVSADR (Tashiro *et al*., 1989). These epitopes would provide the cues for axon outgrowth on the amine surfaces of laminin or fragments adsorped from the serum from cell culture medium. Another physical cue which could have caused the outgrowth of the individual axons is the NCAM which is present on the surface of neurons and glia and is specific to neural cell types where it is expressed on the surface (Noble *et al*., 1985). Therefore neurons do not have direct contact with the surface. Neurospheres in the experiments were used as sources of both neurons and glia on amine functionalised surfaces. Being able to control axon outgrowth with a simple surface is desirable because the principles can be engineered to present ideal conditions to control axonal outgrowth. Along with producing better cell therapies to treat neurodegenerative diseases efforts are required to get rewiring of effected pathways, because often the rate of engraftment of transplanted cells has been low in animal lesion models (Ben-Hur *et al*., 2004a). If

guidance of transplanted cells be guided then the efficacy of neural cell therapies could be improved.

4.3.3 Cell Populations

To assess the effect of the primary and secondary amine functionalised surfaces on the differentiation of neural stem cells and precursors the neural density and neural fraction were measured. The density of neurons provides a corroborative indicator of differentiation which takes into account expression of the tuj1 neural phenotype marker and physiological/morphological condition of the neurons. This indicates whether the neurons want to spread out as highly differentiated neurons forming extensive networks or as clusters where new networks are being established. After the three day time point the neural density measure informs on proliferation of neurons, because if similar densities are retained with expansion in spreading then neurons have proliferated to keep the density at similar levels. The neural fraction was measured to examine surface promotion for differentiation of the useful (in terms of cell therapy) neural cell population. In standard neural cell culture the glia cell populations will dominate, therefore a simple surface treatment to existing materials would be desirable to control pattern formation (van Ooyen, 2011) and make more of the desirable neural populations for cell therapies in the same space.

Another advantage to controlling the neurons over glia with synthetic surfaces is the elimination of expensive reagents, and passive control of the neural cell linages. This is desirable state of because it leads to a more robust closed system where fewer interventions are required elimnating many perturbations.

Over the three time points a clear observation was that the faction of neurons was higher on the secondary amine surfaces. The fraction of neurons started at 0.51 neurons per glia at three days, and declined to 0.39 neurons per glia after seven days of cell culture which was expected. On diamine surface the fraction of neurons started at 0.63 neurons per glia at three days, and slightly declined by 23% to 0.49 neurons per glia by the final seven day time point. The measurements were similar on triamine surface which was the other secondary amine surface with high neural fractions, and a slight decline. The density of neurons started at 0.69 neurons per glia after three days of cell culture, and that was the highest neural fraction. The neural fraction declined slightly more on the triamine surface (29%) 0.49 neurons per glia when the final seven day time point of cell culture was reached.

The neural density measurements showed findings which could be seen with other measurements made such as neurosphere spreading on the primary amine surface which had a primary amine head group the neuron density started at 184 neurons/mm^2 which was the lowest density, because the neurospheres spread rapidly on the primary amine surface. As cell culture advanced to the terminating time point at seven days the neural density declined to 162 neurons/mm^2, and shows that the surface promoted neural proliferation because the density stayed stable even though the spread area kept increasing. The density of neurons was far higher on the two secondary amine surfaces, because the spreading of neurospheres was far lower and the images show that there were more neurons on the secondary amine surfaces. The density of neurons started at 581 neurons/mm^2 at three days. The next time point was at five days which was 200 neurons/mm^2 showing a steep decline, because the spreading increased. The final time point was at seven days where the density stayed steady at 200 neurons/mm^2, but

the spreading decreased which means a declined in the number of neurons on the diamine surface. The observations were similar on the triamine surface which highlights the influence of the secondary amines. The first measurement of neural density on the triamine surface was 360 neurons/mm^2 after three days of incubation in cell culture media. The neural density had declined (222 neurons/mm^2), because the neurospheres had spread a lot. The spread area contracted at the final time point on the triamine surfaces, and the density was 143 neurons/mm^2. The neuron density had been declining on the triamine surface over the course of cell culture, so the neurons were being lost. The diamine surface most notably at the first time point had a massive neuron density. Which means an ideal time and surface to maximise neuron numbers.

An important factor which biomaterials control are the adsorption of proteins which effect cell response. The serum as discussed earlier is important for the attachment of neurospheres to a surface, but serum can also influence the fate of progenitors and neural stem cells (Li *et al*., 2012). When foetal bovine serum was split into fractions based on molecular weight, and the authors observed more MAPK (neural markers) compared to glia markers when the cells were cultured with low molecular weight fractions serum. Providing an explination for changes in glia numbers across the diffent surfaces. In cell culture the cell density and proximity to other cells has been shown to influence cell fate (Tsai and McKay, 2000). At high densities the progenitors and stem cells would produce neurons and astrocytes, however cells would produce smooth muscle cells. Cell density was controllable across the tested surfaces which shows simple changes to the surface can control complicated stem cell responses.

4.4 Chapter Four Conclusions

- At three and five day measurements secondary amine surfaces outperform the primary amine surfaces in all cell surface response metrics such as cell numbers and the higher ratio of neurons.
- At seven days the performance in terms of neural cell response on the surfaces containing secondary amines declines.
- The only measure unaffected by the secondary amines at seven days of cell culture was the neuron to glia ratio
- Incorporation of biological chemistry in to surfaces will have to studied carefully, in order to prevent negative effects on cells.

Chapter V

5 A Chemical Gradient Platform to Controllably Differentiate and Sort Neural Cell Populations

5.1 Introduction

Gradients are a key part of forming the structure and cell fates during development in many organs and tissues in the body (Ashe and Briscoe, 2006). In order to mimic diffusible morphogen gradients during the conversion of stem cells to mature phenotypes, it is common in stem cell differentiation protocols to use multiple diffusible morphogens applied serially at optimal timings (D'Amour *et al*., 2006). The results can produce highly functional tissue as shown in (Kriks *et al*., 2011b and Oldershaw *et al*., 2010). These methods are resource intensive, and cause challenges in repeatability and scalability because of complexity of protocols (Cohen and Melton, 2011). The protein morphoghens and growth factors are expensive, and more than one tend to be used in a lot of protocols. Another problem with the addition of morphogens in cell culture media is the levels are steady-state which means that the natural gradient dynamic is lost (Saha and Schaffer, 2006). The complexity of differentiation has also made repeatability an issue, because all the steps are a source of perturbations to a fragile system. Another way to reduce production costs, tackle repeatability problems and raise efficiency is by removing unit operations and having a consolidated bioprocess (Lynd *et al*., 2002). In the context of cell therapy production it means producing differentiated cells and expanding stem cells simultaneously. Normally separate steps are required to expand and differentiate, so it would be useful to do both simultaneously. In terms of neural cell therapies for brain repair it would be useful to separate out and enrich cell populations that are more likely to engraft because attrition of transplanted cell populations is so high

(Ben-Hur *et al*., 2004b). Equally, with the move towards stem cell-derived therapies (Fricker-Gates and Gates, 2010) there is a need to generate pure, defined cell populations for transplantation, as undifferentiated proliferating stem cells in the transplant present the risk of teratoma formation (Nussbaum *et al*., 2007). Purity of transplanted cells may also be key in preventing unnecessary graft-induced side effects. For example in Parkinson's disease cell therapies serotonergic neuron impurities in dopaminergic grafts have used been shown to sometimes un-intentionally introduce unwanted movements (dyskinesias) in the recipient (Politis *et al*., 2011). A priority for regenerative medicine is to produce pure transplantable populations in order to get higher efficacy in transplanted neural cell therapies.

5.1.1 Natural Biological Gradients

In development and homeostasis, gradients (physical and diffusible morphoghen gradients) play multiple roles in stem cell differentiation (Ashe and Briscoe, 2006), cell proliferation (Lai *et al*., 2003) and migration (Niethammer *et al*., 2004). Various mathematical models have been proposed to explain diffusible morphogen gradients in neural tube development (Rogers, 2011), and the models also provide predictions and explanation of the system. Alan Turing in the 1950's, later Gierer and Meinhardt., 1972 proposed morphogen gradients and diffusion based self-organisation models. Along the length of the gradient there are different concentration zones specifying different cell fates. For example: in a neural context SHH is produced in the notocord ventral to the neural tube (source) and diffuses upwards towards the dorsal neural tube (sink) (Briscoe et al., 2001). Different neural cell fates are found along the gradient (Ye *et al*., 1998, Blaess *et al*., 2006) with further specification obtained through gene regulatory networks (Jaeger *et al*., 2004). A problem with the model is sustaining the gradient because in a diffusion

chemical system, equilibrium will be reached too rapidly to affect development (Kerszberg and Wolpert, 1998). Newer models propose that the gradient is sustained through other parameters. Some models suggest that the combination of diffusion, degradation and endo/exocytosis of bioactive signalling molecules form and sustain the gradient (Eldar *et al*., 2003,′Kerszberg and Wolpert, 1998). Other models add diffusion tortuosity of the morphogen through the extracellular space to solve the problem (Lander *et al*., 2002). Lander recently highlighted that adding parameters can make models unstable because each parameter will bring new perturbations to the system (Lander, 2013).

Cell migration is often directed with biochemical and physical gradients. *In vitro* mechanotaxis has been witnessed where cell movement is directed in the direction of stiffness, so when the cells are in a softer region, migration is easier when compared to the harder regions (Sochol *et al*., 2011). Motile cells especially in the immune system will move towards the source of chemo-attractant (Zigmond, 1977). Gradient directed migration can be seen with fibroblasts in wound healing assays (Seppa *et al*., 1982). Cell adhesion has been shown to be affected by gradients (Cavalcanti-Adam *et al*., 2007) where changing the spacing of a cell adhesive peptide (RGD which is selective for the $\alpha_v\beta_3$ integrin (Haubner *et al*., 1996) altered cell spreading across a surface in response to the spacing. By moving the RGD peptides closer together cells would spread more because of integrin clustering (Cavalcanti-Adam *et al*., 2007). When spacing of the RGD peptide sequence was incorporated into a gradient (Hirschfeld-Warneken *et al*., 2008) the cell's actin filaments (cytoskeletal component) which are anchored to integrins re-orientated in the direction of the focal adhesions. Therefore if cells polarized in the direction of closer spaced RGD sequences then this property could be manipulated to control surface effects on migratory cells. Utililizing gradients in cell culture would add possibilities which were previously not considered.

5.1.2 *In Vitro* Gradient Surfaces for Biological Testing

Cell culture substrates provide an excellent opportunity to control many biological processes because properties such as gradients can be introduced in a controllable fashion. Hapotaxis which is the migration of cells in the direction of a surface attractant gradient, started as hypothesis where thermodynamics could drive cell migration (Carter., 1967). Later it was shown experimentally with laminin with a chamber system of different laminin concentrations (McCarthy., 1983). One of the benefits of developing an orthogonal dual gradient *i.e.* is amenability to high-throughput methods, which require less resources, multiple experimental factors can be tested simultaneously and samples can be analysed rapidly (F. Yang *et al*., 2009, Zelzer *et al*., 2011). The combination of manual operation make tasks slower, and plastic-ware which has not been designed specifically for the job means that resource usage is sub-optimal. In terms of high-throughput surface testing a number of processes are automated, so the keystones of the methodology are miniaturized surface libraries, large scale measurement acquisition and automated analysis (F. Yang *et al*., 2009)(Anderson *et al*., 2004). High-throughput methodologies incorporating gradients are slightly different where the focus is on optimisation of the surface with a known surface parameter for the desired cell response. The key difference between gradient and spots array high-throughput testing is gradient surfaces are continuous, whereas polymer spots are discontinuous (Hook *et al*., 2012), which means biological nuances are easier to observe on surface gradients. Another advantage to using gradients is that the cell's dynamic extracellular micro-environment can be better mimicked *in vitro*, which is overlooked with conventional poly(styrene) tissue culture plastic which is static (Roach *et al*., 2012). A common problem with tissue culture plastic is that there is variability between the brands in terms of cell response, protein adsorption and material characteristics (Zeiger *et al*., 2013). This is surprising

because the products and production process are similar (Barker and LaRocca, 1994). To improve on current tissue culture surfaces then specific cues to ellicit specific biological responses will have to be engineered in to the surface.

5.1.3 Gradient Surface Production

Gradient surfaces have been produced using 'wet chemistry'. Gradient surfaces where produced by simply immersessing samples in non-reactive paraffin, or exposing to reactive chloro-silane vapour. By altering the immersion and exposure time a functional gradient was engineered (Chaudhury and Whitesides, 1992). The Chaudhry and Whitesides method was adapted to produce orthogonal gradients of polymer density and chain length (Wu *et al*., 2003). First an initiator gradient was anchored to the surface that would control density. Next polymer branches of varying length were grown from the initiator, controlled with parameters such as time, monomer concentration and polymerization temperature. Gradients can also be formed through sequential filling of a reactor with a polymerization mixture (monomer, catalyst, ligand, and solvent) (Xu *et al*., 2005). Mixed polymer surfaces can be prepared by adapting the method to use two monomers, for example to create gradients of poly(methylmethacrylate) and poly(styrene). Various methodologies have been used to make gradients which means an array of chemistries and functionalities can be engineered into gradient surfaces.

5.1.4 Gradient Cell Culture Surfaces

It has been established that chemical surface gradients have a profound effect on the biological interface. Protein adsorption from blood serum on to gradients was affected on to gradients of 2-aminoethyl methacrylate and poly(carboxyethylacrylate) that created

a charge gradient (Ekblad *et al*., 2009). Surface plasmon resonance spectroscopy showed protein adsorption followed the (positively charged) 2-aminoethyl methacrylate gradient with greater protein adsorption with greater charge; while protein would resist the highly concentrated poly(carboxyethylacrylate) (negatively charged) end.

The effect of protein adsorption gradients have been used to study cell spreading as a downstream consequence in Mei *et al*., 2006. Poly(2-hydroxyethylmethacrylate) brushes were used to control adsorption of fibronectin, adsorbed volumes of fibronectin were estimated using a mathmatical model. Cell spreading was affected with increased spreading in areas of low poly(2-hydroxyethylmethacrylate) coverage. The authors estimated more fibronectin adsorbed in areas of low poly(2-hydroxyethylmethacrylate) coverage. Similarly cell adhesion has been controlled with RGD ligand density (Harris *et al*., 2006), where cell adhesion increased linearly with RGD density. Plasma polymerised ppHex/ppAAm wettability gradients have been used as a way of controlling cell density (Zelzer *et al*., 2008). 3T3 fibroblasts in the experiments adhered preferentially on the ppAAm, and the density of cells was lower on the more hydrophobic ppHex. ppHex/ppAAm gradients have been multiplexed with topographical gradients to see if cell morphology of the 3T3 fibroblasts could be controlled further (J. Yang *et al*., 2009). Chemical gradients have also been used to culture neurons. A similar gradient of ppHex/plasma etch glass was used to control hippocampal neural adhesion and cell density/proliferation (Zelzer *et al*., 2011). These neural properties where enhanced on hydrophillic regions of the gradient. Multiplexed chemical and topographical gradients (J. Yang *et al*., 2009) have been adapted for neural co-culture (Roach *et al*., 2012). Inclusion of a mixed neuron/glia culture of structural grooves and changes in wettability provided an effective combination for neural guidance. In essense, allowing a mixed co-culture of neurons and glia to develop also resulted in a higher neural density, because glia were

essential to maintenance and proliferation of neurons. Cell adhesion, spreading, density can be controlled with gradients, and the next place to apply gradient substrates is control of stem cell differentiation. This application is extremely challenging because of the complexity in stem cell differentiation which are usually achieved using complex medias.

In chapter three the neural cell response was enhanced on amine functionalised surfaces in terms of neural differentiation and spreading **(Chapter three)** Therefore we focused on amine functionality using gradients of brush length and density of poly(NIPAAm). NIPAAm has been used in chemical gradient surfaces for cell culture in Li *et al*. 2008. HepG2 Cells (hepatocellular carcinoma) cell attachment could be controlled with temperature and individual cell spreading reacted to the gradient. Depending on the brush thickness in terms of position on the gradient the cells would take longer to detach when cooled. Poly(NIPAAm) is more commonly used in regenerative medicine due to its thermo-responsive nature, and cells can be removed from a surface without the use of enzymes (J. Yang *et al*., 2005). The lower critical solution temperature (LCST) is about 32˚C when cells are cultured at 37˚C (physiological temperature). Below the LCST the NIPAAm takes a strand conformation where it is soluble in water, and above the LCST NIPAAm takes a globular form that is immiscible with water ("Poly(N-isopropylacrylamide)-based Smart Surfaces for Cell Sheet Tissue Engineering," n.d.) thus at below 32˚C (**Figure** 5.1).

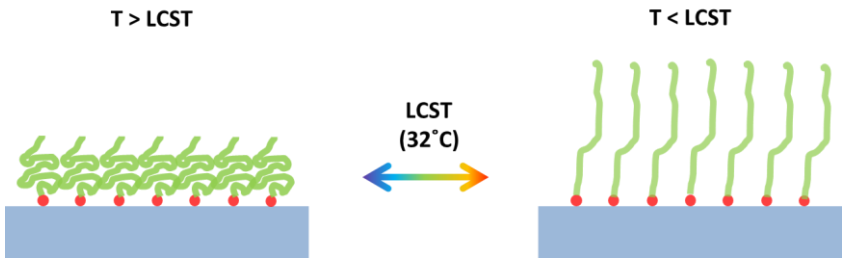

Figure 5.1 - The lower critical solution temperature (LCST). At either end of the LCST the morphology of the NIPAAm polymer chains change.

The next application where gradients which can be used for considerable advantages will be to control problematic stem cell differentiation techniques elimating complexiety and usage of exspensive reagents. NIPAAm gradients provide many advantages which have not been put to full use in previous applications.

5.2 Results

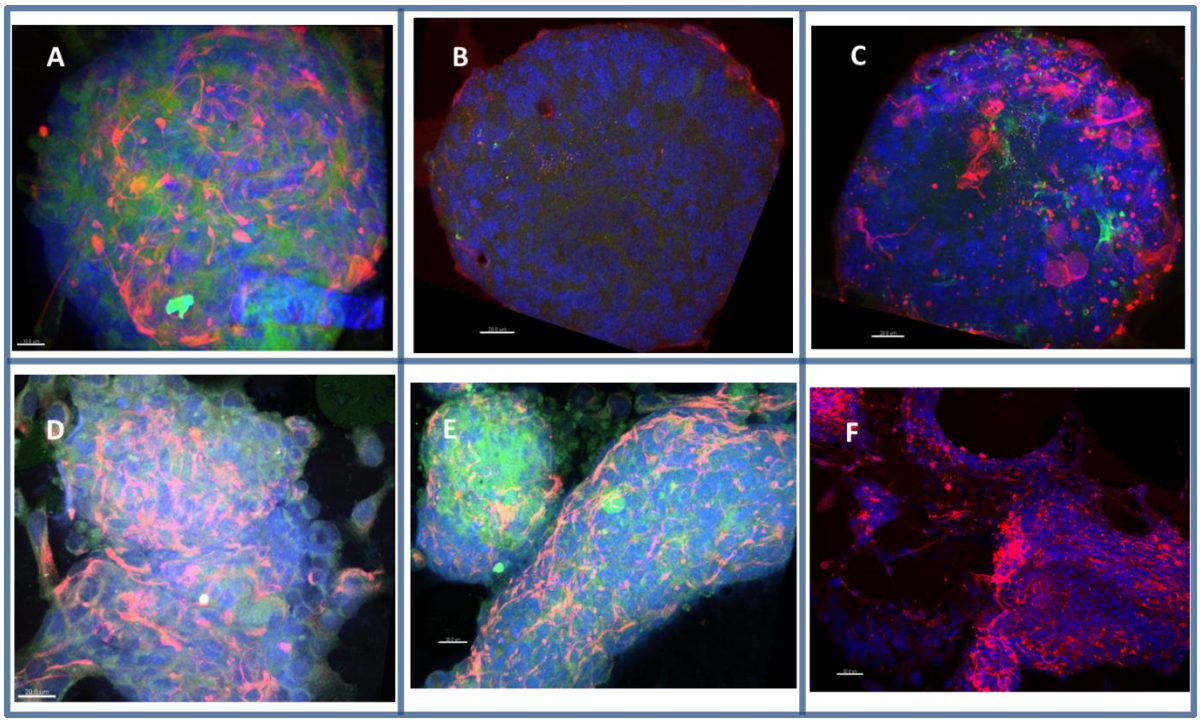

Figure 5 2 – Confocal fluorescence 3D image composits to demonstate organization of the structures on the NIPAAm gradient at different magnifications shown with scale bars. A, B, D & E the images were immunogenically stained for Nestin (red) and Sox2 (green). Pictures C & D were stained for Tuj1 (red) and GFAP (green). (A) show a small spheroid (60X objective lens) lacking organization of the cell lineage. (B) was a bigger more organized spheroid (40X objective lens) with Nestin and morphology positive cells found at the outer cortex. (C) shows neurons and glia in a bigger aggregation and the markers and morphophologies of cell which can be seen at the periphery and core. D & E show very large aggregations (40X nose-peice) which were un-orgaized with no particular localization of phenotypes, persumably sorting would have orccured later. (F) shows a typical neural monolayer (20X objective lens).

5.2.1 Surface Characterisation

Water contact angle (WCA) is a measure of a surface's wettability which will affect the protein conditioning of biomaterial which manefests downstream with cell response. WCA is the measure of polarity at the surface interface with polar parts of the having a lower WCA. Water is used because it is a polar solvent and will maximize its exposure to a polar surface.

5 µL of water was added to the coverslip with a Hamilton syringe. 20 droplets were placed and imaged on the gradient surface with the varying wettabilies recorded and measured using the LBADSA pluggin for ImageJ.

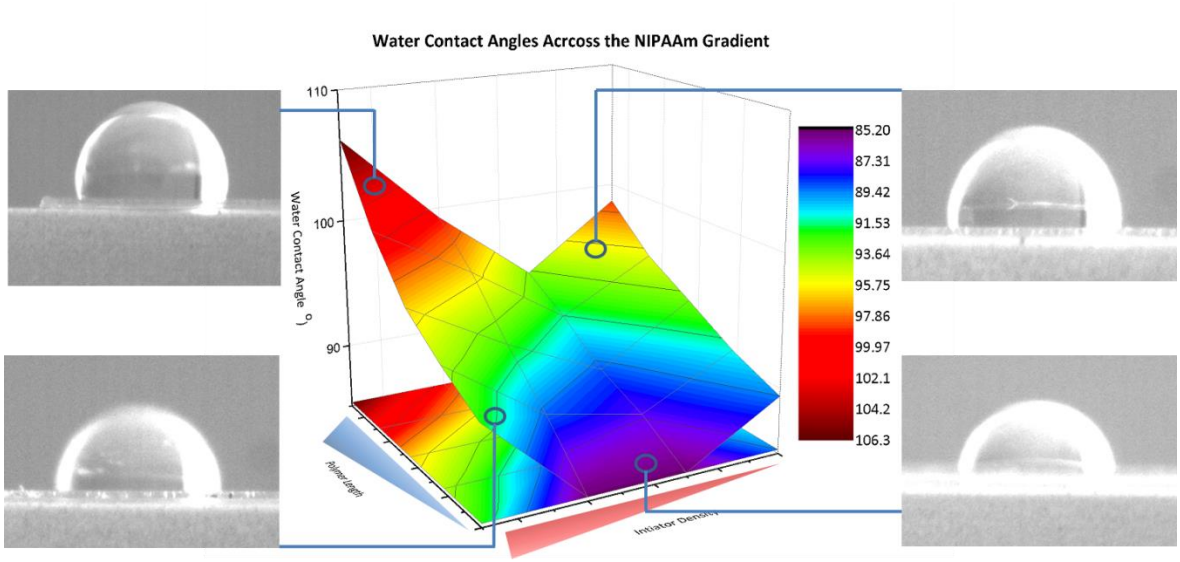

Figure 5.3 (a) – WCA on the gradient surfaces. The surface plot shows wettabilities across the gradient. Red shows the least wettable areas, and purple shows the most weattable areas. Drop shape images and their origins are shown with the graph.

There was a linear trend for wetablities on the gradient surfaces, and with increases in wettability due to increases with polymer lengths. The highest density of polymer brushes and the horizontal axis goes from shortest to longest polymers (**Figure** 5.3 (A)). The most hydrophobic area when the polymer was shortest, and the decline in series one was the sharpest. The increase in wettability (decrease in WCA) was similarly sharp with in regions which had the second highest density of polymers had a linear increase in wettability with increasing polymer length. Following the areas with the second lowest density of the initiator water contact angles were the lowest (most hydrophillic), the increasing wettability was not as sharp as the decreases in initiator density which had the lowest density of polymer brushes had the highest WCA, a linear decline was evident. These areas which were the second most hydrophobic after high intiator density areas. Generally the WCA was more influenced by polymer densities on the NIPAAm gradient. The reason for the high hydrophobicity was probably a result of the WCA being measured at room temperature and the de-ionized water being cold as a result of being in the holding tanks. It is recognised that the wettability of NIPAAm materials change with temperature because at temperatures above the lower critical solution

temperature (LCST) at 32˚C the NIPAAm materials are more wettable (Sun and Qing, 2011).

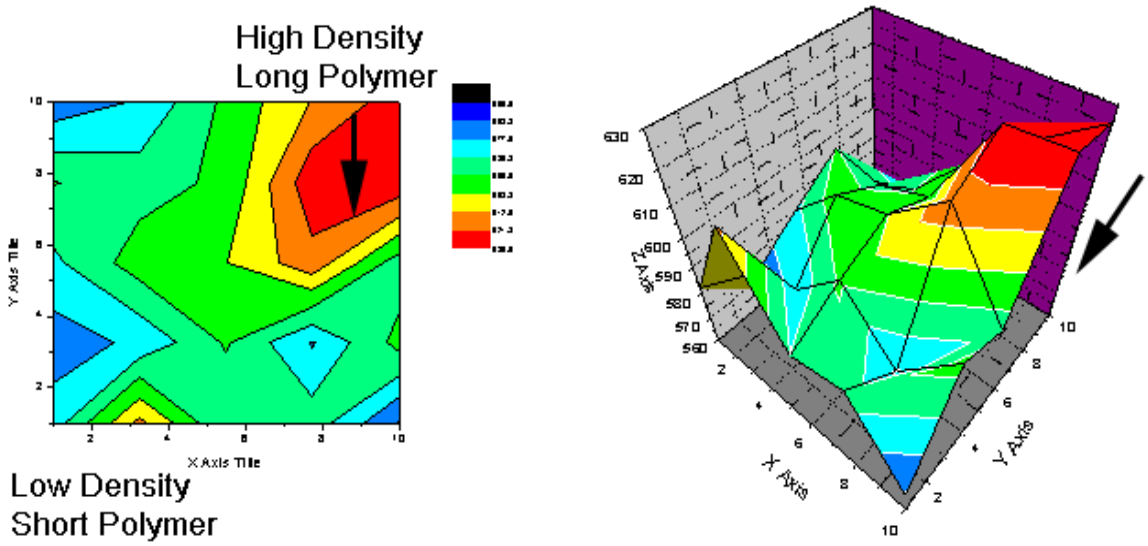

Figure 5.3 (B) – Average amine spectras on the gradient surfaces measured with XPS. Red shows the highest amine intensities, and blue shows the lowest amine intensities. Left graph is a two dimentional heat plot, and the right graph shows a three dimentional perspective on the graph.

To characterise the surface chemistry on the NIPAAm gradient XPS was performed. The XPS data in **Figure** 5.3 (B) shows amine heat maps across the gradient because the principle reason for using NIPAAm polymer was for the amine content. The relative 'heat' in **Figure** 3.5 (B) is a average amine peak height in each of the 25 quantiles. An amine signal was produced in all areas of the gradient which indicates that NIPAAm polymer was grafted to the polymer initiator across the whole surface in low and high densities. The signal intensity was highest in the areas of the gradient where the surface was most exposed to initiator solution longest and polymer solution longest in the production process. Which confirms the hypothesis the highest amine content would be in that area with the highest initiator density and highest polymer density. In the intermediate region of the NIPAAm gradient the signal had intermediate signal intensity. The reduction was caused by that area of the gradient having intermediate exposure to the initiator and NIPAAm solution during the production of the gradients. The lowest intensity amine

signals were in the areas of the gradient where exposure to the initiator and NIPAAm solution for a lower time during production. By decreasing the initiator density and decreasing the NIPAAm polymer length both caused lowest intensity of amine signals on the XPS spectra. The amine spectras analysed with XPS show that NIPPAm was successfully polymerized to varying degrees across the gradient through the production method of different exposures to reaction solutions by filling.

5.2.2 Neural Stem Cells

The presence of neural stem cells on the gradient was proved using a range of phenotyptic and morphological markers such as immunogenic antibody markers Sox2 (Sigma), nestin (BD sciences), as well as counting size and number of neurospheres. Dissociated single cells were initially seeded on to the gradients **(Figure 2.6)**, so the presence of neurospheres on the NIPAAm gradients indicated the surface was direct the cells to form neurospheres. What makes this cell response more striking was that the work was done with a neural differentiation media free of stem cell mitogens such as EGF or bFGF.

The adhesion of the neurospheres was sufficiently strong to stay adhered through the fixing and immunocytochemistry protocols. The highest abundance of the spheres were found in areas with low density and intermediate polymer length (**Figure** 5.4). Neurosphere numbers in this area were almost doubled compared to other higher surface energy regions on the surface. The neurosphere numbers were lowest in regions with the lowest and highest surface energies.

Neurosphere numbers were more responsive to polymer density than to polymer length (**Figure** 5.4). The neurospheres were observed with a highest frequency in regions

of the gradient with low density and intermediate polymer length. A higher average of neurospheres (11.2 neurospheres per quantile) was in the low density areas, compared to other regions on the gradient. The average was at 6.3 neurospheres per quantile in the areas with the high density, so a decrease of neurosphere number by nearly 40%. This shows that there was a *sweet-spot* for growing neurospheres on these surfaces where there was a dual chemical gradient.

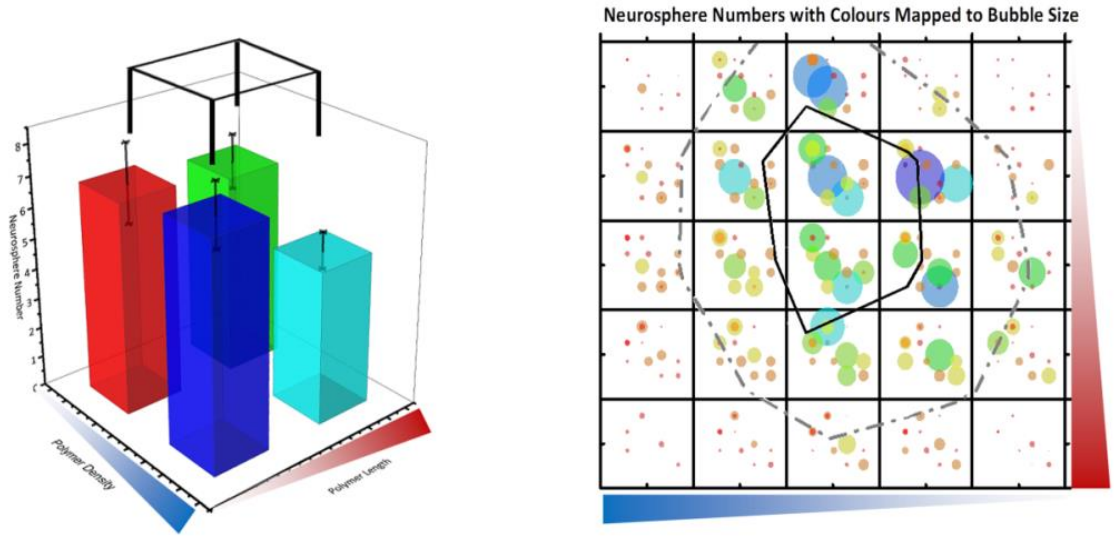

Figure 5.4 – Neurosphere number data on gradient surfaces. The right-hand graph shows a bubble plot where the bubble size and colour is linked to neurosphere numbers and the non-gridline lines show relative 'heat'. The gridlines show the counting squares The left-hand graph is a statistical plot. Where the error bars show standard error of the mean, and the column height corresponds to average neurosphere numbers from the sumised counting squares. The axis on both graphs consists of a red triangle which is the polymer length axis, and a blue triangle which is the polymer initiator density axis.
1 way ANOVA: Significantly Higher Than G1 Significantly Higher Than G2
= Significantly Higher Than G3 = Significantly Higher Than G4
2 way ANOVA: = The Means of Polymer Lengths are Significantly Different
= The Means of Polymer Density are Significantly Different

Neurosphere numbers decreased at the extreme ends of polymer length where they were shortest and longest. When the neurosphere numbers were small the numbers were also regular with an average of 3.37 neurospheres per quantile with the long polymers, and 3.9 neurospheres per quantile with lowest initiator density. Decreasing the density increased the neurosphere numbers on the NIPAAm amine gradients. The reason that the neurosphere numbers were lowest at the edges was probably due to limitations of the cell culturing rather than the surface. That could be because of

poly(dimethylsiloxane) (PDMS) still stuck to the surfaces or excess magic pap pen. Across the whole gradient surface the average number of neurospheres would be around 5.7 neurospheres per quantile, however the average total number of neurospheres across the surface would average total would be around 143.51 neurospheres. 143.51 neurospheres should be considered quite a high number because there were no direct additions of mitogens such as bFGF and it was a two dimensional surface which has a lower surface area compared to the free floating culture systems neurospheres have been culture in.

In the past hydrophobic surfaces in serum free media have been recognised to cause neurosphere formation (Heo *et al*., 2013). Across the NIPAAm gradient there were different wettabilities, but the whole surface was hydrophobic. The largest decrease in hydrophobicity was from 106˚ to 92˚ which is not a wide range compared to the range of wetabilities of the silane surfaces used in chapter one. On the NIPAAm gradient surfaces there was not a strong link between the hydrophobicity and neurosphere formation. In the most hydrophobic and hydrophilic areas of the NIPAAm gradients the numbers of neurospheres were quite similar. Generally the majority of neurospheres were found in the areas with the intermediate wettabilities.

Amine density through the control of polymer length and density is key to neurosphere formation, but amine density requirement is low because high amine densities are more likely to cause neural stem cell differentiation (Lamour *et al*., 2010). This means there is an ideal surface energy to confine neural stem cells which has separation applications. Also there is an optimum surface energy to culture neurospheres in mitogen free conditions which will save money in terms of using recombinant proteins wastefully in cell culture protocols. The sharpest transition in neurosphere number is seen at the two low polymer densities areas on the gradient. The highest neurosphere average was lowest average in the lowest polymer density area.

The neurospheres were in their highest numbers in the areas of the gradient with low energy intermediate polymer lengths. Compared to both the glia cells found to be most abundant at the short polymer lengths and high initiator density areas of the gradient, and the differentiated neurons which were found in highest abundance at the high amine density areas of the gradient.

Quality control and statistical testing was performed on the neurosphere counting data collected from the NIPAAm gradient surfaces. QQ plots were made to compare the data collected from the experiment to a normal distribution (Appendix 8). Data collected from the experiments (the blue circles) were re-plotted by a cumulative distribution function of the random variable, and the red line is a reference line. The QQ plots for neurosphere data collected from the middle of the gradient tended to have a mildly negative skew. Data from the lowest initiator density parts of the gradient followed a more normal distribution as shown in the QQ plots. A little bit of wide tailed data was observed in two parts of the gradient following no pattern. Most of the negatively skewed data was judged to be mildly skew except for (3, 7, 8, 11, 12, 15 quantiles) which were judged to have a negative skew mainly occurring at the high density parts of the gradient. To cope with the mild negative skew the data was transformed following a $\log_n$ transformation.

With the aim of maximizing the power of the ANOVA statistical tests the numbers of groups were cut from 25 sampling squares down to 4. The four squares represented the more extreme ends with the purpose of not including transition data which leads to instability in the statistical model. QQ plots were produced for each set of combined neurosphere data groups, and the graphs revealed very negative skews (Appendix 8). To cope with very negative skews in the combined data sets natural logarithmic transformations were performed using an online calculator

(http://vassarstats.net/trans1.htML) to make the data follow a normal distribution which is an important prerequisite for statistical testing (Howell, 2012). To verify that the distribution of all the data sets used have an equal distribution to test the distributions of data were equal which is another prerequisite for statistical comparisons a Levene's test was performed in Originlab. Levene's test showed that the distribution between the 25 sampling squares was not significantly different after the data transformation.

One-way and two-way ANOVA was performed on the log_n transformed neurosphere data which followed a normal distribution and there was equal variance between the groups. The graph in **Figure** 5.4 shows there was no significant difference between the groups in both one and two way ANOVA. The reason that no significant differences were detected was because the hottest areas with the highest number of neurospheres were omitted from statistical testing because these were transition areas which are problematic for the ANOVA model because a key assumption is that the groups are independent.

At the interface where spheres attached to the surface chain migration of mature neurons out of the sphere was evident. Chain migration is a good indication of differentiation capacity because migration of the precursors is a key stage in stage in neural development (Jacques *et al*., 1998). Initially migrating cells stained positive for anti-Tuj1 which immunologically demonstrates that these cells had differentiated prior to migration. The process leading out of the spheres tended to be quite fine in the low surface energy areas compared to the thick trunks seen in with the less abundant spheres in the high surface energy areas as shown in **Figure** 5.4. Typically the neurons had migrated out on a bed of glia, however due to the dissection originating from the cortex of fairly well developed embryos (E16) the proportion of glia cells was lower. The gradients demonstrated sufficient bio-competence to allow independent neural chain migration.

This work shows that the neurospheres can be produced *in vitro* using a surface in a serum-rich differentiation cell culture media. This means that surface effects are just as important as media adjuncts to control neural differentiation.

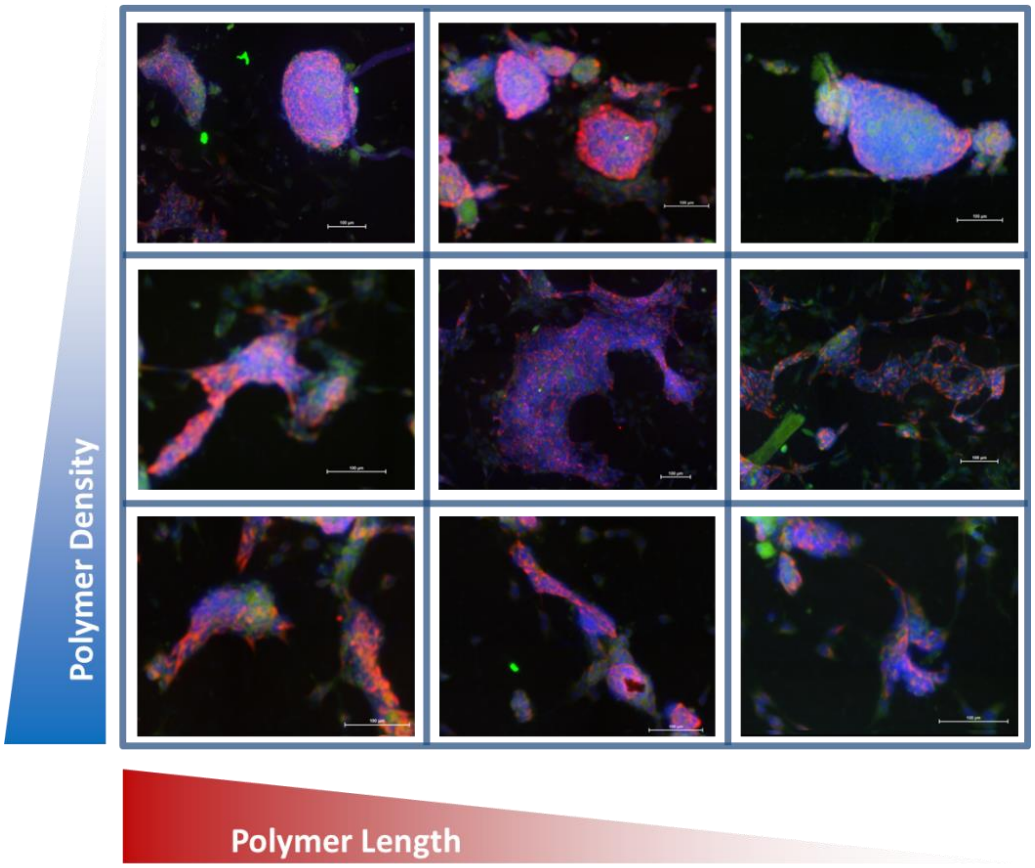

Figure 5.5 – Expression of nestin (red) and sox2 (green) which are immunogenic markers of neural stem cells and progenitors around the gradient. The blue dots show DAPI staining of DNA in the cell nucleus, and the white scale bar represents 100 µm. The pictures were collected after 4 days of cell culture. Nestin and sox2 staining can be found throughout the gradient, but the most abundant staining was found in the areas with lower initiator density.

Further understanding of neural stem cell purification in reference to the different surface conditions presented by the gradient was gained with immunocytochemistry. Cells were stained against anti-nestin, Sox2 and DAPI. The nestin marker shows an intermediate filament within the cell's cytoskelton which is found in neural stem cells and neural progenitors (Dahlstrand *et al*., 1992). Sox2 is a transcription factor located in the perinuclear region of neural stem cells and progenitors (Graham *et al*., 2003). DAPI (4',6-diamidino-2-phenylindol) is florescent stain which binds to A-T in DNA to visualize the cell's nucleus. As expected neurospheres showed strong expression for nestin and Sox2.

Large stitched images were taken with a Nikon Ti epi-fluoresce microscope (phase contrast lens 20X) where the DAPI staining shows that the neurospheres on the gradients were not hollow (Moeller and Dimitrijevich, 2004). Size is probably a key factor because of mass transfer and hollowing would be expected when spheres exceed 200 µm, and the neurospheres in these experiments were rarely exceeding 15 µm diameter. The nestin expressing cells were seen towards the inner perimeter of the neurospheres. Processes tended to run in a perpendicular direction with cells in the neurosphere. When there were large irregular multi-cellular assemblies the processes of nestin expressing cells tended to be randomly orientated. The Sox2 positive cells mostly co-expressed the nestin marker. Another interesting feature of the Sox2 expressing cells was that cells expressing just nestin could be seen in the centre of the neurospheres **(Figure 5.5)**. An interpretation is that the progenitors and neural stem cells reside in different parts in small neurospheres.

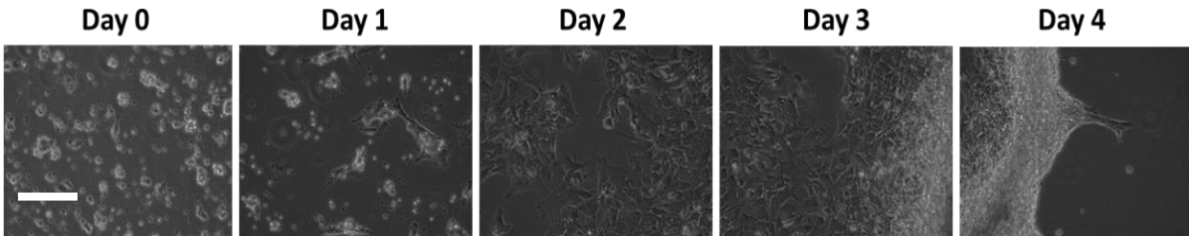

Figure 5.6 - Time lapse imaging taken from the gradients taken over four days showing the attachment in the areas of the gradient where neurospheres formed. Scale bar is 100 µm.

Time-lapse microscopy was performed on CM Technologies' CellIQ phase contrast live cell imager by David Smith at Loughborough University. Neurosphere formation was shown to be a process driven by thermodynamics because cell aggregation was the first part of the process which is indiscriminate with cells minimizing their contact to the surface. The neurospheres attachment was evident, because small processes extend from the sphere which is considered part of colonization. At the same time the neurosphere was increasing in size due to proliferation (**Figure** 5.6). With confocal microscopy cell sorting was evident within the sphere which probably happens at this stage because the

structure was getting bigger. Large irregular multi-cellular assemblies were formed through cells forming into neurospheres. Next a few neurospheres aggregated together at around 5 hours which has been previously described in (Sargent *et al*., 2009) (Singec *et al*., 2006b). In the next stage other sparsely situated neurospheres move towards the aggregate (9 hours). With the merging of new spheres the merged object grew bigger. The neurospheres migration towards the assembly is not random it was directed where there was a strong attraction. Further aggregate was observed, and at 11 hours chain migration happens with the cells colonizing more of the surface. The chain migration was happening simultaneously with the cell aggregates becoming denser due to proliferation. Next the cells that migrated away migrate back to the assembly. The assembly itself begins to migrate towards higher energy parts of the gradient. The NIPAAm gradient was able to cause a range of responses in different areas of gradient, and provides extra control over neural stem cell *in vitro* using surfaces only.

5.2.3 Mature Glial Response to the Surface

The number of neurons to glia vary depending on the location in the brain (Dombrowski *et al*., 2001). The proportion of glia to neurons was lower in these experiments were lower compared to previous experiments in chapter three. The work in chapter three the neural tissue was dissected from E12 VM sprague-dawley rats, and in the work described here the tissue was dissected from E16 cortex in the same type of rat. The cortical glia were mainly found in areas of longer polymer length (**Figure** 5.7). Single glial cells were always co-localized in the same areas with neurons. In the areas with shorter NIPAAm polymer lengths less single dispersed glia cells were observed. The gradients were seeded with single cells and mature glia were present in some parts of the gradient at higher abundance compared to other parts of the surface. Glia differentiation

was controlled by the NIPAAm gradient through sorting to specific parts of the gradient. The glia were present in a mature monolayer morphology at the high energy region. In the low energy region of the amine density gradient the glia were more spindly which indicates that the glia are in a different stage of the lineage. In the area of the gradient with the highest surface energy (highest initiator density and NIPAAm polymers brushes grown for the longest time) the highest number of glia were found, and these numbering an average of 400-500 glia per quantile which is 3x higher than the region with the lowest number of glia. The Atom transfer radical polymerization (ATRP) density and therefore polymer brush density had little effect on glia numbers across the relevent quantiles (0-100).

Glia numbers were highest (152 glia per quantile) in the areas of the gradient with high density of NIPAAm polymer brushes with short lengths. Across The whole NIPAAm gradient glia were present in high numbers (126.6 glia average per quantile) whenever the NIPAAm polymers were short, and that was mostly independent (ranging from 158 to 150 glia average) of polymer initiator density. With the glia similar cell culture type *edge effects* occurred where at the edges of the material lower cell numbers were present where the majority of cells were further towards the central areas of the surface. If the edges and outer borders of the material, then the lowest average glia numbers were in the areas of the NIPAAm gradient with a high density of initiator and long NIPAAm polymers (105 glia average). For cell counting the NIPAAm gradients were split into 25 squares, if an average was taken then there were an average of 96.9 average glia per quantile in any of the 25 squares. Across the whole NIPAAm surfaces the average total of glia cells was 2424.31 which was lower by a more than half the average total neuron numbers. The glia cells were in highest numbers in the areas of the gradient with high polymer density and shortest polymer lengths.

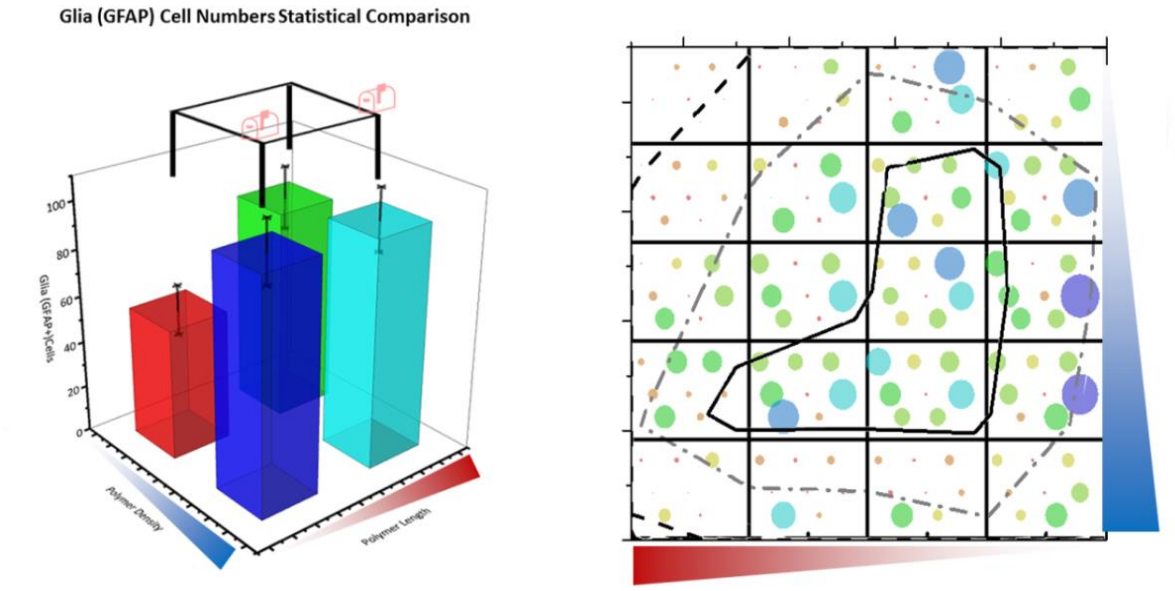

Figure 5.7 – Glia cell number data across gradient surfaces. The right-hand graph shows a bubble plot where the bubble size and colour is linked to glia cell numbers and the non-gridline lines show relative 'heat'. The gridlines show the counting squares The left-hand graph is a statistical plot. Where the error bars show standard error of the mean, and the column height corresponds to average glia cell numbers from the sumised counting squares. The axis on both graphs consists of a red triangle which is the polymer length axis, and a blue triangle which is the polymer initiator density axis.
1 way ANOVA: Significantly Higher Than G1 Significantly Higher Than G2
= Significantly Higher Than G3 = Significantly Higher Than G4
2 way ANOVA: = The Means of Polymer Lengths are Significantly Different
= The Means of Polymer Density are Significantly Different

Roach *et al* 2014 suggested glia were found in their highest numbers in mid-range wettability on gradients moving from ~80 to ~ 60˚ wettability. The NIPAAm gradients were more hydrophobic with an average wettability of 93˚. The glia were generally found in higher abundance in the less hydrophobic regions on the NIPAAm gradient.

Wettability altered over the gradient as shown in **Figure** 5.3 (A) the most hydrophobic region was with the high initiator density, and the hydrophilic areas presented the highest number of glia. Time lapse microscopy showed (**Figure** 5.10) that the high areas of highest cell density were produced through a combination of proliferation at 0-48 hours, and cell migration from 48-96 hours. The number of glia was linked to the number of neurons; with about half as many glia to neurons.

Quality control and statistical testing was performed on the glia cell counting data collected from the NIPAAm gradient surfaces. QQ plots were made to compare the data

collected from the experiment to a normal distribution, and informs on any potential needs of data transformation (Appendix 9). Data collected was re-plotted the blue circles show a cumulative distribution function of the random variable, and the red line is a normal distribution reference line. The QQ plots for glia data collected from the middle of the gradient tended to have a normal distribution, some of the data displayed a mild negative skew. Data from the lowest initiator density parts of the gradient had a slight negative skew in the distribution as shown in the QQ plots. On the whole most of the glia counting data showed a fairly normal distributions, arguably with a slightly negative skew. The most negatively skewed data was found in (4, 5, 16, 21).

QQ plots were produced for each set of combined glia cell count data groups, and the graphs revealed slightly negative skews (Appendix 9). To cope with slightly negative skews in the combined data sets square root transformations were performed using an online calculator (http://vassarstats.net/trans1.htML) to make the data follow a normal distribution which is an important prerequisite for statistical testing (Howell, 2012). To verify that the distribution of all the data sets used have an equal distribution to test the distributions of data were equal which is another prerequisite for statistical comparisons a Levene's test was performed in originlab. Levene's test showed that the distribution between the 25 sampling squares was not significantly different after the data transformation. That meant the data for glia cell count was appropriate for ANOVA statistical testing the variance between groups are tested.

One-way ANOVA and two-way ANOVA with Tukey's *post-hoc* testing was performed on the square root transformed glia cell count data. What the graph shows in **Figure** 5.7 was that there was significant difference between the glia groups in both one way ANOVA (P= 0.04206 & F= 2.81392). The Tukey's *post-hoc* testing from the one way ANOVA showed that when the groups were compared that there were no significant

differences. The two way ANOVA statistical tests provided further testing of the role the polymer lengths and initiator density and their impact on glia numbers. The population means for polymer initiator density were significantly different (P=0.04146 & F=4.24495). The population means for polymer length were not significantly different. The interaction between polymer initiator density and polymer length were not significant.

Compared to work in **chapter 3** when neural progenitors were derived from rat E12 ventral mesencephalon tissue, the proportion of glia was lower. The decrease in the glia is explained in Noctor 2007, and their review shows that the number of glia change depending on time in development and place/structure. Epi-fluorescence microscopy highlighted the glia GFAP marker could be seen within neurospheres, but was difficult to assign the stain to individual cells within the spheroid because of high cell density and morphological indistinction.

Immunocytochemistry showed the glia around the edge of neurospheres have quite an elongated morphology with a distinct pole pointing away from the neurosphere (**Figure** 5.7). The neurosphere was highly immunogenic for the glial marker, but the morphologies of the individual glia in this area were challenging to ascertain. Individual glia cells were counted throughout the surfaces and another observation was that the morphologies of the glia vary depending on the gradient as shown in **Figure** 5.7. In areas where the polymer lengths are short the glia tend to have a more rounded morphology where processes leading out from the cells tend to be short and the marker was localized round the nucleus (important to stress that it was not co-localized with the nucleus). Some astrocytes with the elongated processes more characteristic of the cortex can be seen in much lower numbers. Those type of glia tend to be near neurons with long leading processes. The glia cells in isolation without the neurons tended to have a more spread morphology without clear poles. In areas with longer polymer the glia have a bipolar

morphology. The numbers of mature glia could be controlled with the surface and also the stage of development as we will show with the neurosphere data.

5.2.4 Mature Neurons

Tuj1 is a microtubule protein found in mature neurons, cells positively stained for Tuj1 were judged to be mature neurons. Neurospheres are composed of neural stem cells and progenitors, but contain a small proportion of mature neurons and glia. At the edge of the neurospheres neurons are migrating away in a process called chain migration as explained earlier. These neurons display clearer processes as the cells migrate away from the spheroid. The individual neurons situated near the neurospheres will tend to have long processes, and cells between spheroids have processes which are more curved as the neurons are searching out new connections (Lois, 1996). Clear differentiated neurons are found at the surface interface which shows the importance of surface. Neurons tended to have a long process with numerous finer filapodia, which was expected in cortical neurons (**Figure** 5.8). In the areas of the gradient which had a strong effect on neural differentiation mature neuron morphologies are clearer. Some of the neurons were aggregated together at low amine densities where the cell somas are close, and the primary process extend outwards. These aggregates were small and flat, so they were unlikely to be neurospheres which are three dimentional. When these aggregates are close neural processes join the aggregates. The single neurons in these areas have different morphologies with more pronounced processes. Neurons that have migrated long distances and that are isolated tend to have one distinct process, whereas neurons close to neurospheres have more processes and finer processes. This was textbook cortical neuron behaviour where the cells are forming new connections.

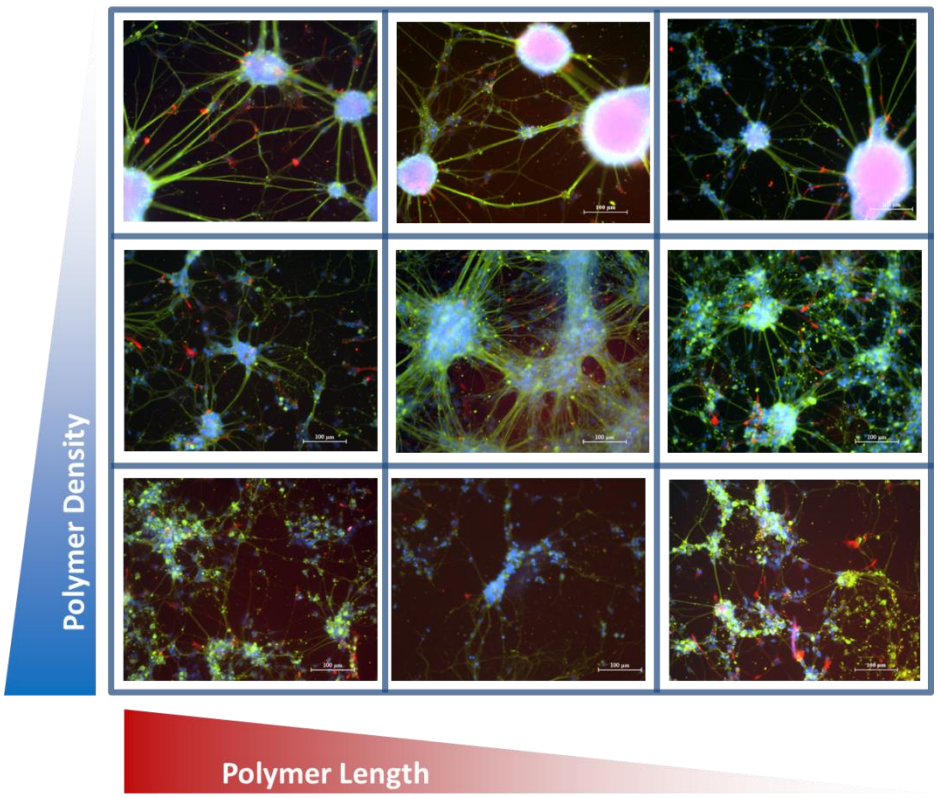

Figure 5.8 – Immunocytochemistry shows the localazation of tuj1 (green) and glia (red) phenotypes along the orthoganoal NIPAAm gradient. The blue dots show DAPI staining of genetic material in the cell nucleus, and the white scale bar represents 100 µm. The pictures were collected after 4 days of cell culture. Tuj1 and GFAP posative cells were observed in all areas of the gradient. The highest density areas show the tuj1 positive cells in the differentiated monolayer morphology. Intermediate density shows neurosphere attachment. The low density areas caused the localization of tuj1 positive cells to neurospheres.

Cells on the gradient surfaces were fixed, stained and counted to assess distributions of various neural phenotypes after 4 days of cell culture. Neurons (**Figure** 5.9) differentiated cortical neurons were found all over the coverslip in different numbers. Highlighting poly NIPAAm is perfectly capable of culturing primary neural cell *in vitro*. In the parts of the gradient with a low density of polymer differentiated neuron numbers are low averaging 148 neurons per quantile. In the areas of the gradient with an intermediate to low density the average neuron number was 202 neurons per quantile. The areas of the gradient which had an intermediate/high of polymer had a lower average of 206 neurons per quantile. Similar to the intermediate/high density areas more neurons are found in areas with a long NIPAAm polymers, and lower in the areas with shorter NIPAAm polymers. The embryonic cortical rat neurons which were used in these experiments were

highly responsive to NIPAAm polymer length. In general higher numbers of differentiated neurons were found in areas with longer polymers. The tissue showed the clearest differentiation into mature neurons in the area with the longest polymers and highest polymer density.

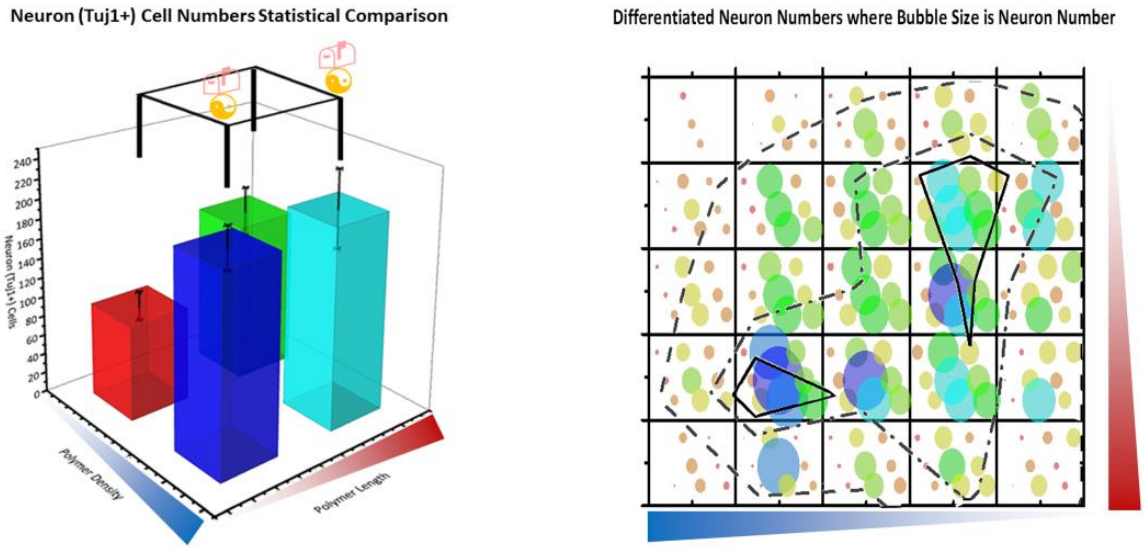

Figure 5.9 – Differentiated neuron cell number data on the NIPAAm gradient. The right-hand graph shows a bubble plot where the bubble size and colour is linked to differentiated neuron cell numbers and the non-gridline lines show relative 'heat'. The gridlines show the counting squares The left-hand graph is a statistical plot. Where the error bars show standard error of the mean, and the column height corresponds to average differentiated neuron cell numbers from the sumised counting squares. The axis on both graphs consists of a red triangle which is the polymer length axis, and a blue triangle which is the polymer initiator density axis.
1 way ANOVA: Significantly Higher Than G1 Significantly Higher Than G2
= Significantly Higher Than G3 Significantly Higher Than G4
2 way ANOVA: = The Means of Polymer Lengths are Significantly Different
= The Means of Polymer Density are Significantly Different

The highest numbers of differentiated neurons were in the areas of the gradient with long polymers and high initiator density where amine density would have been highest. The highest average in the counting squares was 312 in a high amine density area of the gradient. Low numbers of differentiated neurons were in the boarder and edge areas of the gradient which was common for neurospheres and glia too. Generally mature differentiated neurons responded more to polymer length than polymer initiator density with more neurons found in the parts of the gradients with long polymers. The average number of neurons per square would be 179.4 on the NIPAAm gradient. The sum total

average number of differentiated neurons over the whole surface was 4486 neurons. At the low initiator density areas neuron numbers increased with decreasing polymer length. Such responses were not repeated elsewhere. Compared to glia neurons enriched at far higher numbers in some of counting squares on the gradient. In the high amine density area of the gradient there were double the number of differentiated neurons, however in the long polymer low initiator density areas there were only 55% more neurons compared to glia. Across the low initiator density areas not taking into account polymer lengths the neurons very much outnumber the glia, which was not evident at high initiator densities.

The three cell populations (neural stem cells, glia and neurons) which were investigated in terms of cell response showed preferences for different areas of the amine density gradient. The differentiated neurons were found in highest abundance at the high amine density areas of the gradient with long polymers and high initiator densities. Compared to both the neurospheres found to be most abundant at the low energy intermediate polymer lengths, and the glia cells were in their highest numbers in the areas of the gradient with high initiator density and short polymers.

Quality control and statistical testing was performed to judge the difference in neural differentiation on different parts of the NIPAAm gradient surfaces. QQ plots were made to compare the data collected from the experiment to a normal distribution, and informs on any potential needs of data transformation (**Appendix 10**). Data collected was re-plotted the blue circles show a cumulative distribution function of the random variable, and the red line is a normal distribution reference line. The QQ plots for differentiated neuron cell count data collected from the middle of the gradient tended to have a normal distribution, some of the data displayed a mild negative skew. Data from the lowest initiator density parts of the gradient had a negative skews ranging from very skewed to slightly skewed in the distribution as shown in the QQ plots. The most negatively skewed

differentiated neuron cell data was found in squares (1, 3, 7 20, 22). Different from the neurospheres and glia was that the neuron cell counts had some wide tail distributions.

With the aim of maximizing the power of the ANOVA statistical tests the numbers of groups were cut from 25 sampling squares down to 4. The four squares represented the more extreme ends with the purpose of not including transition data which leads to instability in the model. QQ plots were produced for each set of combined neuron cell count data groups, and the graphs revealed very negative skews (**Appendix 10**). To cope with very negative skews in the combined data sets natural logarithmic transformations were performed using an online calculator found at (http://vassarstats.net/trans1.htML) to make the data follow a normal distribution which is an important prerequisite for statistical testing (Howell, 2012). To verify that the distribution of all the data sets used have an equal distribution to test the distributions of data were equal which is another prerequisite for statistical comparisons a Levene's test was performed in originlab. Levene's test showed that the distribution between the 25 sampling squares was not significantly different after the data transformation. That meant the data for differentiated neuron cell count was appropriate for ANOVA statistical testing the variance between groups are tested to judge the impact of surfaces on differentiated neurons.

One way ANOVA with Tukey's *post-hoc* testing was performed on the square root transformed differentiated neuron cell count data. What the graph shows in **Figure** 5.9 was that there was significant difference between the glia groups in both one way ANOVA (P= 0.00202 & F= 5.17182). The Tukey's *post-hoc* testing from the one way ANOVA showed that there were significant differences between G4 with G1 and G4 and G2. The two way ANOVA statistical tests provided further testing of the role the polymer lengths and initiator density and their impact on differentiated neuron numbers. The population means for polymer initiator density were significantly different (P= 0.00134 &

F= 10.70647). The population means for polymer length were not significantly different. The interaction between polymer initiator density and polymer length were not significant.

Neural migration is one factor which contributed to the high numbers which was shown with time-lapse microscopy (**Figure** 5.10). Therefore cells differentiated in one area, but migrate and reside in another part of the gradient. The gradient has two effects on cells causing differentiation and chemotactic migration, and these points further enhance the application of the NIPAAm polymer gradients for the separation of stem cells and rare cell populations.

Neural differentiation was also monitored with time-lapse microscopy. The cell response to certain parts of the gradient had a resemblance to neurons cultured on laminin coated surfaces as shown in **Figure** 3.4 in terms of morphology. A strong feature is that the neurons are highly elongated and the cells are in a low density monolayer. This cell response was captured with time lapse microscopy low density long polymer area of the gradient. The cell adhesion process was rapid with cells becoming rounded and attaching after 4 hours. Some cells migrated towards other cells to form multicellular aggregates, and longer processes start to extend out from the agregates at 8.25 hours. Cells proliferate and the aggregates were completely flat after 22.5 hours. The cells individually are spreading out more and migrating towards other, and some cells can be seen to rapidly migrate from one collection of cells to another. Neurons, even once differentiated from stem cells still divide (in a limited capacity) because the cell numbers increase. At about 60 hours the surface is nearly saturated with cells, and cell migration is common. Towards the end of the 96 hours the cells migrated closer together which creates a few gaps making a part of the surface visible again. The key stages of the cell response are attachment and proliferation.

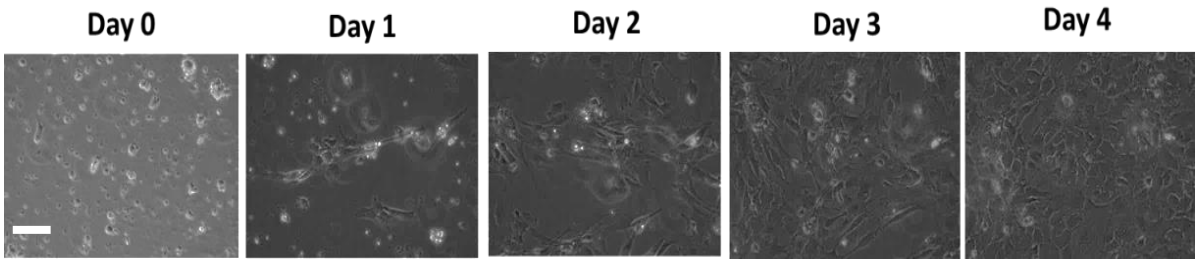

Figure 5.10 – Time lapse imaging taken from the gradients taken over four days showing the attachment in the areas of the gradient where neurons proliferated (scale bar is 100 μm).

The highest number of the neurons was observed on the highest energy part of the NIPAAm gradient the cell response to this area was recorded with timelapse microscopy. In the high surface energy part of the gradient attachment starts about 3.5 hours after the cells were seeded on to the gradient. With the clumps processes elongate out after 8.25 hours and were extended at the 13.5 hours mark. After 27.5 hours lots of flattening has occurred and extensive proliferation can be seen. About two thirds of the surface is covered with cells and next more cells migrate into the area. At about 3.5 days the surface is fully saturated with cells, in a highly dense monolayer taking on the morphology of a cell sheet. The cell response to the high surface energy area on the gradient occurs in three stages: attachment, proliferation and long range migration to the high energy area.

5.2.5 Controlling Neurosphere Size

The differentiation of neural stem cells was controllable with the gradient, raising the possibility of controlling the neural stem cell micro-environment with the surface. The orthogonal gradient was designed to present a continuous range of amine densities to control the rates, volumes and types of proteins to adsorb. The continuous nature of the surface was also designed to examine the effects across many multiple combinations of the chemical surface in a high throughput assessment of cell response. The samples were fixed at the four day time time-point and bright-field images of the whole surface were

collected. The spheres imaged had a fairly robust attachment to the surface to remain attached through the fixing process.

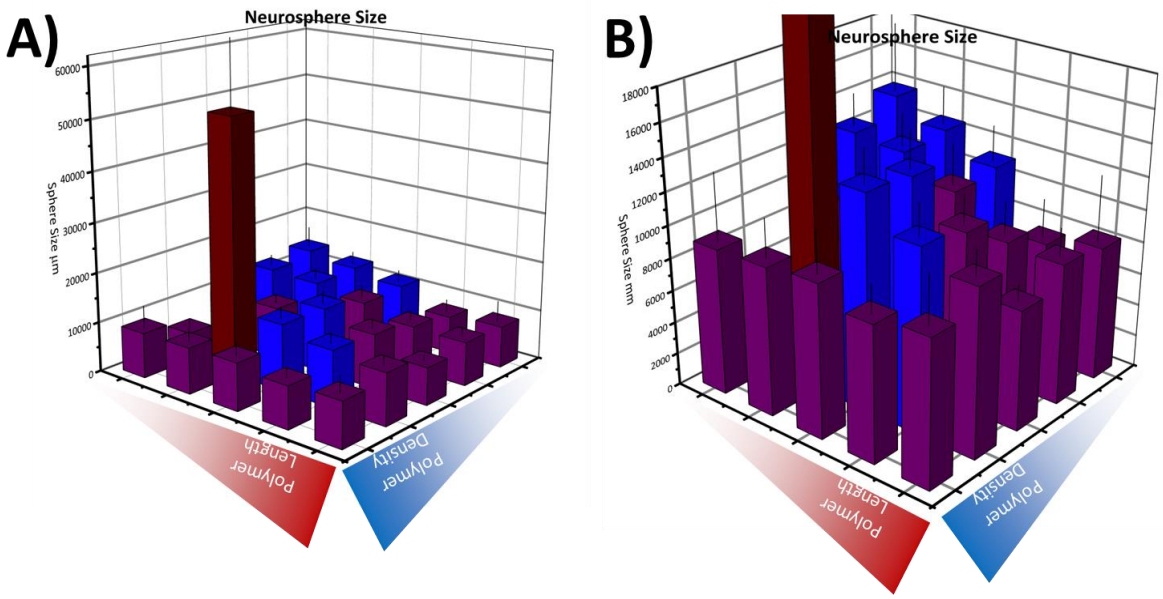

Figure 5.11 – Neurosphere size on the NIPAAm gradient. The error bars show SEM. A) Zoomed out verision of the graph. B) Zoomed in verision of the graph.

Figure 5.11 provides evidence that neurosphere size was very responsive to the orthogonal NIPAAm gradient surface. In the high polymer density regions of the surface neurospheres were where small (around 80000 µm) regardless of whether the polymer was long or short in that area. In all the areas of the gradient with short polymers the size of neurosphere was small around the 8000 µm. **Figure** 5.11 proves that neurosphere size is controllable with polymer length, and this type of observation would have been impossible without the dual orthogonal gradient where we could observe gradual changes in cell response. When the polymer initiator density was lowest the neurospheres size increased with polymer length. In the parts of the gradient within the areas with intermediate polymer density the effect of polymer length on neurosphere size becomes clearer. With the shorter the neurospheres are smallest (6000 µm) when its an intermediate polymer length the neurosphere area increases to 10000 µm. The combination of intermediate polymer density and long polymers the neurospheres the spheres had an area of 12000 µm. The increasing polymer length would increase the size

of spheres in the areas with intermediate density. Control of the neural cell niche was evident in these areas of the gradient (**Figure** 5.2). The clearest effects of the gradient surface can be seen in the areas of the gradient with second lowest polymer density because the relationship between neurosphere size and polymer length is linear. In terms of process control linear parameters are extremely desirable because results are easier to predict. In lower polymer initiator regions of the gradient the sphere size at the short polymer is at 8000 µm. The area of the neurospheres increases linearly to 14000 µm, and the linear trend in this area has an R^2=0.9. In the areas of the gradient with the lowest polymer density the increase in neurosphere size was starker. With the short polymer the spheres have an average size of just under 8000 µm. In the areas of lowest polymer density and intermediate NIPAAm polymer length the neurosphere area increased to 11000 µm, and at longest polymer length the sphere size increased to just under 14000 µm. Changes to neurosphere size were controllable using the NIPAAm gradient, and the control was demonstrated to happen simultaneously. Previously the best efforts have been capable of producing homogeneous populations (**Figure** 5.12).

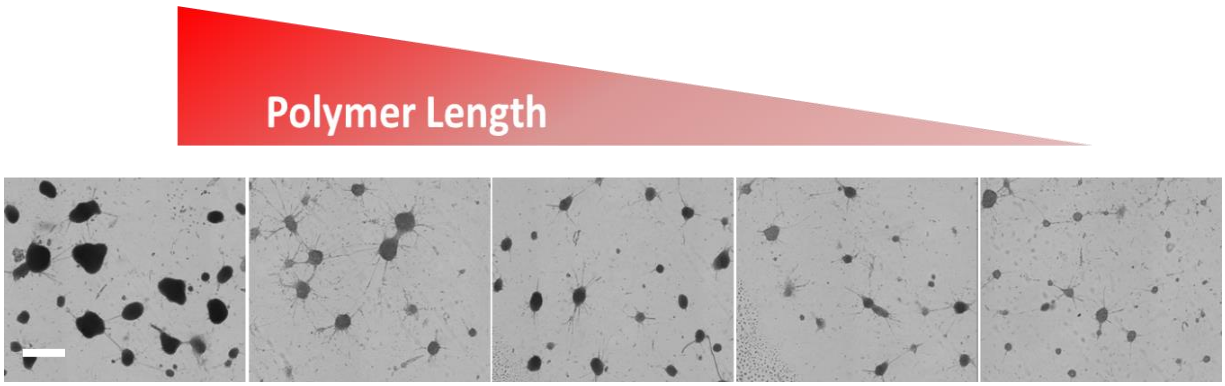

Figure 5.12 – Pictures from the low initiator density areas of the gradient. By increasing the polymer lengths the neurospheres got bigger (scale bar is 100 µm).

5.3 Discussion

The aim of the experiments was to investigate cell response using a high-throughput approach. The gradient surface allowed controlled differentiation of neural stem cells and progenitors in a simple way which is flexible enough to engineer into other techniques for widespread adoption (**Figure** 5.13). Currently differentiation protocols employ expensive recombinant proteins which were discovered in such development investigations. Using cocktails of relevant proteins a wide variety of tissues can be produced such as: blood from pluripotent stem cells (Samuel *et al*., 2013), bone from pluripotent stem cells (Schuldiner *et al*., 2000), and liver from embryonic stem cells (Funakoshi *et al*., 2011) to name a few. The tissue produced from these protocols can provide accurate functional tissue from potentially infinitely expandable cell sources (Kriks *et al*., 2011a) (Oldershaw *et al*., 2010). These two protocols use over nine different sources of both purified and recombinant protein reagents which creates problems. Financially these protocols are expensive with an inelastic reagent supplies making it difficult to move prices down. Significant simplification of protocols is required because they are out of reach for a lot of scientists due to expense and complexity. Also, cell therapies based on the highlighted techniques would be extremely challenging to translate because some of these reagents might not be produced in GMP conditions (Felicia M. Rosenthal, 2013). Other problems include:

- variations in cell responses which are difficult to synchronise in culture.
- additions of developmental proteins to cell culture media means steady-state levels arise meaning natural gradient dynamics are lost (Saha and Schaffer, 2006).
- a lot of the proteins in embryonic development have overlapping roles, for example the WNTs (Wingless patterning protein) causes differentiation (Davidson *et al*., 2012), prevents stem cell differentiation (Berge *et al*., 2011), and the response to

WNT signalling varies depending on the stage of the cell cycle (Niehrs and Acebron, 2012). Adding further complexeity oligodendrogliogenic and neurogenic adult subependymal zone neural stem cells responded differently to WNT (Ortega *et al*., 2013). Neurogenic adult subependymal zone neural stem cells generate oligodendroglia or neurons in response to WNT, but WNT caused oligodendrogliogenesis in oligodendrogliogenic stem cells with no change in linage.

The addition of these factors will lead to mixed populations, so a more efficient process would eliminate many of these factors and purify populations. Here we adopted an alternative strategy to using expensive reagents to control differentiation in cell culture, and that was to use a dynamic surface. The design philosophy comes from Whitesides team which produced a surface gradient which could make 'water flow uphill' (Chaudhury and Whitesides, 1992). Whitesides said in a recent commentary, new devices need to solve *real problems* in the *simplest* fashion (Whitesides, 2013). The idea was to evaluate the use of linear gradient surfaces to better control native/intrinsic cell behaviours to produce the desired response. Local paracrine signalling influences cell response depending on the cell density (Bauwens *et al*., 2011) which was type of factor which surfaces were effective at controlling.

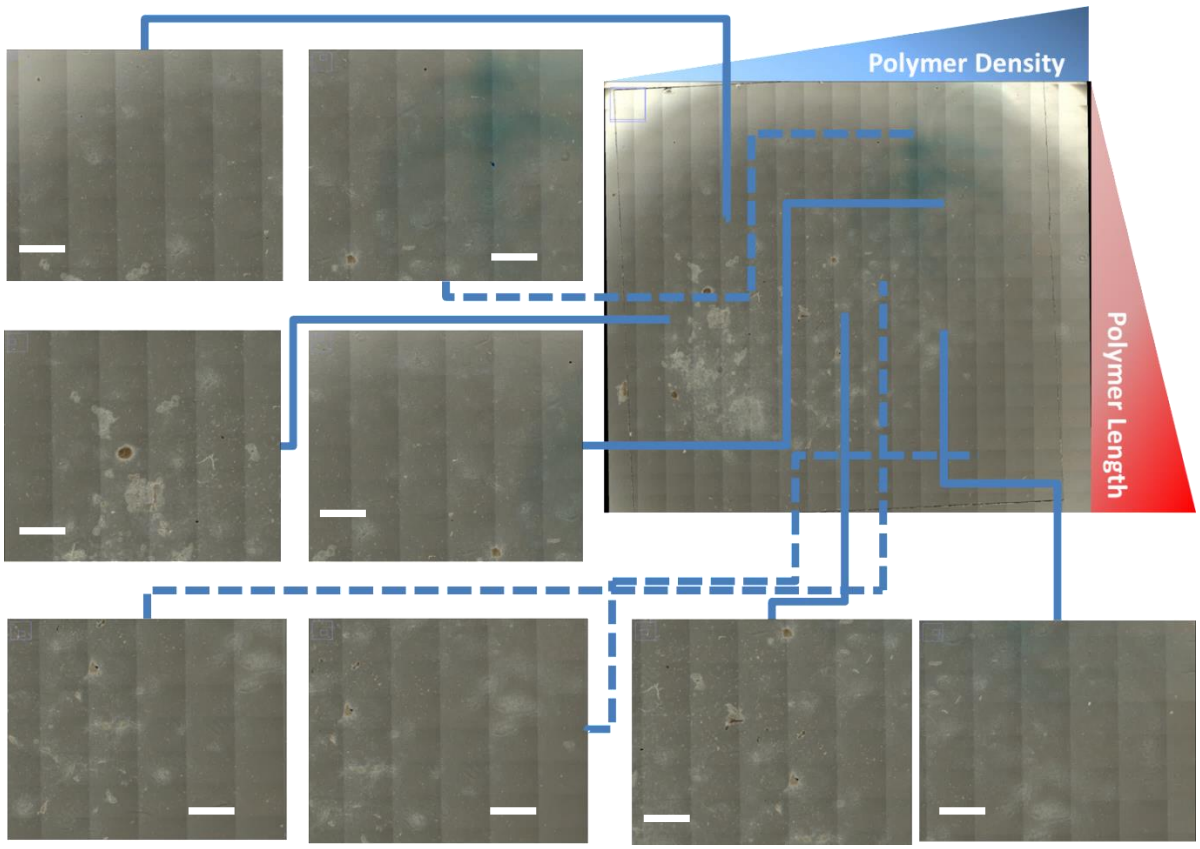

Figure 5.13 – Phase-contrast image (10X) of fixed NIPAAm gradient after four days of cell culture. Large pane is the whole surface. The samller panes are zoomed-in images from around the gradient (white scale bars are 1000 µm).

5.3.1 Sorting and Spheroids

Cells have a natural ability to sort in terms of self organisation in tissue development creating the hierarchy of tissues with layers of different cell types segregated to different areas to fulfil specific needs. The neurospheres on the NIPAAm gradient rarely exceeded 15µm diameter and in βFGF containing media. Confocal microscopy showed cells expressing nestin were seen towards the inner perimeter of the neurospheres (**Figure** 5.2). Nestin fibril processes tended to run in a perpendicular direction with cells in the neurosphere. When there were far larger irregular multi-cellular assemblies which were composed of multiple neurospheres. Here nestin expressing cells tended to be randomly orientated. If the experiment had gone on longer cells would have probably sorted in the mass based on Steinberg's differential adhesion hypothesis. The Sox2 positive cells mostly co-expressed the nestin marker. Another interesting feature of

the Sox2 expressing cells was that cells expressing just nestin could be seen in the centre of the neurospheres. A possible explanation is that the progenitors and neural stem cells reside in different parts in small neurospheres as the structuring of the neurospheres was controllable, so was the size. In the areas of the gradient with a low initiator density, the size of neurospheres was responsive to polymer length. The clearest effects of the gradient surface can be seen in the areas of the gradient with second lowest polymer density because the relationship between neurosphere size and polymer length was linear. The neurospheres increased in size with increasing polymer length. In terms of process control linear parameters are extremely desirable because results are easier to predict. In this cross-section of the gradient the sphere size at the short polymer is at 8000 µm. The area of the neurospheres increases linearly to 14000 µm. With the short polymer the spheres have an average size of just under 8000 µm. In the areas of lowest polymer density and intermediate NIPAAm polymer length the neurosphere area increased to 11000 µm, and at longest polymer length the sphere size increased to just under 14000 µm.

Previously it has been shown that spheroid formation and size can be controlled with hydrodynamics by using a rotary shaker. At low speeds the spheroids would form faster and have a uniform size distribution (Kinney *et al*., 2012). Similar approaches have been used with static matrigel islands where the colony size would affect the differentiation of stem cells. Spheroids are therefore a powerful because they are controllable, and differentiation can be achieved with minimum input. This is the most overlooked factor when it comes to scale-up because not enough work goes into reducing complexity (Whitesides, 2013). By reducing amine density can form and control the neurospheres.

Others using a more interventionist approach have controlled spheroid size in special moulds, but the strict simultaneous size control of aggregates shown on the NIPAAm gradients has not been reported before. Using hydrophobic PDMS funnel moulds aggregate size was controlled (Bratt-Leal *et al*., 2011). Fluid shear has also been shown to homogenize the size of pluripotent stem cell aggregates, which has led to better protocols to scale-up stem cell expansion (Kinney *et al*., 2012). With regards to neurospheres, alternative methods have been developed to enhance clonality of neurospheres. Neuroscientists perceive the lack of neurosphere clonality as an issue, and that is where one neural stem cell generates a neurosphere. When studied it was not always the case, because in typical non-adherent culture the neurospheres can merge which affects clonality (Singec *et al*., 2006b), and neurospheres did not necessarily contain neural stem cells but the biochemical environment can generate them (Clarke *et al*., 2000b).

To improve clonality, microwells and encapsulation strategies have been developed (Cordey *et al*., 2008b, Coles-Takabe *et al*., 2008). The microwells improved the clonality of the neurospheres through restriction, but not the size distribution. Agarose encapsulation worked as a method to maintain clonality of neurospheres, and low cell densities could be used in agarose encapsulations (Coles-Takabe *et al*., 2008). Controlling the densities means that clonality of neurospheres could be controlled better with prevention of chimeric spheres. The sizes of the spheres reported were also quite variable ranging from 50 to 200 µm with the encapsulation technique, which is a surprising result from clonal neurospheres which would be expected to have more uniform size distribution. Time-lapse microscopy shows that a key mechanism for the formation of the neurospheres on the NIPAAm surface energy gradients was that the cells in the low density areas would first aggregate together. The phenomena of neurosphere merging and thus effecting clonality were also witnessed with time lapse microscopy. Here we do

question the importance of clonality because neurosphere merging was not part of a random process? In the videos in the low density area there was no random movement of the spheres towards each other. The merging involved the spheres moving towards each other in directed fashion, because the neurospheres were responding to the surface energy gradient with further evidence of migration of the merged sphere derived aggregate to a higher energy region of the gradient.

On the NIPAAm gradients visual evidence showed that the cell populations based on immunogenic markers would sort within neurospheres. There are few examples of biomaterials which have been developed to harness this natural process. Such biomaterials would improve biomedical research and cell therapy production. An explanation of how cell types sort in natural tissues was put forward by Steinberg in the 1960s (Steinberg, 1963). Steinberg labelled mesoderm cells green the endoderm cells red, and cells were observed to agglomerate which was followed by sorting where the red cells resided next to the red cells and the green with green. The cells which are less adhesive accumulate at the outer edges of such cell aggregates outside, and the inner core consists of more adhesive cells. Steinberg later demonstrated that the surface tension of the aggregate had a linear relationship the number of cadherins (Foty and Steinberg, 2005). Another interesting finding is that the aggregates can elongate and are not restricted to being spheroids *in vitro* (Ninomiya and Winklbauer, 2008). In a endothelial/mesoderm aggregate system endotheial wrapping would cause elongation and flattening of the aggregates. Also the authors show that the less cohesive cells do not have to be on the outside by mixing in a less cohesive cell line. A factor which favours differential adhesion hypothesis is that when cells divide the distribution of cellular components between the two daughter cells is not always symmetrical (Neumüller and Knoblich, 2009), therefore one would expect the structure to be lost when daughter cells of the same tissue are

asymmetrical. Neurospheres derived from primary sub-ventricular neural stem cells have been shown to have structure and organization (Lia S. Campos *et al*., 2004) which is consistent with differential adhesion hypothesis. Dividing bromodeoxyuridine positive cells where at the periphery which was the location of the neural stem cells, and the differentiated neurons and glia at the centre. This organization is logical because in full differentiation neurons and glia are in a low density monolayer, because they are more adhesive compared to stem cells. Confocal microscopy of the neurospheres on the NIPAAm gradient showed structuring within the neurospheres **(Figure 5.2**). Key differences with our culture system and (Lia S. Campos *et al*., 2004) included:

- Free-floating neurosphere culture system
- Cell culture media contained bFGF and EGF
- Forebrain cells (cortex and limbic) from rat pups,
- Larger neurospheres based on seeding density (size data was not shown)

The NIPAAm gradients have simplyified control of spheroid size. Useful applications would include scale-up of *in vitro* organ formation (Eiraku et al., 2008) where small cues stimulate self-organsized patteren from cells.

5.3.2 Neurosphere Numbers

Neurospheres adhered strongly enough to stay adhered through the fixing and immunocytochemistry protocols. Neurospheres have always been part of non-adherent free-floating cultures (Vescovi *et al*., 1993b). In chapter three and four surfaces were seeded with whole neurospheres where surfaces such as methyl functionalised were effective at retaining neurospheres, and in contrast the NIPAAm gradients neurospheres formed from single cells.

The highest abundance of the spheres was found in areas with low density and intermediate polymer length **(Figure 5.4)**. Neurosphere numbers in this area are almost doubled compared to other higher surface energy regions on the surface. The neurosphere numbers are lowest in regions with the lowest and highest surface energies.

Neural stem cells are typically cultured *in vitro* following two principle methods: adhered monolayers (Conti *et al*., 2005) and free-floating spheroid (Vescovi *et al*., 1993b). The spheroid techniques have distinct advantages including simplicity, scalability and developmental potential demonstrated in seminal work (Takebe *et al*., 2013, Eiraku *et al*., 2008). Neural stem cells and progenitors are cultured *in vitro* using stem cell mitogens such as βFGF and EGF.

On the NIPAAm gradient surfaces neurospheres could be found throughout the surface, and obviously present in higher numbers in certain areas. The highest abundance of the spheres was found in areas with low density and intermediate polymer length (**Figure** 5.12). The NIPAAm gradient delivered neural stem cell maintainace (cross-validated by neurosphere counting and expression of the Nestin and Sox2 markers) in a simpler protocol compared to (Vescovi *et al*., 1993b). Also the NIPAAm gradient provided a source of adhered neural stem cells but in a productive way compared to (Conti *et al*., 2005) monolayer method.

If applied commericailly the gradient would save alot of production costs because no low volume high value reagents were used in these experiments. Productivity in terms of producing more per unit area was increased and unit-operations were removed through consolidatedation of stem cell expansion and differentiation.

5.3.3 Differentiated Neurons and Glia

The counted neurons in **Figure** 5.9 were defined on a taxinomical basis with long spindly processes, and cross exspression of Tuj1 and DAPI to show the main cell body. Differentiated cortical neurons were found all over the coverslip. This shows that poly(NIPAAm) is perfectly capable of neural cell culture. The reason could be a resemblance of NIPAAm to poly(lysine) (in terms of amine content) which is a popular substrate for cell culture (Yavin and Yavin, 1974).

Differentiation of neurons was controlled by the gradient because different neuron numbers were counted around the gradient. The highest numbers of differentiated neurons were in the areas of the gradient with long polymers and high initiator density where amine density would have been highest. Low numbers of differentiated neurons were in the border and edge areas of the gradient which was common for neurospheres and glia too. Generally mature differentiated neurons responded more to polymer length than polymer density with more neurons found in the parts of the gradients with long polymers.

Glia tended to be found in similar places to neurons due to the maintenance role at the surface interface (Roach *et al*., 2012). In these experiments the neurons outnumbered the glia, because of the area where the cell were dissected from (Dombrowski *et al*., 2001).

Differentiated glia populations responded in terms of cell number to the NIPAAm gradient. The highest glia numbers were in the high density of NIPAAm polymer brushes with short lengths areas of the gradient. Across The whole NIPAAm gradient glia were present in consistently high numbers whenever the NIPAAm polymers were short, and that was mostly independent (ranging from 158 to 150 glia per quantile average) of

polymer initiator density. The areas of the gradient had about 3X more glia than the areas of the gradient with the lowest numbers.

Lutolf and Hubbell highlighted the morphogenic potential of surfaces the authors placed the emphasis on extracellular matrix proteins (Lutolf and Hubbell, 2005). The approach has worked well in an array format demonstrated by Flaim but the purpose of that platform was to probe the key cell extracellular matrix interactions to inform on future biomaterial design. Also the authors use mitogens such as retinoic acid and leukemia inhibitory factor (LIF).

Differentiation of cortical neurons could be controlled purely using these surfaces. Neurons and neurospheres are a powerful model to study surface induced differentiation with, because the cells are in two un-ambiguous states. As neural stem cells resided in three dimentional neurospheres, and as differentiated mature neurons we have low density two dimentional monolayer which resembles a 'honeycomb' collective morphology. It is long establish that poly(d-lysine)/poly(ornithine) laminin coated surfaces that neurons differentiate (Drago *et al*., 1991). Chapter 3 demonstrated that the *gold standard* performance of laminin coated surfaces could be achieved by harnessing the physical sciences of protein adsorption. Results were achieved by using aminopropyl silane terminated glass cover slides, and we observed similar responses in multiple outputs including spreading and lengthening. We demonstrated that surfaces can cause differentiation, and we show that gradient surfaces control differentiation of neurons because different stages of the cortical neural linages can be seen in different areas of the gradient. Therefore surface energy of a surface can precisely control neural stem cell differentiation. In areas of low surface amine density was host to neural stem cells, and mature differentiated neurons are found in areas with high amine density. Neurons can be purified by up to 700% when comparing the areas with highest neurons number to areas

with the lowest neuron numbers. Mature neurons in these experiments were defined as being positive for the Tuj1 antibody, the cells had to have a clear soma and nucleus, and processes had to be running out from the soma.

The experiments demonstrated that stem cell differentiation can be made into a more controllable process with principles of consolidated bioprocesses. To show that neural progenitors /stem cells were simultaneously being expanded and differentiated, the immunocytochemistry was performed only at the four day time point. There are numerous ways to cause differentiation such as contact dependent proteins (Drago *et al*., 1991), combinations of factors (Jaeger *et al*., 2011) and biomaterials alone (chapter 3). These methods highlight important principles, but not the control of the gradients where responses can be localised.

5.3.4 Possible Mechanisms

The NIPAAm gradients presented a two dimentional linear amine density gradient, where aggregates would arise because of the surface. Normally aggregates are normally produced by the classic hanging-drop technique to look at tissue sorting within. In an effort to simplify the argument behind thermodynamic and mechanical sorting we wanted to test the factors on a two dimentional planar surface to eliminate the influence of other factors un-intentionally introduced to the experiment. To simplify we developed a gradient which mixed brush density with varying NIPAAm polymer length to produce an orthogonal surface gradient aiming to control cell organization, and differentiation with thermodynamics at the cell surface-interface. For example in charge density studies with nanoparticles more plasma protein adsorbed onto particles with a higher charge density (Gessner *et al*., 2002). The authors found that the composition of adsorbed proteins did not differ significantly between the particles; the big differences were in specific adsorbed

volumes. Others have seen a superior cell response on surfaces by increasing surface energies, compared to materials with a lower surface energy (Zhao *et al*., 2005). Specifically with NIPAAm the response of bone marrow stem cell adhesion, spreading and growth alters by changing the ratio of NIPAAm in composite biomaterials (Allen *et al*., 2003). In contrast to our finding the authors found a less favourable response to the addition of NIPPAm in a linear fashion. In the previous experiments (chapter three) we reasoned that laminin or laminin fragments adsorb on to surfaces with amine groups, because of the similarity between amine surfaces to the poly(D-lysine)/laminin *gold standard*.

Certain parts of the gradient caused differentiation while other parts of the gradient caused maintenance of neural stem cells. Neurospheres on the gradient surfaces were studied with confocal microscopy to identify and localize neural markers. The relationship between neurosphere size and organization was bigger spheres were more sorted. Which means the greater adhesion forces in the bigger spheroids enhances cell sorting. The findings show that the thermodynamic surface gradient effected the organization within the spheroids, and size of the neurospheres was also affected. The clearest affects were based on adhesion and cell affinity with long NIPAAm polymer brushes at low density. The finding show in a vivid fashion that the neurosphere response was linear in places which adds a predictable level of control. Other scientists have shown in slightly different single cell systems (opposed to these aggregates) that the spreading of individual cells was effected by adhesion ligand density (Cavalcanti-Adam *et al*., 2006b). By functionalizing nanoparticles with arginylglycylaspartic acid (RGD) peptide sequences and having various densities of the particles (so therefore the RGD peptides), cell spreading could be controlled. Cells spread more with a higher ligand density, because of focal adhesions. That means for strong adhesion the adhesive molecules cluster, so in weaker

adhesions have less ligand density driven adhesive molecule clustering. Others have found different fibronectin densities different cell adhesive forces are generated. In a combination of surfaces coated with different fibronectin densities and a spinning-disk device it was calculated that if clustering is below 0.11 clusters/μm^2 a cell will not generate an adhesive force (Coyer *et al*., 2012). The reason highlighted by the authors was that the focal adhesions are key to organizing the cytoskeleton which generates the force (Dalby *et al*., 2004).

5.4 Chapter Five Conclusions

- Markers for stem cell and differentiated neurons concentrated at different parts of the surface.
- Neurospheres were in higher numbers in the lower amine density areas on the gradient.
- Differentiated neurons were more abundant in the higher amine density areas on the gradient.
- Effective high throughput platform with cell attachment in all areas
- Controlled neural cell differentiation with density and length pNIPAAm gradient

Chapter VI

6 Conclusions

The aim of PhD thesis was to find some simple principle to improve biomaterials, and to improve surfaces to better control neural cell culture. There have been various high-throughput approaches to biomaterial design, but the idea behind a lot of the work was to look at a parameter in the simplest form and ascertain the effects. For example the start of the project was to assess cell response to surface functionality, which was moved-on to multiple functionalities on the same surface in the final chapter.

In chapter three properties of the biomaterial interface with silane functalities to cause different cell responses. The surface chemical functionalities were shown to have dramatic impact on neural stem and daughter cell responses. Clear differences were observed between all the surfaces and the cell response metrics, with amine surfaces giving rise to similar attachment, spreading and differentiation capacity as that shown by poly(lysine)-laminin conditioned surfaces. The study presented shows that a simple and cheap chemical modification to a material's surface controls various aspects (attach, spreading, proliferation) of cell response, being of major benefit in terms of improve cell culture practices and scale-up, scale-out of cellular therapies for neural tissue.

In chapter four the aim to take the amine functionality further by incorporating secondary amines in the alkyl chains of silane molecules, so the surface were coated with secondary amines along with a primary amine head groups. One hypothesis for the success of the amine functionalised surfaces in chapter three was the relevance to biology, because secondary amines being found in amino acids such as arginine and histidine. Therefore the aim was to present the amine surface functionalities in a biologically relevant fashion by using silanes with secondary amine groups. In all the

metrics such as neurosphere spreading and neuron to glia ratio, the two surfaces with secondary amines would equal or exceed the primary amine surface between the three and five day time point to statistically significant levels. At the final seven day time point the secondary amine surfaces had a sharp decline in surface influenced cell responses. A possible explanation is bio-degradation where the surfaces changed as a result of the cell or the cell culture media. Retractions of neurosphere spreading were observed, and if that was a result of degradation, then having degradable materials would adversely affect cell response over time.

In chapter five the amine functionalites were put into a gradient. Currently *in vitro* differentiation of stem cells is achieved by using high value/low volume soluble factors, and functional tissue has been derived *in vitro* from pluripotent stem cells using relevant soluble signalling factors from the developmental process. The problem with using soluble signalling factors is expense and lack of control, because a lot signal proteins have overlapping roles. In these experiments we manged to control neural differentiation using chemo-physical gradient surfaces. The gradients allowed simultaneous culture of neural stem cells/progenitors (in neurospheres) with differentiated neurons in a differentiation media excluding expensive reagents, and the gradient surfaces concentrated the lineages to different areas of the surface. Principle to the gradient design was Steinberg's differential adhesion hypothesis, which made neurosphere size and organisation controllable allowing engineering of micro-environments. The chemical reaction used to make the gradients is translatable between many materials including metals and polymer. Therefore we provide a cheap and flexible solution which would be easy to incorporate into many experiments and processes to bring improvements with basic science and cell therapy production.

Chapter VII

7 References

Aguirre, A., Rubio, M.E., Gallo, V., 2010. Notch and EGFR pathway interaction regulates neural stem cell number and self-renewal. Nature 467, 323–327. doi:10.1038/nature09347

Alberti, K., Davey, R.E., Onishi, K., George, S., Salchert, K., Seib, F.P., Bornhäuser, M., Pompe, T., Nagy, A., Werner, C., Zandstra, P.W., 2008. Functional immobilization of signaling proteins enables control of stem cell fate. Nat. Methods 5, 645–650. doi:10.1038/nmeth.1222

Allen, L.T., Fox, E.J.P., Blute, I., Kelly, Z.D., Rochev, Y., Keenan, A.K., Dawson, K.A., Gallagher, W.M., 2003. Interaction of soft condensed materials with living cells: Phenotype/transcriptome correlations for the hydrophobic effect. Proc. Natl. Acad. Sci. 100, 6331–6336. doi:10.1073/pnas.1031426100

Altman, J., Bayer, S.A., 1981. Development of the brain stem in the rat. V. Thymidine-radiographic study of the time of origin of neurons in the midbrain tegmentum. J. Comp. Neurol. 198, 677–716. doi:10.1002/cne.901980409

Altman, J., Das, G.D., 1965. Autoradiographic and histological evidence of postnatal hippocampal neurogenesis in rats. J. Comp. Neurol. 124, 319–335. doi:10.1002/cne.901240303

Anderson, D.G., Levenberg, S., Langer, R., 2004. Nanoliter-scale synthesis of arrayed biomaterials and application to human embryonic stem cells. Nat. Biotechnol. 22, 863–866. doi:10.1038/nbt981

Anderson, N.L., Anderson, N.G., 2002. The human plasma proteome: history, character, and diagnostic prospects. Mol. Cell. Proteomics MCP 1, 845–867.

Angst, B.D., Marcozzi, C., Magee, A.I., 2001. The cadherin superfamily: diversity in form and function. J. Cell Sci. 114, 629–641.

Arima, Y., Iwata, H., 2007. Effect of wettability and surface functional groups on protein adsorption and cell adhesion using well-defined mixed self-assembled monolayers. Biomaterials 28, 3074–3082. doi:10.1016/j.biomaterials.2007.03.013

Asenath Smith, E., Chen, W., 2008. How To Prevent the Loss of Surface Functionality Derived from Aminosilanes. Langmuir 24, 12405–12409. doi:10.1021/la802234x

Ashall, L., Horton, C.A., Nelson, D.E., Paszek, P., Harper, C.V., Sillitoe, K., Ryan, S., Spiller, D.G., Unitt, J.F., Broomhead, D.S., Kell, D.B., Rand, D.A., Sée, V., White, M.R.H., 2009. Pulsatile Stimulation Determines Timing and Specificity of NF-κB-Dependent Transcription. Science 324, 242–246. doi:10.1126/science.1164860

Ashe, H.L., Briscoe, J., 2006. The interpretation of morphogen gradients. Development 133, 385–394. doi:10.1242/dev.02238

Astete, C.E., Sabliov, C.M., 2006. Synthesis and characterization of PLGA nanoparticles. J. Biomater. Sci. Polym. Ed. 17, 247–289.

Atthoff, B., Hilborn, J., 2007. Protein adsorption onto polyester surfaces: is there a need for surface activation? J. Biomed. Mater. Res. B Appl. Biomater. 80, 121–130. doi:10.1002/jbm.b.30576

Ayala, R., Zhang, C., Yang, D., Hwang, Y., Aung, A., Shroff, S.S., Arce, F.T., Lal, R., Arya, G., Varghese, S., 2011. Engineering the cell–material interface for controlling stem cell adhesion, migration, and differentiation. Biomaterials 32, 3700–3711. doi:10.1016/j.biomaterials.2011.02.004

Bain, C., Whitesides, G., 1988. Depth Sensitivity of Wetting - Monolayers of Omega-Mercapto Ethers on Gold. J. Am. Chem. Soc. 110, 5897–5898. doi:10.1021/ja00225a050

Ballestrem, C., Wehrle-Haller, B., Imhof, B.A., 1998. Actin dynamics in living mammalian cells. J. Cell Sci. 111 (Pt 12), 1649–1658.

Barbey, R., Lavanant, L., Paripovic, D., Schuewer, N., Sugnaux, C., Tugulu, S., Klok, H.-A., 2009. Polymer Brushes via Surface-Initiated Controlled Radical Polymerization: Synthesis, Characterization, Properties, and Applications. Chem. Rev. 109, 5437–5527. doi:10.1021/cr900045a

Barker, S.L., LaRocca, P.J., 1994. Method of production and control of a commercial tissue culture surface. J. Tissue Cult. Methods 16, 151–153. doi:10.1007/BF01540642

Batlle, E., Henderson, J.T., Beghtel, H., van den Born, M.M.W., Sancho, E., Huls, G., Meeldijk, J., Robertson, J., van de Wetering, M., Pawson, T., Clevers, H., 2002. Beta-catenin and TCF mediate cell positioning in the intestinal epithelium by controlling the expression of EphB/ephrinB. Cell 111, 251–263.

Bauwens, C.L., Song, H., Thavandiran, N., Ungrin, M., Massé, S., Nanthakumar, K., Seguin, C., Zandstra, P.W., 2011. Geometric Control of Cardiomyogenic Induction in Human Pluripotent Stem Cells. Tissue Eng. Part A 17, 1901–1909. doi:10.1089/ten.tea.2010.0563

Beck, K., Hunter, I., Engel, J., 1990. Structure and function of laminin: anatomy of a multidomain glycoprotein. FASEB J. Off. Publ. Fed. Am. Soc. Exp. Biol. 4, 148–160.

Bergenudd. H., 2011. Understanding the Mechanisms Behind Atom Transfer Radical Polymerization – Exploring the Limit of Control. Thesis Available from KTH Library

Ben-Hur, T., Idelson, M., Khaner, H., Pera, M., Reinhartz, E., Itzik, A., Reubinoff, B.E., 2004a. Transplantation of Human Embryonic Stem Cell–Derived Neural Progenitors Improves Behavioral Deficit in Parkinsonian Rats. STEM CELLS 22, 1246–1255. doi:10.1634/stemcells.2004-0094

Ben-Hur, T., Idelson, M., Khaner, H., Pera, M., Reinhartz, E., Itzik, A., Reubinoff, B.E., 2004b. Transplantation of human embryonic stem cell-derived neural progenitors improves behavioral deficit in Parkinsonian rats. Stem Cells Dayt. Ohio 22, 1246–1255. doi:10.1634/stemcells.2004-0094

Berge, Kurek, D., Blauwkamp, T., Koole, W., Maas, A., Eroglu, E., Siu, R.K., Nusse, R., 2011. Embryonic stem cells require Wnt proteins to prevent differentiation to epiblast stem cells. Nat. Cell Biol. 13.

Besnard, J., Ruda, G.F., Setola, V., Abecassis, K., Rodriguiz, R.M., Huang, X.-P., Norval, S., Sassano, M.F., Shin, A.I., Webster, L.A., Simeons, F.R.C., Stojanovski, L., Prat, A., Seidah, N.G., Constam, D.B., Bickerton, G.R., Read, K.D., Wetsel, W.C., Gilbert, I.H., Roth, B.L., Hopkins, A.L., 2012. Automated design of ligands to polypharmacological profiles. Nature 492, 215–220. doi:10.1038/nature11691

Bez, A., Corsini, E., Curti, D., Biggiogera, M., Colombo, A., Nicosia, R.F., Pagano, S.F., Parati, E.A., 2003. Neurosphere and neurosphere-forming cells: morphological and ultrastructural characterization. Brain Res. 993, 18–29.

Bjornson, C.R., Rietze, R.L., Reynolds, B.A., Magli, M.C., Vescovi, A.L., 1999. Turning brain into blood: a hematopoietic fate adopted by adult neural stem cells in vivo. Science 283, 534–537.

Blaess, S., Corrales, J.D., Joyner, A.L., 2006. Sonic hedgehog regulates Gli activator and repressor functions with spatial and temporal precision in the mid/hindbrain region. Development 133, 1799–1809. doi:10.1242/dev.02339

Boehler, M.D., Leondopulos, S.S., Wheeler, B.C., Brewer, G.J., 2012. Hippocampal networks on reliable patterned substrates. J. Neurosci. Methods 203, 344–353. doi:10.1016/j.jneumeth.2011.09.020

Bradbury, E.J., Khemani, S., Von, R., King, Priestley, J.V., McMahon, S.B., 1999. NT-3 promotes growth of lesioned adult rat sensory axons ascending in the dorsal columns of the spinal cord. Eur. J. Neurosci. 11, 3873–3883.

Bratt-Leal, A.M., Carpenedo, R.L., Ungrin, M.D., Zandstra, P.W., McDevitt, T.C., 2011. Incorporation of biomaterials in multicellular aggregates modulates pluripotent stem cell differentiation. Biomaterials 32, 48–56. doi:10.1016/j.biomaterials.2010.08.113

Braunecker, W.A., Matyjaszewski, K., 2007. Controlled/living radical polymerization: Features, developments, and perspectives. Prog. Polym. Sci. 32, 93–146. doi:10.1016/j.progpolymsci.2006.11.002

Briscoe, J., Chen, Y., Jessell, T.M., Struhl, G., 2001. A hedgehog-insensitive form of patched provides evidence for direct long-range morphogen activity of sonic hedgehog in the neural tube. Mol. Cell 7, 1279–1291.

Cai, L., Lu, J., Sheen, V., Wang, S., 2012. Promoting Nerve Cell Functions on Hydrogels Grafted with Poly(L-lysine). Biomacromolecules 13, 342–349. doi:10.1021/bm201763n

Caldwell, M.A., He, X., Wilkie, N., Pollack, S., Marshall, G., Wafford, K.A., Svendsen, C.N., 2001. Growth factors regulate the survival and fate of cells derived from human neurospheres. Nat. Biotechnol. 19, 475–479. doi:10.1038/88158

Campos, L.S., 2004. Neurospheres: insights into neural stem cell biology. J. Neurosci. Res. 78, 761–769. doi:10.1002/jnr.20333

Campos, L.S., Leone, D.P., Relvas, J.B., Brakebusch, C., Fässler, R., Suter, U., ffrench-Constant, C., 2004. Beta1 integrins activate a MAPK signalling pathway in neural stem cells that contributes to their maintenance. Dev. Camb. Engl. 131, 3433–3444. doi:10.1242/dev.01199

Campos, L.S., Leone, D.P., Relvas, J.B., Brakebusch, C., Fässler, R., Suter, U., Ffrench-Constant, C., 2004. B1 Integrins Activate a MAPK Signalling Pathway in Neural Stem Cells That Contributes to Their Maintenance. Development 131, 3433–3444. doi:10.1242/dev.01199

Capurro, M.I., Xu, P., Shi, W., Li, F., Jia, A., Filmus, J., 2008. Glypican-3 inhibits Hedgehog signaling during development by competing with patched for Hedgehog binding. Dev. Cell 14, 700–711. doi:10.1016/j.devcel.2008.03.006

Carter, S.B., (1967) Haptotaxis and the mechanism of cell motility. Nature. 213, 256

Castner, D.G., Ratner, B.D., 2002. Biomedical surface science: Foundations to frontiers. Surf. Sci. 500, 28–60. doi:10.1016/S0039-6028(01)01587-4

Cavalcanti-Adam, E.A., Micoulet, A., Blümmel, J., Auernheimer, J., Kessler, H., Spatz, J.P., 2006a. Lateral spacing of integrin ligands influences cell spreading and focal adhesion assembly. Eur. J. Cell Biol. 85, 219–224.

Cavalcanti-Adam, E.A., Micoulet, A., Blümmel, J., Auernheimer, J., Kessler, H., Spatz, J.P., 2006b. Lateral spacing of integrin ligands influences cell spreading and focal adhesion assembly. Eur. J. Cell Biol. 85, 219–224. doi:10.1016/j.ejcb.2005.09.011

Cavalcanti-Adam, E.A., Volberg, T., Micoulet, A., Kessler, H., Geiger, B., Spatz, J.P., 2007. Cell spreading and focal adhesion dynamics are regulated by spacing of integrin ligands. Biophys. J. 92, 2964–2974. doi:10.1529/biophysj.106.089730

Celiz, A.D., Smith, J.G.W., Langer, R., Anderson, D.G., Winkler, D.A., Barrett, D.A., Davies, M.C., Young, L.E., Denning, C., Alexander, M.R., 2014. Materials for stem cell factories of the future. Nat. Mater. 13, 570–579. doi:10.1038/nmat3972

Chang, E.-J., Kim, H.-H., Huh, J.-E., Kim, I.-A., Seung Ko, J., Chung, C.-P., Kim, H.-M., 2005. Low proliferation and high apoptosis of osteoblastic cells on hydrophobic surface are associated with defective Ras signaling. Exp. Cell Res. 303, 197–206. doi:10.1016/j.yexcr.2004.09.024

Charonis, A.S., Tsilibary, E.C., Yurchenco, P.D., Furthmayr, H., 1985. Binding of laminin to type IV collagen: a morphological study. J. Cell Biol. 100, 1848–1853.

Charron, F., Stein, E., Jeong, J., McMahon, A.P., Tessier-Lavigne, M., 2003. The Morphogen Sonic Hedgehog Is an Axonal Chemoattractant that Collaborates with Netrin-1 in Midline Axon Guidance. Cell 113, 11–23. doi:10.1016/S0092-8674(03)00199-5

Chaudhury, M.K., Whitesides, G.M., 1992. How to Make Water Run Uphill. Science 256, 1539–1541. doi:10.1126/science.256.5063.1539

Chen, J., Salas, A., Springer, T.A., 2003. Bistable regulation of integrin adhesiveness by a bipolar metal ion cluster. Nat. Struct. Biol. 10, 995–1001. doi:10.1038/nsb1011

Cheng, Y.-S., Champliaud, M.-F., Burgeson, R.E., Marinkovich, M.P., Yurchenco, P.D., 1997. Self-assembly of Laminin Isoforms. J. Biol. Chem. 272, 31525–31532. doi:10.1074/jbc.272.50.31525

Chieh, H.-F., Su, F.-C., Lin, S.-C., Shen, M.-R., Liao, J.-D., 2013. Migration Patterns and Cell Functions of Adipose-Derived Stromal Cells on Self-Assembled Monolayers with Different Functional Groups. J. Biomater. Sci. Polym. Ed. 24, 94–117. doi:10.1163/156856212X626208

Chin, M.H., Mason, M.J., Xie, W., Volinia, S., Singer, M., Peterson, C., Ambartsumyan, G., Aimiuwu, O., Richter, L., Zhang, J., Khvorostov, I., Ott, V., Grunstein, M., Lavon, N., Benvenisty, N., Croce, C.M., Clark, A.T., Baxter, T., Pyle, A.D., Teitell, M.A., Pelegrini, M., Plath, K., Lowry, W.E., 2009. Induced Pluripotent Stem Cells and Embryonic Stem Cells Are Distinguished by Gene Expression Signatures. Cell Stem Cell 5, 111–123. doi:10.1016/j.stem.2009.06.008

Clarke, D.L., Johansson, C.B., Wilbertz, J., Veress, B., Nilsson, E., Karlström, H., Lendahl, U., Frisén, J., 2000a. Generalized potential of adult neural stem cells. Science 288, 1660–1663.

Clarke, D.L., Johansson, C.B., Wilbertz, J., Veress, B., Nilsson, E., Karlström, H., Lendahl, U., Frisén, J., 2000b. Generalized potential of adult neural stem cells. Science 288, 1660–1663.

Cohen, D.E., Melton, D., 2011. Turning straw into gold: directing cell fate for regenerative medicine. Nat. Rev. Genet. 12, 243–252. doi:10.1038/nrg2938

Cole, M.A., Voelcker, N.H., Thissen, H., Griesser, H.J., 2009. Stimuli-responsive interfaces and systems for the control of protein-surface and cell-surface interactions. Biomaterials 30, 1827–1850. doi:10.1016/j.biomaterials.2008.12.026

Coles-Takabe, B.L.K., Brain, I., Purpura, K.A., Karpowicz, P., Zandstra, P.W., Morshead, C.M., van der Kooy, D., 2008. Don't look: growing clonal versus nonclonal neural stem cell colonies. Stem Cells Dayt. Ohio 26, 2938–2944. doi:10.1634/stemcells.2008-0558

Conti, L., Pollard, S.M., Gorba, T., Reitano, E., Toselli, M., Biella, G., Sun, Y., Sanzone, S., Ying, Q.-L., Cattaneo, E., Smith, A., 2005. Niche-Independent Symmetrical Self-Renewal of a Mammalian Tissue Stem Cell. PLoS Biol 3, e283. doi:10.1371/journal.pbio.0030283

Cookson, S., Ostroff, N., Pang, W.L., Volfson, D., Hasty, J., 2005. Monitoring dynamics of single-cell gene expression over multiple cell cycles. Mol. Syst. Biol. 1, 2005.0024. doi:10.1038/msb4100032

Cooper, A.R., Kurkinen, M., Taylor, A., Hogan, B.L.M., 1981. Studies on the Biosynthesis of Laminin by Murine Parietal Endoderm Cells. Eur. J. Biochem. 119, 189–197. doi:10.1111/j.1432-1033.1981.tb05593.x

Cordey, M., Limacher, M., Kobel, S., Taylor, V., Lutolf, M.P., 2008a. Enhancing the reliability and throughput of neurosphere culture on hydrogel microwell arrays. Stem Cells 26, 2586–2594.

Cordey, M., Limacher, M., Kobel, S., Taylor, V., Lutolf, M.P., 2008b. Enhancing the Reliability and Throughput of Neurosphere Culture on Hydrogel Microwell Arrays. STEM CELLS 26, 2586–2594. doi:10.1634/stemcells.2008-0498

Couture, L.A., n.d. Scalable pluripotent stem cell culture. Nat. Biotechnol. 28, 562–563. doi:10.1038/nbt0610-562

Coyer, S.R., Singh, A., Dumbauld, D.W., Calderwood, D.A., Craig, S.W., Delamarche, E., Garcia, A.J., 2012. Nanopatterning reveals an ECM area threshold for focal adhesion assembly and force transmission that is regulated by integrin activation and cytoskeleton tension. J. Cell Sci. 125, 5110–5123. doi:10.1242/jcs.108035

Cunningham, B.A., Hoffman, S., Rutishauser, U., Hemperly, J.J., Edelman, G.M., 1983. Molecular topography of the neural cell adhesion molecule N-CAM: surface orientation and location of sialic acid-rich and binding regions. Proc. Natl. Acad. Sci. U. S. A. 80, 3116–3120.

Curran, J.M., Chen, R., Hunt, J.A., 2005. Controlling the phenotype and function of mesenchymal stem cells in vitro by adhesion to silane-modified clean glass surfaces. Biomaterials 26, 7057–7067. doi:10.1016/j.biomaterials.2005.05.008

Curran, J.M., Chen, R., Hunt, J.A., 2006. The guidance of human mesenchymal stem cell differentiation in vitro by controlled modifications to the cell substrate. Biomaterials 27, 4783–4793. doi:10.1016/j.biomaterials.2006.05.001

Curtis, A.S., Forrester, J.V., 1984. The competitive effects of serum proteins on cell adhesion. J. Cell Sci. 71, 17–35.

D'Amour, K.A., Bang, A.G., Eliazer, S., Kelly, O.G., Agulnick, A.D., Smart, N.G., Moorman, M.A., Kroon, E., Carpenter, M.K., Baetge, E.E., 2006. Production of pancreatic hormone-expressing endocrine cells from human embryonic stem cells. Nat. Biotechnol. 24, 1392–1401. doi:10.1038/nbt1259

Daadi, M.M., Steinberg, G.K., 2009. Manufacturing neurons from human embryonic stem cells: biological and regulatory aspects to develop a safe cellular product for stroke cell therapy. Regen. Med. 4, 251–263. doi:10.2217/17460751.4.2.251

Dahlstrand, J., Zimmerman, L.B., McKay, R.D., Lendahl, U., 1992. Characterization of the human nestin gene reveals a close evolutionary relationship to neurofilaments. J. Cell Sci. 103, 589–597.

Dalby, M.J., Gadegaard, N., Riehle, M.O., Wilkinson, C.D.W., Curtis, A.S.G., 2004. Investigating filopodia sensing using arrays of defined nano-pits down to 35 nm diameter in size. Int. J. Biochem. Cell Biol. 36, 2005–2015. doi:10.1016/j.biocel.2004.03.001

Dalby, M.J., Gadegaard, N., Tare, R., Andar, A., Riehle, M.O., Herzyk, P., Wilkinson, C.D.W., Oreffo, R.O.C., 2007. The control of human mesenchymal cell differentiation using nanoscale symmetry and disorder. Nat. Mater. 6, 997–1003. doi:10.1038/nmat2013

Dalton, P.D., Flynn, L., Shoichet, M.S., 2002. Manufacture of poly(2-hydroxyethyl methacrylate-co-methyl methacrylate) hydrogel tubes for use as nerve guidance channels. Biomaterials 23, 3843–3851.

Darr, H., Mayshar, Y., Benvenisty, N., 2006. Overexpression of NANOG in human ES cells enables feeder-free growth while inducing primitive ectoderm features. Dev. Camb. Engl. 133, 1193–1201. doi:10.1242/dev.02286

Davidson, K.C., Adams, A.M., Goodson, J.M., McDonald, C.E., Potter, J.C., Berndt, J.D., Biechele, T.L., Taylor, R.J., Moon, R.T., 2012. Wnt/β-catenin signaling promotes differentiation, not self-renewal, of human embryonic stem cells and is repressed by Oct4. Proc. Natl. Acad. Sci. 201118777. doi:10.1073/pnas.1118777109

DeLong, S.A., Moon, J.J., West, J.L., 2005. Covalently immobilized gradients of bFGF on hydrogel scaffolds for directed cell migration. Biomaterials 26, 3227–3234. doi:10.1016/j.biomaterials.2004.09.021

Dimos, J.T., Rodolfa, K.T., Niakan, K.K., Weisenthal, L.M., Mitsumoto, H., Chung, W., Croft, G.F., Saphier, G., Leibel, R., Goland, R., Wichterle, H., Henderson, C.E., Eggan, K., 2008. Induced pluripotent stem cells generated from patients with ALS can be differentiated into motor neurons. Science 321, 1218–1221. doi:10.1126/science.1158799

Discher, D.E., Mooney, D.J., Zandstra, P.W., 2009. Growth factors, matrices, and forces combine and control stem cells. Science 324, 1673–1677. doi:10.1126/science.1171643

Dityatev, A., Schachner, M., 2003. Extracellular matrix molecules and synaptic plasticity. Nat. Rev. Neurosci. 4, 456–468. doi:10.1038/nrn1115

Doetsch, F., Petreanu, L., Caille, I., Garcia-Verdugo, J.M., Alvarez-Buylla, A., 2002. EGF converts transit-amplifying neurogenic precursors in the adult brain into multipotent stem cells. Neuron 36, 1021–1034.

Dombrowski, S.M., Hilgetag, C.C., Barbas, H., 2001. Quantitative Architecture Distinguishes Prefrontal Cortical Systems in the Rhesus Monkey. Cereb. Cortex 11, 975–988. doi:10.1093/cercor/11.10.975

Dowell-Mesfin, N.M., Abdul-Karim, M.-A., Turner, A.M.P., Schanz, S., Craighead, H.G., Roysam, B., Turner, J.N., Shain, W., 2004. Topographically modified surfaces affect orientation and growth of hippocampal neurons. J. Neural Eng. 1, 78–90. doi:10.1088/1741-2560/1/2/003

Drago, J., Nurcombe, V., Bartlett, P.F., 1991. Laminin through its long arm E8 fragment promotes the proliferation and differentiation of murine neuroepithelial cells in vitro. Exp. Cell Res. 192, 256–265. doi:10.1016/0014-4827(91)90184-V

Dubey, G., Mequanint, K., 2011. Conjugation of fibronectin onto three-dimensional porous scaffolds for vascular tissue engineering applications. Acta Biomater. 7, 1114–1125. doi:10.1016/j.actbio.2010.11.010

Dubiel, E.A., Martin, Y., Vermette, P., 2011. Bridging the Gap Between Physicochemistry and Interpretation Prevalent in Cell−Surface Interactions. Chem. Rev. 111, 2900–2936. doi:10.1021/cr9002598

Duval, N., Gomès, D., Calaora, V., Calabrese, A., Meda, P., Bruzzone, R., 2002. Cell coupling and Cx43 expression in embryonic mouse neural progenitor cells. J. Cell Sci. 115, 3241–3251.

E S Anton, J.A.K., 1999. Distinct functions of alpha3 and alpha(v) integrin receptors in neuronal migration and laminar organization of the cerebral cortex. Neuron 22, 277–89.

Edmondson, J.C., Hatten, M.E., 1987. Glial-guided granule neuron migration in vitro: a high-resolution time-lapse video microscopic study. J. Neurosci. Off. J. Soc. Neurosci. 7, 1928–1934.

Eiraku, M., Takata, N., Ishibashi, H., Kawada, M., Sakakura, E., Okuda, S., Sekiguchi, K., Adachi, T., Sasai, Y., 2011. Self-organizing optic-cup morphogenesis in three-dimensional culture. Nature 472, 51–56. doi:10.1038/nature09941

Eiraku, M., Watanabe, K., Matsuo-Takasaki, M., Kawada, M., Yonemura, S., Matsumura, M., Wataya, T., Nishiyama, A., Muguruma, K., Sasai, Y., 2008. Self-Organized Formation of Polarized Cortical Tissues from ESCs and Its Active Manipulation by Extrinsic Signals. Cell Stem Cell 3, 519–532. doi:10.1016/j.stem.2008.09.002

Ekblad, T., Andersson, O., Tai, F.-I., Ederth, T., Liedberg, B., 2009. Lateral Control of Protein Adsorption on Charged Polymer Gradients. Langmuir 25, 3755–3762. doi:10.1021/la803443d

Eldar, A., Rosin, D., Shilo, B.-Z., Barkai, N., 2003. Self-enhanced ligand degradation underlies robustness of morphogen gradients. Dev. Cell 5, 635–646.

Elisseeff, J., McIntosh, W., Fu, K., Blunk, B.T., Langer, R., 2001. Controlled-release of IGF-I and TGF-beta1 in a photopolymerizing hydrogel for cartilage tissue engineering. J. Orthop. Res. Off. Publ. Orthop. Res. Soc. 19, 1098–1104. doi:10.1016/S0736-0266(01)00054-7

Emerling, D.E., Lander, A.D., 1996. Inhibitors and Promoters of Thalamic Neuron Adhesion and Outgrowth in Embryonic Neocortex: Functional Association with Chondroitin Sulfate. Neuron 17, 1089–1100. doi:10.1016/S0896-6273(00)80242-1

Evans, M.J., Kaufman, M.H., 1981. Establishment in culture of pluripotential cells from mouse embryos. Nature 292, 154–156.

Evans, N.R., Davies, E.M., Dare, C.J., Oreffo, R.O., 2013. Tissue engineering strategies in spinal arthrodesis: the clinical imperative and challenges to clinical translation. Regen. Med. 8, 49–64. doi:10.2217/rme.12.106

Faham, S., Hileman, R.E., Fromm, J.R., Linhardt, R.J., Rees, D.C., 1996. Heparin Structure and Interactions with Basic Fibroblast Growth Factor. Science 271, 1116–1120. doi:10.1126/science.271.5252.1116

Faucheux, N., Schweiss, R., Lützow, K., Werner, C., Groth, T., 2004. Self-assembled monolayers with different terminating groups as model substrates for cell adhesion studies. Biomaterials 25, 2721–2730. doi:10.1016/j.biomaterials.2003.09.069

Felicia M. Rosenthal, F.A., Nicole M. Provost, 2013. Standards for Ancillary Materials Used in Cell- and Tissue-Based Therapies. BioProcess Int. 11, 12–22.

Ferrari, A., Cecchini, M., Serresi, M., Faraci, P., Pisignano, D., Beltram, F., 2010. Neuronal polarity selection by topography-induced focal adhesion control. Biomaterials 31, 4682–4694. doi:10.1016/j.biomaterials.2010.02.032

Finke, B., Luethen, F., Schroeder, K., Mueller, P.D., Bergemann, C., Frant, M., Ohl, A., Nebe, B.J., 2007. The effect of positively charged plasma polymerization on initial osteoblastic focal adhesion on titanium surfaces. Biomaterials 28, 4521–4534. doi:10.1016/j.biomaterials.2007.06.028

Fisher, O.Z., Khademhosseini, A., Langer, R., Peppas, N.A., 2010. Bio-inspired Materials for Controlling Stem Cell Fate. Acc. Chem. Res. 43, 419–428. doi:10.1021/ar900226q

Flaim, C.J., Chien, S., Bhatia, S.N., 2005. An extracellular matrix microarray for probing cellular differentiation. Nat. Methods 2, 119–125. doi:10.1038/nmeth736

Flanagan, L.A., Rebaza, L.M., Derzic, S., Schwartz, P.H., Monuki, E.S., 2006. Regulation of human neural precursor cells by laminin and integrins. J. Neurosci. Res. 83, 845–856. doi:10.1002/jnr.20778

Foty, R.A., Steinberg, M.S., 2005. The differential adhesion hypothesis: a direct evaluation. Dev. Biol. 278, 255–263. doi:10.1016/j.ydbio.2004.11.012

Franz, C.K., Rutishauser, U., Rafuse, V.F., 2005. Polysialylated Neural Cell Adhesion Molecule Is Necessary for Selective Targeting of Regenerating Motor Neurons. J. Neurosci. 25, 2081–2091. doi:10.1523/JNEUROSCI.4880-04.2005

Freire, E., Gomes, F.C.A., Linden, R., Neto, V.M., Coelho-Sampaio, T., 2002. Structure of laminin substrate modulates cellular signaling for neuritogenesis. J. Cell Sci. 115, 4867–4876. doi:10.1242/jcs.00173

Fricker-Gates, R.A., Gates, M.A., 2010. Stem cell-derived dopamine neurons for brain repair in Parkinson's disease. Regen. Med. 5, 267–278. doi:10.2217/rme.10.3

Fuentealba, L.C., Obernier, K., Alvarez-Buylla, A., 2012. Adult neural stem cells bridge their niche. Cell Stem Cell 10, 698–708. doi:10.1016/j.stem.2012.05.012

Funakoshi, N., Duret, C., Pascussi, J.-M., Blanc, P., Maurel, P., Daujat-Chavanieu, M., Gerbal-Chaloin, S., 2011. Comparison of Hepatic-like Cell Production from Human Embryonic Stem Cells and Adult Liver Progenitor Cells: CAR Transduction Activates a Battery of Detoxification Genes. Stem Cell Rev. 7, 518–531. doi:10.1007/s12015-010-9225-3

Fusaoka-Nishioka, E., Shimono, C., Taniguchi, Y., Togawa, A., Yamada, A., Inoue, E., Onodera, H., Sekiguchi, K., Imai, T., 2011. Differential effects of laminin isoforms on axon and dendrite development in hippocampal neurons. Neurosci. Res. 71, 421–426. doi:10.1016/j.neures.2011.08.012

Garcion, E., Halilagic, A., Faissner, A., ffrench-Constant, C., 2004. Generation of an environmental niche for neural stem cell development by the extracellular matrix molecule tenascin C. Development 131, 3423–3432. doi:10.1242/dev.01202

Geim, A.K., Dubonos, S.V., Grigorieva, I.V., Novoselov, K.S., Zhukov, A.A., Shapoval, S.Y., 2003. Microfabricated adhesive mimicking gecko foot-hair. Nat. Mater. 2, 461–463. doi:10.1038/nmat917

Genet, G., Guilbeau-Frugier, C., Honton, B., Dague, E., Schneider, M.D., Coatrieux, C., Calise, D., Cardin, C., Nieto, C., Payré, B., Dubroca, C., Marck, P., Heymes, C., Dubrac, A., Arvanitis, D., Despas, F., Altié, M.-F., Seguelas, M.-H., Delisle, M.-B., Davy, A., Sénard, J.-M., Pathak, A., Galés, C., 2012. Ephrin-B1 Is a Novel Specific Component of the Lateral Membrane of the Cardiomyocyte and Is Essential for the Stability of Cardiac Tissue Architecture Cohesion. Circ. Res. 110, 688–700. doi:10.1161/CIRCRESAHA.111.262451

Georges-Labouesse, E., Mark, M., Messaddeq, N., Gansmüller, A., 1998. Essential role of alpha 6 integrins in cortical and retinal lamination. Curr. Biol. CB 8, 983–986.

Gessner, A., Lieske, A., Paulke, B.R., Müller, R.H., 2002. Influence of surface charge density on protein adsorption on polymeric nanoparticles: analysis by two-dimensional electrophoresis. Eur. J. Pharm. Biopharm. 54, 165–170. doi:10.1016/S0939-6411(02)00081-4

Giam, L.R., Massich, M.D., Hao, L., Shin Wong, L., Mader, C.C., Mirkin, C.A., 2012. Scanning probe-enabled nanocombinatorics define the relationship between fibronectin feature size and stem cell fate. Proc. Natl. Acad. Sci. U. S. A. 109, 4377–4382. doi:10.1073/pnas.1201086109

Gierer, A., Meinhardt, H., 1972. A theory of biological pattern formation. Kybernetik 12, 30–39.

Goetz, A.K., Scheffler, B., Chen, H.-X., Wang, S., Suslov, O., Xiang, H., Bruestle, O., Roper, S.N., Steindler, D.A., 2006a. Temporally restricted substrate interactions direct fate and specification of neural precursors derived from embryonic stem cells. Proc. Natl. Acad. Sci. U. S. A. 103, 11063–11068. doi:10.1073/pnas.0510926103

Goetz, A.K., Scheffler, B., Chen, H.-X., Wang, S., Suslov, O., Xiang, H., Brüstle, O., Roper, S.N., Steindler, D.A., 2006b. Temporally restricted substrate interactions direct fate and specification of neural precursors derived from embryonic stem cells. Proc. Natl. Acad. Sci. U. S. A. 103, 11063–11068. doi:10.1073/pnas.0510926103

Gomez, P.F., Morcuende, J.A., 2005. A Historical and Economic Perspective on Sir John Charnley, Chas F. Thackray Limited, and the Early Arthroplasty Industry. Iowa Orthop. J. 25, 30–37.

Goodman, S.L., Aumailley, M., von der Mark, H., 1991. Multiple cell surface receptors for the short arms of laminin: alpha 1 beta 1 integrin and RGD-dependent proteins mediate cell attachment only to domains III in murine tumor laminin. J. Cell Biol. 113, 931–941.

Goodman, S.L., Deutzmann, R., von der Mark, K., 1987. Two distinct cell-binding domains in laminin can independently promote nonneuronal cell adhesion and spreading. J. Cell Biol. 105, 589–598.

Graham, V., Khudyakov, J., Ellis, P., Pevny, L., 2003. SOX2 Functions to Maintain Neural Progenitor Identity. Neuron 39, 749–765. doi:10.1016/S0896-6273(03)00497-5

Grandbarbe, L., Bouissac, J., Rand, M., Hrabé de Angelis, M., Artavanis-Tsakonas, S., Mohier, E., 2003. Delta-Notch signaling controls the generation of neurons/glia from neural stem cells in a stepwise process. Dev. Camb. Engl. 130, 1391–1402.

Griesser, H., Chatelier, R., Gengenbach, T., Johnson, G., Steele, J., 1994. Growth of Human-Cells on Plasma Polymers - Putative Role of Amine and Amide Groups. J. Biomater. Sci.-Polym. Ed. 5, 531–554. doi:10.1163/156856294X00194

Haile, Y., Haastert, K., Cesnulevicius, K., Stummeyer, K., Timmer, M., Berski, S., Dräger, G., Gerardy-Schahn, R., Grothe, C., 2007. Culturing of glial and neuronal cells on polysialic acid. Biomaterials 28, 1163–1173. doi:10.1016/j.biomaterials.2006.10.030

Hanna, J., Saha, K., Pando, B., van Zon, J., Lengner, C.J., Creyghton, M.P., van Oudenaarden, A., Jaenisch, R., 2009. Direct cell reprogramming is a stochastic process amenable to acceleration. Nature 462, 595–601. doi:10.1038/nature08592

Hanna, J.H., Saha, K., Jaenisch, R., 2010. Pluripotency and cellular reprogramming: facts, hypotheses, unresolved issues. Cell 143, 508–525. doi:10.1016/j.cell.2010.10.008

Harder, P., Grunze, M., Dahint, R., Whitesides, G.M., Laibinis, P.E., 1998. Molecular Conformation in Oligo(ethylene glycol)-Terminated Self-Assembled Monolayers on Gold and Silver Surfaces Determines Their Ability To Resist Protein Adsorption. J. Phys. Chem. B 102, 426–436. doi:10.1021/jp972635z

Harris, B.P., Kutty, J.K., Fritz, E.W., Webb, C.K., Burg, K.J.L., Metters, A.T., 2006. Photopatterned Polymer Brushes Promoting Cell Adhesion Gradients. Langmuir 22, 4467–4471. doi:10.1021/la053417x

Haubner, R., Gratias, R., Diefenbach, B., Goodman, S.L., Jonczyk, A., Kessler, H., 1996. Structural and Functional Aspects of RGD-Containing Cyclic Pentapeptides as Highly Potent and Selective Integrin αVβ3 Antagonists. J. Am. Chem. Soc. 118, 7461–7472. doi:10.1021/ja9603721

Heo, J.S., Choi, S.-M., Kim, H.O., Kim, E.H., You, J., Park, T., Kim, E., Kim, H.-S., 2013. Neural transdifferentiation of human bone marrow mesenchymal stem cells on hydrophobic polymer-modified surface and therapeutic effects in an animal model of ischemic stroke. Neuroscience 238, 305–318. doi:10.1016/j.neuroscience.2013.02.011

Hirschfeld-Warneken, V.C., Arnold, M., Cavalcanti-Adam, A., López-García, M., Kessler, H., Spatz, J.P., 2008. Cell adhesion and polarisation on molecularly defined spacing gradient surfaces of cyclic RGDfK peptide patches. Eur. J. Cell Biol. 87, 743–750. doi:10.1016/j.ejcb.2008.03.011

Hook, A.L., Chang, C.-Y., Yang, J., Luckett, J., Cockayne, A., Atkinson, S., Mei, Y., Bayston, R., Irvine, D.J., Langer, R., Anderson, D.G., Williams, P., Davies, M.C., Alexander, M.R., 2012. Combinatorial discovery of polymers resistant to bacterial attachment. Nat. Biotechnol. 30, 868–875. doi:10.1038/nbt.2316

Howell, D., 2012. Statistical Methods for Psychology. Cengage Learning.

Humphries, J.D., Byron, A., Humphries, M.J., 2006. Integrin ligands at a glance. J. Cell Sci. 119, 3901–3903. doi:10.1242/jcs.03098

Hung, C.-H., Young, T.-H., 2006. Differences in the effect on neural stem cells of fetal bovine serum in substrate-coated and soluble form. Biomaterials 27, 5901–5908. doi:10.1016/j.biomaterials.2006.08.009

Hussain, S.-A., Carafoli, F., Hohenester, E., 2011. Determinants of laminin polymerization revealed by the structure of the α5 chain amino-terminal region. EMBO Rep. 12, 276–282. doi:10.1038/embor.2011.3

Hyafil, F., Babinet, C., Jacob, F., 1981. Cell-cell interactions in early embryogenesis: a molecular approach to the role of calcium. Cell 26, 447–454.

Hynes, R., 1992. Integrins - Versatility, Modulation, and Signaling in Cell-Adhesion. Cell 69, 11–25. doi:10.1016/0092-8674(92)90115-S

Hynes, R.O., 2002. Integrins: bidirectional, allosteric signaling machines. Cell 110, 673–687.

Jacques, T.S., Relvas, J.B., Nishimura, S., Pytela, R., Edwards, G.M., Streuli, C.H., ffrench-Constant, C., 1998. Neural precursor cell chain migration and division are regulated through different beta1 integrins. Development 125, 3167–3177.

Jaeger, I., Arber, C., Risner-Janiczek, J.R., Kuechler, J., Pritzsche, D., Chen, I.-C., Naveenan, T., Ungless, M.A., Li, M., 2011. Temporally controlled modulation of FGF/ERK signaling

directs midbrain dopaminergic neural progenitor fate in mouse and human pluripotent stem cells. Dev. Camb. Engl. 138, 4363–4374. doi:10.1242/dev.066746

Jaeger, J., Surkova, S., Blagov, M., Janssens, H., Kosman, D., Kozlov, K.N., Manu, Myasnikova, E., Vanario-Alonso, C.E., Samsonova, M., Sharp, D.H., Reinitz, J., 2004. Dynamic control of positional information in the early Drosophila embryo. Nature 430, 368–371. doi:10.1038/nature02678

James, D., Levine, A.J., Besser, D., Hemmati-Brivanlou, A., 2005. TGFbeta/activin/nodal signaling is necessary for the maintenance of pluripotency in human embryonic stem cells. Dev. Camb. Engl. 132, 1273–1282. doi:10.1242/dev.01706

Jeon, O., Alt, D.S., Linderman, S.W., Alsberg, E., 2013. Biochemical and Physical Signal Gradients in Hydrogels to Control Stem Cell Behavior. Adv. Mater. n/a–n/a. doi:10.1002/adma.201302364

Jeon, S.., Andrade, J.., 1991. Protein—surface interactions in the presence of polyethylene oxide: II. Effect of protein size. J. Colloid Interface Sci. 142, 159–166. doi:10.1016/0021-9797(91)90044-9

Joddar, B., Guy, A.T., Kamiguchi, H., Ito, Y., 2013. Spatial gradients of chemotropic factors from immobilized patterns to guide axonal growth and regeneration. Biomaterials 34, 9593–9601. doi:10.1016/j.biomaterials.2013.08.019

Kalyani, A., Hobson, K., Rao, M.S., 1997. Neuroepithelial Stem Cells from the Embryonic Spinal Cord: Isolation, Characterization, and Clonal Analysis. Dev. Biol. 186, 202–223. doi:10.1006/dbio.1997.8592

Kam, L., Shain, W., Turner, J.N., Bizios, R., 2002. Selective adhesion of astrocytes to surfaces modified with immobilized peptides. Biomaterials 23, 511–515.

Kanczler, J.M., Mirmalek-Sani, S.-H., Hanley, N.A., Ivanov, A.L., Barry, J.J.A., Upton, C., Shakesheff, K.M., Howdle, S.M., Antonov, E.N., Bagratashvili, V.N., Popov, V.K., Oreffo, R.O.C., 2009. Biocompatibility and osteogenic potential of human fetal femur-derived cells on surface selective laser sintered scaffolds. Acta Biomater. 5, 2063–2071. doi:10.1016/j.actbio.2009.03.010

Kane, D.A., McFarland, K.N., Warga, R.M., 2005. Mutations in half baked/E-cadherin block cell behaviors that are necessary for teleost epiboly. Dev. Camb. Engl. 132, 1105–1116. doi:10.1242/dev.01668

Kasper, C., Rasmussen, H., Kastrup, J.S., Ikemizu, S., Jones, E.Y., Berezin, V., Bock, E., Larsen, I.K., 2000. Structural basis of cell–cell adhesion by NCAM. Nat. Struct. Mol. Biol. 7, 389–393. doi:10.1038/75165

Kato, M., Kamigaito, M., Sawamoto, M., Higashimura, T., 1995. Polymerization of Methyl Methacrylate with the Carbon Tetrachloride/Dichlorotris-(triphenylphosphine)ruthenium(II)/Methylaluminum Bis(2,6-di-tert-butylphenoxide) Initiating System: Possibility of Living Radical Polymerization. Macromolecules 28, 1721–1723. doi:10.1021/ma00109a056

Kawamura, R., Mishima, M., Ryu, S., Arai, Y., Okose, M., Silberberg, Y.R., Rao, S.R., Nakamura, C., 2013. Controlled Cell Adhesion Using a Biocompatible Anchor for Membrane-Conjugated Bovine Serum Albumin/Bovine Serum Albumin Mixed Layer. Langmuir 29, 6429–6433. doi:10.1021/la4012229

Kearns, S.M., Laywell, E.D., Kukekov, V.K., Steindler, D.A., 2003. Extracellular matrix effects on neurosphere cell motility. Exp. Neurol. 182, 240–244. doi:10.1016/S0014-4886(03)00124-9

Kerever, A., Schnack, J., Vellinga, D., Ichikawa, N., Moon, C., Arikawa-Hirasawa, E., Efird, J.T., Mercier, F., 2007. Novel extracellular matrix structures in the neural stem cell niche capture the neurogenic factor fibroblast growth factor 2 from the extracellular milieu. Stem Cells Dayt. Ohio 25, 2146–2157. doi:10.1634/stemcells.2007-0082

Kerszberg, M., Wolpert, L., 1998. Mechanisms for positional signalling by morphogen transport: a theoretical study. J. Theor. Biol. 191, 103–114. doi:10.1006/jtbi.1997.0575

Keselowsky, B.G., Collard, D.M., García, A.J., 2003. Surface chemistry modulates fibronectin conformation and directs integrin binding and specificity to control cell adhesion. J. Biomed. Mater. Res. A 66A, 247–259. doi:10.1002/jbm.a.10537

Keung, A.J., Kumar, S., Schaffer, D.V., 2010. Presentation counts: microenvironmental regulation of stem cells by biophysical and material cues. Annu. Rev. Cell Dev. Biol. 26, 533–556. doi:10.1146/annurev-cellbio-100109-104042

Kim, H.-J., 2011. Stem cell potential in Parkinson's disease and molecular factors for the generation of dopamine neurons. Biochim. Biophys. Acta 1812, 1–11.

Kim, M., Morshead, C.M., 2003. Distinct Populations of Forebrain Neural Stem and Progenitor Cells Can Be Isolated Using Side-Population Analysis. J. Neurosci. 23, 10703–10709.

Kinney, M.A., Saeed, R., McDevitt, T.C., 2012. Systematic analysis of embryonic stem cell differentiation in hydrodynamic environments with controlled embryoid body size. Integr. Biol. 4, 641–650. doi:10.1039/C2IB00165A

Kinoshita, Y., Kinoshita, C., Heuer, J.G., Bothwell, M., 1993. Basic fibroblast growth factor promotes adhesive interactions of neuroepithelial cells from chick neural tube with extracellular matrix proteins in culture. Dev. Camb. Engl. 119, 943–956.

Kirouac, D.C., Zandstra, P.W., 2008. The Systematic Production of Cells for Cell Therapies. Cell Stem Cell 3, 369–381. doi:10.1016/j.stem.2008.09.001

Kleene, R., Schachner, M., 2004. Glycans and neural cell interactions. Nat. Rev. Neurosci. 5, 195–208. doi:10.1038/nrn1349

Kleinfeld, D., Kahler, K.H., Hockberger, P.E., 1988. Controlled outgrowth of dissociated neurons on patterned substrates. J. Neurosci. 8, 4098–4120.

Ko, I.K., Kato, K., Iwata, H., 2005. Parallel analysis of multiple surface markers expressed on rat neural stem cells using antibody microarrays. Biomaterials 26, 4882–4891. doi:10.1016/j.biomaterials.2004.11.049

Koc, Y., de Mello, A.J., McHale, G., Newton, M.I., Roach, P., Shirtcliffe, N.J., 2008. Nano-scale superhydrophobicity: suppression of protein adsorption and promotion of flow-induced detachment. Lab. Chip 8, 582–586. doi:10.1039/b716509a

Koh, H.S., Yong, T., Chan, C.K., Ramakrishna, S., 2008. Enhancement of neurite outgrowth using nano-structured scaffolds coupled with laminin. Biomaterials 29, 3574–3582. doi:10.1016/j.biomaterials.2008.05.014

Konagaya, S., Kato, K., Nakaji-Hirabayashi, T., Iwata, H., 2011. Design of culture substrates for large-scale expansion of neural stem cells. Biomaterials 32, 992–1001. doi:10.1016/j.biomaterials.2010.10.008

Konagaya, S., Kato, K., Nakaji-Hirabayashi, T., Iwata, H., 2013. Selective and rapid expansion of human neural progenitor cells on substrates with terminally anchored growth factors. Biomaterials 34, 6008–6014. doi:10.1016/j.biomaterials.2013.04.041

Kriks, S., Shim, J.-W., Piao, J., Ganat, Y.M., Wakeman, D.R., Xie, Z., Carrillo-Reid, L., Auyeung, G., Antonacci, C., Buch, A., Yang, L., Beal, M.F., Surmeier, D.J., Kordower, J.H., Tabar, V., Studer, L., 2011a. Dopamine neurons derived from human ES cells efficiently engraft in animal models of Parkinson/'s disease. Nature 480, 547–551. doi:10.1038/nature10648

Kriks, S., Shim, J.-W., Piao, J., Ganat, Y.M., Wakeman, D.R., Xie, Z., Carrillo-Reid, L., Auyeung, G., Antonacci, C., Buch, A., Yang, L., Beal, M.F., Surmeier, D.J., Kordower, J.H., Tabar, V., Studer, L., 2011b. Dopamine neurons derived from human ES cells efficiently engraft in animal models of Parkinson/'s disease. Nature 480, 547–551. doi:10.1038/nature10648

Kwiat, M., Elnathan, R., Pevzner, A., Peretz, A., Barak, B., Peretz, H., Ducobni, T., Stein, D., Mittelman, L., Ashery, U., Patolsky, F., 2012. Highly Ordered Large-Scale Neuronal Networks of Individual Cells - Toward Single Cell to 3D Nanowire Intracellular Interfaces. ACS Appl. Mater. Interfaces. doi:10.1021/am300602e

Lagna, G., Hemmati-Brivanlou, A., 1999. A molecular basis for Smad specificity. Dev. Dyn. Off. Publ. Am. Assoc. Anat. 214, 269–277. doi:10.1002/(SICI)1097-0177(199903)214:3<269::AID-AJA10>3.0.CO;2-#

Lagunas, A., Comelles, J., Oberhansl, S., Hortigüela, V., Martínez, E., Samitier, J., 2013. Continuous bone morphogenetic protein-2 gradients for concentration effect studies on C2C12 osteogenic fate. Nanomedicine Nanotechnol. Biol. Med. 9, 694–701. doi:10.1016/j.nano.2012.12.002

Lai, K., Kaspar, B.K., Gage, F.H., Schaffer, D.V., 2003. Sonic hedgehog regulates adult neural progenitor proliferation in vitro and in vivo. Nat. Neurosci. 6, 21–27. doi:10.1038/nn983

Lamour, G., Eftekhari-Bafrooei, A., Borguet, E., Souès, S., Hamraoui, A., 2010. Neuronal adhesion and differentiation driven by nanoscale surface free-energy gradients. Biomaterials 31, 3762–3771. doi:10.1016/j.biomaterials.2010.01.099

Lamour, G., Journiac, N., Souès, S., Bonneau, S., Nassoy, P., Hamraoui, A., 2009. Influence of surface energy distribution on neuritogenesis. Colloids Surf. B Biointerfaces 72, 208–218. doi:10.1016/j.colsurfb.2009.04.006

Lancaster, M.A., Renner, M., Martin, C.-A., Wenzel, D., Bicknell, L.S., Hurles, M.E., Homfray, T., Penninger, J.M., Jackson, A.P., Knoblich, J.A., 2013. Cerebral organoids model human brain development and microcephaly. Nature 501, 373–379. doi:10.1038/nature12517

Lander, A.D., 2013. How cells know where they are. Science 339, 923–927. doi:10.1126/science.1224186

Lander, A.D., Nie, Q., Wan, F.Y.M., 2002. Do morphogen gradients arise by diffusion? Dev. Cell 2, 785–796.

Lawrence, B.J., Madihally, S.V., 2008. Cell colonization in degradable 3D porous matrices. Cell Adhes. Migr. 2, 9–16.

Leone, D.P., Relvas, J.B., Campos, L.S., Hemmi, S., Brakebusch, C., Fässler, R., Ffrench-Constant, C., Suter, U., 2005. Regulation of neural progenitor proliferation and survival by beta1 integrins. J. Cell Sci. 118, 2589–2599. doi:10.1242/jcs.02396

Leroy, E., Boyer, R., Auburger, G., Leube, B., Ulm, G., Mezey, E., Harta, G., Brownstein, M.J., Jonnalagada, S., Chernova, T., Dehejia, A., Lavedan, C., Gasser, T., Steinbach, P.J., Wilkinson, K.D., Polymeropoulos, M.H., 1998. The ubiquitin pathway in Parkinson's disease. Nature 395, 451–452. doi:10.1038/26652

Letourneau, P., Condic, M., Snow, D., 1994. Interactions of Developing Neurons with the Extracellular-Matrix. J. Neurosci. 14, 915–928.

Levenstein, M.E., Ludwig, T.E., Xu, R.-H., Llanas, R.A., VanDenHeuvel-Kramer, K., Manning, D., Thomson, J.A., 2006. Basic fibroblast growth factor support of human embryonic stem cell self-renewal. Stem Cells Dayt. Ohio 24, 568–574. doi:10.1634/stemcells.2005-0247

Levi-Montalcini, R., 1987. The nerve growth factor: thirty-five years later. EMBO J. 6, 1145–1154.

Li, L., Zhu, Y., Li, B., Gao, C., 2008. Fabrication of Thermoresponsive Polymer Gradients for Study of Cell Adhesion and Detachment. Langmuir 24, 13632–13639. doi:10.1021/la802556e

Li, Q., Chau, Y., 2010. Neural differentiation directed by self-assembling peptide scaffolds presenting laminin-derived epitopes. J. Biomed. Mater. Res. A 94A, 688–699. doi:10.1002/jbm.a.32707

Li, Y.-C., Lin, Y.-C., Young, T.-H., 2012. Combination of media, biomaterials and extracellular matrix proteins to enhance the differentiation of neural stem/precursor cells into neurons. Acta Biomater. 8, 3035–3048. doi:10.1016/j.actbio.2012.04.036

Lindholm, D., Carroll, P., Tzimagiogis, G., Thoenen, H., 1996. Autocrine-paracrine regulation of hippocampal neuron survival by IGF-1 and the neurotrophins BDNF, NT-3 and NT-4. Eur. J. Neurosci. 8, 1452–1460.

Lindvall, O., Björklund, A., 2004. Cell Therapy in Parkinson's Disease. NeuroRx 1, 382–393.

Lindvall, O., Kokaia, Z., Martinez-Serrano, A., 2004. Stem cell therapy for human neurodegenerative disorders–how to make it work. Publ. Online 01 July 2004 Doi101038nm1064 10, S42–S50. doi:10.1038/nm1064

Liu, B.F., Ma, J., Xu, Q.Y., Cui, F.Z., 2006. Regulation of charged groups and laminin patterns for selective neuronal adhesion. Colloids Surf. B Biointerfaces 53, 175–178. doi:10.1016/j.colsurfb.2006.08.018

Liu, S., Tian, Z., Yin, F., Zhao, Q., Fan, M., 2009. Generation of dopaminergic neurons from human fetal mesencephalic progenitors after co-culture with striatal-conditioned media and exposure to lowered oxygen. Brain Res. Bull. 80, 62–68.

Lois, C., 1996. Chain migration of neuronal precursors. Science 271, 978.

Louis, S.A., Rietze, R.L., Deleyrolle, L., Wagey, R.E., Thomas, T.E., Eaves, A.C., Reynolds, B.A., 2008. Enumeration of Neural Stem and Progenitor Cells in the Neural Colony-Forming Cell Assay. STEM CELLS 26, 988–996. doi:10.1634/stemcells.2007-0867

Lu, S., Bansal, A., Soussou, W., Berger, T.W., Madhukar, A., 2006. Receptor-ligand-based specific cell adhesion on solid surfaces: hippocampal neuronal cells on bilinker functionalized glass. Nano Lett. 6, 1977–1981. doi:10.1021/nl061139w

Ludwig, T.E., Levenstein, M.E., Jones, J.M., Berggren, W.T., Mitchen, E.R., Frane, J.L., Crandall, L.J., Daigh, C.A., Conard, K.R., Piekarczyk, M.S., Llanas, R.A., Thomson, J.A., 2006. Derivation of human embryonic stem cells in defined conditions. Nat. Biotechnol. 24, 185–187. doi:10.1038/nbt1177

Lutolf, M.P., Hubbell, J.A., 2005. Synthetic biomaterials as instructive extracellular microenvironments for morphogenesis in tissue engineering. Nat. Biotechnol. 23, 47–55. doi:10.1038/nbt1055

Lynch, I., Dawson, K.A., 2008. Protein-nanoparticle interactions. Nano Today 3, 40–47. doi:10.1016/S1748-0132(08)70014-8

Lynd, L.R., Laser, M.S., Bransby, D., Dale, B.E., Davison, B., Hamilton, R., Himmel, M., Keller, M., McMillan, J.D., Sheehan, J., Wyman, C.E., 2008. How biotech can transform biofuels. Nat. Biotechnol. 26, 169–172. doi:10.1038/nbt0208-169

Lynd, L.R., Weimer, P.J., van Zyl, W.H., Pretorius, I.S., 2002. Microbial cellulose utilization: Fundamentals and biotechnology. Microbiol. Mol. Biol. Rev. 66, 506–+. doi:10.1128/MMBR.66.3.506-577.2002

Maheshwari, G., Brown, G., Lauffenburger, D.A., Wells, A., Griffith, L.G., 2000. Cell adhesion and motility depend on nanoscale RGD clustering. J. Cell Sci. 113 (Pt 10), 1677–1686.

Malinda, K.M., Kleinman, H.K., 1996. The laminins. Int. J. Biochem. Cell Biol. 28, 957–959. doi:10.1016/1357-2725(96)00042-8

Mammoto, T., Mammoto, A., Torisawa, Y., Tat, T., Gibbs, A., Derda, R., Mannix, R., de Bruijn, M., Yung, C.W., Huh, D., Ingber, D.E., 2011. Mechanochemical control of mesenchymal condensation and embryonic tooth organ formation. Dev. Cell 21, 758–769. doi:10.1016/j.devcel.2011.07.006

Mandal, S., Bhaskar, S., Lahann, J., 2009. Micropatterned Fiber Scaffolds for Spatially Controlled Cell Adhesion. Macromol. Rapid Commun. 30, 1638–1644. doi:10.1002/marc.200900340

Marklein, R.A., Burdick, J.A., 2010. Controlling stem cell fate with material design. Adv. Mater. Deerfield Beach Fla 22, 175–189. doi:10.1002/adma.200901055

Masand, S.N., Perron, I.J., Schachner, M., Shreiber, D.I., 2012. Neural cell type-specific responses to glycomimetic functionalized collagen. Biomaterials 33, 790–797. doi:10.1016/j.biomaterials.2011.10.013

Massia, S.P., and Hubbell, J.A., 1991. An RGD Spacing of 440 nm Is Sufficient for Integrin αvβ3 mediated Fibroblast Spreading and 140 nm for Focal Contact and Stress Fiber Formation. J. Cell Biol., 114, 1089-1100.

Matsushima, H., Bogenmann, E., 1990. Nerve growth factor (NGF) induces neuronal differentiation in neuroblastoma cells transfected with the NGF receptor cDNA. Mol. Cell. Biol. 10, 5015–5020.

Matyjaszewski, K., Patten, T.E., Xia, J., 1997. Controlled/“Living” Radical Polymerization. Kinetics of the Homogeneous Atom Transfer Radical Polymerization of Styrene. J. Am. Chem. Soc. 119, 674–680. doi:10.1021/ja963361g

McGuire, P.G., Seeds, N.W., 1990. Degradation of underlying extracellular matrix by sensory neurons during neurite outgrowth. Neuron 4, 633–642. doi:10.1016/0896-6273(90)90121-U

McCARTHY, J.B. , PALM, S.L., and FURCHT, L.T., 1983. Migration by haptotaxis of a Schwann cell tumor line to the basement membrane glycoprotein laminin. J Cell Biol. 97, 772–777

McKeown, S.J., Wallace, A.S., Anderson, R.B., 2013. Expression and function of cell adhesion molecules during neural crest migration. Dev. Biol. 373, 244–257. doi:10.1016/j.ydbio.2012.10.028

McMurray, R.J., Gadegaard, N., Tsimbouri, P.M., Burgess, K.V., McNamara, L.E., Tare, R., Murawski, K., Kingham, E., Oreffo, R.O.C., Dalby, M.J., 2011. Nanoscale surfaces for the

long-term maintenance of mesenchymal stem cell phenotype and multipotency. Nat. Mater. 10, 637–644. doi:10.1038/nmat3058

Mei, Y., Elliott, J.T., Smith, J.R., Langenbach, K.J., Wu, T., Xu, C., Beers, K.L., Amis, E.J., Henderson, L., 2006. Gradient substrate assembly for quantifying cellular response to biomaterials. J. Biomed. Mater. Res. A 79, 974–988. doi:10.1002/jbm.a.30883

Mei, Y., Gerecht, S., Taylor, M., Urquhart, A.J., Bogatyrev, S.R., Cho, S.-W., Davies, M.C., Alexander, M.R., Langer, R.S., Anderson, D.G., 2009. Mapping the Interactions among Biomaterials, Adsorbed Proteins, and Human Embryonic Stem Cells. Adv. Mater. 21, 2781–2786. doi:10.1002/adma.200803184

Mei, Y., Saha, K., Bogatyrev, S.R., Yang, J., Hook, A.L., Kalcioglu, Z.I., Cho, S.-W., Mitalipova, M., Pyzocha, N., Rojas, F., Vliet, K.J.V., Davies, M.C., Alexander, M.R., Langer, R., Jaenisch, R., Anderson, D.G., 2010. Combinatorial development of biomaterials for clonal growth of human pluripotent stem cells. Nat. Mater. 9, 768–778. doi:10.1038/nmat2812

Melkoumian, Z., Weber, J.L., Weber, D.M., Fadeev, A.G., Zhou, Y., Dolley-Sonneville, P., Yang, J., Qiu, L., Priest, C.A., Shogbon, C., Martin, A.W., Nelson, J., West, P., Beltzer, J.P., Pal, S., Brandenberger, R., 2010. Synthetic peptide-acrylate surfaces for long-term self-renewal and cardiomyocyte differentiation of human embryonic stem cells. Nat. Biotechnol. 28, 606–610. doi:10.1038/nbt.1629

Meng, Y., Eshghi, S., Li, Y.J., Schmidt, R., Schaffer, D.V., Healy, K.E., 2010. Characterization of integrin engagement during defined human embryonic stem cell culture. FASEB J. 24, 1056–1065. doi:10.1096/fj.08-126821

Mercier, F., Kitasako, J.T., Hatton, G.I., 2003. Fractones and other basal laminae in the hypothalamus. J. Comp. Neurol. 455, 324–340. doi:10.1002/cne.10496

Mezey, É., Chandross, K.J., Harta, G., Maki, R.A., McKercher, S.R., 2000. Turning Blood into Brain: Cells Bearing Neuronal Antigens Generated in Vivo from Bone Marrow. Science 290, 1779–1782. doi:10.1126/science.290.5497.1779

Miner, J.H., Yurchenco, P.D., 2004. Laminin functions in tissue morphogenesis. Annu. Rev. Cell Dev. Biol. 20, 255–284. doi:10.1146/annurev.cellbio.20.010403.094555

Mirzadeh, Z., Merkle, F.T., Soriano-Navarro, M., Garcia-Verdugo, J.M., Alvarez-Buylla, A., 2008. Neural stem cells confer unique pinwheel architecture to the ventricular surface in neurogenic regions of the adult brain. Cell Stem Cell 3, 265–278. doi:10.1016/j.stem.2008.07.004

Miyata, T., Kawaguchi, A., Saito, K., Kawano, M., Muto, T., Ogawa, M., 2004. Asymmetric production of surface-dividing and non-surface-dividing cortical progenitor cells. Development 131, 3133–3145. doi:10.1242/dev.01173

Moeller, M.L., Dimitrijevich, S.D., 2004. A new strategy for analysis of phenotype marker antigens in hollow neurospheres. J. Neurosci. Methods 139, 43–50. doi:10.1016/j.jneumeth.2004.04.014

Moon, L.D.F., Asher, R.A., Rhodes, K.E., Fawcett, J.W., 2001. Regeneration of CNS axons back to their target following treatment of adult rat brain with chondroitinase ABC. Nat. Neurosci. 4, 465–466. doi:10.1038/87415

Morgenthaler, M., Schweizer, E., Hoffmann-Röder, A., Benini, F., Martin, R.E., Jaeschke, G., Wagner, B., Fischer, H., Bendels, S., Zimmerli, D., Schneider, J., Diederich, F., Kansy, M., Müller, K., 2007. Predicting and tuning physicochemical properties in lead optimization: amine basicities. ChemMedChem 2, 1100–1115. doi:10.1002/cmdc.200700059

Morizane, A., Darsalia, V., Guloglu, M.O., Hjalt, T., Carta, M., Li, J.-Y., Brundin, P., 2010. A simple method for large-scale generation of dopamine neurons from human embryonic stem cells. J. Neurosci. Res. 88, 3467–3478. doi:10.1002/jnr.22515

Mrksich, M., 2000. A surface chemistry approach to studying cell adhesion. Chem. Soc. Rev. 29, 267–273. doi:10.1039/A705397E

Muir, E.M., Adcock, K.H., Morgenstern, D.A., Clayton, R., von Stillfried, N., Rhodes, K., Ellis, C., Fawcett, J.W., Rogers, J.H., 2002. Matrix metalloproteases and their inhibitors are produced by overlapping populations of activated astrocytes. Mol. Brain Res. 100, 103–117. doi:10.1016/S0169-328X(02)00132-8

Naimy, H., Buczek-Thomas, J.A., Nugent, M.A., Leymarie, N., Zaia, J., 2011. Highly sulfated nonreducing end-derived heparan sulfate domains bind fibroblast growth factor-2 with high affinity and are enriched in biologically active fractions. J. Biol. Chem. 286, 19311–19319. doi:10.1074/jbc.M110.204693

Nakajima, M., Ishimuro, T., Kato, K., Ko, I.-K., Hirata, I., Arima, Y., Iwata, H., 2007. Combinatorial protein display for the cell-based screening of biomaterials that direct neural stem cell differentiation. Biomaterials 28, 1048–1060. doi:10.1016/j.biomaterials.2006.10.004

Nasef, A., Ashammakhi, N., Fouillard, L., 2008. Immunomodulatory effect of mesenchymal stromal cells: possible mechanisms. Regen. Med. 3, 531–546. doi:10.2217/17460751.3.4.531

Navarro, M., Engel, E., Planell, J.A., Amaral, I., Barbosa, M., Ginebra, M.P., 2008. Surface characterization and cell response of a PLA/CaP glass biodegradable composite material. J. Biomed. Mater. Res. A 85, 477–486. doi:10.1002/jbm.a.31546

Neumüller, R.A., Knoblich, J.A., 2009. Dividing cellular asymmetry: asymmetric cell division and its implications for stem cells and cancer. Genes Dev. 23, 2675–2699. doi:10.1101/gad.1850809

Niehrs, C., Acebron, S.P., 2012. Mitotic and mitogenic Wnt signalling. EMBO J. doi:10.1038/emboj.2012.124

Niethammer, P., Bastiaens, P., Karsenti, E., 2004. Stathmin-tubulin interaction gradients in motile and mitotic cells. Science 303, 1862–1866. doi:10.1126/science.1094108

Ninomiya, H., Winklbauer, R., 2008. Epithelial coating controls mesenchymal shape change through tissue-positioning effects and reduction of surface-minimizing tension. Nat. Cell Biol. 10, 61–69. doi:10.1038/ncb1669

Nisbet, D.R., Yu, L.M.Y., Zahir, T., Forsythe, J.S., Shoichet, M.S., 2008. Characterization of neural stem cells on electrospun poly(ε-caprolactone) submicron scaffolds: evaluating their potential in neural tissue engineering. J. Biomater. Sci. Polym. Ed. 19, 623–634. doi:10.1163/156856208784089652

Noble, M., Albrechtsen, M., Møller, C., Lyles, J., Bock, E., Goridis, C., Watanabe, M., Rutishauser, U., 1985. Glial cells express N-CAM/D2-CAM-like polypeptides in vitro. Nature 316, 725–728.

Noctor, S.C., Martínez-Cerdeño, V., Ivic, L., Kriegstein, A.R., 2004. Cortical neurons arise in symmetric and asymmetric division zones and migrate through specific phases. Nat. Neurosci. 7, 136–144. doi:10.1038/nn1172

Nurcombe, V., Ford, M.D., Wildschut, J.A., Bartlett, P.F., 1993. Developmental regulation of neural response to FGF-1 and FGF-2 by heparan sulfate proteoglycan. Science 260, 103–106. doi:10.1126/science.7682010

Nur-E-Kamal, A., Ahmed, I., Kamal, J., Babu, A.N., Schindler, M., Meiners, S., 2008. Covalently attached FGF-2 to three-dimensional polyamide nanofibrillar surfaces demonstrates enhanced biological stability and activity. Mol. Cell. Biochem. 309, 157–166. doi:10.1007/s11010-007-9654-8

Nussbaum, J., Minami, E., Laflamme, M.A., Virag, J.A.I., Ware, C.B., Masino, A., Muskheli, V., Pabon, L., Reinecke, H., Murry, C.E., 2007. Transplantation of undifferentiated murine embryonic stem cells in the heart: teratoma formation and immune response. FASEB J. Off. Publ. Fed. Am. Soc. Exp. Biol. 21, 1345–1357. doi:10.1096/fj.06-6769com

Nuzzo, R., 2014. Scientific method: statistical errors. Nature 506, 150–152. doi:10.1038/506150a

Ogawa, K., Wada, H., Okada, N., Harada, I., Nakajima, T., Pasquale, E.B., Tsuyama, S., 2006. EphB2 and ephrin-B1 expressed in the adult kidney regulate the cytoarchitecture of medullary tubule cells through Rho family GTPases. J. Cell Sci. 119, 559–570. doi:10.1242/jcs.02777

Oldershaw, R.A., Baxter, M.A., Lowe, E.T., Bates, N., Grady, L.M., Soncin, F., Brison, D.R., Hardingham, T.E., Kimber, S.J., 2010. Directed differentiation of human embryonic stem cells toward chondrocytes. Nat. Biotechnol. 28, 1187–1194. doi:10.1038/nbt.1683

Orme, R.P., Gates, M.A., Fricker-Gates, R.A., 2010. A multiplexed quantitative proteomics approach for investigating protein expression in the developing central nervous system. J. Neurosci. Methods 191, 75–82. doi:10.1016/j.jneumeth.2010.06.009

Ornitz, D.M., 2000. FGFs, heparan sulfate and FGFRs: complex interactions essential for development. BioEssays News Rev. Mol. Cell. Dev. Biol. 22, 108–112. doi:10.1002/(SICI)1521-1878(200002)22:2<108::AID-BIES2>3.0.CO;2-M

Ortega, F., Gascón, S., Masserdotti, G., Deshpande, A., Simon, C., Fischer, J., Dimou, L., Chichung Lie, D., Schroeder, T., Berninger, B., 2013. Oligodendrogliogenic and neurogenic adult subependymal zone neural stem cells constitute distinct lineages and exhibit differential responsiveness to Wnt signalling. Nat. Cell Biol. 15, 602–613. doi:10.1038/ncb2736

Ostenfeld, T., Joly, E., Tai, Y.T., Peters, A., Caldwell, M., Jauniaux, E., Svendsen, C.N., 2002. Regional specification of rodent and human neurospheres. Brain Res. Dev. Brain Res. 134, 43–55.

Panman, L., Andersson, E., Alekseenko, Z., Hedlund, E., Kee, N., Mong, J., Uhde, C.W., Deng, Q., Sandberg, R., Stanton, L.W., Ericson, J., Perlmann, T., 2011. Transcription Factor-Induced Lineage Selection of Stem-Cell-Derived Neural Progenitor Cells. Cell Stem Cell 8, 663–675. doi:10.1016/j.stem.2011.04.001

Paragkumar N, T., Edith, D., Six, J.-L., 2006. Surface characteristics of PLA and PLGA films. Appl. Surf. Sci. 253, 2758–2764. doi:10.1016/j.apsusc.2006.05.047

Park, J.Y., Kim, S.-K., Woo, D.-H., Lee, E.-J., Kim, J.-H., Lee, S.-H., 2009. Differentiation of Neural Progenitor Cells in a Microfluidic Chip-Generated Cytokine Gradient. STEM CELLS 27, 2646–2654. doi:10.1002/stem.202

Pashuck, E.T., Stevens, M.M., 2012. Designing Regenerative Biomaterial Therapies for the Clinic. Sci. Transl. Med. 4, 160sr4–160sr4. doi:10.1126/scitranslmed.3002717

Pastrana, E., Silva-Vargas, V., Doetsch, F., 2011. Eyes Wide Open: A Critical Review of Sphere-Formation as an Assay for Stem Cells. Cell Stem Cell 8, 486–498. doi:10.1016/j.stem.2011.04.007

Patten, T.E., Matyjaszewski, K., 1998. Atom Transfer Radical Polymerization and the Synthesis of Polymeric Materials. Adv. Mater. 10, 901–915. doi:10.1002/(SICI)1521-4095(199808)10:12<901::AID-ADMA901>3.0.CO;2-B

Pearson, K., 1914. Tables for statisticians and biometricians. Cambridge, University press.

Peerani, R., Rao, B.M., Bauwens, C., Yin, T., Wood, G.A., Nagy, A., Kumacheva, E., Zandstra, P.W., 2007. Niche-mediated control of human embryonic stem cell self-renewal and differentiation. EMBO J. 26, 4744–4755. doi:10.1038/sj.emboj.7601896

Perrier, A.L., Tabar, V., Barberi, T., Rubio, M.E., Bruses, J., Topf, N., Harrison, N.L., Studer, L., 2004. Derivation of Midbrain Dopamine Neurons from Human Embryonic Stem Cells. Proc. Natl. Acad. Sci. U. S. A. 101, 12543–12548. doi:10.1073/pnas.0404700101

Persohn, E., Pollerberg, G.E., Schachner, M., 1989. Immunoelectron-microscopic localization of the 180 kD component of the neural cell adhesion molecule N-CAM in postsynaptic membranes. J. Comp. Neurol. 288, 92–100. doi:10.1002/cne.902880108

Pickard, M.R., Barraud, P., Chari, D.M., 2011. The transfection of multipotent neural precursor/stem cell transplant populations with magnetic nanoparticles. Biomaterials 32, 2274–2284.

Politis, M., Oertel, W.H., Wu, K., Quinn, N.P., Pogarell, O., Brooks, D.J., Bjorklund, A., Lindvall, O., Piccini, P., 2011. Graft-induced dyskinesias in Parkinson's disease: High striatal serotonin/dopamine transporter ratio. Mov. Disord. Off. J. Mov. Disord. Soc. 26, 1997–2003. doi:10.1002/mds.23743

Poly(N-isopropylacrylamide)-based Smart Surfaces for Cell Sheet Tissue Engineering [WWW Document], n.d. Sigma-Aldrich. URL http://www.sigmaaldrich.com/technical-documents/articles/material-matters/poly-n-isopropylacrylamide.html (accessed 5.10.13).

Pons, S., Marti, E., 2000. Sonic hedgehog synergizes with the extracellular matrix protein vitronectin to induce spinal motor neuron differentiation. Development 127, 333–342.

Prestwich, G.D., Bhatia, S., Breuer, C.K., Dahl, S.L.M., Mason, C., McFarland, R., McQuillan, D.J., Sackner-Bernstein, J., Schox, J., Tente, W.E., Trounson, A., 2012. What Is the Greatest Regulatory Challenge in the Translation of Biomaterials to the Clinic? Sci. Transl. Med. 4, 160cm14–160cm14. doi:10.1126/scitranslmed.3004915

Rais, Y., Zviran, A., Geula, S., Gafni, O., Chomsky, E., Viukov, S., Mansour, A.A., Caspi, I., Krupalnik, V., Zerbib, M., Maza, I., Mor, N., Baran, D., Weinberger, L., Jaitin, D.A., Lara-Astiaso, D., Blecher-Gonen, R., Shipony, Z., Mukamel, Z., Hagai, T., Gilad, S., Amann-Zalcenstein, D., Tanay, A., Amit, I., Novershtern, N., Hanna, J.H., 2013. Deterministic direct reprogramming of somatic cells to pluripotency. Nature 502, 65–70. doi:10.1038/nature12587

Rao, Y., Wu, X.F., Gariepy, J., Rutishauser, U., Siu, C.H., 1992. Identification of a peptide sequence involved in homophilic binding in the neural cell adhesion molecule NCAM. J. Cell Biol. 118, 937–949.

Ratner, B.D., Bryant, S.J., 2004. BIOMATERIALS: Where We Have Been and Where We are Going. Annu. Rev. Biomed. Eng. 6, 41–75. doi:10.1146/annurev.bioeng.6.040803.140027

Ratner, B.D., Tyler, B.J., Chilkoti, A., 1993. Analysis of biomedical polymer surfaces: polyurethanes and plasma-deposited thin films. Clin. Mater. 13, 71–84.

Rawsterne, R.E., Todd, S.J., Gough, J.E., Farrar, D., Rutten, F.J.M., Alexander, M.R., Ulijn, R.V., 2007. Cell spreading correlates with calculated logP of amino acid-modified surfaces RID C-2506-2009 RID C-3998-2009. Acta Biomater. 3, 715–721. doi:10.1016/j.actbio.2007.02.006

Ray, J., Peterson, D.A., Schinstine, M., Gage, F.H., 1993. Proliferation, differentiation, and long-term culture of primary hippocampal neurons. Proc. Natl. Acad. Sci. U. S. A. 90, 3602–3606.

Rayment, E.A., Williams, D.J., 2010. Concise Review: Mind the Gap: Challenges in Characterizing and Quantifying Cell- and Tissue-Based Therapies for Clinical Translation. STEM CELLS 28, 996–1004. doi:10.1002/stem.416

Ren, Y.-J., Zhang, H., Huang, H., Wang, X.-M., Zhou, Z.-Y., Cui, F.-Z., An, Y.-H., 2009. In vitro behavior of neural stem cells in response to different chemical functional groups. Biomaterials 30, 1036–1044. doi:10.1016/j.biomaterials.2008.10.028

Reticker-Flynn, N.E., Malta, D.F.B., Winslow, M.M., Lamar, J.M., Xu, M.J., Underhill, G.H., Hynes, R.O., Jacks, T.E., Bhatia, S.N., 2012. A combinatorial extracellular matrix platform identifies cell-extracellular matrix interactions that correlate with metastasis. Nat. Commun. 3, 1122. doi:10.1038/ncomms2128

Reynolds, B.A., Rietze, R.L., 2005. Neural stem cells and neurospheres--re-evaluating the relationship. Nat. Methods 2, 333–336. doi:10.1038/nmeth758

Reynolds, B.A., Tetzlaff, W., Weiss, S., 1992. A multipotent EGF-responsive striatal embryonic progenitor cell produces neurons and astrocytes. J. Neurosci. Off. J. Soc. Neurosci. 12, 4565–4574.

Reynolds, B.A., Weiss, S., 1992. Generation of neurons and astrocytes from isolated cells of the adult mammalian central nervous system. Science 255, 1707–1710.

Reynolds, B.A., Weiss, S., 1996. Clonal and population analyses demonstrate that an EGF-responsive mammalian embryonic CNS precursor is a stem cell. Dev. Biol. 175, 1–13.

Ribes, V., Briscoe, J., 2009. Establishing and Interpreting Graded Sonic Hedgehog Signaling during Vertebrate Neural Tube Patterning: The Role of Negative Feedback. Cold Spring Harb. Perspect. Biol. 1. doi:10.1101/cshperspect.a002014

Richard, B.L., Nomizu, M., Yamada, Y., Kleinman, H.K., 1996. Identification of synthetic peptides derived from laminin alpha1 and alpha2 chains with cell type specificity for neurite outgrowth. Exp. Cell Res. 228, 98–105. doi:10.1006/excr.1996.0304

Risner-Janiczek, J.R., Ungless, M.A., Li, M., 2011. Electrophysiological Properties of Embryonic Stem Cell-Derived Neurons. PLoS ONE 6, e24169. doi:10.1371/journal.pone.0024169

Roach, P., Eglin, D., Rohde, K., Perry, C.C., 2007. Modern biomaterials: a review - bulk properties and implications of surface modifications. J. Mater. Sci. Mater. Med. 18, 1263–1277. doi:10.1007/s10856-006-0064-3

Roach, P., Farrar, D., Perry, C.C., 2005. Interpretation of protein adsorption: surface-induced conformational changes. J. Am. Chem. Soc. 127, 8168–8173. doi:10.1021/ja042898o

Roach, P., Farrar, D., Perry, C.C., 2006. Surface Tailoring for Controlled Protein Adsorption: Effect of Topography at the Nanometer Scale and Chemistry. J. Am. Chem. Soc. 128, 3939–3945. doi:10.1021/ja056278e

Roach, P., Parker, T., Gadegaard, N., Alexander, M.R., 2010. Surface strategies for control of neuronal cell adhesion: A review. Surf. Sci. Rep. 65, 145–173. doi:10.1016/j.surfrep.2010.07.001

Roach, P., Parker, T., Gadegaard, N., Alexander, M.R., 2012. A bio-inspired neural environment to control neurons comprising radial glia, substrate chemistry and topography. Biomater. Sci. 1, 83–93. doi:10.1039/C2BM00060A

Roach, P., Shirtcliffe, N.J., Newton, M.I., 2008. Progess in superhydrophobic surface development. Soft Matter 4, 224–240. doi:10.1039/B712575P

Robertson, M., Chambers, I., Rathjen, P., Nichols, J., Smith, A., 1993. Expression of alternative forms of differentiation inhibiting activity (DIA/LIF) during murine embryogenesis and in neonatal and adult tissues. Dev. Genet. 14, 165–173. doi:10.1002/dvg.1020140303

Roccio, M., Gobaa, S., Lutolf, M.P., 2012. High-throughput clonal analysis of neural stem cells in microarrayed artificial niches. Integr. Biol. Quant. Biosci. Nano Macro 4, 391–400. doi:10.1039/c2ib00070a

Rodin, S., Domogatskaya, A., Ström, S., Hansson, E.M., Chien, K.R., Inzunza, J., Hovatta, O., Tryggvason, K., 2010. Long-term self-renewal of human pluripotent stem cells on human recombinant laminin-511. Nat. Biotechnol. 28, 611–615. doi:10.1038/nbt.1620

Rössler, R., Boddeke, E., Copray, S., 2010. Differentiation of non-mesencephalic neural stem cells towards dopaminergic neurons. Neuroscience 170, 417–428.

Rottner, K., Hall, A., Small, J.V., 1999. Interplay between Rac and Rho in the control of substrate contact dynamics. Curr. Biol. CB 9, 640–648.

Ruoslahti, E., 1996. RGD and other recognition sequences for integrins. Annu. Rev. Cell Dev. Biol. 12, 697–715. doi:10.1146/annurev.cellbio.12.1.697

Ruppert, R., Hoffmann, E., Sebald, W., 1996. Human bone morphogenetic protein 2 contains a heparin-binding site which modifies its biological activity. Eur. J. Biochem. FEBS 237, 295–302.

Rutishauser, U., Acheson, A., Hall, A.K., Mann, D.M., Sunshine, J., 1988. The neural cell adhesion molecule (NCAM) as a regulator of cell-cell interactions. Science 240, 53–57.

Saha, K., Irwin, E.F., Kozhukh, J., Schaffer, D.V., Healy, K.E., 2007. Biomimetic interfacial interpenetrating polymer networks control neural stem cell behavior. J. Biomed. Mater. Res. A 81, 240–249. doi:10.1002/jbm.a.30986

Saha, K., Schaffer, D.V., 2006. Signal dynamics in Sonic hedgehog tissue patterning. Dev. Camb. Engl. 133, 889–900. doi:10.1242/dev.02254

Sakaguchi, M., Imaizumi, Y., Shingo, T., Tada, H., Hayama, K., Yamada, O., Morishita, T., Kadoya, T., Uchiyama, N., Shimazaki, T., Kuno, A., Poirier, F., Hirabayashi, J., Sawamoto, K., Okano, H., 2010. Regulation of adult neural progenitor cells by Galectin-1/beta1 Integrin interaction. J. Neurochem. 113, 1516–1524. doi:10.1111/j.1471-4159.2010.06712.x

Sakai, Y., Yoshida, S., Yoshiura, Y., Mori, R., Tamura, T., Yahiro, K., Mori, H., Kanemura, Y., Yamasaki, M., Nakazawa, K., 2010. Effect of microwell chip structure on cell microsphere production of various animal cells. J. Biosci. Bioeng. 110, 223–9. doi:10.1016/j.jbiosc.2010.01.021

Salvati, A., Pitek, A.S., Monopoli, M.P., Prapainop, K., Bombelli, F.B., Hristov, D.R., Kelly, P.M., Åberg, C., Mahon, E., Dawson, K.A., 2013. Transferrin-functionalized nanoparticles lose their targeting capabilities when a biomolecule corona adsorbs on the surface. Nat. Nanotechnol. 8, 137–143. doi:10.1038/nnano.2012.237

Samuel, R., Daheron, L., Liao, S., Vardam, T., Kamoun, W.S., Batista, A., Buecker, C., Schäfer, R., Han, X., Au, P., Scadden, D.T., Duda, D.G., Fukumura, D., Jain, R.K., 2013. Generation of functionally competent and durable engineered blood vessels from human induced pluripotent stem cells. Proc. Natl. Acad. Sci. 201310675. doi:10.1073/pnas.1310675110

Saneinejad, S., Shoichet, M.S., 1998. Patterned glass surfaces direct cell adhesion and process outgrowth of primary neurons of the central nervous system. J. Biomed. Mater. Res. 42, 13–19. doi:10.1002/(SICI)1097-4636(199810)42:1<13::AID-JBM3>3.0.CO;2-R

Sargent, C.Y., Berguig, G.Y., McDevitt, T.C., 2009. Cardiomyogenic Differentiation of Embryoid Bodies Is Promoted by Rotary Orbital Suspension Culture. Tissue Eng. Part A 15, 331–342. doi:10.1089/ten.tea.2008.0145

Scadden, D.T., 2006. The stem-cell niche as an entity of action. Nature 441, 1075–1079. doi:10.1038/nature04957

Schuger, L., Yurchenco, P., Relan, N.K., Yang, Y., 1998. Laminin fragment E4 inhibition studies: basement membrane assembly and embryonic lung epithelial cell polarization requires laminin polymerization. Int. J. Dev. Biol. 42, 217–220.

Schuldiner, M., Yanuka, O., Itskovitz-Eldor, J., Melton, D.A., Benvenisty, N., 2000. Effects of eight growth factors on the differentiation of cells derived from human embryonic stem cells. Proc. Natl. Acad. Sci. 97, 11307–11312. doi:10.1073/pnas.97.21.11307

Schwartz, D.K., 2001. Mechanisms and Kinetics of Self-Assembled Monolayer Formation. Annu. Rev. Phys. Chem. 52, 107.

Scopelliti, P.E., Borgonovo, A., Indrieri, M., Giorgetti, L., Bongiorno, G., Carbone, R., Podestà, A., Milani, P., 2010. The Effect of Surface Nanometre-Scale Morphology on Protein Adsorption. PLoS ONE 5, e11862. doi:10.1371/journal.pone.0011862

Sehgal, B.U., DeBiase, P.J., Matzno, S., Chew, T.-L., Claiborne, J.N., Hopkinson, S.B., Russell, A., Marinkovich, M.P., Jones, J.C.R., 2006. Integrin β4 Regulates Migratory Behavior of Keratinocytes by Determining Laminin-332 Organization. J. Biol. Chem. 281, 35487–35498. doi:10.1074/jbc.M606317200

Selkoe, D.J., 2001. Alzheimer's disease: genes, proteins, and therapy. Physiol. Rev. 81, 741–766.

Seppa, H., Grotendorst, G., Seppa, S., Schiffmann, E., Martin, G., 1982. Platelet-Derived Growth-Factor Is Chemotactic for Fibroblasts. J. Cell Biol. 92, 584–588. doi:10.1083/jcb.92.2.584

Shen, Q., Goderie, S.K., Jin, L., Karanth, N., Sun, Y., Abramova, N., Vincent, P., Pumiglia, K., Temple, S., 2004. Endothelial Cells Stimulate Self-Renewal and Expand Neurogenesis of Neural Stem Cells. Science 304, 1338–1340. doi:10.1126/science.1095505

Shimura, H., Schlossmacher, M.G., Hattori, N., Frosch, M.P., Trockenbacher, A., Schneider, R., Mizuno, Y., Kosik, K.S., Selkoe, D.J., 2001. Ubiquitination of a New Form of α-Synuclein by Parkin from Human Brain: Implications for Parkinson's Disease. Science 293, 263–269. doi:10.1126/science.1060627

Sick, S., Reinker, S., Timmer, J., Schlake, T., 2006. WNT and DKK determine hair follicle spacing through a reaction-diffusion mechanism. Science 314, 1447–1450. doi:10.1126/science.1130088

Sigal, G.B., Mrksich, M., Whitesides, G.M., 1998. Effect of Surface Wettability on the Adsorption of Proteins and Detergents. J. Am. Chem. Soc. 120, 3464–3473. doi:10.1021/ja970819l

Silva, G., Czeisler, C., Niece, K., Beniash, E., Harrington, D., Kessler, J., Stupp, S., 2004. Selective differentiation of neural progenitor cells by high-epitope density nanofibers RID B-6737-2009. Science 303, 1352–1355. doi:10.1126/science.1093783

Silver, J., Miller, J.H., 2004. Regeneration beyond the glial scar. Nat. Rev. Neurosci. 5, 146–156. doi:10.1038/nrn1326

Singec, I., Knoth, R., Meyer, R.P., Maciaczyk, J., Volk, B., Nikkhah, G., Frotscher, M., Snyder, E.Y., 2006a. Defining the actual sensitivity and specificity of the neurosphere assay in stem cell biology. Nat. Methods 3, 801–806.

Singec, I., Knoth, R., Meyer, R.P., Maciaczyk, J., Volk, B., Nikkhah, G., Frotscher, M., Snyder, E.Y., 2006b. Defining the actual sensitivity and specificity of the neurosphere assay in stem cell biology. Nat. Methods 3, 801–806. doi:10.1038/nmeth926

Singer, I.I., Scott, S., Kawka, D.W., Kazazis, D.M., Gailit, J., Ruoslahti, E., 1988. Cell surface distribution of fibronectin and vitronectin receptors depends on substrate composition and extracellular matrix accumulation. J. Cell Biol. 106, 2171–2182.

Skubitz, A.P., Letourneau, P.C., Wayner, E., Furcht, L.T., 1991. Synthetic peptides from the carboxy-terminal globular domain of the A chain of laminin: their ability to promote cell adhesion and neurite outgrowth, and interact with heparin and the beta 1 integrin subunit. J. Cell Biol. 115, 1137–1148.

Smyth, N., Vatansever, H.S., Murray, P., Meyer, M., Frie, C., Paulsson, M., Edgar, D., 1999. Absence of Basement Membranes after Targeting the LAMC1 Gene Results in Embryonic Lethality Due to Failure of Endoderm Differentiation. J. Cell Biol. 144, 151–160. doi:10.1083/jcb.144.1.151

Sochol, R.D., Higa, A.T., Janairo, R.R.R., Li, S., Lin, L., 2011. Unidirectional mechanical cellular stimuli via micropost array gradients. Soft Matter 7, 4606–4609. doi:10.1039/C1SM05163F

Soen, Y., Mori, A., Palmer, T.D., Brown, P.O., 2006. Exploring the regulation of human neural precursor cell differentiation using arrays of signaling microenvironments. Mol. Syst. Biol. 2, 37. doi:10.1038/msb4100076

Solanki, A., Shah, S., Memoli, K.A., Park, S.Y., Hong, S., Lee, K.-B., 2010. Controlling differentiation of neural stem cells using extracellular matrix protein patterns. Small Weinh. Bergstr. Ger. 6, 2509–2513. doi:10.1002/smll.201001341

Soldner, F., Hockemeyer, D., Beard, C., Gao, Q., Bell, G.W., Cook, E.G., Hargus, G., Blak, A., Cooper, O., Mitalipova, M., Isacson, O., Jaenisch, R., 2009. Parkinson's Disease Patient-Derived Induced Pluripotent Stem Cells Free of Viral Reprogramming Factors. Cell 136, 964–977. doi:10.1016/j.cell.2009.02.013

Solozobova, V., Wyvekens, N., Pruszak, J., 2012. Lessons from the Embryonic Neural Stem Cell Niche for Neural Lineage Differentiation of Pluripotent Stem Cells. Stem Cell Rev. 8, 813–829. doi:10.1007/s12015-012-9381-8

Song, H., Zandstra, P.W., Radisic, M., 2011. Engineered heart tissue model of diabetic myocardium. Tissue Eng. Part A 17, 1869–1878. doi:10.1089/ten.TEA.2010.0617

Song, X., Wong, M.D., Kawase, E., Xi, R., Ding, B.C., McCarthy, J.J., Xie, T., 2004. Bmp signals from niche cells directly repress transcription of a differentiation-promoting gene, bag of marbles, in germline stem cells in the Drosophila ovary. Dev. Camb. Engl. 131, 1353–1364. doi:10.1242/dev.01026

Sørensen, A., Alekseeva, T., Katechia, K., Robertson, M., Riehle, M.O., Barnett, S.C., 2007. Long-term neurite orientation on astrocyte monolayers aligned by microtopography. Biomaterials 28, 5498–5508. doi:10.1016/j.biomaterials.2007.08.034

Sousa, S.R., Moradas-Ferreira, P., Barbosa, M.A., 2005. TiO2 type influences fibronectin adsorption. J. Mater. Sci. Mater. Med. 16, 1173–1178. doi:10.1007/s10856-005-4725-4

STEINBERG, M.S., 1963. Reconstruction of tissues by dissociated cells. Some morphogenetic tissue movements and the sorting out of embryonic cells may have a common explanation. Science 141, 401–408.

Stenger, D.A., Georger, J.H., Dulcey, C.S., Hickman, J.J., Rudolph, A.S., Nielsen, T.B., McCort, S.M., Calvert, J.M., 1992. Coplanar molecular assemblies of amino- and perfluorinated alkylsilanes: characterization and geometric definition of mammalian cell adhesion and growth. J. Am. Chem. Soc. 114, 8435–8442. doi:10.1021/ja00048a013

Studer, L., Csete, M., Lee, S.H., Kabbani, N., Walikonis, J., Wold, B., McKay, R., 2000. Enhanced proliferation, survival, and dopaminergic differentiation of CNS precursors in lowered oxygen. J. Neurosci. 20, 7377–7383.

Sun, T., Qing, G., 2011. Biomimetic Smart Interface Materials for Biological Applications. Adv. Mater. 23, H57–H77. doi:10.1002/adma.201004326

Sun, Y., Yong, K.M.A., Villa-Diaz, L.G., Zhang, X., Chen, W., Philson, R., Weng, S., Xu, H., Krebsbach, P.H., Fu, J., 2014. Hippo/YAP-mediated rigidity-dependent motor neuron differentiation of human pluripotent stem cells. Nat. Mater. 13, 599–604. doi:10.1038/nmat3945

Sun, Y.-M., Cooper, M., Finch, S., Lin, H.-H., Chen, Z.-F., Williams, B.P., Buckley, N.J., 2008. Rest-Mediated Regulation of Extracellular Matrix Is Crucial for Neural Development. PLoS ONE 3. doi:10.1371/journal.pone.0003656

Suzuki, Y., Yanagisawa, M., Yagi, H., Nakatani, Y., Yu, R.K., 2010. Involvement of ?1-Integrin Up-regulation in Basic Fibroblast Growth Factor- and Epidermal Growth Factor-induced Proliferation of Mouse Neuroepithelial Cells. J. Biol. Chem. 285, 18443–18451. doi:10.1074/jbc.M110.114645

Sweetman, M.J., Shearer, C.J., Shapter, J.G., Voelcker, N.H., 2011. Dual silane surface functionalization for the selective attachment of human neuronal cells to porous silicon. Langmuir ACS J. Surf. Colloids 27, 9497–9503. doi:10.1021/la201760w

Swistowski, A., Peng, J., Liu, Q., Mali, P., Rao, M.S., Cheng, L., Zeng, X., 2010. Efficient Generation of Functional Dopaminergic Neurons from Human Induced Pluripotent Stem Cells Under Defined Conditions. Stem Cells Dayt. Ohio 28, 1893–1904. doi:10.1002/stem.499

Takahashi, K., Yamanaka, S., 2006. Induction of pluripotent stem cells from mouse embryonic and adult fibroblast cultures by defined factors. Cell 126, 663–676. doi:10.1016/j.cell.2006.07.024

Takebe, T., Sekine, K., Enomura, M., Koike, H., Kimura, M., Ogaeri, T., Zhang, R.-R., Ueno, Y., Zheng, Y.-W., Koike, N., Aoyama, S., Adachi, Y., Taniguchi, H., 2013. Vascularized and functional human liver from an iPSC-derived organ bud transplant. Nature advance online publication. doi:10.1038/nature12271

Tashiro, K., Sephel, G.C., Weeks, B., Sasaki, M., Martin, G.R., Kleinman, H.K., Yamada, Y., 1989. A synthetic peptide containing the IKVAV sequence from the A chain of laminin mediates cell attachment, migration, and neurite outgrowth. J. Biol. Chem. 264, 16174–16182.

Tavazoie, M., Van der Veken, L., Silva-Vargas, V., Louissaint, M., Colonna, L., Zaidi, B., Garcia-Verdugo, J.M., Doetsch, F., 2008. A specialized vascular niche for adult neural stem cells. Cell Stem Cell 3, 279–288. doi:10.1016/j.stem.2008.07.025

Tay, S., Hughey, J.J., Lee, T.K., Lipniacki, T., Quake, S.R., Covert, M.W., 2010. Single-cell NF-kappaB dynamics reveal digital activation and analogue information processing. Nature 466, 267–271. doi:10.1038/nature09145

Tayalia, P., Mooney, D.J., 2009. Controlled growth factor delivery for tissue engineering. Adv. Mater. Deerfield Beach Fla 21, 3269–3285. doi:10.1002/adma.200900241

Taylor, C.J., Bolton, E.M., Pocock, S., Sharples, L.D., Pedersen, R.A., Bradley, J.A., 10. Banking on human embryonic stem cells: estimating the number of donor cell lines

needed for HLA matching. The Lancet 366, 2019–2025. doi:10.1016/S0140-6736(05)67813-0

Tekin, H., Sanchez, J.G., Landeros, C., Dubbin, K., Langer, R., Khademhosseini, A., 2012. Controlling spatial organization of multiple cell types in defined 3D geometries. Adv. Mater. Deerfield Beach Fla 24, 5543–5547, 5542. doi:10.1002/adma.201201805

Teng, Y.D., Lavik, E.B., Qu, X., Park, K.I., Ourednik, J., Zurakowski, D., Langer, R., Snyder, E.Y., 2002. Functional recovery following traumatic spinal cord injury mediated by a unique polymer scaffold seeded with neural stem cells. Proc. Natl. Acad. Sci. 99, 3024–3029. doi:10.1073/pnas.052678899

Tenzer, S., Docter, D., Kuharev, J., Musyanovych, A., Fetz, V., Hecht, R., Schlenk, F., Fischer, D., Kiouptsi, K., Reinhardt, C., Landfester, K., Schild, H., Maskos, M., Knauer, S.K., Stauber, R.H., 2013. Rapid formation of plasma protein corona critically affects nanoparticle pathophysiology. Nat. Nanotechnol. 8, 772–781. doi:10.1038/nnano.2013.181

Terada, N., Hamazaki, T., Oka, M., Hoki, M., Mastalerz, D.M., Nakano, Y., Meyer, E.M., Morel, L., Petersen, B.E., Scott, E.W., 2002. Bone marrow cells adopt the phenotype of other cells by spontaneous cell fusion. Nature 416, 542–545. doi:10.1038/nature730

Terranova, V.P., DiFlorio, R., Hujanen, E.S., Lyall, R.M., Liotta, L.A., Thorgeirsson, U., Siegal, G.P., Schiffmann, E., 1986. Laminin promotes rabbit neutrophil motility and attachment. J. Clin. Invest. 77, 1180–1186.

Terranova, V.P., Rohrbach, D.H., Martin, G.R., 1980. Role of laminin in the attachment of PAM 212 (epithelial) cells to basement membrane collagen. Cell 22, 719–726. doi:10.1016/0092-8674(80)90548-6

Theodosis, D.T., Bonhomme, R., Vitiello, S., Rougon, G., Poulain, D.A., 1999. Cell Surface Expression of Polysialic Acid on NCAM Is a Prerequisite for Activity-Dependent Morphological Neuronal and Glial Plasticity. J. Neurosci. 19, 10228–10236.

Thomson, J.A., Itskovitz-Eldor, J., Shapiro, S.S., Waknitz, M.A., Swiergiel, J.J., Marshall, V.S., Jones, J.M., 1998. Embryonic Stem Cell Lines Derived from Human Blastocysts. Science 282, 1145–1147. doi:10.1126/science.282.5391.1145

Timpl, R., Rohde, H., Robey, P.G., Rennard, S.I., Foidart, J.M., Martin, G.R., 1979. Laminin--a glycoprotein from basement membranes. J. Biol. Chem. 254, 9933–9937.

Tropepe, V., Sibilia, M., Ciruna, B.G., Rossant, J., Wagner, E.F., van der Kooy, D., 1999. Distinct neural stem cells proliferate in response to EGF and FGF in the developing mouse telencephalon. Dev. Biol. 208, 166–88. doi:10.1006/dbio.1998.9192

Tsai, R.Y.L., McKay, R.D.G., 2000. Cell Contact Regulates Fate Choice by Cortical Stem Cells. J. Neurosci. 20, 3725–3735.

Tucker, R.P., 2004. Antisense knockdown of the beta1 integrin subunit in the chicken embryo results in abnormal neural crest cell development. Int. J. Biochem. Cell Biol. 36, 1135–1139. doi:10.1016/j.biocel.2004.01.010

Turing, A.M., 1952. The Chemical Basis of Morphogenesis. Philos. Trans. R. Soc. Lond. B. Biol. Sci. 237, 37–72. doi:10.1098/rstb.1952.0012

Ulman, A., 1996. Formation and Structure of Self-Assembled Monolayers. Chem. Rev. 96, 1533–1554. doi:10.1021/cr9502357

Ungrin, M.D., Joshi, C., Nica, A., Bauwens, C., Zandstra, P.W., 2008. Reproducible, Ultra High-Throughput Formation of Multicellular Organization from Single Cell Suspension-Derived Human Embryonic Stem Cell Aggregates. PLoS ONE 3. doi:10.1371/journal.pone.0001565

Valamehr, B., Jonas, S.J., Polleux, J., Qiao, R., Guo, S., Gschweng, E.H., Stiles, B., Kam, K., Luo, T.-J.M., Witte, O.N., Liu, X., Dunn, B., Wu, H., 2008. Hydrophobic surfaces for enhanced differentiation of embryonic stem cell-derived embryoid bodies. Proc. Natl. Acad. Sci. U. S. A. 105, 14459–14464. doi:10.1073/pnas.0807235105

Van Ooyen, A., 2011. Using theoretical models to analyse neural development. Nat. Rev. Neurosci. 12, 311–326. doi:10.1038/nrn3031

Vescovi, A.L., Reynolds, B.A., Fraser, D.D., Weiss, S., 1993a. bFGF regulates the proliferative fate of unipotent (neuronal) and bipotent (neuronal/astroglial) EGF-generated CNS progenitor cells. Neuron 11, 951–966.

Vescovi, A.L., Reynolds, B.A., Fraser, D.D., Weiss, S., 1993b. bFGF regulates the proliferative fate of unipotent (neuronal) and bipotent (neuronal/astroglial) EGF-generated CNS progenitor cells. Neuron 11, 951–966.

Vik-Mo, E.O., Sandberg, C., Joel, M., Stangeland, B., Watanabe, Y., Mackay-Sim, A., Moe, M.C., Murrell, W., Langmoen, I.A., 2011. A comparative study of the structural organization of spheres derived from the adult human subventricular zone and glioblastoma biopsies. Exp. Cell Res. 317, 1049–1059.

Villa-Diaz, L.G., Nandivada, H., Ding, J., Nogueira-de-Souza, N.C., Krebsbach, P.H., O'Shea, K.S., Lahann, J., Smith, G.D., 2010. Synthetic polymer coatings for long-term growth of human embryonic stem cells. Nat. Biotechnol. 28, 581–583. doi:10.1038/nbt.1631

Vogler, E.A., 2012. Protein adsorption in three dimensions. Biomaterials 33, 1201–1237. doi:10.1016/j.biomaterials.2011.10.059

Vroman, L., Adams, A.L., Fischer, G.C., Munoz, P.C., 1980. Interaction of high molecular weight kininogen, factor XII, and fibrinogen in plasma at interfaces. Blood 55, 156–159.

Wang, A., Tang, H., Cao, T., Salley, S.O., Ng, K.Y.S., 2005. In vitro stability study of organosilane self-assemble monolayers and multilayers. J. Colloid Interface Sci. 291, 438–447. doi:10.1016/j.jcis.2005.05.008

Wang, J.-S., Matyjaszewski, K., 1995. Controlled/"living" radical polymerization. atom transfer radical polymerization in the presence of transition-metal complexes. J. Am. Chem. Soc. 117, 5614–5615. doi:10.1021/ja00125a035

Wang, N., Butler, J., Ingber, D., 1993. Mechanotransduction Across the Cell-Surface and Through the Cytoskeleton. Science 260, 1124–1127. doi:10.1126/science.7684161

Wang, T.Y., Sen, A., Behie, L.A., Kallos, M.S., 2006. Dynamic behavior of cells within neurospheres in expanding populations of neural precursors. Brain Res. 1107, 82–96.

Wei, J., Igarashi, T., Okumori, N., Igarashi, T., Maetani, T., Liu, B., Yoshinari, M., 2009. Influence of surface wettability on competitive protein adsorption and initial attachment of osteoblasts. Biomed. Mater. 4, 045002. doi:10.1088/1748-6041/4/4/045002

Weinhold, B., Seidenfaden, R., Röckle, I., Mühlenhoff, M., Schertzinger, F., Conzelmann, S., Marth, J.D., Gerardy-Schahn, R., Hildebrandt, H., 2005. Genetic ablation of polysialic acid causes severe neurodevelopmental defects rescued by deletion of the neural cell adhesion molecule. J. Biol. Chem. 280, 42971–42977. doi:10.1074/jbc.M511097200

Weiss, P., 1934. In vitro experiments on the factors determining the course of the outgrowing nerve fiber. J. Exp. Zool. 68, 393–448. doi:10.1002/jez.1400680304

Wenk, G.L., 2003. Neuropathologic changes in Alzheimer's disease. J. Clin. Psychiatry 64 Suppl 9, 7–10.

Whitesides, G.M., 2013. Cool, or simple and cheap? Why not both? Lab. Chip 13, 11–13. doi:10.1039/c2lc90109a

Willems, E., Cabral-Teixeira, J., Schade, D., Cai, W., Reeves, P., Bushway, P.J., Lanier, M., Walsh, C., Kirchhausen, T., Izpisua Belmonte, J.C., Cashman, J., Mercola, M., 2012. Small

molecule-mediated TGF-β type II receptor degradation promotes cardiomyogenesis in embryonic stem cells. Cell Stem Cell 11, 242–252. doi:10.1016/j.stem.2012.04.025

Willerth, S.M., Rader, A., Sakiyama-Elbert, S.E., 2008. The effect of controlled growth factor delivery on embryonic stem cell differentiation inside fibrin scaffolds. Stem Cell Res. 1, 205–218. doi:10.1016/j.scr.2008.05.006

Williams, R.L., Hilton, D.J., Pease, S., Willson, T.A., Stewart, C.L., Gearing, D.P., Wagner, E.F., Metcalf, D., Nicola, N.A., Gough, N.M., 1988. Myeloid leukaemia inhibitory factor maintains the developmental potential of embryonic stem cells. Nature 336, 684–687. doi:10.1038/336684a0

Wu, T., Tomlinson, M., Efimenko, K., Genzer, J., 2003. A combinatorial approach to surface anchored polymers. J. Mater. Sci. 38, 4471–4477. doi:10.1023/A:1027373216389

Wylie, R.G., Ahsan, S., Aizawa, Y., Maxwell, K.L., Morshead, C.M., Shoichet, M.S., 2011. Spatially controlled simultaneous patterning of multiple growth factors in three-dimensional hydrogels. Nat. Mater. 10, 799–806. doi:10.1038/nmat3101

Xu, C., Inokuma, M.S., Denham, J., Golds, K., Kundu, P., Gold, J.D., Carpenter, M.K., 2001. Feeder-free growth of undifferentiated human embryonic stem cells. Nat. Biotechnol. 19, 971–974. doi:10.1038/nbt1001-971

Xu, C., Wu, T., Mei, Y., Drain, C.M., Batteas, J.D., Beers, K.L., 2005. Synthesis and Characterization of Tapered Copolymer Brushes via Surface-Initiated Atom Transfer Radical Copolymerization. Langmuir 21, 11136–11140. doi:10.1021/la051853d

Xu, R.-H., Barron, T.L., Gu, F., Root, S., Peck, R.M., Pan, G., Yu, J., Antosiewicz-Bourget, J., Tian, S., Stewart, R., Thomson, J.A., 2008. NANOG is a Direct Target of TGF?/Activin Mediated SMAD Signaling in Human ES Cells. Cell Stem Cell 3, 196–206. doi:10.1016/j.stem.2008.07.001

Yan, Y., Yang, D., Zarnowska, E.D., Du, Z., Werbel, B., Valliere, C., Pearce, R.A., Thomson, J.A., Zhang, S.-C., 2005. Directed Differentiation of Dopaminergic Neuronal Subtypes from Human Embryonic Stem Cells. Stem Cells Dayt. Ohio 23, 781–790. doi:10.1634/stemcells.2004-0365

Yanagisawa, M., Nakashima, K., Taga, T., 1999. STAT3-mediated astrocyte differentiation from mouse fetal neuroepithelial cells by mouse oncostatin M. Neurosci. Lett. 269, 169–172. doi:10.1016/S0304-3940(99)00447-4

Yang, F., Mei, Y., Langer, R., Anderson, D.G., 2009. High Throughput Optimization of Stem Cell Microenvironments. Comb. Chem. High Throughput Screen. 12, 554–561.

Yang, F., Murugan, R., Wang, S., Ramakrishna, S., 2005. Electrospinning of nano/micro scale poly(L-lactic acid) aligned fibers and their potential in neural tissue engineering RID E-1937-2011 RID C-9542-2009. Biomaterials 26, 2603–2610. doi:10.1016/j.biomaterials.2004.06.051

Yang, J., Rose, F.R.A.J., Gadegaard, N., Alexander, M.R., 2009. A High-Throughput Assay of Cell-Surface Interactions using Topographical and Chemical Gradients. Adv. Mater. 21, 300–304. doi:10.1002/adma.200801942

Yang, J., Yamato, M., Kohno, C., Nishimoto, A., Sekine, H., Fukai, F., Okano, T., 2005. Cell sheet engineering: recreating tissues without biodegradable scaffolds. Biomaterials 26, 6415–6422. doi:10.1016/j.biomaterials.2005.04.061

Yao, Y., Ma, Y.-Z., Qin, M., Ma, X.-J., Wang, C., Feng, X.-Z., 2008. NHS-ester functionalized poly(PEGMA) brushes on silicon surface for covalent protein immobilization. Colloids Surf. B Biointerfaces 66, 233–239. doi:10.1016/j.colsurfb.2008.06.015

Yavin, E., Yavin, Z., 1974. ATTACHMENT AND CULTURE OF DISSOCIATED CELLS FROM RAT EMBRYO CEREBRAL HEMISPHERES ON POLYLYSINE-COATED SURFACE. J. Cell Biol. 62, 540–546.

Ye, W., Shimamura, K., Rubenstein, J.L.., Hynes, M.A., Rosenthal, A., 1998. FGF and Shh Signals Control Dopaminergic and Serotonergic Cell Fate in the Anterior Neural Plate. Cell 93, 755–766. doi:10.1016/S0092-8674(00)81437-3

Ying, Q.-L., Stavridis, M., Griffiths, D., Li, M., Smith, A., 2003. Conversion of embryonic stem cells into neuroectodermal precursors in adherent monoculture. Nat. Biotechnol. 21, 183–186. doi:10.1038/nbt780

Yu, Y., Gu, S., Huang, H., Wen, T., 2007. Combination of bFGF, heparin and laminin induce the generation of dopaminergic neurons from rat neural stem cells both in vitro and in vivo. J. Neurol. Sci. 255, 81–86.

Zanella, F., Lorens, J.B., Link, W., 2010. High content screening: seeing is believing. Trends Biotechnol. 28, 237–245. doi:10.1016/j.tibtech.2010.02.005

Zeiger, A.S., Hinton, B., Van Vliet, K.J., 2013. Why the dish makes a difference: Quantitative comparison of polystyrene culture surfaces. Acta Biomater. doi:10.1016/j.actbio.2013.02.035

Zelzer, M., Alexander, M.R., Russell, N.A., 2011. Hippocampal cell response to substrates with surface chemistry gradients. Acta Biomater. 7, 4120–4130. doi:10.1016/j.actbio.2011.07.021

Zelzer, M., Majani, R., Bradley, J.W., Rose, F.R.A.J., Davies, M.C., Alexander, M.R., 2008. Investigation of cell–surface interactions using chemical gradients formed from plasma polymers. Biomaterials 29, 172–184. doi:10.1016/j.biomaterials.2007.09.026

Zhang, H., Klumperman, B., Ming, W., Fischer, H., van der Linde, R., 2001. Effect of Cu(II) on the Kinetics of the Homogeneous Atom Transfer Radical Polymerization of Methyl Methacrylate. Macromolecules 34, 6169–6173. doi:10.1021/ma0104736

Zhang, J., Woodhead, G.J., Swaminathan, S.K., Noles, S.R., McQuinn, E.R., Pisarek, A.J., Stocker, A.M., Mutch, C.A., Funatsu, N., Chenn, A., 2010. Cortical neural precursors inhibit their own differentiation via N-cadherin maintenance of beta-catenin signaling. Dev. Cell 18, 472–479. doi:10.1016/j.devcel.2009.12.025

Zhang, K., Sugawara, A., Tirrell, D.A., 2009. Generation of surface-bound multicomponent protein gradients. Chembiochem Eur. J. Chem. Biol. 10, 2617–2619. doi:10.1002/cbic.200900542

Zhao, G., Schwartz, Z., Wieland, M., Rupp, F., Geis-Gerstorfer, J., Cochran, D.L., Boyan, B.D., 2005. High surface energy enhances cell response to titanium substrate microstructure. J. Biomed. Mater. Res. A 74A, 49–58. doi:10.1002/jbm.a.30320

Zhao, T., Zhang, Z.-N., Rong, Z., Xu, Y., 2011. Immunogenicity of induced pluripotent stem cells. Nature 474, 212–215. doi:10.1038/nature10135

Zigmond, S.H., 1977. Ability of polymorphonuclear leukocytes to orient in gradients of chemotactic factors. J. Cell Biol. 75, 606–616.

Chapter IX

9 Appendix

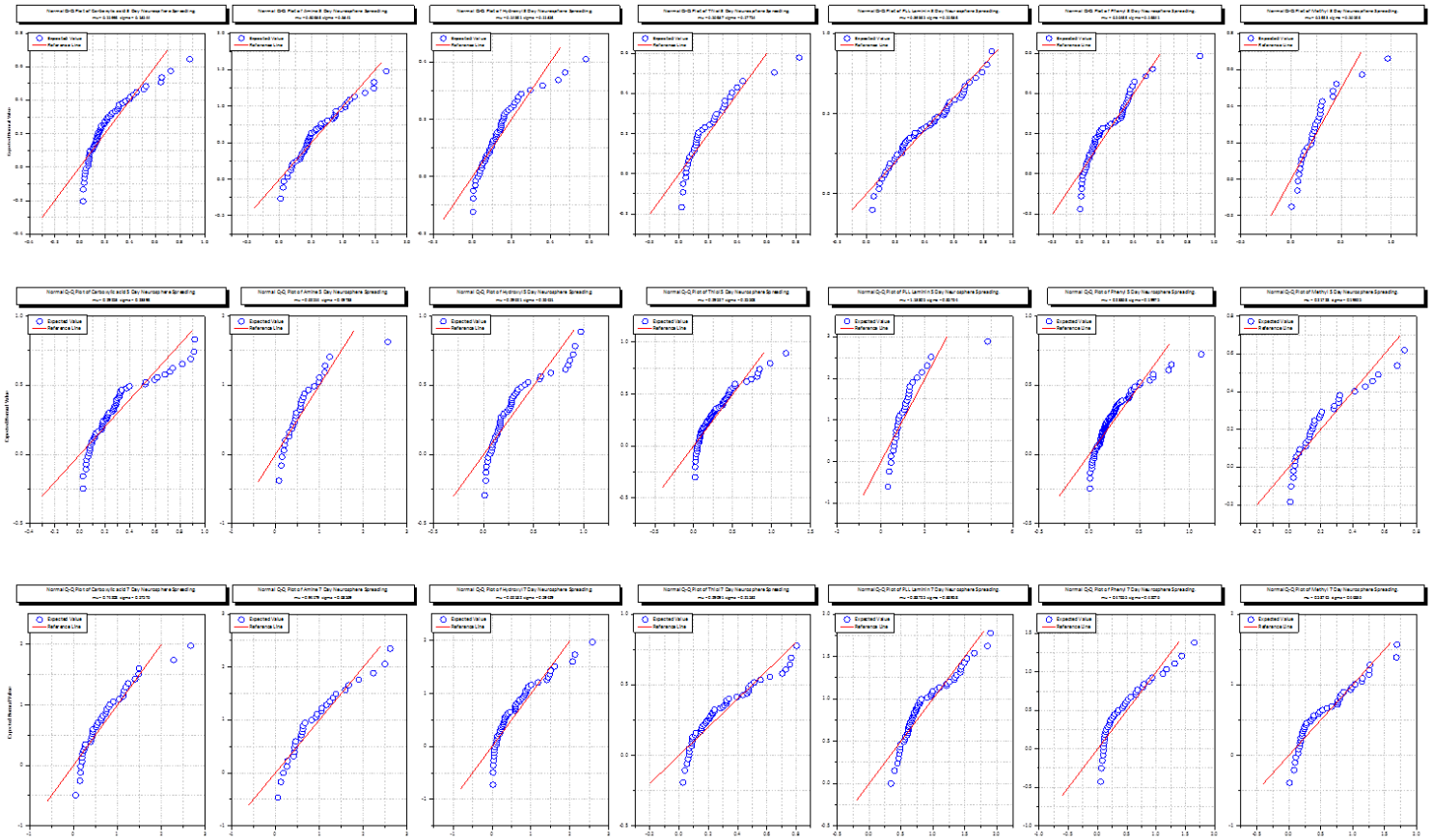

Appendix 1 – Neurosphere spread area QQ plots for chapter three. From the plots skews in the data could be shown which meant data treatments which improve the statistical testing could be applied. Row one is day 3, Row two is the tested surfaces at the day 3 timepoint, and row three is the day 7 timepoint. On the heading: mean is Mu, and sigma is standard deviation.

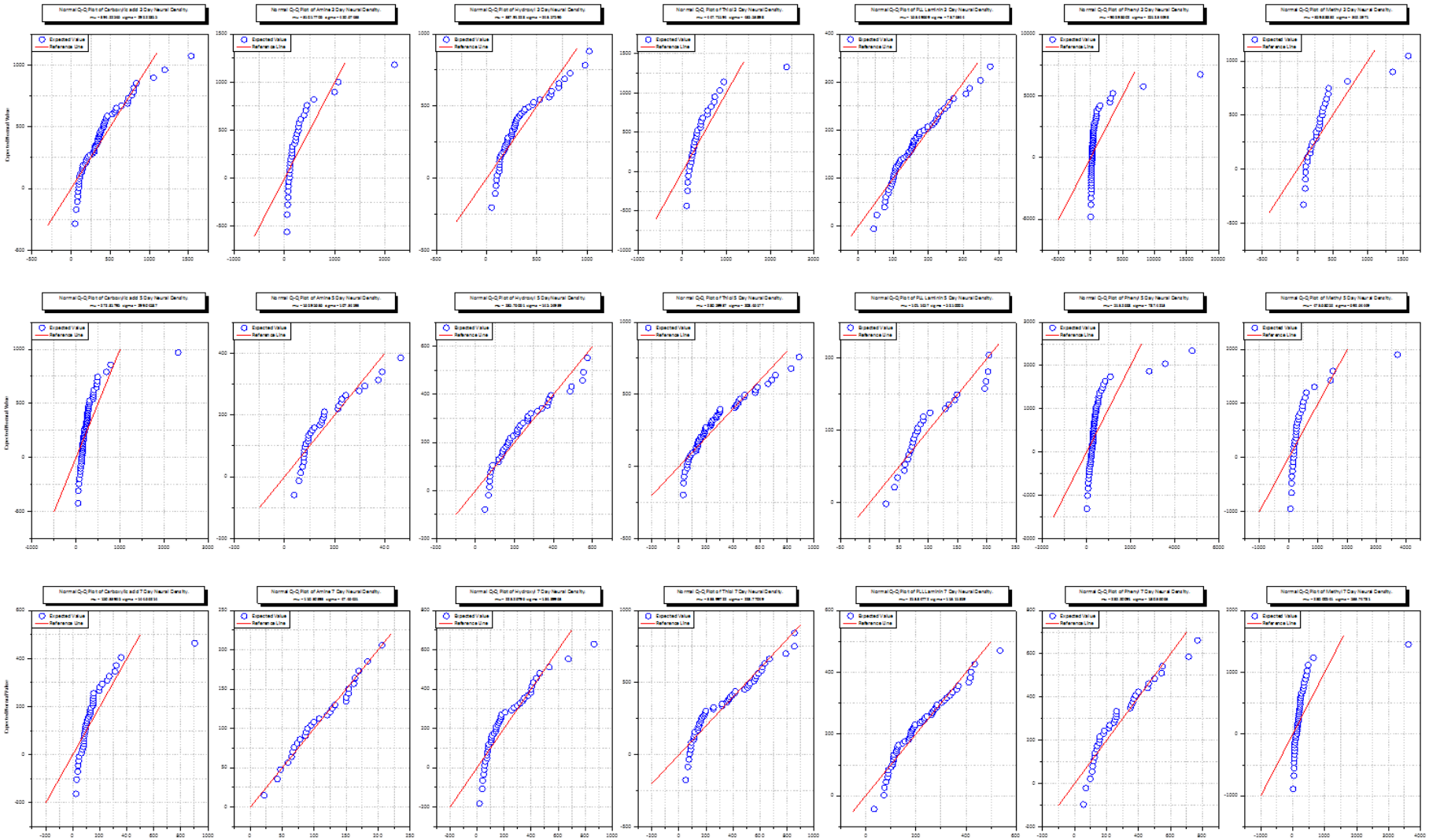

Appendix 2 – Neural density QQ plots for chapter three. From the plots skews in the data could be shown which meant data treatments which improve the statistical testing could be applied. Row one is day 3, Row two is the tested surfaces at the day 3 timepoint, and row three is the day 7 timepoint. On the heading: mean is Mu, and sigma is standard deviation.

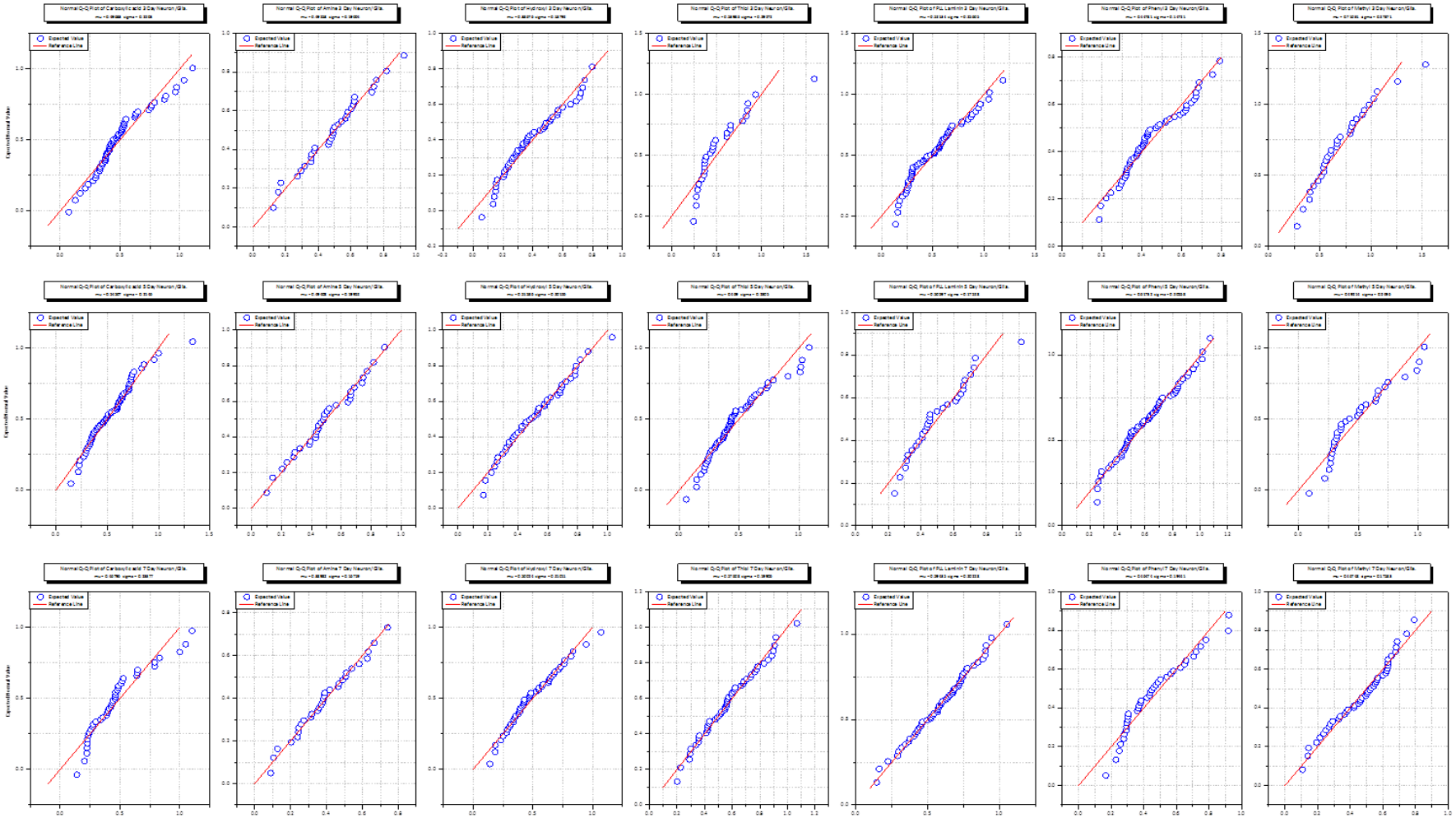

Appendix 3 – Neuron to glia ratio QQ plots for chapter three. From the plots skews in the data could be shown which meant data treatments which improve the statistical testing could be applied. Row one is day 3, Row two is the tested surfaces at the day 3 timepoint, and row three is the day 7 timepoint. On the heading: mean is Mu, and sigma is standard deviation.

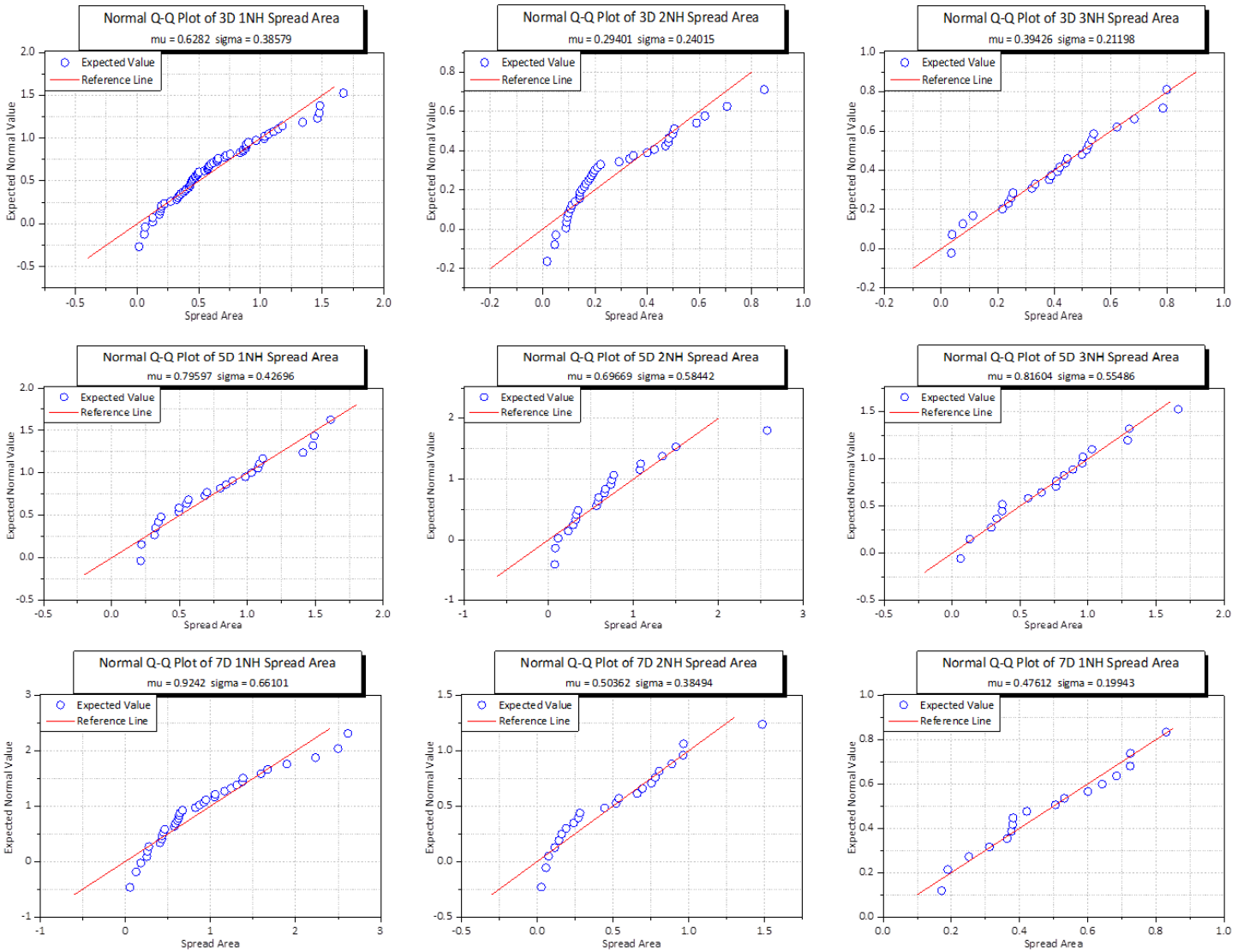

Appendix 4 – Neurosphere spread area QQ plots for chapter four. From the plots skews in the data could be shown which meant data treatments which improve statistical testing could be applied. Row one is day 3, Row two is the tested surfaces at the day 5 timepoint, and row three is the day 7 timepoint. On the heading: mean is Mu, and sigma is standard deviation.

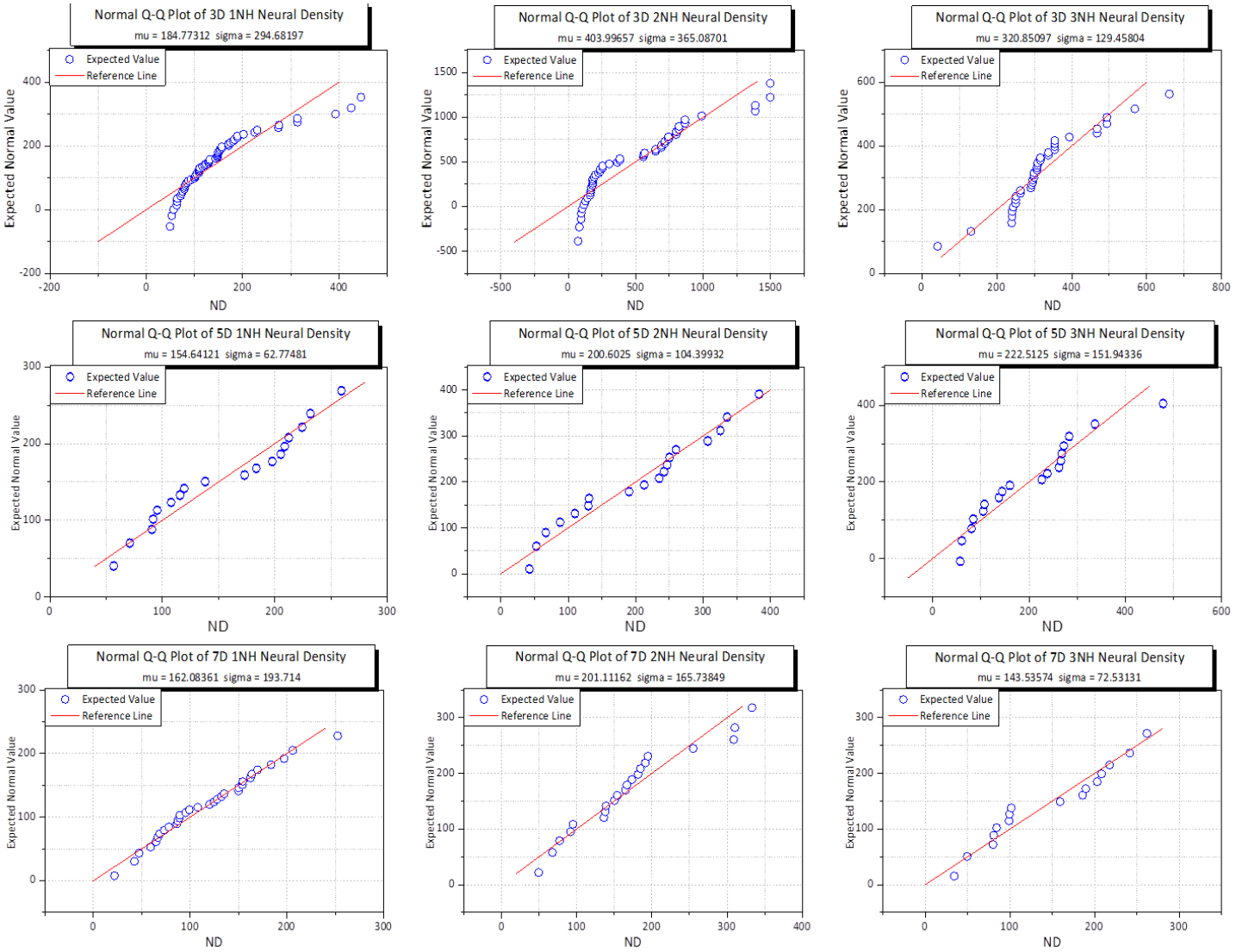

Appendix 5 – Neural density QQ plots for chapter four. From the plots skews in the data could be shown which meant data treatments which improve the statistical testing could be applied. Row one is day 3, Row two is the tested surfaces at the day 5 timepoint, and row three is the day 7 timepoint. On the heading: mean is Mu, and sigma is standard deviation.

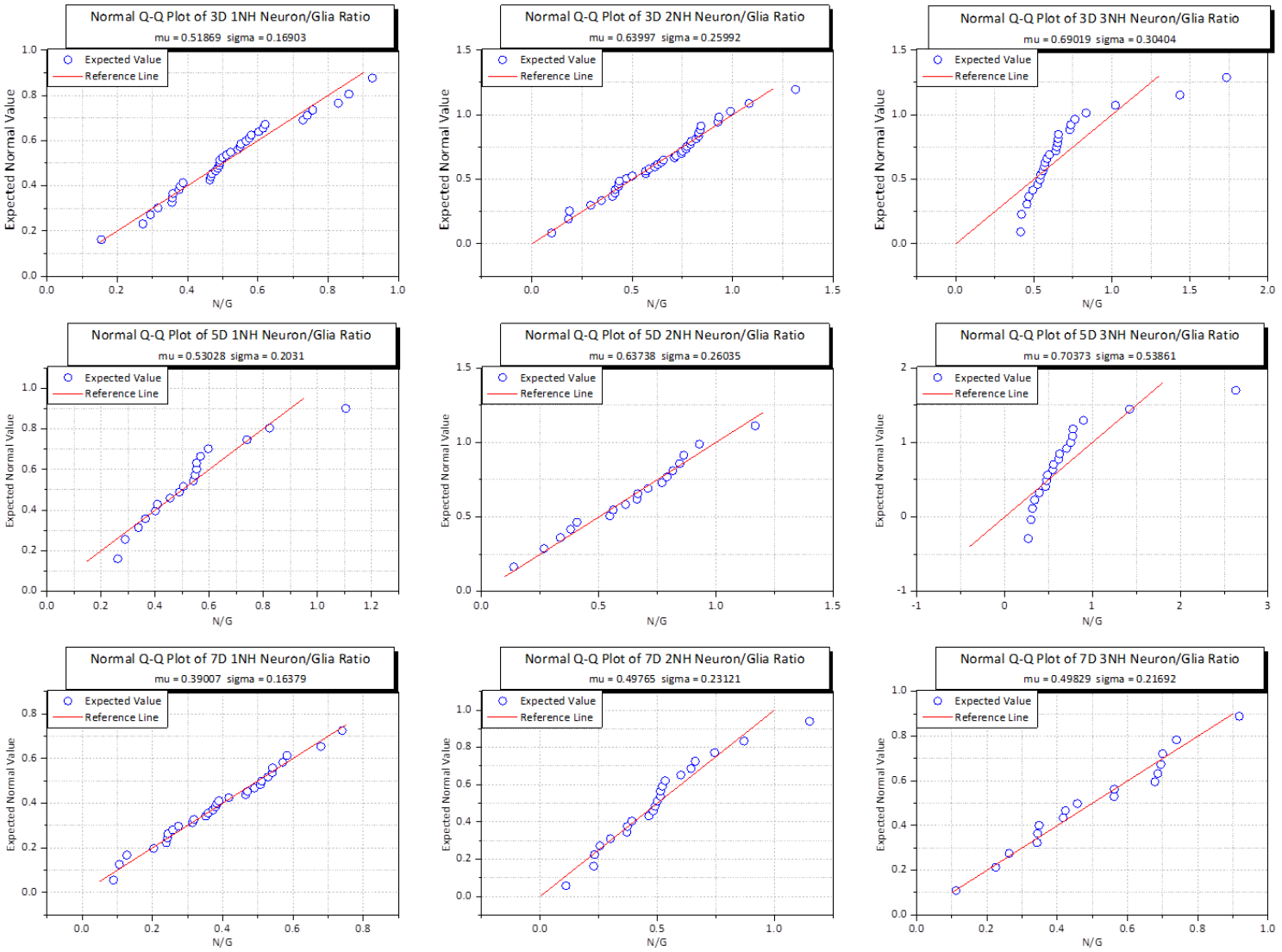

Appendix 6 – Neuron to glia ratio QQ plots for chapter four. From the plots skews in the data could be shown which meant data treatments which improve the statistical testing could be applied. Row one is day 3, Row two is the tested surfaces at the day 5 timepoint, and row three is the day 7 timepoint. On the heading: mean is Mu, and sigma is standard deviation.

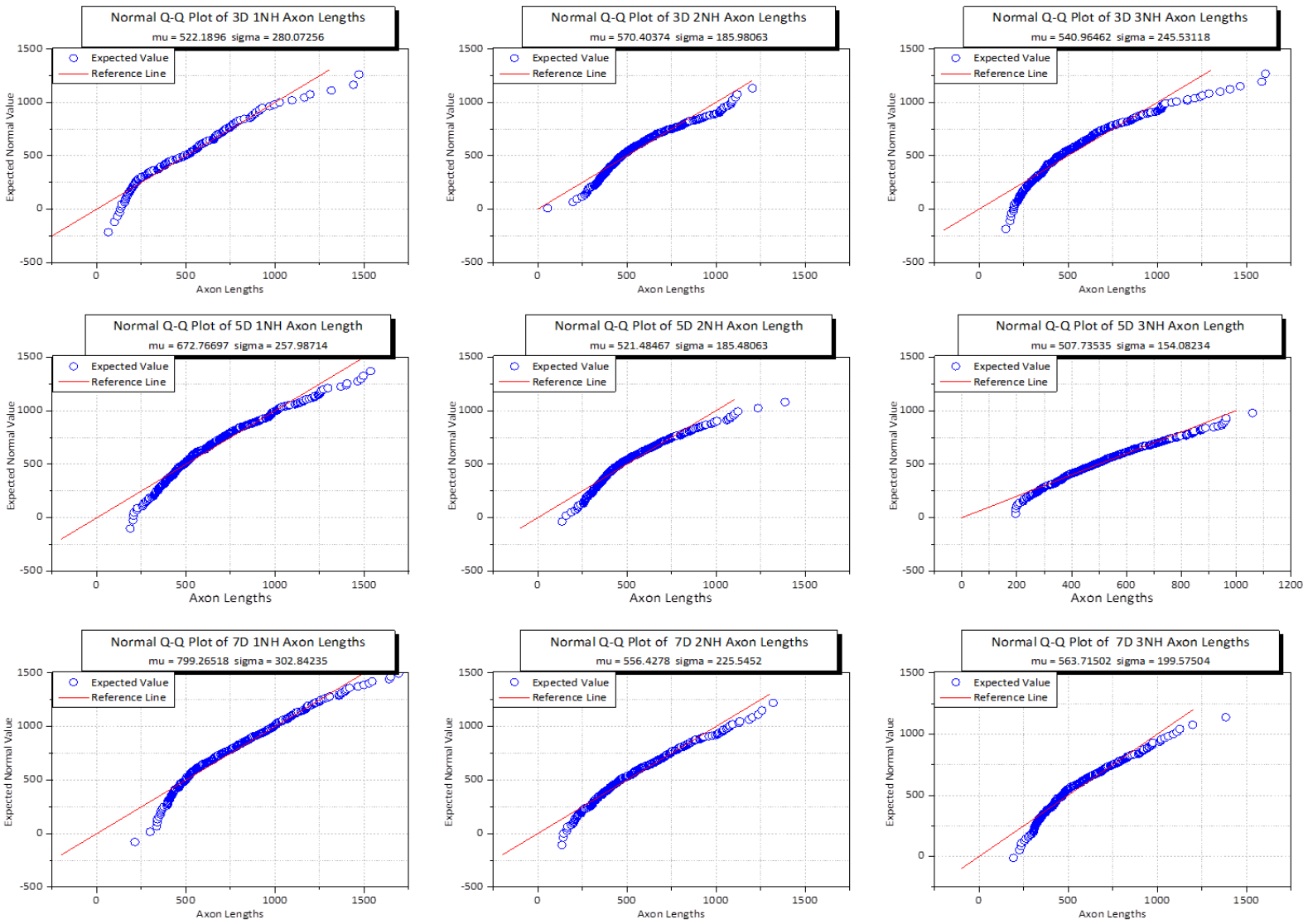

Appendix 7 - Axon process lengths QQ plots for chapter four. From the plots skews in the data could be shown which meant data treatments which improve the statistical testing could be applied. Row one is day 3, Row two is the tested surfaces at the day 5 timepoint, and row three is the day 7 timepoint. On the heading: mean is Mu, and sigma is standard deviation.

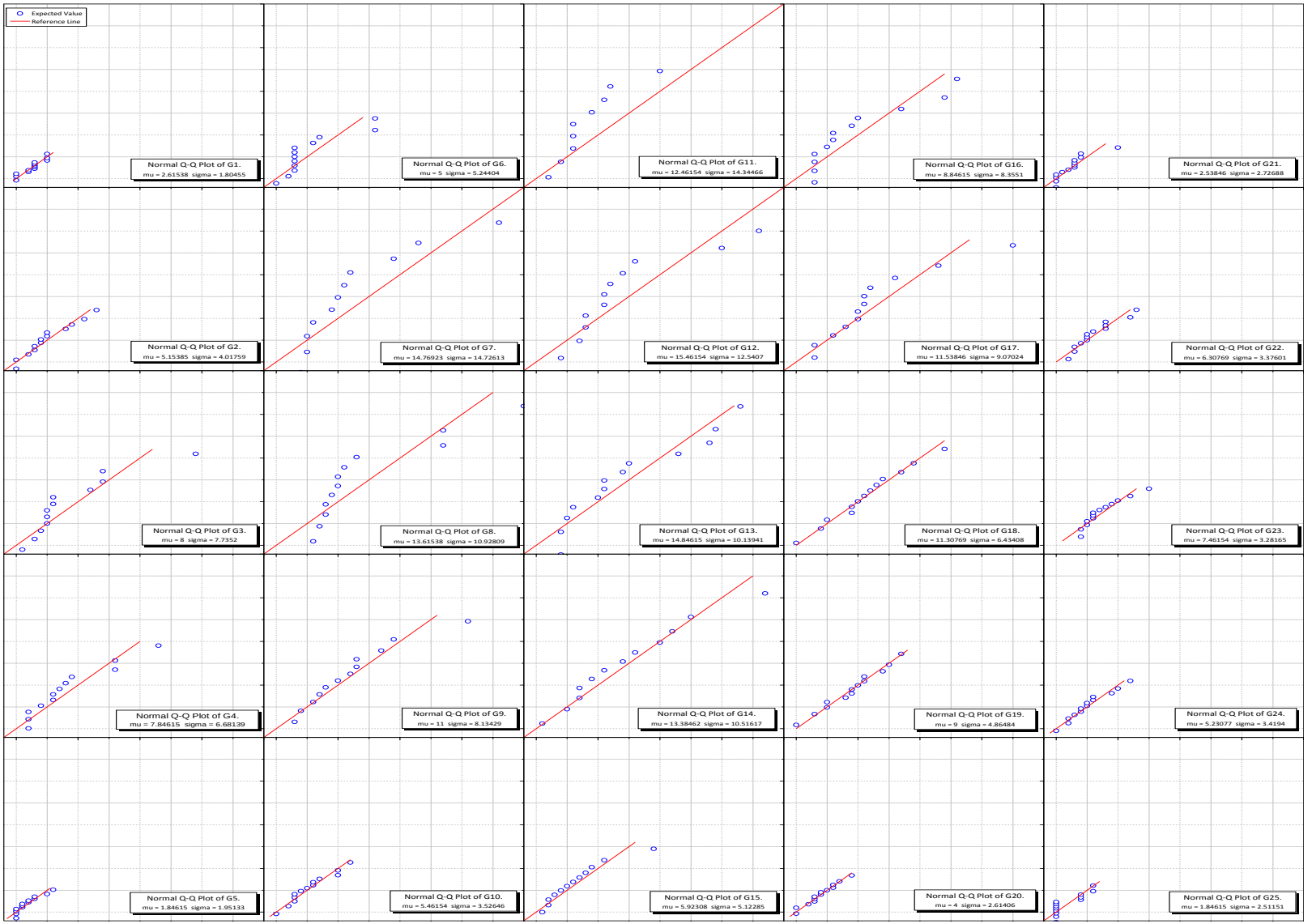

Appendix 8-Neursphere counting data from the Nipaam gradients in chapter five. Each graph is the data from counting square replicates. From the plots skews in the data could be shown which meant data treatments which improve the statistical testing could be applied. In the dialog box: mean is Mu, and sigma is standard deviation.

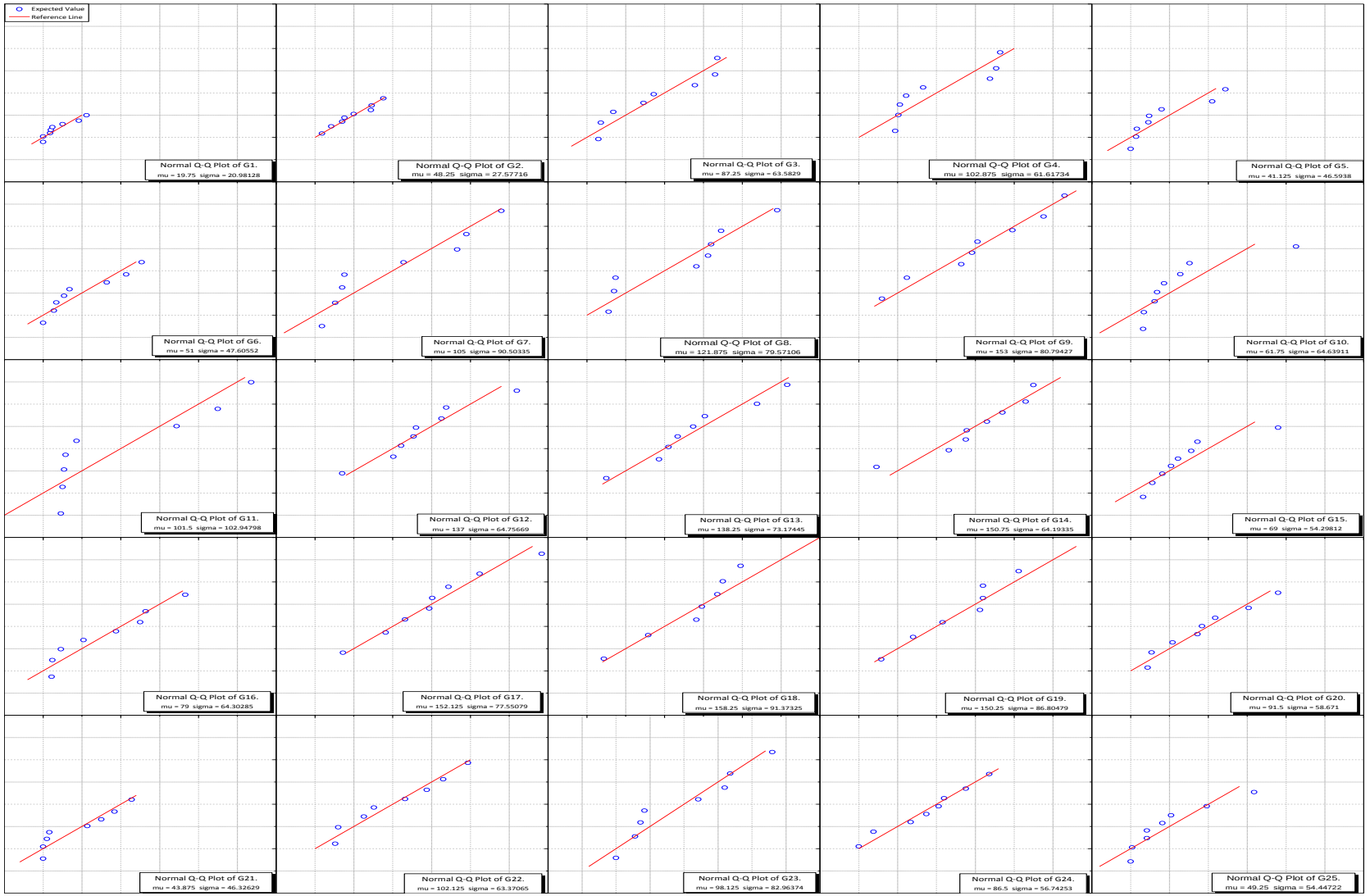

Appendix 9 - Glia counting data from the Nipaam gradients in chapter five. Each graph is the data from counting square replicates. From the plots skews in the data could be shown which meant data treatments which improve the statistical testing could be applied. In the dialog box: mean is Mu, and sigma is standard deviation.

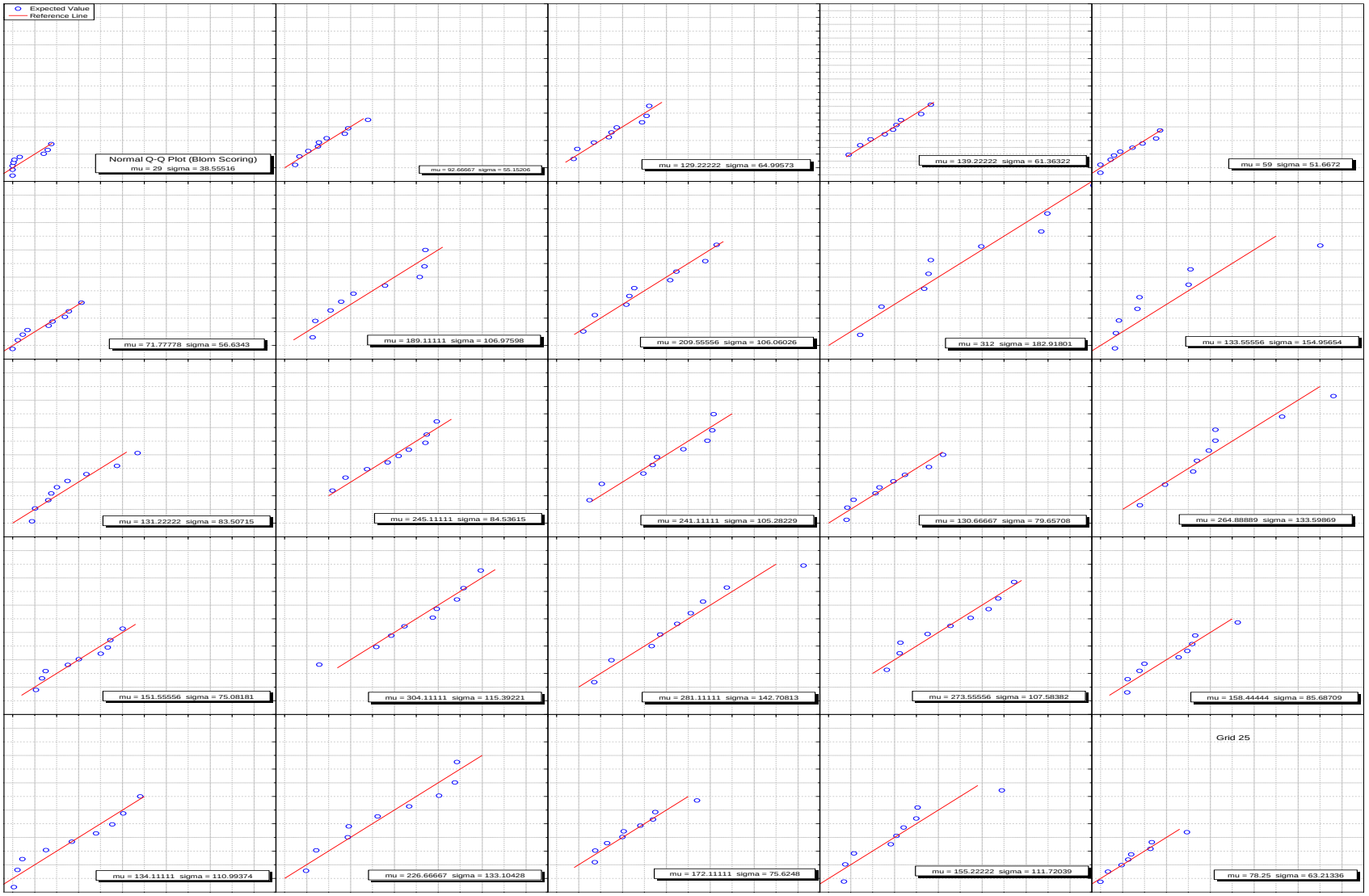

Appendix 10 – Neuron counting data from the Nipaam gradients in chapter five. Each graph is the data from counting square replicates. From the plots skews in the data could be shown which meant data treatments which improve the statistical testing could be applied. In the dialog box: mean is Mu, and sigma is standard deviation.

Media	Name of Component	Volume in 50 mL	Source
NPC (50 mls Total)	Neurobasal Media	47.8mls	Gibco (sub-division Life Technologies), Paisley
	B27 Supplement	0.5mls	Gibco (sub-division Life Technologies), Paisley
	penicillin streptomycin fungizone (PSF	0.5mls	
	l-Glutamine	0.125mls	Sigma-Aldrich Llc, Gillingham
	30% Glucose Solution	0.375mls	Sigma-Aldrich Llc, Gillingham
	Basic Fibroblast Growth Factor (bFGF)	20µl	
Dissection Media (50 mls Total)	Dulbecco's modified Eagle's medium (DMEM)	47.5mls	Sigma-Aldrich Llc, Gillingham
	30% Glucose Solution	1ml	Sigma-Aldrich Llc, Gillingham
	Sodium bicarbonate	0.8mls	Sigma-Aldrich Llc, Gillingham
	1M HEPES solution	0.25mls	Sigma-Aldrich Llc, Gillingham
Differentiation Media (50 mls Total)	Neurobasal media	42.5mls	Gibco (sub-division Life Technologies), Paisley
	Foetal calf serum	5mls	Biocera Ltd, Ringmer
	B27 supplement	0.5mls	Gibco (sub-division Life Technologies), Paisley
	glucose solution	0.375mls	Sigma-Aldrich Llc, Gillingham
	PSF	0.5mls	
	L-glutamine	0.125mls	Sigma-Aldrich Llc, Gillingham

Appendix 11 - The cell culture medias used in all experiments are shown above.

Solution	Name of Component	Volume in 7 mls	Source
Block Solution (6.94mls Total)	TBS (1 in 4 dilution)	6.6	
	Triton x	0.066 mls	Sigma-Aldrich Llc, Gillingham
	Normal goat serum (NGS)	0.33 mls	PAA Laboratories Ltd, Yeovil
Primary Antibody Solution 1 (7.1mls Total)	TBS (1 in 4 dilution)	7 mls	
	Triton x	0.007 mls	Sigma-Aldrich Llc, Gillingham
	Normal goat serum (NGS)	0.07 mls	PAA Laboratories Ltd, Yeovil
	β-III-tubulin (neuronal microtubial protein) murine antibody	1:500 Dilution	DSHB, University of Iowa, USA
	Rabbit glia fibrillary acidic protein (GFAP) antibody	1:1000 Dilution	DAKO UK Ltd, Ely
Primary Antibody Solution 1 (7.1mls Total)	TBS (1 in 4 dilution)	7 mls	
	Triton x	0.007 mls	Sigma-Aldrich Llc, Gillingham
	Nestin murine antibody	1:500 Dilution	BD Biosciences, USA
	Sox2 rabbit antibody	1:1000	Sigma-Aldrich Llc, Gillingham
Secondary Antibody Solution (7.1ml Total)	TBS (1 in 4 dilution)	7 mls	
	Triton x	0.007 mls	Sigma-Aldrich Llc, Gillingham
	Normal goat serum (NGS)	0.07 mls	PAA Laboratories Ltd, Yeovil
	TRITc tagged 547nm Goat anti-Rabbit Antibody	1:300 Dilution	Cheshire Sciences LTD, Aldford
	FITc tagged 490nm Goat anti-Mouse Antibody	1:300 Dilution	Cheshire Sciences LTD, Aldford

Appendix 12 – Antibody solutions used in all experiments.